DEVELOPMENT OF MATHEMATICAL MODELS AND INVESTIGATION OF FBR PLANT BEHAVIOUR DURING TRANSIENTS BY A COUPLED SINGLE AND MULTI-DIMENSIONAL APPROACH

By

K. NATESAN

Enrolment No :ENGG02201304010

Indira Gandhi Centre for Atomic Research, Kalpakkam

A thesis submitted to the

Board of Studies in Engineering Sciences

In partial fulfillment of requirements

for the Degree of

DOCTOR OF PHILOSOPHY

of

HOMI BHABHA NATIONAL INSTITUTE

May, 2020

Homi Bhabha National Institute

Recommendations of the Viva Voce Committee

As members of the Viva Voce Committee, we certify that we have read the dissertation prepared by Shri K. Natesan entitled "Development of Mathematical Models and Investigation of FBR Plant behaviour during Transients by a Coupled Single and Multi-Dimensional Approach" and recommend that it may be accepted as fulfilling the thesis requirement for the award of Degree of Doctor of Philosophy.

Chairman : **Dr. A. K. Bhaduri**		**Date :** 21/5/2020
Guide / Convener : **Dr. K. Velusamy**		**Date:** 21/05/2020
Examiner : **Dr. A. Sameen**		**Date :** 27/5/2020
Member 1 : **Dr. V. S. Srinivasan**	V. S. Srinivasan	**Date :** 21/05/2020
Member 2 : **Dr. T. S. Lakshmi Narasimhan**		**Date :** 21/05/20
Member 3 : **Dr. T. Sundararajan**		**Date :** 29/5/2020

Final approval and acceptance of this thesis is contingent upon the candidate's submission of the final copies of the thesis to HBNI.

I hereby certify that I have read this thesis prepared under my direction and recommend that it may be accepted as fulfilling the thesis requirement.

Date: 21/5/2020

Place: Kalpakkam

Dr. K. Velusamy

(Guide)

STATEMENT BY AUTHOR

This dissertation has been submitted in partial fulfillment of requirements for an advanced degree at Homi Bhabha National Institute (HBNI) and is deposited in the Library to be made available to borrowers under rules of the HBNI.

Brief quotations from this dissertation are allowable without special permission, provided that accurate acknowledgement of source is made. Requests for permission for extended quotation from or reproduction of this manuscript in whole or in part may be granted by the Competent Authority of HBNI when in his or her judgment the proposed use of the material is in the interests of scholarship. In all other instances, however, permission must be obtained from the author.

Natesan

K. Natesan

DECLARATION

I, hereby declare that the investigation presented in the thesis has been carried out by me. The work is original and has not been submitted earlier as a whole or in part for a degree / diploma at this or any other Institution / University.

Natesan.

K. Natesan

List of Publications arising from the thesis

International Journal Papers

1. **K. Natesan**, K. Velusamy, P. Selvaraj, and P. Chellapandi, 2014. Safety Improvement of Pool type FBR against Loss of Flow Accident, Nuclear Engineering and Design, Vol. 278, 29–38.

2. **K. Natesan**, K. Velusamy, P. Selvaraj, and P. Chellapandi, 2015. Significance of Coast Down Time on Safety and Availability of a Pool Type Fast Breeder Reactor, Nuclear engineering and Design, Vol. 286, 77-88.

3. **K. Natesan** and K. Velusamy, 2019. Coupled System Dynamics and Computational Fluid Dynamics Simulation of Plant Transients in Sodium Cooled Fast Reactors, Nuclear Engineering and Design, Vol. 342, 157-169.

4. **K. Natesan** and K. Velusamy, 2019. Synthesis of Pool Modeling of Fast Reactors in System Dynamics Codes, Annals of Nuclear Energy, Vol. 132, 24-33.

Conference Proceedings

1. Amit K. Chauhan, **K. Natesan**, K. Velusamy and P. Puthiyavinayagam, 2016. Safety Benefits of Increasing Number of Primary Coolant Pumps and Pipes in Future FBR, Proceedings of the 6thInternational and 43rdNational Conference on Fluid Mechanics and Fluid Power (FMFP), MNNITA, Allahabad, India.

2. **K. Natesan**, K. Velusamy, N. Kasinathan and P. Puthiyavinayagam, 2018. Consideration for Thermal Stratification in the Thermal Hydraulic Design of Fast Reactor, Proceedings of the 7thInternational and 45thNational Conference on Fluid Mechanics and Fluid Power (FMFP), 2018, IIT Bombay, Mumbai, India.

3. **K. Natesan**, K. Velusamy and N. Kasinathan, 2019. Transient Thermal Stratification in Sodium Pool of a Fast Reactor, Proceedings of the 46thNational Conference on Fluid Mechanics and Fluid Power (FMFP), 2019, PSG College of Technology, Coimbatore, India.

Natesan.

K. Natesan

Dedicated to all my teachers and family

ACKNOWLEDGEMENTS

I am very much delighted to take up my Ph.D work with **Dr. K. Velusamy** as the research guide. I gratefully acknowledge Dr. K. Velusamy, Associate Director, Nuclear Systems Analysis Group, IGCAR for his valuable guidance during the course of this work. Dr. K. Velusamy's overwhelming knowledge, keen insight and persistent encouraging nature make him so endearingly unforgettable as a great teacher and researcher.

I express my profound thanks to **Shri. N. Kasinathan,** Head, Thermal Hydraulics Division, IGCAR, who initiated interest in me to work in the area of plant dynamics of fast reactor systems. I am deeply gratified to his knowledge on this subject.

I thank the Chairman and members of the Doctoral Committee, **Dr. A. K. Bhaduri** (Director IGCAR), **Dr. N. Saibaba** (Former AD, RMG), **Dr. V. S. Srinivasan** (Head, SIRD), **Dr. T. S. Lakshmi Narasimhan** (AD, RMG) and **Prof. T. Sundararajan** (IIT, Madras) for their periodic assessment of the work at various stages. I gratefully acknowledge **Dr. P. Selvaraj** (Director FRTG& RDG)**,** **Shri. P. Puthiyavinayagam** (Former Director RDG) and **Dr. P. Chellapandi** (Former CMD, BHAVINI) for their motivation to pursue my higher studies. I also thank all the colleagues of Thermal Hydraulics Division, IGCAR, **Shri M. Asokkumar** in particular, for their encouragement and support throughout my research.

I express my heartfelt thanks to all my family members who have been a great moral support for me.

K. Natesan

CONTENTS

List of Figures

List of Tables

ABBREVATIONS

ANL	Argonne national laboratory
ATWS	Anticipated transients without SCRAM
BNL	Brookhaven national laboratory
BWR	Boiling water reactor
CEA	French Alternative Energies and Atomic Energy Commission
CFD	Computational fluid dynamics
CRBRP	Clinch river breeder reactor project
DHX	Decay heat exchanger
EBR	Experimental breeder reactor
FBTR	Fast breeder test reactor
FFTF	Fast flux test facility
FHT	Flow halving time
FVM	Finite volume model
HP	High pressure
IHX	Intermediate heat exchanger
IAEA	International atomic energy agency
IGCAR	Indira Gandhi Centre for atomic research
IP	Intermediate pressure
IPPE	Institute of Physics and Power Engineering
IRSN	Institut de radioprotection et de sûreténucléaire
JNC	Japan Nuclear Cycle Development Institute
KAERI	Korea atomic energy research institute
KALIMER	Korea advanced liquid metal reactor
LANL	Los Alamos National Laboratory

LP	Low pressure
NSSS	Nuclear steam supply system
NPSH	Net positive suction head
PFBR	Prototype fast breeder reactor
PFR	Prototype fast reactor
PSI	Das Paul Scherrer Institute
PSP	Primary sodium pump
PWR	Pressurized water reactor
RANS	Reynolds average Navier Stokes
RNG	Re-normalization group
RSTM	Reynolds stress model
SCRAM	Safety control rod accelerated movement
SFR	Sodium cooled fast reactor
SG	Steam generator
SPX	Superphenix
SSC	Super system code
TDMA	Tri-diagonal matrix algorithm
ULOF	Unprotected loss of flow
VVER	Water-water energetic reactor

LIST OF SYMBOLS

A_I	Flow area of cross section of the I^{th} subassembly
a	ratio of longitudinal pitch to diameter of sleeves
b	ratio of transverse pitch to diameter of sleeves
C_N	Correction factor for number of rows
c_n	Empirical correction parameter for number of rows
Cp	Specific heat capacity, J/kg K
D	Diffusive flux
d	Diameter, m
Eu	Euler number
F	Convective flux
Gr	Grashoff number
g	Acceleration due to gravity, m/s^2
K	Molecular thermal conductivity of fluid, W/m-K
K_{eff}	Effective thermal conductivity of fluid, W/m-K
k	Turbulent kinetic energy, m^2/s^2
M_{HP}	Mass of hot pool sodium, kg
M_{CP}	Mass of cold pool sodium, kg
N	Number of rows of sleeves
Nu	Nusselt number
P	Pressure, Pa
Q_{CI}	Flow rate through i^{th} subassembly, kg/s
Q_f	Flow faction between control volumes, kg/s
Q_I	Sodium flow rate through IHX, kg/s
Q_{PP}	Flow entering primary sodium pump

Re	Reynolds number
Ri	Richardson number
S_T	Heat source, W/m^3
S_U	Momentum source in the U-momentum equation, N/m^3
S_V	Momentum source in the V- momentum equation, N/m^3
r	distance in the radial coordinate direction (Cylindrical)
T	Temperature, K
T_{Ci}	Sodium outlet temperature of ith subassembly, K
T_{CP}	Mixed mean temperature of cold pool, K
T_{HP}	Mixed mean temperature of hot pool, K
T_I	Temperature of sodium leaving IHX, K
t	time
U	Velocity in 'x - coordinate' or 'r - coordinate' direction, m/s
V	Velocity in 'y - coordinate' or 'z - coordinate' direction, m/s
v	Average fluid velocity, m/s
x	distance in the x-coordinate direction (Cartesian)
y	distance in the y-coordinate direction (Cartesian)
z	distance in the axial coordinate direction (Cylindrical)
β	Volumetric expansion coefficient, K^{-1}
γ	Porosity
ΔP	Pressure drop, Pa
δ	thickness of plate, mm
ε	Rate of dissipation of turbulent kinetic energy, m^2/s^3
κ	Empirial constant
μ	Molecular viscosity, N-s/m^2

μ_{eff} Effctive viscosity, N-s/m^2

Ω Pressure drop coefficient

φ Diameter of holes, mm

ρ Density, kg/m^3

σ Prandtl number

CHAPTER – 7

CONCLUSIONS AND SCOPE FOR FUTURE WORK

7.1 SUMMARY OF STUDIES

In order to account for the multi-dimensional phenomenon involved in various systems and components of a fast reactor, models capable of simulating such phenomenon are to be adopted for the accurate prediction of transient thermal hydraulic phenomenon involved during plant transients. A survey of various codes developed for plant dynamic analysis of fast reactor systems has shown that benchmarking exercises have been undertaken internationally to assess the relative performance of various codes. The recent studies in this direction have indicated a strong need for incorporating multi-dimensional modeling approach for sodium pools of fast reactor systems. Accordingly, several codes have been improved through incorporation of multi-dimensional thermal hydraulic features for predicting phenomenon such as thermal stratification in the outlet plenum (hot pool) of reactor. Nevertheless, the real benefits of including such models on the predictions of plant behavior during transients are not reported in literature. There are also other sub-domains in the plant where the multidimensional modeling plays important roles. In this direction, an investigation adopting computational tools has been carried out towards identification of sub-domains in the sodium cooled fast reactor that need multi-dimensional modeling in plant dynamic analyses.

Hydraulic studies carried for grid plate have shown that plant dynamics modeling of this component does not require special consideration for simulation flow re-distribution caused by the grid plate. The flow distribution among various subassemblies is found to be not affected even during primary pipe rupture condition during which the pipe boundaries supplying coolant to the grid plate are highly un-symmetric and some of the pipes bypass coolant flow. The point pressure approximation for grid plate is valid for all transients including primary pipe rupture event addressed by plant dynamics codes. Thermal hydraulic studies on hot pool during plant transients involving thermal stratification in hot pool have shown that axi-symmetric modeling can predict the associated phenomenon in a realistic manner compared to one dimensional model predictions. The deviations between axi-symmetric and three dimensional model predictions are acceptable for plant dynamics studies while comparing against the large computational effort associated with three dimensional model studies. Hence, axi-symmetric model for hot pool is recommended for plant dynamics studies. Based on the insight derived from the above studies, an axi-symmetric 2-D turbulent code (STITH-2D) for hot pool has been developed. The CFD code has been validated against standard benchmark solution. The pool hydraulics predictions of this code for large size sodium pools for fast reactor have also been compared against those predicted by general purpose commercial CFD codes. Subsequently, the CFD code is coupled with system dynamics code (DYANA-P) for the rest of the plant. The coupled hybrid code system is named as DYANA-HM. Analysis of typical plant transients in a fast reactor is carried out with the coupled code system and predictions are compared against those obtained with fully one dimensional code.

It is seen that during transients in which heat removal is continued to be available through steam generators, the prediction of hot leg temperatures of heat exchangers are affected due to thermal stratification effects in hot pool. Prediction of cold leg temperatures and hence the core temperature evolutions under these class of transients are not affected. During other transients, when heat removal through steam generators is not available, consideration of thermal stratification in hot pool is essential for the realistic prediction of temperature evolution in the entire plant. The evolution of natural convection flow in the secondary sodium circuit is also found to be influenced by the thermal stratification effects in hot pool. However, when both primary and secondary sodium circuits are under natural convection conditions, the buoyancy effects in the primary circuit manifest in such that the temperature evolution of sodium pool is governed by diffusion rather than convection.

As far the plant dynamics studies towards design of plant protection system and demonstration of core safety are concerned, multi-dimensional model based studies are not essential. This is due to the hot pool being in well mixed condition during normal operating conditions and plant protection system gets triggered within a few seconds after the occurrence of initiating events. However, multi-dimensional model based studies provide accurate prediction of transient thermal loading on various structures and components for their fatigue design. Conservatism cannot be guaranteed in the design based on fully one-dimensional model predictions. Moreover, realistic prediction of transient scenario in the plant under post shutdown cooling conditions requires the incorporation of advanced models. DYANA-HM has the extra capability of providing accurate information for the above design requirements of the plant.

Comparison of transient phenomenon predicted in the cold pool with single zone, multi-zone and three dimensional model during plant transients originating from one secondary sodium loop and both secondary loops have clearly brought out the advantages and disadvantages of the multi-zone model. Multi-zone model can realistically predict the thermal hydraulics in cold pool during events in which both secondary sodium loops participate in a similar manner. However, this model is not found to be conservative for transients originating from one secondary sodium loop. Hence, for accurate representation of transients in the cold pool in plant dynamic studies three dimensional modeling is essential.

Further, studies have been carried out to optimize the coast down of primary sodium pumps and to bring out the benefits of the sympathetic safety action (coast down of sodium pumps after reactor trip). In order to limit the consequences of power failure event within design safety limits, a primary flow halving time of 8 s has been found to be essential. Apart from safety benefits, the large coast down time has also an operational benefit by way of improving plant availability through the elimination of reactor SCRAM during short term power failure events. Optimization of threshold values of various SCRAM parameters is also essential to accomplish this effectively. With this optimization and a selection of primary flow halving time of 8 s can eliminate reactor SCRAM during short term power failure for a duration extending up to 0.75 s. Analysis of hot pool with and without the consideration of sympathetic safety action shows that though the sympathetic safety action results in development of thermal stratification in hot pool for about 15 minutes after reactor SCRAM, a significant reduction in thermal shock faced by components from ~ 110 ^{0}C/min to 30 ^{0}C/min is benefitted from this procedure. With the incorporation of sympathetic safety action in the operating strategy of the plant, in order to have accurate prediction of thermal hydraulic scenario during reactor transients, models incorporating multi-dimensional analysis capability for sodium pools becomes essential.

7.2 SCOPE FOR FUTURE WORK

The following are the domains identified for future work.

- Only the multi-dimensional hydraulic nature of grid plate has been assessed in the present investigations. However, the need for multi-dimensional model for realistic prediction of thermal mixing in grid plate needs to be assessed. If necessary, a simplified thermal mixing model for grid plate based on the point hydraulic model assumption needs to be developed and interfaced with the system models of the plant dynamics code.
- The need for a three dimensional modeling cold pool for realistic simulation of thermal stratification and mixing phenomenon has been demonstrated from the studies carried out. However, interfacing a detailed CFD model for cold pool may make the plant dynamics studies computationally complex and defeat its all intended objectives

including its application for development of training simulator. Therefore, an optimum model with minimum modeling features and control volumes adequate enough to represent the multi-dimensional phenomenon can be developed through numerical experimentation.

- Presently, coupling between axi-symmetric model for hot pool and one dimensional model for rest of the plant has only been achieved. Further development of a coupled code system involving multi-dimensional thermal mixing model for grid plate, axi-symmetric modeling for hot pool, three dimensional model for cold pool and one dimensional system dynamics model for rest of the plant can be undertaken.

ABSTRACT

KEYWORDS : Fast breeder reactor, plant dynamics, system dynamics, computational fluid dynamics, thermal stratification, flow halving time, event analysis

Sodium cooled Fast breeder reactors (SFR) constitute the second stage of Indian nuclear power program. SFR are poised to play a significant role in providing energy security to India. Future designs of SFR require focused enhancements in safety and economy to become a major contributor to the energy matrix. This requires advanced design and analysis tools with reduced uncertainties in the prediction to be utilized in the design.

Dynamic simulation is one of the important analysis domains which play a significant role right from conception to decommissioning of a nuclear power plant. This is important in the design of plant protection system, demonstration of plant safety, establishment of safe plant operation and training of operators. These simulations are carried out using system level thermal hydraulic computer codes (known as plant dynamic codes) which predict the neutronic/thermal hydraulic behaviours of entire plant. Plant dynamic codes have computational models to represent various phenomena involved in normal operation as well as transient conditions involving reactor physics, coolant flow and heat transport in various coupled loops and components of the plant. Traditionally, one dimensional transient codes are adopted for this purpose which enables faster computation of transient evolution of various critical parameters of the plant including reactor power, coolant flow rates, temperature, coolant levels, pump speeds etc. Significant uncertainties in the prediction by these codes have been observed during situations involving multi-dimensional thermal hydraulic features. One such phenomenon is the thermal stratification in large size sodium pools of fast reactors. Thus, there is a need for systematic investigations into (i) the sub-systems/components where multi-dimensional models are essential, (ii) the level of multi dimensional models, viz., 2-D/3-D, required, (iii) applicability of generalized sub domain models, (iv) the role of flow halving time of coolant pumps, (v) the parameters that are

affected by multi-dimensional physics and (vi) the extent to which these parameters are affected. This is the primary focus of this work.

For the present research work, a medium size pool type SFR of 500 MWe capacity has been considered. The sub-systems taken for the present investigation are grid plate, hot pool and cold pool. In the first part of the research work, the hydraulics within the grid plate where sodium from the primary sodium pumps enter before distributing to the various subassemblies of the core, is considered. For the 3-D analysis, a porous body approach has been adopted wherein the presence of ~1950 subassembly sleeves is represented by surface/volume porosities. Both the normal and accidental rupture of one pipe have been considered. It is established that a single point pressure approximation is adequate for representing the hydraulics within grid plate under normal and accident conditions of one pipe rupture.

Single and multi-dimensional thermal hydraulic characteristics of hot pool and cold pool under various transients have been predicted. It is seen that the single control volume based 1-D model is unable to represent the mixing and thermal stratification phenomenon in hot and cold pools. Further, it is seen that two dimensional model is a reasonable optimum (from computational cost and accuracy considerations) approach for representing the thermal stratification in hot pool. However, to account for stratification and mixing of sodium in cold pool under all types of plant transients, a three dimensional modelling is found to be essential.

Based on the above investigations, a coupled analysis tool by combining two dimensional CFD model for hot pool along with one dimensional model for rest of the plant has been developed. The two dimensional code solves the conservation equations of mass, momentum and energy employing the Finite Volume Method. The pressure-velocity coupling in the incompressible form of the governing equations is solved using the SIMPLE algorithm. Turbulence is modelled using the high Reynolds number k-epsilon model. Predictions of the code have been validated against standard benchmark solutions as well as through code-to-code comparison. Subsequently, two dimensional model of hot pool of the reactor developed using this code is coupled with one dimensional models of rest of the plant to form a hybrid code system. Typical plant transients have been analysed using this hybrid code and predictions are compared against the traditional fully one-dimensional approach. It is seen that consideration of thermal stratification not only affects the temperature evolution in the entire plant, predictions of transient thermal loading on the components and natural convection evolution in secondary sodium circuit are also significantly influenced. With incorporation of multi-dimensional modelling feature, the analysis capability of code is enhanced with respect to realistic prediction of above thermal hydraulic transient conditions in the plant.

The extent and duration of thermal stratification in the primary systems are functions of primary sodium flow rate which is dependent on flow halving time of sodium pump. Traditionally, on confirmation of reactor trip, the primary sodium flow is reduced to 20 % value to reduce thermal shock to reactor structures. This is referred as sympathetic safety action. The roles of coast down time of primary sodium pumps and speed reduction of sodium pumps following reactor trip have been investigated to determine (i) the minimum flow halving time to ensure core safety and (ii) the associated duration of short-term power fluctuation which can eliminate reactor trip. Though the sympathetic safety action causes stratification in hot pool following reactor trip, it reduces the thermal shock experienced by the hot pool components. Thus, the subtle benefits of appropriate choice of flow halving time and sympathetic safety action in the plant have been brought out based on investigations performed by incorporating multi-dimensional modelling for hot pool.

CHAPTER – 1

INTRODUCTION

1.1 FOREWORD

Dynamic simulation studies of a nuclear power plant are important throughout the entire lifetime of the plant starting from conceptual design phase to decommissioning. These studies are carried out using system level thermal hydraulic computer codes which predict the thermal hydraulic behaviour of entire plant. These codes are known as plant dynamic codes. Plant dynamic analysis plays an important role,

(i) in the assessment of operability and controllability of the plant

(ii) as a tool for design and testing of control systems

(iii) as a device for establishing various operating and testing procedures such as startup, shut-down, power changeover, etc.

(iv) in safety assessment and design of plant protection systems, residual heat removal systems etc.

(v) in environmental studies for prediction of emissions generated during plant upsets/failures and

(vi) in training of operators

Results of studies carried out using plant dynamics codes form an essential part in the licensing process of nuclear power plants in order to demonstrate that acceptance criteria which ensure safety of the plant are met. Dynamic simulation is also important in the computer based training of operators and it can be used for development of on-line operator decision support tool in which the dynamic simulation models run parallel to the actual plant. The simulators are designed to provide insight and understanding of the general design and operational characteristics of various reactor systems.

Plant dynamics codes have computational models representing various physical phenomena involved in the plant operation. Thus, the codes developed for nuclear power plants generally have neutronic modeling to simulate power generated in the reactor core, hydraulic models to simulate coolant flow in heat transport circuits, thermal models to represent heat exchange process involved in various systems and components, and torque balance to simulate the pumping systems. Depending on the nature of the coolant and the behavior of fuel and coolant during plant transients, compressible behavior as well as phase change phenomenon may also have to be modeled in these codes. Generally, these codes are of one dimensional in space coordinate due to the need for representing the behavior of entire plant. Therefore, systems and components in which multi-dimensional thermal hydraulic features are involved are approximated to be one dimensional in nature. It should be ensured that such approximations do not compromise the required level of accuracy of simulation with respect to the objectives. In order to overcome this difficulty, certain phenomenological models such as multi-zone modeling are sometimes incorporated in these codes.

Development and validation of plant dynamic codes is an important task to be carried out to guarantee that the predictions are physically realistic and the code is able to represent the specific plant design. Several physical phenomena can occur during the operation of a plant, especially during operational transients and accidents. The models developed and their validation should adequately cover all these phenomena. Computer codes developed for water reactor systems are not suitable for analyzing the dynamics of sodium cooled fast reactors (SFR). In order to evaluate the dynamic behaviour of SFRs, it is necessary to develop specialized codes. Many transient thermal-hydraulic analysis codes have been developed for SFRs worldwide.

Validation of computer codes form an important phase in the development process. The validation exercise is classified into several types. In order to validate the code against various types of phenomenon such as sub-cooled boiling, dryout etc., experimental data from separate effect tests are utilized. Due to the large size of the reactor and the plant, experiments for code validation are usually performed in test facilities of smaller scale or with only a few important components. For example, in order to study the main thermal hydraulic features of core, tests with only one fuel assembly may be performed for simplicity. Nevertheless, real time data from operating plants or from large scale experimental facilities are also adopted in the final validation exercise to investigate the integrated behaviour of the code.

1.2 SCOPE OF THE THESIS

The one dimensional modeling adopted in plant dynamics analyses of SFRs results in neglecting of some of the important multi-dimensional thermal hydraulic features which govern the plant behavior during transients. Due to the large size of coolant pools, multi-dimensional flow features are predominant in them. One such phenomenon is the occurrence of thermal stratification in coolant pools. Significant effects due to thermal stratification occur in the coolant pools where reactor core is located when the coolant emanating from the reactor core becomes colder than that prevailing in the pool. Under such conditions, the flow pattern within the pool gets altered due to the dominance of buoyancy force over inertial force. This condition arises in the reactor pool after reactor trip (SCRAM) when the power generation in the core is suddenly stopped. One dimensional codes represent coolant pools as single control volumes and hence the thermal hydraulic behavior of pools are modeled based on perfect mixing assumption. Therefore, one dimensional codes are not capable of simulating thermal stratification effects in the pools. However, such one dimensional modeling approach is adequate for pipe lines and heat exchangers.

Thermal stratification affects the evolution of coolant temperature in components located in the pools. Through these components, the effects of thermal stratification get propagated in the entire plant. Similar multi-dimensional effects such as redistribution of coolant flow and thermal mixing pattern are also possible in some of the plant components. Scope of the thesis involves identification of sub-systems in the plant that require multi-dimensional modeling for accurate simulation of transient behavior. Thermal stratification behavior of coolant pool at the exit of reactor core is proposed to be addressed through a multi-dimensional approach in the plant dynamics studies. Some of the codes adopt multi zone based phenomenological approach to represent the stratification effects. However, the phenomenological approach is very difficult to be generalized to make it applicable for all the transient conditions. Realistic representation of the thermal stratification phenomenon requires multi-dimensional modeling for the coolant pool. For this, a computational fluid dynamics (CFD) based multi-dimensional model for the coolant pool is developed. Subsequently, a hybrid simulation approach combining the multi-dimensional modeling for coolant pool and one dimensional modeling for the rest of the plant is developed. A comparative study on the predictions of plant behavior using the hybrid approach against those obtained from the fully one dimensional model is carried out to bring out the benefits of the hybrid approach in plant dynamic studies.

Some of the design studies necessarily require the consideration of the multi-dimensional features in arriving at the design parameters. For example, establishment of operational scheme to eliminate thermal stratification effects in coolant pool requires multi-dimensional modeling of pool. Thermal stratification depends on the coast down behavior of coolant pumps following reactor trip. The influences of (i) speed halving time of coolant pumps and (ii) the extent of core flow reduction employed after reactor trip are some of the important parameters affecting the thermal stratification in coolant pools. Appropriate selection of the above design parameters requires due consideration to core safety aspects also. Objectives of the thesis can be summarized as follows:

- identification of critical components of the FBR system that require multi-dimensional modeling
- development of 2-dimensional axi-symmetric model for hot pool and coupling the same with the 1-dimensional plant dynamic model for the rest of the FBR systems to formulate a hybrid code system
- comparison of the hybrid code predictions against that of 1-D plant dynamics code
- investigations into flow halving time and sympathetic safety action and their effects on plant behavior

Studies in this thesis are carried out with respect to a typical design of a pool type sodium cooled fast reactor based nuclear power plant [1] of 1250 MWt (500 MWe) power capacity. Details of the plant considered for the study are elaborated in the following sections.

1.3 DESCRIPTION OF SODIUM COOLED FAST REACTOR

Heat transport layout of the sodium cooled fast reactor (SFR) is shown in Fig. 1.1. There are three heat transport circuits in the plant, viz., primary sodium circuit, secondary sodium circuit and steam water circuit. Reactor core in which nuclear heat generation takes place is located in the primary sodium circuit. In the pool type SFR, the entire primary sodium circuit along with associated components is located inside a single cylindrical vessel called main vessel. The primary sodium circulating in the loop picks up the heat generated in the reactor core and transfers it to the secondary sodium circuit through shell and tube heat exchangers known as intermediate heat exchangers (IHX). Secondary sodium circuit transfers the heat to steam water system to produce steam in the steam generators (SG). The superheated steam produced in SG is used for driving the turbo generators operating based on Reheat and Regenerative Rankine cycle to produce electricity. Heat rejection from the plant to sea water takes place in condensers.

A nuclear power plant continues to produce thermal power in its reactor core even after shutdown due to radioactive decay of fission products known as residual heat or decay heat. In order to remove this heat, dedicated heat removal systems are provided in the reactor. These systems extract heat from the reactor pool and transfer it to an intermediate sodium circuit before ultimately transferring it to atmospheric air. There are primary sodium to intermediate sodium heat exchangers immersed in the sodium pool and intermediate sodium to air heat exchangers located at a higher elevation in the plant. Coolant flow in the intermediate sodium circuit takes place by natural convection. In order to promote natural convection flow of air through the intermediate sodium to air heat exchangers, stacks are provided above them.

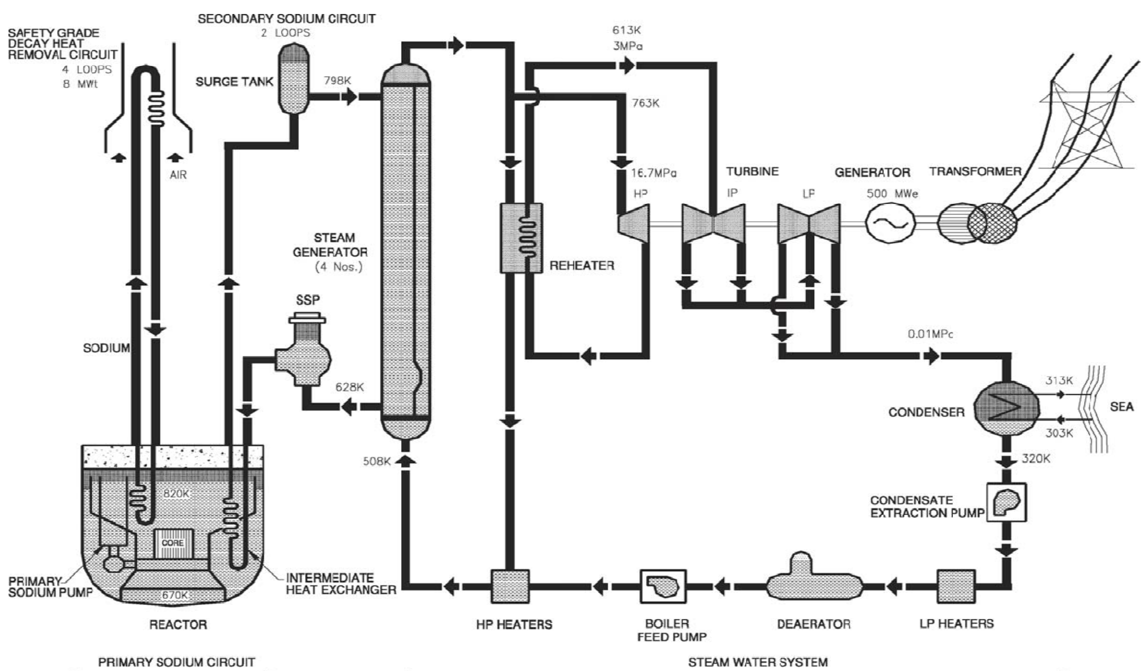

Fig. 1.1: Heat transport flow sheet of SFR

As already mentioned all the components of primary sodium circuit, viz., pumps and heat exchangers are contained in a pool of sodium within the main vessel. The assembly of all the components of primary sodium circuit, the reactor core and associated components is known as reactor assembly. Section view of reactor assembly is shown in Fig. 1.2. The sodium volume within the main vessel is divided into two parts by a structural member called inner vessel. The outer and inner pools formed by the inner vessel are known as cold pool and hot pool respectively. Primary sodium pumps take their suction from the cold pool and supply it to the inlet plenum to reactor core known as grid plate. The grid plate distributes sodium flow through various subassemblies of reactor core mounted on it. Sodium flowing through the core subassemblies picks up the heat produced by nuclear fission in the reactor core and comes out hot to enter the hot pool. From the hot pool, sodium flows through the IHX and transfer heat to secondary sodium circuit before reaching back to the cold pool.

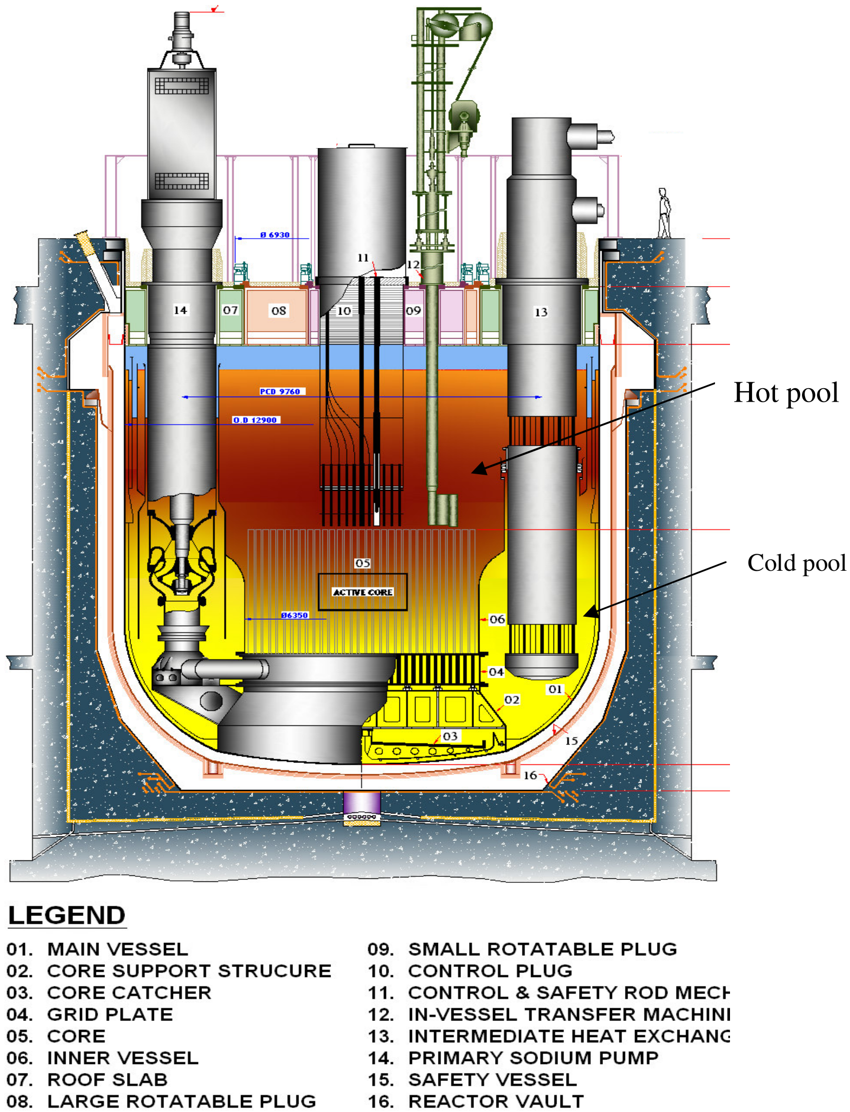

Fig. 1.2: Schematic of reactor assembly

Schematic of IHX is shown in Fig. 1.3. Primary sodium enters the IHX through an inlet window located in the hot pool and flows downwards in the shell side before exiting through an outlet window located in the cold pool. Secondary sodium enters the IHX through the top of reactor assembly and flows downwards through a central down comer to reach the inlet header. From the inlet header, secondary sodium flows upwards inside the tubes to reach an outlet header. There are 4 IHX, each containing 3600 tubes. Sodium flow in the primary sodium circuit is maintained by two primary sodium pumps operating in parallel.

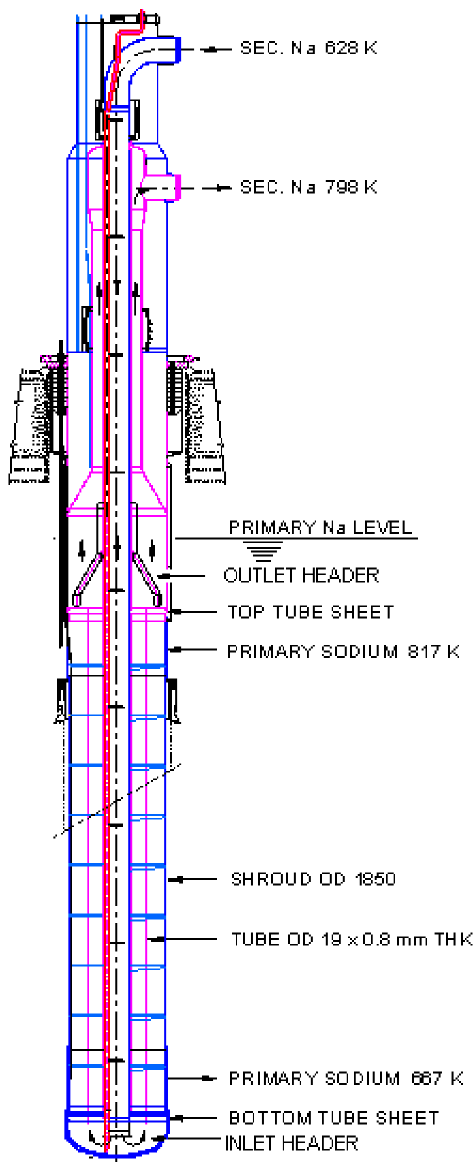

Fig. 1.3: Schematic of intermediate heat exchangers

The steam generators (SG) in the secondary sodium circuit are also shell and tube heat exchangers (Fig. 1.4) wherein, sodium flows in the shell side and water/steam flows in the tube side. There are four SG, each having 547 tubes in each secondary sodium circuit. There are two secondary sodium circuits in the reactor. Mechanical centrifugal pumps known as secondary sodium pumps are used for pumping of secondary sodium in the circuit. Surge tanks provided in the circuit to surge out the dynamic pressure generated in the circuit in the unlikely event of a sodium- water reaction in the SG.

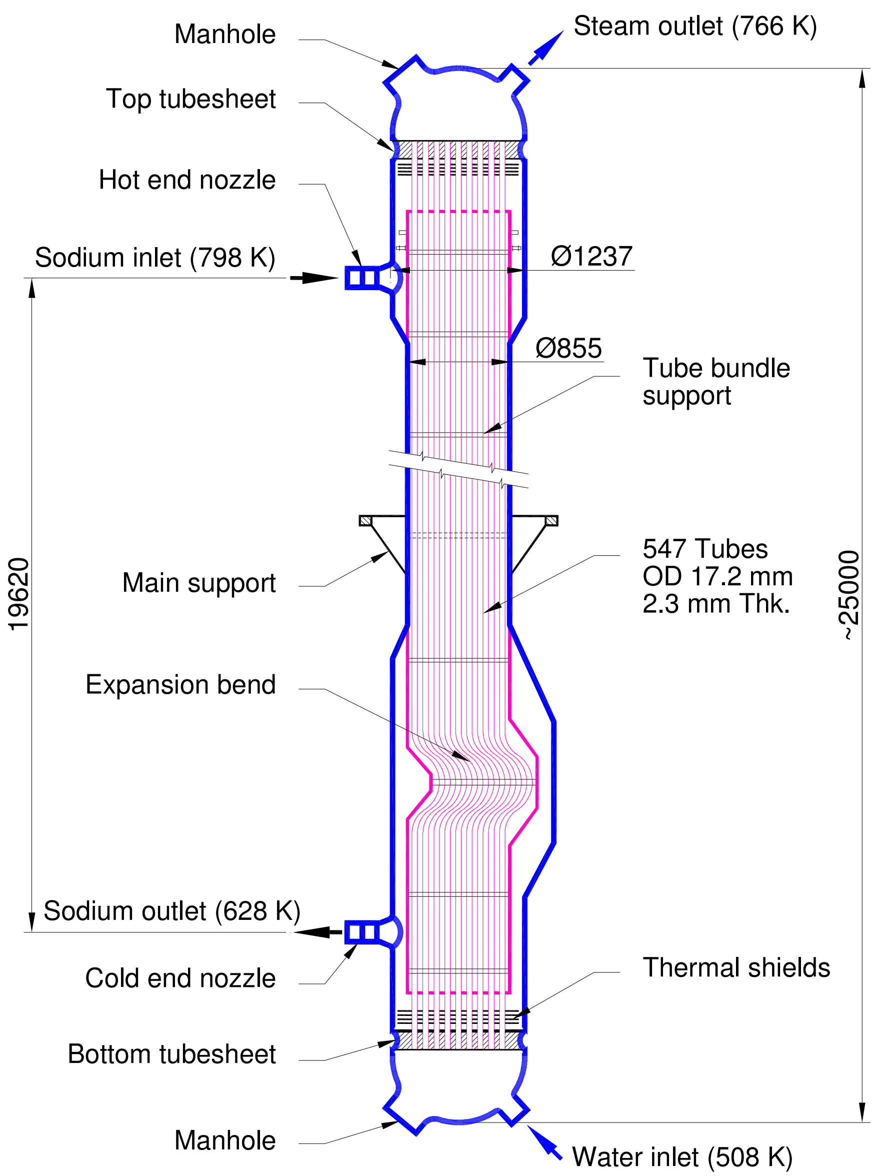

Fig. 1.4: Schematic of SG

The reactor core comprises of various types of subassemblies such as fuel (where the actual nuclear heat is generated), breeder (where conversion of fertile nuclear material into fissile, takes place), shielding (serving as a radiological shield for the surrounding structures) and reflector (preventing escape of neutrons from core), as shown in Fig. 1.5. Fuel subassemblies are the important elements in a nuclear reactor where the majority of the fissile heat is generated. Schematic of a fuel subassembly in the reactor is shown in Fig. 1.6 wherein the fuel pins are arranged in a triangular pitch. A bundle of 217 pins form a hexagonal layout and the bundle of 6.6 mm diameter pins is housed inside a hexagonal structural member known as wrapper with a geometrical dimension of 132 mm as the 'width across the flats'. The wrapper also acts as the conduit for coolant flow through the fuel subassembly. A thin spacer wire of 1.65 mm diameter is wound helically over each of the fuel rods to separate them from one another and create paths for the coolant flow surrounding them.

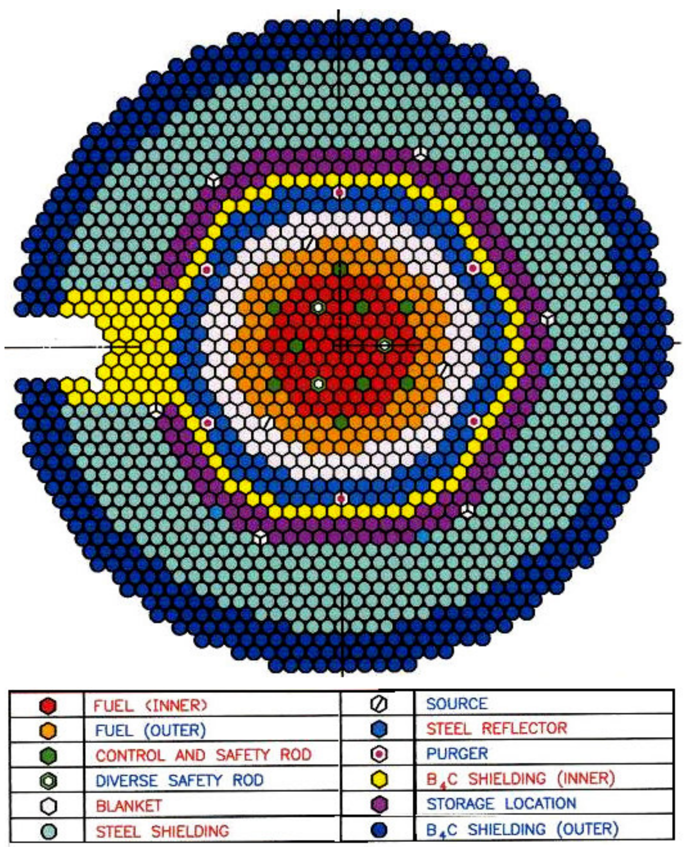

Fig. 1.5: Core plan

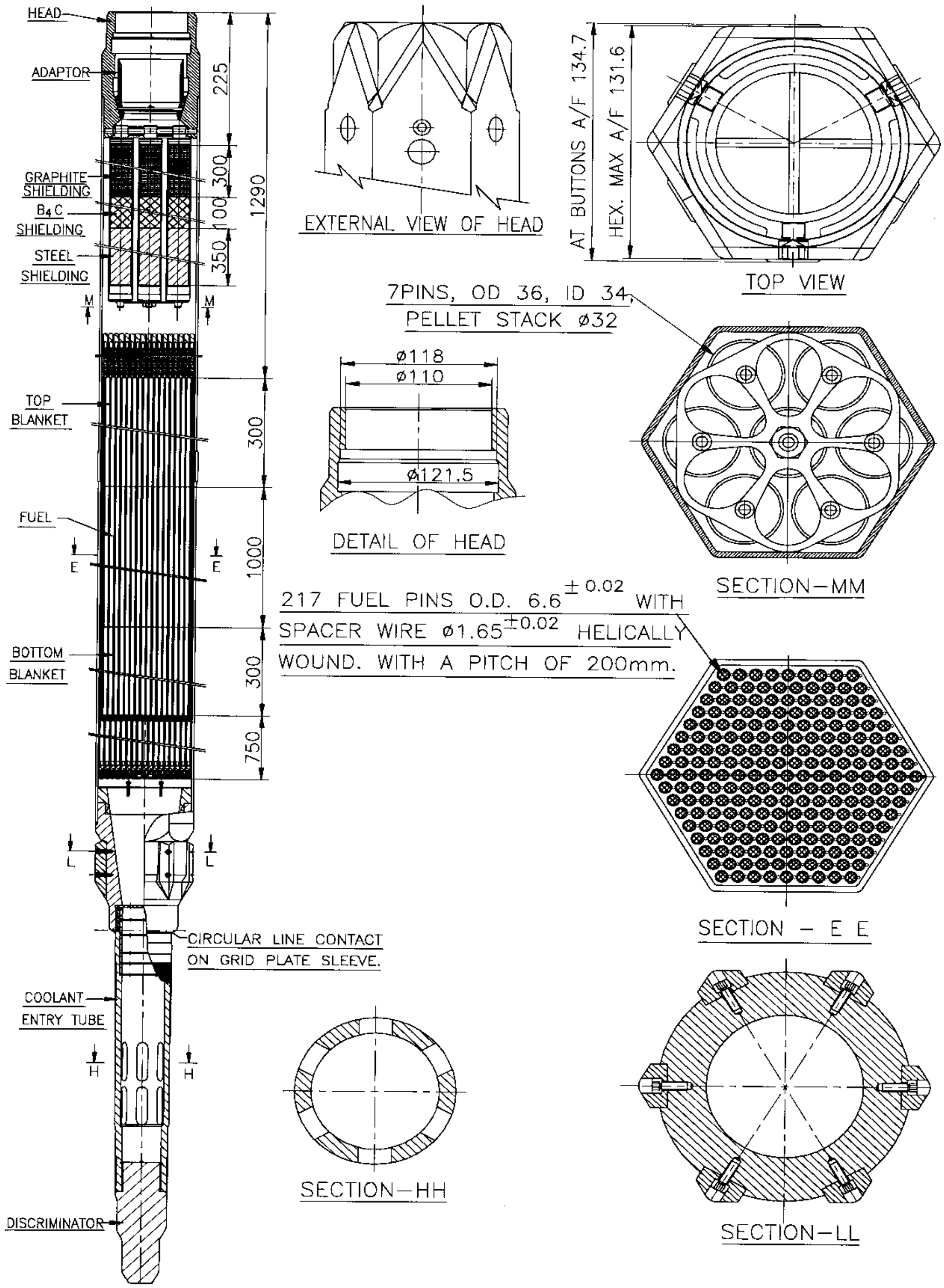

Fig. 1.6: Schematic of fuel subassembly

Each fuel pin is ~ 2.5 m long with many subsections, viz., bottom fission gas plenum, bottom axial blanket, active fuel, top axial blanket and top fission gas plenum. The actual fission heat generation takes place in the active fuel region. The length of active fuel region is

1 m. Apart from the pin bundle, the fuel subassmebly has other sections, viz., foot, orifice block, axial shielding bundle and head. It is through the foot that coolant enters fuel subassembly. Orifice block is a passive device that admits coolant flow proportional to the heat generation rate in the fuel subassembly. Axial shielding bundle provides neutronic shielding for the above core structures and head is the part through which the coolant flow comes out of fuel subassembly. The head has arrangements for handling fuel subassembly from the top using special mechanisms. The shielding bundle and head of the assembly also act as devices for thermal mixing of the coolant before it comes out of the fuel subassembly.

The turbine in the steam water system is tandem compound design with separate HP, IP and LP cylinders. The steam cycle employs regenerative feed water heating based on steam bled from the turbine. A steam separator is provided at the common outlet of 8 steam generator units to take care of two phase flow during startup and shutdown of the plant. The important plant parameters are outlined below [1]:

Reactor thermal power	-	1250 MWt
Electrical output	-	500 MWe
Reactor coolant inlet temperature	-	397 ^{0}C
Reactor coolant outlet temperature	-	547 ^{0}C
Feedwater inlet temperature to SG	-	235 ^{0}C
Steam temperature at turbine inlet	-	490 ^{0}C
Steam pressure at HP turbine inlet	-	16.7 MPa
Primary sodium flow rate	-	8.26 m^3/s
Secondary sodium flow rate per loop	-	3.34 m^3/s
Feedwater flow rate per SG module	-	70.3 kg/s
Number of primary sodium pumps	-	2
Number of secondary sodium loops	-	2

Number of IHX per secondary loop	-	2
Number of SG modules per loop	-	4

1.4 ORGANIZATION OF THE THESIS

Chapter 1 deals with general features of pool type sodium cooled reactors, coupling of multiple heat transport loops, need for large pool of primary sodium, heat exchange among the pools, thermal stratification potential in the pools, multi dimensional modeling needs for the pools, current practice in plant dynamics simulations, including scope and motivation for the thesis work. Chapter 2 presents the literature review carried out towards synthesizing the capabilities of various plant dynamics codes developed world wide, strengths & weaknesses of these codes, considerations for thermal stratification in SFR design and capability of plant dynamics codes in addressing thermal stratification issues. Further developments required in the modeling approach adopted in plant dynamics codes towards improving their predictions are also discussed in the second chapter. Chapter 3 deals with numerical studies carried out towards identification of domains in an SFR plant that require multi-dimensional modeling through inter-model comparison studies. Chapter 4 provides the details of the development and validation of a CFD based two-dimensional axi-symmetric code for turbulent flow simulations using finite volume based approach. Coupling of this code with plant dynamics code is also discussed. Chapter 5 deals with analysis of typical plant transients using the coupled code system having multi-dimensional modeling of thermal stratification phenomenon and comparison of the results against those predicted using traditional fully one dimensional analysis approach. The role of flow halving time and sympathetic safety action on thermal stratification and safety of an SFR are discussed in Chapter 6. Important conclusions and scope for future work are assimilated in Chapter 7 of the thesis.

CHAPTER 2

LITERATURE SURVEY

2.1 INTRODCUTION

Traditionally, system level thermal hydraulic computer codes are used for predicting the combined thermal hydraulic behaviour of entire plant. Development of appropriate mathematical models and their validation is an important phase in the development of these codes to ensure that the predictions are physically realistic and the code is able to represent the plant behaviour accurately. In order to evaluate the dynamic behaviour of SFRs, it is necessary to develop specialized transient thermal hydraulic analysis codes. Many transient thermal-hydraulic analysis codes have been developed in different countries for their fast reactor systems. The following sections give details of important plant dynamics codes developed for fast reactor systems.

2.2 PLANT DYNAMICS CODES DEVELOPED FOR SFR SYSTEMS

2.2.1 DEMO

DEMO [2] is a transient analysis code developed for Clinch River Breeder Reactor Project (CRBRP) plant in US. A detailed description of the modeling adopted in this code is discussed in this section due to the fact that most of the plant dynamics codes developed for fast reactors are based on this approach. This code has thermal hydraulic models for primary, secondary and steam generator systems. Point kinetics model with prompt jump approximation is adopted for neutronic modeling in this code. As far as thermal modeling of core is concerned, average channel of the core alone is modeled which contains five axial and five radial nodes. Radial nodes represent two sub-volumes for fuel, one volume for clad, one volume for coolant and another volume for the wrapper. Coolant nodes are staggered with respect to the structural nodes of components (fuel, clad and wrapper). However, for the blanket zone, one node each to represent the structure and coolant is adopted. The governing equations are solved by explicit finite difference method. Initial version of the code considered complete power generation in fuel region while in the later versions, power generated in fuel, structural and coolant nodes have been resolved separately.

Possible stratification effects in the upper plenum during transients are simulated using a phenomenological model. However, the same approach is not adopted for the inlet plenum. Perfect mixing of coolant is approximated for the inlet plenum. Another important approximation adopted in this code is that distribution of coolant flow among various regions of core, viz., fuel, blanket and bypass is assumed to be unchanged under all conditions through the core. Coolant flow is assumed to be single phase and incompressible that can undergo thermal expansion to account for buoyancy effects. For computational simplicity, three primary coolant loops are modeled as two in which the first one represents single loop and the second one represents double loop. Homologous pump characteristics is employed for modeling of sodium pumps and torque balance based on Newton's law is used for torque balancing of the pump. Performance of the pump under cavitation conditions is also modeled in this code.

Intermediate heat exchangers (IHX) are modeled based on lumped volume approach with multiple axial nodes. The radial nodalization involves one node each for primary coolant, secondary coolant, tube wall and shell wall. Check valves are modeled as prescribed pressure drops. Filling of the guard vessel as a result of the rupture in pipe lines having double envelope is also modeled. The later version of the code includes a steady state calculation module which solves the governing equation by making the time derivative term to zero. The prediction of the transient behavior in the plant during a station blackout event is reported by Gregory [3].

2.2.2 IANUS

IANUS [4] is the transient analysis code developed for Fast Flux Test Facility (FFTF) plant in US. In this code also the coolant flow is considered to be one dimensional, single phase and incompressible. Mathematical models adopted in this code are similar to those used in the DEMO code.

2.2.3 SSC-L

The Super System Code for loop type (SSC-L) [5] reactors was developed by Brookhaven National-Laboratory (BNL) in US. This code has the capability to perform thermal hydraulic analysis of operational as well as natural circulation transients in nuclear power plants. It has models for in-vessel components, heat transport loops, plant protection systems and plant control systems based on best estimate approach. It has been coupled with MINET code models of steam water system to analyze transients in the balance of plant along with that in the nuclear steam supply system. Main feature of SSC-L code with respect to DEMO code is the incorporation of model for predicting transient flow redistribution in the core. Inter-subassembly and intra-subassembly heat transfers are not modeled in this code. The characteristic integration time steps for various processes/components can vary over a wide range. To improve computing efficiency, a multiple time step scheme approach has been used in this code [6]. In conjunction with partitioning of various analysis models, five resultant time steps are worked out based on a time step hierarchy. This code has been validated through inter-code comparison and simulation of experimental studies carried out in FFTF reactor [7].

2.2.4 SSC-K

The super system code of KAERI (SSC-K) [8] has been developed at the Korea Atomic Energy Research Institute (KAERI) based on SSC-L code for loop type reactors. In order to account for the specific thermal hydraulic features of pool type reactors especially the hot pool, several modifications have been incorporated to make it applicable for safety analysis of KALIMER (Korea Advanced Liquid Metal Reactor). Significant improvements in (i) pool and core thermo-hydraulic model, (ii) reactivity model and (iii) passive decay heat removal system model have been made. As already mentioned, thermal stratification can occur in the hot pool during reactor SCRAM due to cold sodium emanating from core. Therefore, in SSC-K code, a two-dimensional model for hot pool is developed in place of one-dimensional model to predict temperature and velocity distributions of sodium in hot pool accurately.

In the one dimensional multi-zone representation of hot pool, a two-zone model is incorporated in the SSC-K code. In this model, the hot pool volume is divided into two perfect mixing zones. The interface between these zones is determined by the maximum penetration distance of the core flow which is determined based on empirical function of Froude number of the average core flow. In the two dimensional representation of hot pool, the governing equations for conservation of mass, momentum, energy, turbulent kinetic energy and rate of dissipation of turbulent kinetic energy (for k -ε turbulence model) are solved in a generalized coordinate system. The solution domain is divided into a finite number of quadrilateral control volumes as shown in Fig. 2.1 and discretization of the governing equation is performed following the finite volume approach. The convection terms are approximated by a higher-order bounded scheme HLPA developed by Zhu [9] and the unsteady terms are treated by the backward differencing scheme. The SIMPLEC algorithm by Van Doormal and Raithby [10] is used for pressure-velocity coupling. In this algorithm, the momentum equations are implicitly solved at cell-centered locations. Then the cell-face velocities are evaluated. More investigations through both analytical and experimental efforts are being carried out for verification and validation of the hot pool model in the SSC-K computer code.

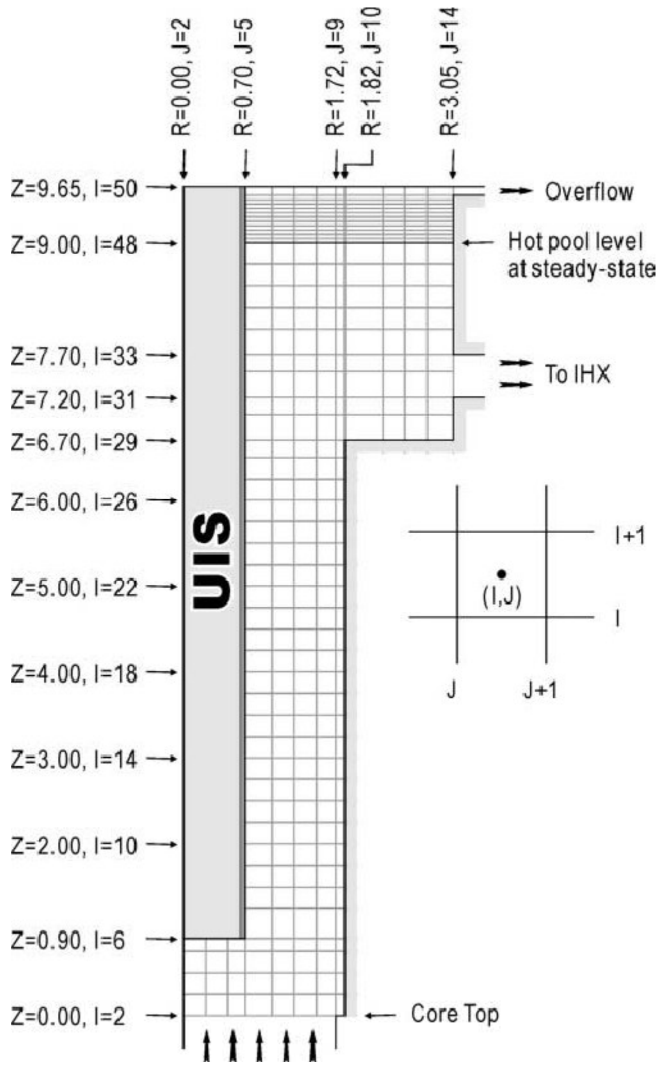

Fig. 2.1: Computational meshes considered for modeling hot pool in SSC-K code [8]

2.2.5 MINET

MINET code [11] is developed based on momentum integral method in US in which the pressure in the coolant circuit is calculated dynamically only in a few key locations. The pressure evaluation is based on integral momentum balance equation. The initial momentum integral model for steam generator did not have a reverse flow modelling capability. By employing matrix techniques, a generalized momentum integral network model was developed for use in the current version of the SSC code. The formulation has been validated against data from once-through and U-tube steam generators and the EBR-II facility. In addition, several qualitative and quantitative comparisons against other code calculations have also been performed.

Many computer codes currently used for simulating the thermal-hydraulics of nuclear reactor systems are based on the local pressure formulation. In this approach, a staggered mesh nodalization is adopted with pressure as cell average parameter calculated through conservation of mass and momentum equations. Cell junction flows are evaluated. When two phase flow formulations are also included, the actual number of equations per cell becomes much large in number. Since the time constants for pressure wave propagation generally fall in the millisecond range, all thermal-hydraulic systems analysis codes adopt implicit or semi-implicit time stepping scheme. In momentum integral method, since the number of pressure values solved is less, the computational effort involved is also less.

2.2.6 CATHARE 2

CATHARE 2 [12] is evolving as a multi-purpose multi-reactor system code in France. The CATHARE 2 code was originally devoted to best estimate calculations of thermal hydraulic transients in water-cooled reactors such as pressurized water reactor (PWR), water-water energetic reactor (VVER) or boiling water reactor (BWR). New developments are under way to extend the code to sodium cooled fast reactors [13]. CATHARE 2 can now describe several circuits with various fluids either in single-phase gas or liquid, or in two-fluid conditions possibly with non-condensable gases, which allows simulating any kind of reactor concept and any kind of transient.

CATHARE 2 has a flexible modular structure for the thermal hydraulic modeling. It can be applied for simulating thermal hydraulic transients in all types of facilities varying from simple experimental loops to large installations like nuclear power plants. The main hydraulic components of the code include pipes (one dimensional), volumes (zero dimensional) and three dimensional vessels. Components are connected to each other through junctions. Other modeling features of the code include pumps, turbo-machines, control valves, T-junctions, sinks, sources, breaks, etc. Various modules are formulated with six-equation based two-fluid model (mass, energy and momentum equations for each phase), with additional equations for non-condensable gases. Discretization of terms of equation is fully implicit in one dimensional and zero dimensional modules and semi implicit in three dimensional elements. The resulting nonlinear equations are solved by iterative newton solver.

The neutronics module of CATHARE-2 has been validated by comparison with the OASIS code [14] which was previously used by CEA. Transient calculations have been made for the small and modular fast reactor (SMFR) pool-loop type reactor, a small innovative SFR studied by ANL and JNC. A large program of validation is currently underway using available experimental data measured in the SFRs such as SPX, MONJU and PHENIX.

2.2.7 NETFLOW ++

NETFLOW++ [15] is an integrated network code developed in Japan to simulate the nuclear steam supply system (NSSS) and the balance of the plant. It has the capability to simulate not only light water reactors but also liquid metal cooled reactors. The code has been validated using transient data from various facilities, viz., the experimental sodium facility PLANDTL, experimental fast reactor ‘JOYO’ and the prototype fast reactor ‘MONJU’. As far as liquid metal cooled reactors are concerned, the simulation of thermal hydraulics of nuclear steam supply system is possible with this code along with models for the turbine and the feed-water systems comprising of deaerator, feedwater heaters, flow control valves and steam extraction lines from the turbine incorporated using network models. Detailed comparison studies demonstrate that predictions of SSC-L and NETFLOW++ match very closely for natural circulation in loop-type sodium cooled fast reactors.

2.2.8 GRIF

GRIF [16] is a Russian computational tool for single-phase thermal hydraulics analysis of transients in the plant as a whole as well as detailed analysis of specific systems and components. This code can be regarded as a system dynamics code with capabilities for simulation of velocity and temperature distributions in large coolant volumes. Models for secondary and auxiliary circuits are also included in the code. Prediction of three dimensional velocity, pressure and temperature distributions of sodium in the primary circuit as well as inter-wrapper space is possible with this code. Other important modules of the code include models for pump, IHX, core and reactor kinetics. Three dimensional form of mass, momentum and energy conservation equations for viscous incompressible liquid flowing in the porous body are solved for the simulation of thermal hydraulic phenomena in the inter-wrapper space. Buoyancy effects are taken into account in the model using Boussinesq approximation.

2.2.9 THACOS

The transient thermal-hydraulic code THACOS [17] is under development for analysis of China Demonstration Fast Reactor. This is an one dimensional code for simulation of reactor transients. Point reactor kinetics equations with six-group delayed neutrons have been applied to calculate the core power considering reactivity feedbacks caused by the Doppler effect, coolant density, axial expansion of fuel rods and radial expansion of the core. Thermal modelling of the core is through a multiple-channel based approach. Compressible homogenous flow model is used for the two-phase flow of sodium. The code has been validated against benchmark results reported in IAEA report [18]. Recently, multi-bubble model similar to that adopted in SAS4A code has been incorporated in the code to simulate sodium boiling scenario in the reactor core [19] with enhanced accuracy.

2.2.10 DYANA-P

DYANA-P [20] is a system dynamics code developed by Indira Gandhi Centre for Atomic Research (IGCAR), India for performing plant dynamics studies for fast reactor systems. DYANA-P has models for reactor core, primary sodium circuit, secondary sodium circuit, sodium pumps, heat exchangers and sodium pools. Steam water system is not modelled in the code. However, steam generator is modelled with appropriate boundary conditions for the water side. Mathematical models in the DYANA-P code are based on those used for most of the fast reactors. Thermal models are based on heat balance between various sections exchanging heat such as fuel and sodium through the clad in subassembly, primary sodium and secondary sodium through the tube wall in IHX, sodium and ambient air through the pipe wall and insulation in sodium piping, secondary sodium and water through the tube wall in steam generators etc. Hydraulic model is based on integral momentum balance between various flow segments in the primary and secondary sodium circuits.

Torque balance is adopted for the modelling of pump with the characteristics derived from generalized homologous characteristics. Cavitation performance of pump is modelled through simulation of NPSH condition in the pump as well as in the circuit. Fluid levels in the tanks are modelled through dynamic mass balance. Neutronic model for the core is based on point kinetics approximation, with prompt jump approximation for transient solution. Detailed models are also incorporated for the calculation of various reactivity feedback effects due to radial expansion of grid plate where subassembly are supported, control rod expansion, volumetric expansion of sodium inside the fuel and blanket portion of core, axial clad steel expansion, axial fuel expansion, Doppler effect due to changes in fuel temperature, etc. Thermal modelling of core is through multiple parallel channels with a capability to simulate flow reversal as well as flow redistribution amongst the channels. Liquid sodium flow is assumed to be one dimensional and incompressible. The assumption of Perfecting mixing is invoked to model mixing of coolant in the sodium pools and thermal stratification effects are not simulated.

Initial steady state conditions are calculated in the code through the solution of steady state balance equations. For the transient solution, numerical integration of hydraulic models is obtained by utilizing a standard ordinary differential equation solver based on the Hamming's Predictor-Corrector method. Semi-implicit formulation has been adopted for the integration of thermal balance equations. A similar methodology is adopted in the formulation of computer codes such as DYNAM [21] and SIFDYN developed for performing the dynamic calculations in Fast Breeder Test Reactor (FBTR), which have been validated through various tests carried out in FBTR.

2.2.11 SASSYS & SAS4A

The SAS4A and SASSYS computer codes are developed at Argonne National Laboratory in US for transient analysis of liquid metal cooled reactors. SASSYS-1 [22] is applicable for both loop type and pool type reactor concepts. Cavitation modeling pump is added to the code which computes net positive suction head required by the pump as a function of flow and pump speed. The required net positive suction head is compared against that available in the circuit to determine the onset of pump cavitation. After the onset of cavitation the pump head drops rapidly until the applied net positive suction head exceeds the required net positive suction head and cavitation ceases.The SASSYS code, has evolved into a tool to analyse response of the plant during anticipated transients without SCRAM (ATWS). To enable this facility, the SASSYS code contains fuel element heat transfer and single and two-phase coolant hydraulics models as in SAS4A.

The SAS4A [23] code is designed to analyse severe loss-of-coolant flow and overpower accidents involving coolant boiling, cladding failures, and fuel melting and relocation. SAS4A contains detailed, mechanistic models of transient thermal, hydraulic, neutronic, and mechanical phenomena to describe the response of the reactor core, coolant, fuel elements, and structural members under accident conditions. This code has been applied to analyse of the consequences of cladding rupture failures in high-burnup metal fuel elements in EBR-II reactor. Apart from these models, SAS4A code has models for predicting fuel failure and disruption in binary (U-Zr) and ternary (U-Pu-Zr) metal fuel alloys.

2.2.12 TRACE

In the FAST code framework developed by Paul Scherrer Institute, Germany, the thermal-hydraulics code TRACE [24, 25] was extended for simulation of sodium two-phase flow. The non-homogeneous, non-equilibrium two-fluid model, which is available in the TRACE for steam-water system simulation is extended to sodium two-phase flow simulation. Results obtained from the extended code have been validated against out-of-pile sodium boiling tests, conducted on a 37-pin bundle under simulated loss-of-flow-accident conditions. Comparison of predicted results using one-dimensional models showed the importance of including 2D effects in the two phase flow of sodium. With the two dimensional model incorporated, the predictions using the new version of TRACE (with capability for predicting radial and axial expansion of the boiling region, dryout on fuel cladding surfaces, wall temperature and flow reversal) demonstrated the applicability of the equations of state and constitutive relations incorporated in the two-fluid model. Comparison of TRACE prediction of inlet and outlet coolant flow rates in the boiling experiment [26] has demonstrated the ability of the extended TRACE code to predict, boiling inception, void fraction, radial and axial expansion of the boiling region, pressure evolution, coolant and clad temperature, etc.

2.2.13 SIMMER

The development of a next-generation code, SIMMER-III [27, 28], was initiated in the late 1980s at the Japan Nuclear Cycle Development Institute (JNC), initially in collaboration with Los Alamos National Laboratory (LANL).The entire code consists of three modules, viz., the fluid-dynamics module, the structure (fuel-pin) module, and the neutronics module. The fluid-dynamics module is interfaced with the structure module through heat and mass transfer at structure surfaces. The neutronics provides nuclear heat sources based on the time-dependent neutron flux distribution consistent with the mass and energy distributions. Since the three-dimensional representation of the core enables realistic distribution of the materials constituting the core, including control rods, SIMMER-IV has been developed as a direct extension of SIMMER-III to three dimensions retaining the physical modules of SIMMER-III. Recently, the parallelization of SIMMER-IV has been achieved, allowing application to reactor calculations within available computational resources. A three-dimensional simulation using SIMMER-IV has drawn more realistic accident scenario including the transition phase.

2.3 SUMMARY OF CAPABILITIES OF VARIOUS CODES

Summary of capabilities of various codes is given in Table 2.1. Based on the capability and application of various codes they can be broadly classified into three types, viz., (i) codes for analysis of transients in the plant without coolant boiling in the core, (ii) codes for analysis of transients along with coolant boiling situations in the core and (iii) codes for analysis of severe accident conditions in the core. The first category of codes have models for reactor core kinetics along with thermal hydraulic modeling of nuclear steam supply system (NSSS). The second category of codes have modeling of sodium boiling inside the core as an added feature. The third category of codes have special models for simulating core failure which includes thermal hydraulic, material movement and neutronic models under severe accident conditions. The first category of codes are matured enough and further improvements in them are being taken up to include multi-dimensional models for large sodium volumes to represent special phenomenon such as thermal stratification in sodium pools. The second category of codes are being improved with respect to multidimensional modeling for sodium boiling inside the core. Further, development in the third category of codes is focused on inclusion of whole plant simulation models along with detailed simulation of accident progression inside the core.

Table 2.1: Summary of capabilities of various thermal hydraulic codes

Code	Main features	Weakness	Application
DEMO	• Heat generation in fuel and other parts of core modeled separately • Stratification through phenomenological model • Modeling of pump operation under cavitation • Simplified models for steam water system	• No modeling for coolant boiling • Phenomenological modeling for multidimensional flow features	Transients in CRBRP
IANUS	• Similar to DEMO	• No modeling for coolant boiling	Transients in FFTF
SSC-L	• BoP modeling through MINET code • Modeling of transient flow redistribution in core • Multiple time step scheme approach	• Inter-subassembly and intra-subassembly heat transfer not modeled • No modeling for coolant boiling	Transients in loop type
SSC-K	• Two dimensional modeling for hot pool	• No modeling for coolant boiling	Transients in KALIMER
MINET	• Code developed based momentum integral method • Simplified modeling for two phase flow situations	• Approximations in the simulation of pressure transient in compressible flow	Linked with SSC-L for simulation of steam water system
CATHARE-2	• 6 Equations for two fluid model • Possible to link 3D models along with system models	--	Transients in ASTRID reactor
NETFLOW++	• Integrated network code for NSSS and steam water system	• Approximate simulation of stratification in pools	Transients in MONJU
GRIF	• Modeling of multi-dimensional flow features along with inter-wrapper flow	---	Transients in Russian SFRs
THACOS	• Multi bubble based model for two phase	Multi zone approach for sodium pools	Transients in Chinese reactor

Table 2.1: Summary of capabilities of various thermal hydraulic codes (Contd…)

Code	Main features	Weakness	Application
DYANA-P	• Modeling of NSSS including steam generator • Modeling of pump operation under cavitation	• Stratification in pools not modeled • No modeling for coolant boiling • Steam water system models are absent	Transients in PFBR
SASSYS	• Coolant boiling models are present • Steam water system models are present	• Multidimensional flow features not considered • Absence of spatial neutron kinetics model	Transients in EBR-II reactor
SAS4A	• Coolant boiling and fuel failure models are incorporated	• Multidimensional flow features not considered • Absence of spatial neutron kinetics model	Severe accident situations in EBR-II reactor
TRACE	• Non homogeneous 2 fluid model for boiling simulation • 2D effects in 2 phase sodium flow simulated • Spatial neutron kinetics	• Modeling of primary circuit alone	Severe accident situations in SFR
SIMMER	• Three-dimensional multi-velocity-field, multiphase, multi-component, Eulerian fluid-dynamics code • Fuel-pin failure model • Space and energy-dependent neutron kinetics model	• Modeling for core alone	Severe accident situations in SFR

2.4 INTER COMPARISON OF PLANT DYNAMICS CODES

It may be highlighted that the pool type sodium cooled fast reactor PHENIX [29] which was in operation in France was shutdown permanently in the year 2009. The French nuclear design group carried out several tests in the reactor before its permanent shutdown to generate valuable data and knowledge base on various aspects of reactor design and operation. As a part of this activity, natural convection tests in the primary circuit of the reactor were carried out. The data generated during this exercise was made available to all the researchers to test the capability of plant dynamics codes through an IAEA sponsored collaborative research project [30]. Several countries including India participated in this exercise. The international benchmark on the natural convection test was organized with "blind" calculations in a first step, then "post-test" calculations and sensitivity studies compared with reactor measurements. Eight organizations from seven Member States took part in the benchmark: ANL (USA), CEA (France), IGCAR (India), IPPE (Russian Federation), IRSN (France), KAERI (Korea), PSI (Switzerland) and University of Fukui (Japan). Each organization performed computations and contributed to the analysis and global recommendations.

PHENIX is a pool type reactor composed of a main primary reactor vessel, three sodium secondary circuits, three tertiary water/steam circuits and one turbine. Nominal full power of the reactor is 560 MWt /250 MWe. However, during the natural convection tests, one secondary circuit was out of operation and the reactor was operating at a reduced power of 120 MWt. Schematic of reactor assembly is shown in Fig. 2.2. The standard instrumentation available in the reactor and a special instrumentation for the final tests were used simultaneously. The following are the important measurements made in the plant during the tests.

- Primary and secondary pumps' speed, which can be used to estimate the flow rate, via., the pumps characteristics, when the pumps are operating.
- Secondary mass flow rate on each secondary loop.
- Sodium inlet temperature to each primary pump.
- Fuel subassembly sodium outlet temperature measured a few centimetres above each fuel subassembly.
- Intermediate heat exchanger inlet and outlet sodium temperatures on both the primary and secondary sides.

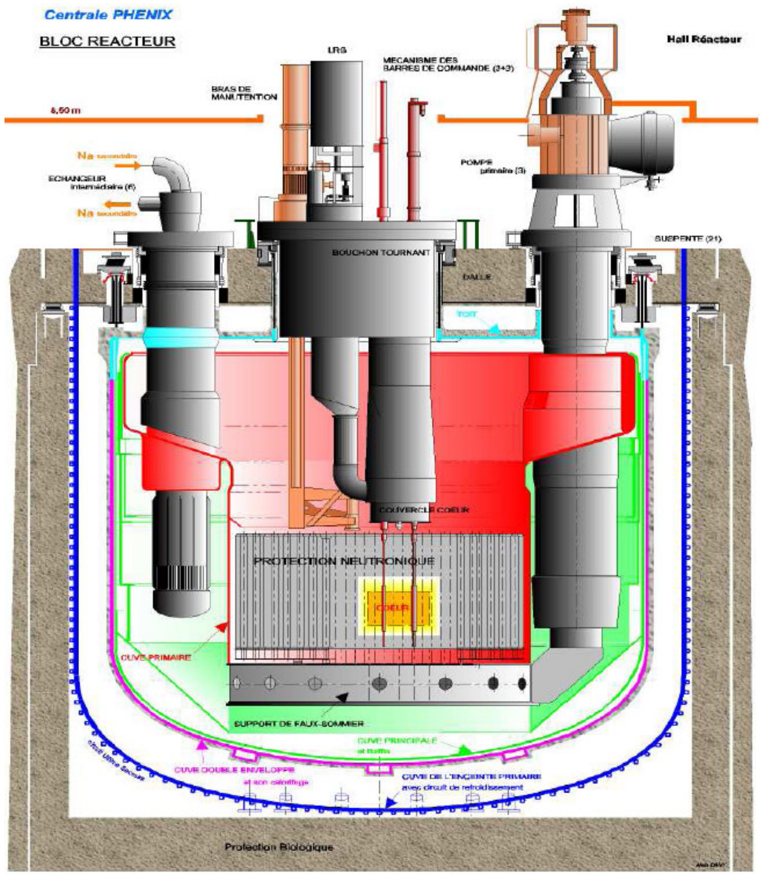

Fig. 2.2: Schematic of reactor assembly of PHENIX reactor [29]

The natural convection test in the primary circuit is divided into two phases, viz., (i) with no significant heat sink in the secondary circuits, except the heat losses along the piping and through the casing of the steam generator and (ii) with significant heat sink in the secondary circuits, by opening the casing of SG at the bottom and at the top which promotes large scale air draft in the SG casing. The main objective of the computational studies is to qualify the prediction capability of the onset of sodium natural circulation in the primary circuit. The codes used by the benchmark participants are listed below:

- ANL with SAS4A/SASSYS-1 : 1D-code
- CEA with CATHARE_2 : 1D-code
- IGCAR with DYANA-P : 1D code
- IPPE with GRIF : 3D-code

- IRSN with CATHARE_2 : 1D-code
- KAERI with MARS-LMR : 1D-code
- PSI with TRACE : 1D-code
- Univ. of Fukui with NETFLOW++ : 1D-code

Natural convection flow evolution in the core predicted by various participants is shown in Fig. 2.3. Large deviations can be observed between the predictions made by different participants. Unfortunately, there is no measurement of natural convection flow rate in the reactor for comparison against the computational predictions. The predicted values of primary coolant temperature at the inlet and outlet of heat exchanger in the primary sodium circuit are shown in Figs. 2.4 and 2.5 respectively. The inlet temperature is not well predicted by the computational codes. This is judged to be due to the strong influence of thermal stratification effects in the hot pool which is not predicted by the system codes accurately. The other plant parameters predicted by the various codes match reasonably well with experimental data.

Discrepancies were observed in the code-to-code comparisons of the core flow rate predictions in the natural convection regime, but there was overall coherence between computed and measured temperature evolutions. Limitations were observed in the capability of 1D system codes to deal with buoyancy effects such as thermal stratification in pools. Use of 3D codes or coupling 1D system with 3D codes is required for a better estimation of such complicated flow conditions.

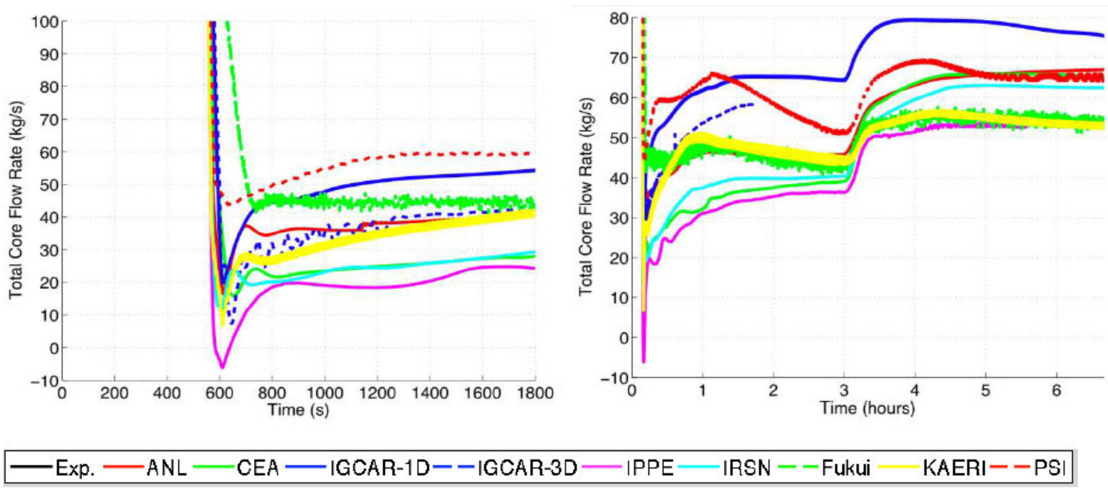

Fig. 2.3: Prediction of natural convection evolution in the core by different participants [29]

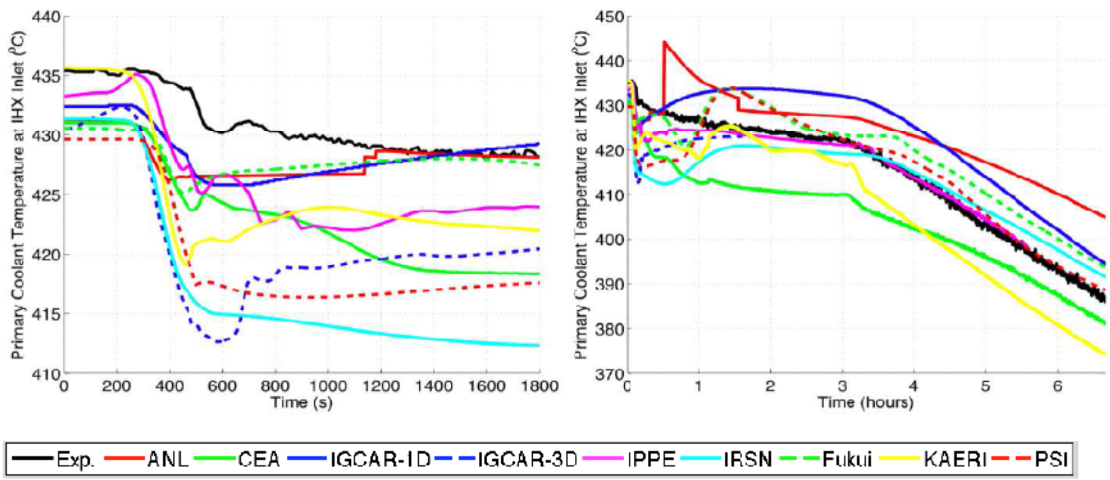

Fig. 2.4: Primary coolant temperature predicted at heat exchanger inlet [29]

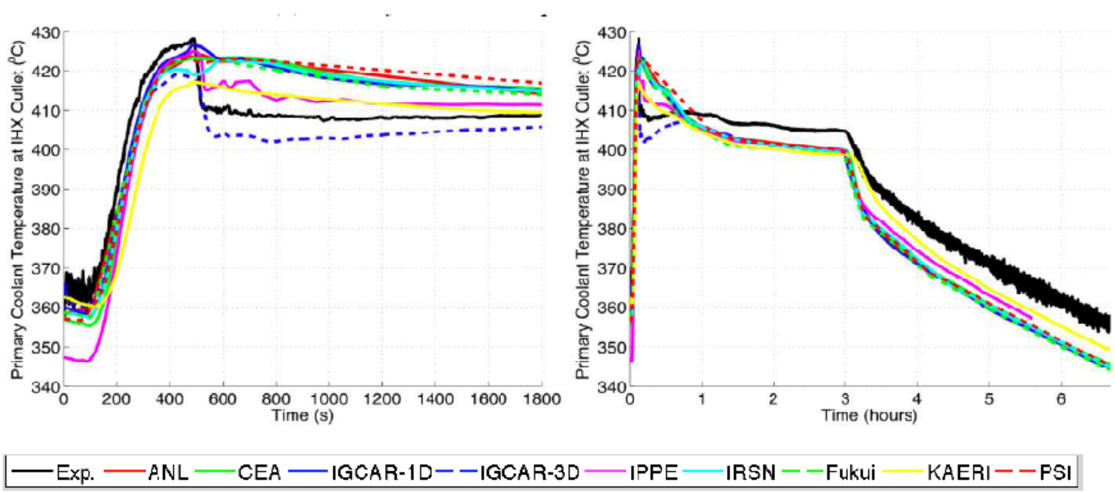

Fig. 2.5: Primary coolant temperature predicted at heat exchanger outlet [29]

2.5 CONSIDERATION FOR THERMAL STRATIFICATION IN DESIGN

As already indicated, the reactor core comprises of different types of subassemblies with varying power generation due to which the temperature of coolant at the exit of these subassemblies is not the same. The temperature distribution at the exit of reactor core causes specific thermal hydraulic issues such as thermal striping, thermal stratification and temperature gradient in structures. Among these, thermal stratification is a phenomenon of concern both during steady state operation as well as during transient conditions. The thermal interface in the stratification layers are generally unstable and lead to thermal fatigue of adjoining structures. Special attention towards this phenomenon is devoted in fast reactor design [31] due to the high heat transfer coefficient of liquid sodium resulting in the transmission of temperature fluctuations caused in coolant to structure with minimal attenuation. During some transient situations such as that following reactor trip, due to the specific flow and temperature evolution at the outlet of reactor core, the hot pool would be subjected to thermal stratification [32]. This can significantly affect the temperature of sodium stream reaching the heat exchanger in the sodium pool. Thermal hydraulic effects due to thermal stratification can get propagated to the entire plant through the heat exchangers.

Based on the detailed thermal hydraulic investigations of hot pool, a porous skirt is introduced below control plug in most of the fast reactor designs as shown in Fig. 2.6 to eliminate the formation of thermal stratification layers [33]. The porous skirt diverts the flow and induces mixing of coolant streams emanating from various subassemblies. The configuration of the skirt is decided based on pool hydraulics studies for full power operating conditions. However, the reactor may be operating at low power operating conditions also. It is essential to establish that the stratification conditions do not happen under these conditions also. This is generally achieved by keeping the sodium flow rate through the core sufficient enough to overcome the buoyancy effects. Moreover, during transients such as reactor trip, when cold sodium emanates from reactor core, significant thermal stratification may occur in the hot pool which has to be addressed in the reactor design. Moreover, when the buoyancy dominates over the inertia the resulting flow field can become unsteady or oscillating in nature in spite of the boundary conditions being steady [34, 35]. Such effects can be addressed only through multi-dimensional models.

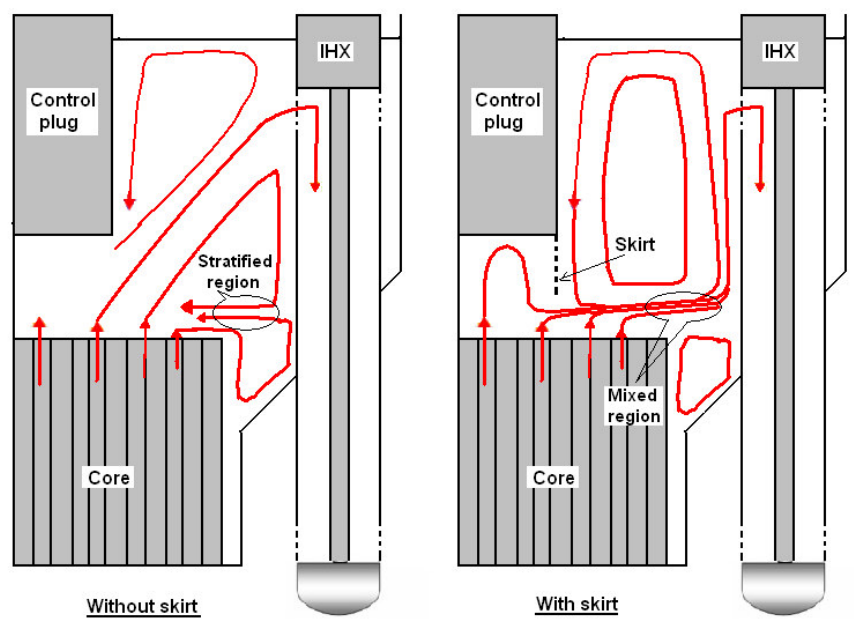

Fig. 2.6: Porous skirt incorporated to modify flow pattern to eliminate thermal stratification in hot pool of an SFR

2.6 CLOSURE

A survey of various codes developed in different countries for the analysis of thermal hydraulic transients in fast reactor systems has been carried out. Computer codes developed in the earlier days were based on integral momentum balance approach and one dimensional single phase formulations. Later on, some of these codes have been improved with multi-zone modelling of core with capability to simulate flow reversal as well as flow redistribution in the core. Subsequently, models accounting for pump performance under cavitating conditions and sodium boiling in the core have been added to some of the codes. Recent development in these codes is the incorporation of multi-dimensional thermal hydraulic features such as thermal stratification in the hot pool of reactor. Incorporating of multi-dimensional modelling features in plant dynamics code make the analysis process computationally expensive. The real benefits of including such models on the predictions of plant behaviour during transients are not widely reported in literature. There are also other subsystems in the reactor where the multidimensional modelling plays important roles. The current thesis is aimed at identifying the regions in the reactor where multi-dimensional modelling is important. An attempt is also made to bring out the benefits of including such multidimensional models for simulating thermal stratification phenomenon in the hot pool and the results prediction of plant behaviour during important plant transients.

CHAPTER - 3

IDENTIFICATION OF DOMAINS REQUIRING MULTI-DIMENSIONAL MODELING

3.1 OVERVIEW

For most of the components of fast reactor, viz., reactor core, heat exchangers, pumps, valves and piping, one dimensional modelling is adequate as the thermal hydraulic phenomenon involved in them is truly one dimensional in nature. Multi-dimensional flow features are involved in large sodium volumes. A detailed review of reactor design from this consideration reveals that multi-dimensional flow features are involved mainly in three components of primary sodium circuit, viz., inlet plenum or grid plate, cold pool and hot pool. Detailed investigations of thermal hydraulics of these components have been carried out to arrive at the need for representing these components through multi-dimensional modelling approach in plant dynamics studies. The numerical scheme to be followed for representing them in the plant dynamics codes is also discussed based of the results of investigation.

3.2 THREE DIMENSIONAL ANALYSIS OF GRID PLATE

Grid plate is an important component of reactor assembly, which supports the core subassemblies and serves as a plenum to distribute primary coolant flow through various subassemblies. The primary sodium pumped by the primary sodium pumps (PSP) is supplied to the grid plate through multiple pipes. In a typical design of SFR, considered in the present analysis, there are two primary sodium pumps supplying flow to grid plate through eight pipes (four pipes connected to each pump) as shown in Fig. 3.1. The schematic of grid plate considered for the present investigation is shown in Fig. 3.2. This design of grid plate is special due to the fact that the coolant plenum accommodates only those subassemblies (fuel, blanket, reflector and storage) which receive sodium flow through them. Shielding assemblies which do not have internal flow through them are accommodated outside plenum.

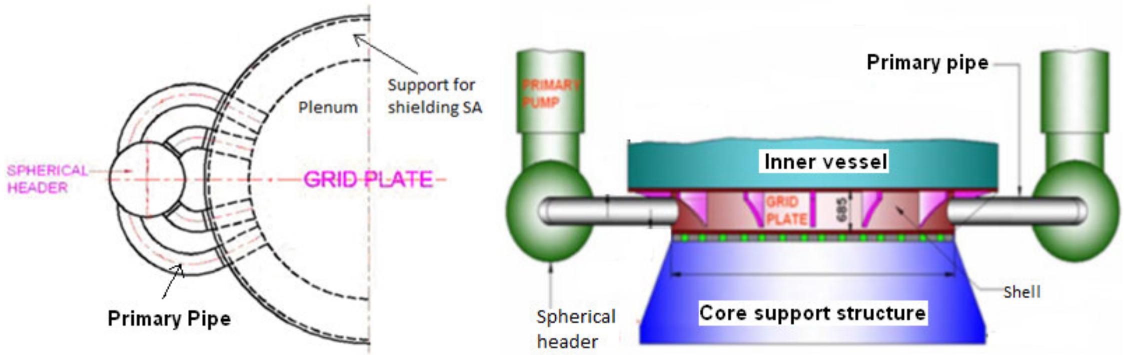

Fig. 3.1: Layout of primary pipes connected to grid plate

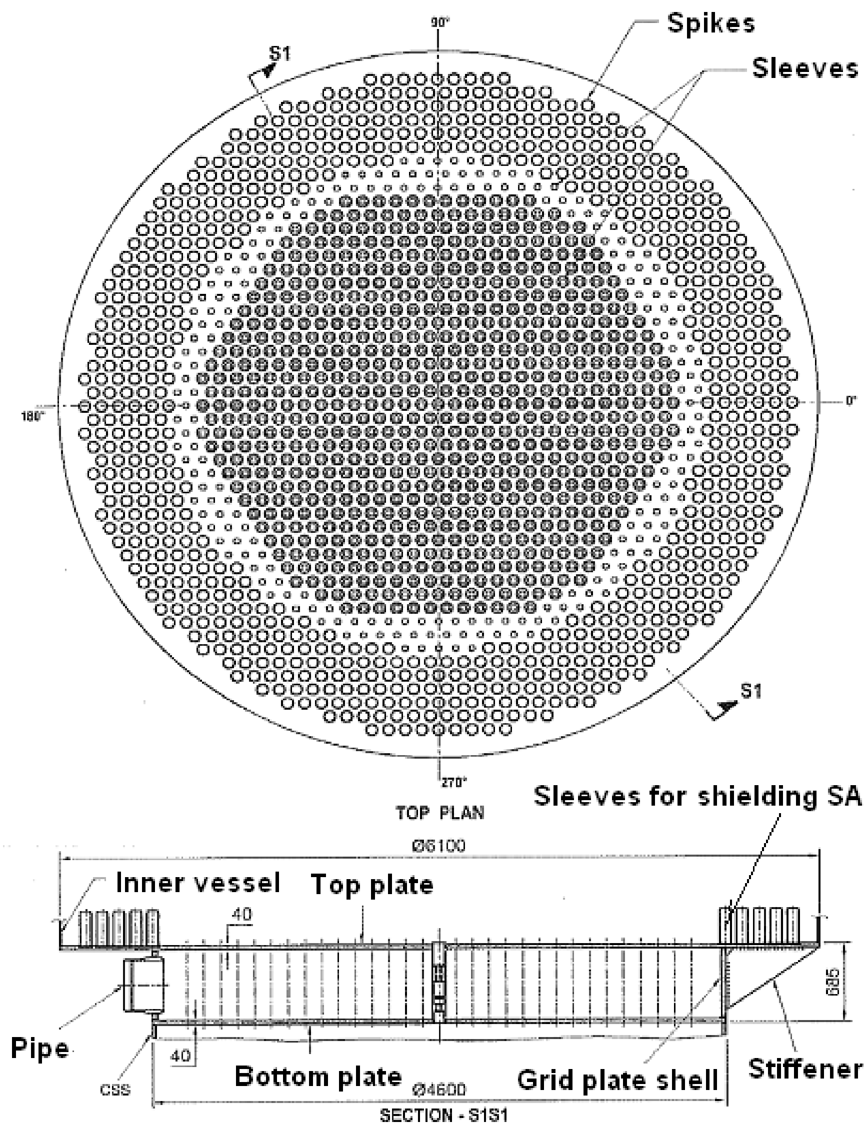

Fig. 3.2: Schematic of grid plate

Therefore, the size of the plenum is reduced in this design compared to a design which accommodates all the subassemblies of the core. The size being smaller, primary pipes are located close to the fuel subassembly in the core. Grid plate contains several cylindrical sleeves in which core subassemblies are mounted. Primary sodium supplied to the grid plate through the primary pipes enters the subassembly through slots provided in the sleeves. In order to mount shielding subassembly, spikes are provided over the top plate (Fig. 3.2).

Under a primary pipe rupture condition, the sodium flow supplied to the grid plate becomes highly unsymmetrical. Sodium flow would bypass from the grid plate to the cold pool through the ruptured pipe, while the flow supplied to the grid plate through the other pipes connected to the same pump falls to a low value. During this condition, the other four pipes (connected to the second pump) supply increased amount of flow (125 %) corresponding to the cavitating flow conditions of PSP. In one dimensional plant dynamics studies, it is assumed that core flow through various subassemblies would remain symmetrical even under pipe rupture condition in spite of unsymmetry in the inlet. A point pressure model is generally adopted to represent the grid plate. This assumption is applied due to the smaller pressure drop offered by the grid plate compared to the pressure drop suffered by the flow in the core subassembly. However, it is likely that the subassembly close to the ruptured pipe may receive comparatively lower flow rate than the subassembly close to the intact pipes. Such multi-dimensional effects on the flow rate through fuel subassemblies located in the central region of grid plate become more pronounced in a design with shielding subassemblies located outside the plenum. It is worth mentioning here that as far as the application of plant dynamics studies for reactor safety is concerned, it is the flow through fuel subassemblies which is of most concern. Hence, it is essential to carry out a three dimensional analysis of grid plate under a pipe rupture condition to understand the unsymmetry nature of core flow among various fuel subassemblies.

3.2.1 Computational Model of Grid Plate

Since there is no symmetry in the circumferential direction for the ruptured state of the grid plate, a full 360^o model has to be considered. The grid pattern and the boundary conditions adopted for this investigation are shown in Fig. 3.3. As already mentioned, grid plate contains several sleeves and modeling them in exact sense is computationally very expensive. Hence, a porous medium approximation is adopted for the sleeve modeling wherein the presence of sleeves in the grid plate is represented by porosities in various coordinate directions. The in-flow to the domain is modeled at the location of intact pipes and outlet from the domain is modeled at the ruptured pipe location and in the top most grid of the domain which represents core flow. Pressure drops offered by sleeves in the radial and circumferential directions are modeled through the correlation for cross flow over bank of tubes available in literature [36] which is given below for the sake of completion.

<u>Radial and circumferential pressure drop</u>

The radial pressure drop due to cross flow over a bank of sleeves is given by

$$\Delta P = Eu \frac{\rho V^2}{2} C_N \ N \tag{3.1}$$

where, Eu is the Euler number, ρ is fluid density, v is fluid velocity, C_N is correction factor for number of rows of sleeves and N is the number of rows of sleeves in control volume. Eu is given by

$$\frac{Eu}{\kappa} = 0.245 + \frac{0.339E4}{\mathrm{Re}} - \frac{0.984E7}{\mathrm{Re}^2} + \frac{0.132E11}{\mathrm{Re}^3} - \frac{0.599E13}{\mathrm{Re}^4} \tag{3.2}$$

Where Re is the Reynolds number defined as

$\mathrm{Re} = \frac{\rho v d}{\mu}$, d is the diameter of the sleeve

$$\kappa = 2.016 - 1.675\left(\frac{a}{b}\right) + 0.948\left(\frac{a}{b}\right)^2 - 0.234\left(\frac{a}{b}\right)^3 + 0.021\left(\frac{a}{b}\right)^4 \tag{3.3}$$

$$a = \frac{\text{longitudinal pitch}}{\text{dia. of sleeve}} \qquad b = \frac{\text{transverse pitch}}{\text{dia. of sleeve}} = \frac{\sqrt{3}}{2}a$$

$$C_N = \frac{1}{N}\sum_{n=1}^{N} c_n \tag{3.4}$$

$$c_n = 0.62 + \frac{1.467}{n + 0.667} \qquad c_n = 1 \text{ for } n > 4 \tag{3.5}$$

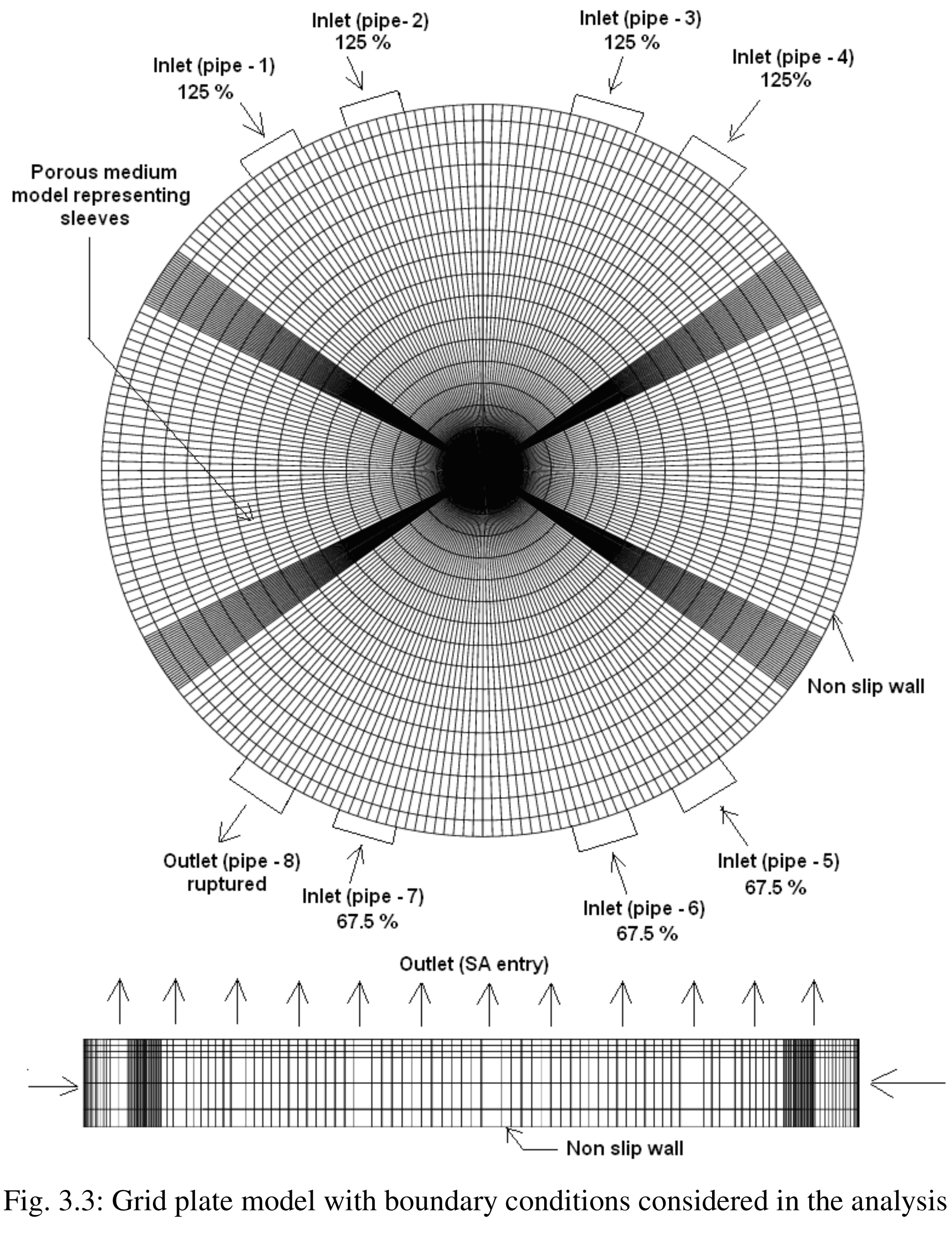

Fig. 3.3: Grid plate model with boundary conditions considered in the analysis

The axial pressure drop specified at the top of the grid plate represents the hydraulic resistance offered by various subassemblies mounted over the grid plate. This is modeled by considering a nominal pressure drop (64 m of sodium column in each subassembly). The axial pressure drop coefficients for various control volumes have been arrived at as shown below.

<u>Axial pressure drop</u>

For a nominal flow rate of Q_{CI} through I^{th} subassembly, the axial pressure drop coefficient is given by $\Omega_I = \dfrac{64*2*g}{(Q_{CI}/\rho A_I)^2}$ where A_I is the flow area of subassembly of type I and Q_{CI} is the nominal flow rate through this subassembly.

If there are n1 subassemblies of type-1 and n2 subassemblies of type-2 etc in a control volume, then effective axial pressure drop coefficient of the control volume Ω_{eff} is given by

$$A_{1F} = \frac{A_1}{A_1+A_2+---}, \quad A_{2F} = \frac{A_2}{A_1+A_2+---}, \ ---- \tag{3.6}$$

$$\Omega_{eff} = \left(\frac{1}{\frac{A_{1F}}{\sqrt{\Omega_1}} + \frac{A_{2F}}{\sqrt{\Omega_2}} + ---} \right)^2 \tag{3.7}$$

The pressure drop on the bypass flow through the ruptured pipe is represented as a sum of pipe resistance (rupture considered at the header end of pipe) and the resistance due to free expansion to the cold pool (k = 1). The grid pattern considered for the study in the (r - θ - Z) directions is 24 X 52 X 8. The three dimensional steady state CFD analysis adopting the k-ε turbulence model has been carried out using the commercial CFD code PHOENICS [37]. The fundamental governing equations (three dimensional momentum and continuity equations) are discretized based on finite volume method. This code is selected for the present analysis due to the structured mesh approach adopted in the code. Structured mesh approach is a convenient way for representing surface porosities of modeled zones. Therefore, the flow velocity simulated through such simulation represents the actual (physical) velocity of flow in between sleeves of grid plate.

3.2.2 Grid Plate Hydraulics during Nominal Operating Conditions

Before analysing the flow distribution during ruptured state, flow distribution during nominal steady state condition is obtained when all the primary pipes are intact. The predicted velocity vector profiles in horizontal and vertical planes of the primary pipes are shown in Figs. 3.4 and 3.5 respectively. It can be observed that sodium flow enters the grid plate through eight primary pipes and flows radially towards the sleeves housing fuel subassemblies in the core. This is located in the central region of the grid plate. The maximum cross flow velocity on the sleeves occurs at the mid radial location in the grid plate due to the reduction in flow area as we proceed radially inwards into the grid plate. As we move further inwards, the cross flow velocity decreases in spite of the flow area reduction. This is due to the out flow through various subassemblies mounted on the grid plate. The maximum cross flow velocity has been found to be 9 m/s.

The predicted distribution of axial velocity at the top of the model along the radial direction at the primary pipe location is shown in Fig. 3.6. Along with the predicted values, the expected velocity distribution based on the theoretical flow distribution in the core is also shown. Axial surface porosity at the top of the domain is specified according to the flow area available in the mid plane of the core. Therefore, the predicted velocities correspond to that inside the subassembly in the mid plane of core. A good comparison is seen between the two justifying the porous medium model considered in the simulation.

3.2.3 Grid Plate Hydraulics during Pipe Rupture Condition

In order to obtain the inlet flow conditions at various pipe locations which is required as input for the CFD analysis, a resistance network calculation is carried out. The hydraulic network considered for the analysis is shown in Fig. 3.7. The resistance coefficient representing the grid plate pressure drop is evaluated based on the calculation of pressure drop estimated for the normal operating condition using the three dimensional model. Within

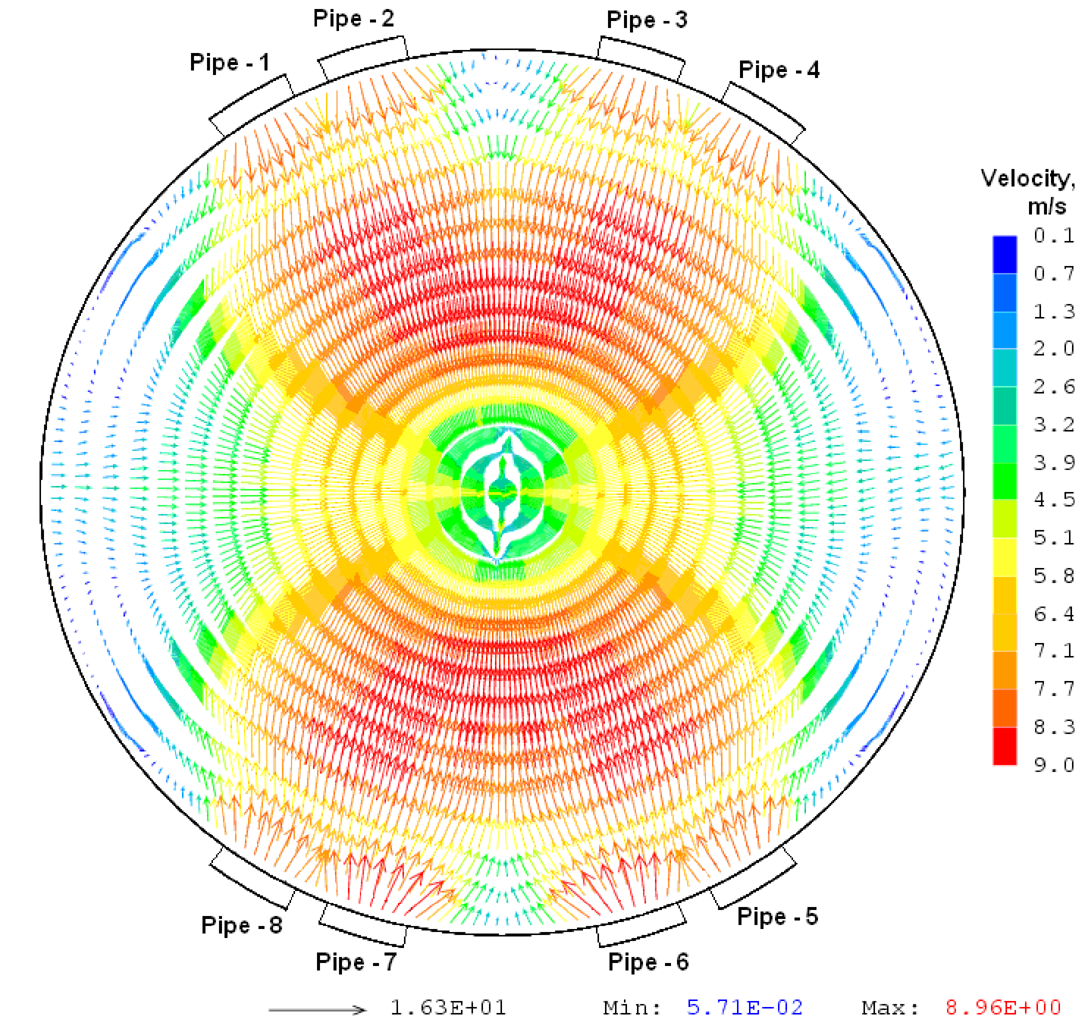

Fig. 3.4: Velocity profile in the horizontal plane through primary pipes during nominal operating conditions

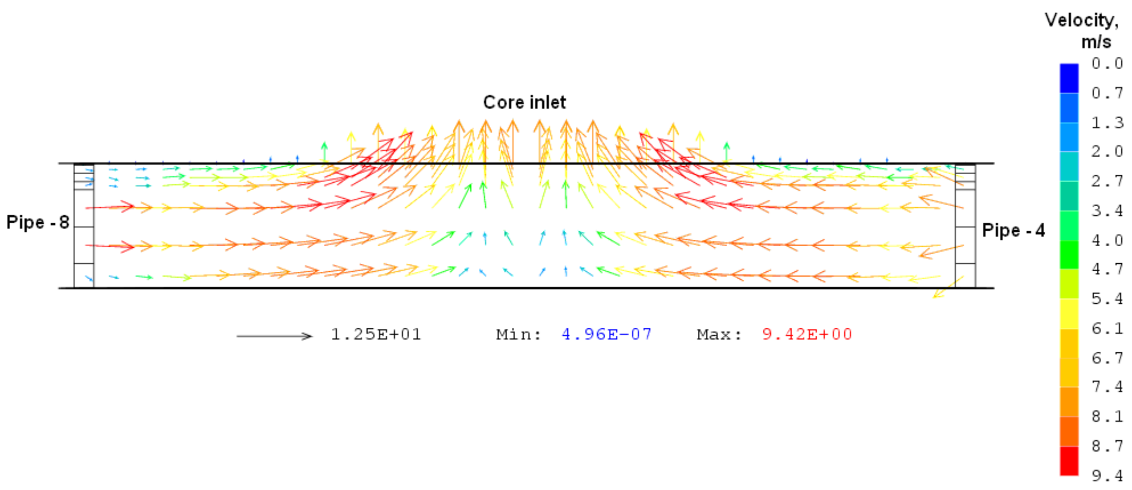

Fig. 3.5: Velocity profile in the vertical plane through discharge pipes during nominal operating conditions

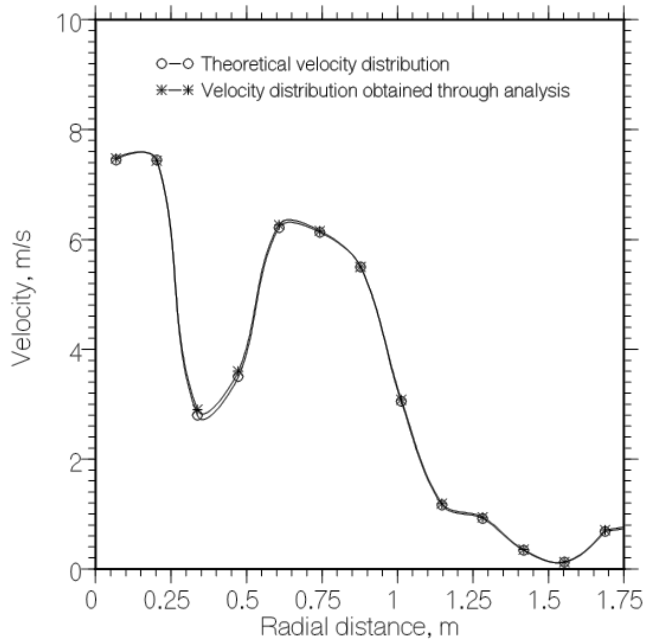

Fig. 3.6.Predicted axial velocity distribution the axial exit of the domain

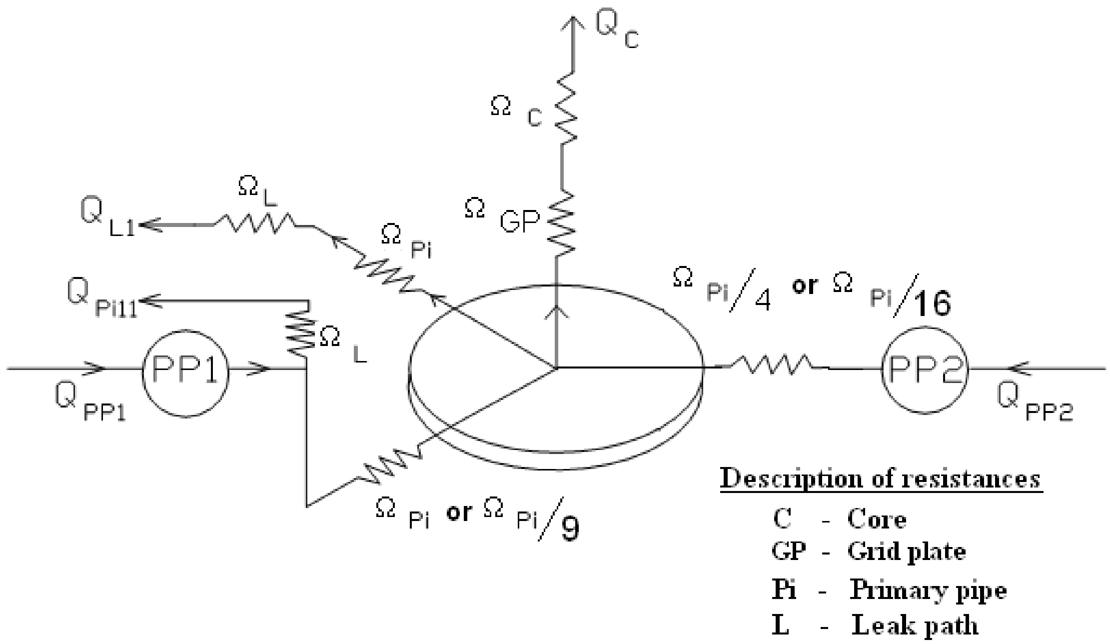

Fig. 3.7: Resistance network considered for obtaining boundary conditions

the grid plate, there is a low resistance path for sodium from intact pipes to the ruptured pipe. This region between the last row of support sleeves and grid plate shell is known as calming zone. The effect of calming zone has been considered conservatively in the mathematical model by treating the grid plate resistance to be not acting on the leak flow paths and the same is treated in series with the core flow. The resistances of three intact pipes are combined as a single resistance path. Similarly, the resistances of four intact pipes connected to the second pump are combined as another single resistance path. A flow rate of 125 % of nominal (Pump flow under cavitating conditions) is considered to be supplied by the two pumps when one of the primary pipes is ruptured. The network model estimates an average core flow rate of 57.5 %.The predicted flow rate through various pipes is supplied as boundary conditions for the three dimensional analysis (Fig. 3.3).

The predicted velocity fields in horizontal and vertical planes through primary pipes are shown in Figs. 3.8 and 3.9 respectively. The maximum cross flow velocity is found to be 10.5 m/s occurring on the sleeves near the intact pipes 1 to 4. The sodium flow rate through the core is found to be 55 % of nominal. The rest of the flow by-passes through the ruptured pipe. On the other hand, the core flow rate estimated through 1-D calculation is 57.5 %. The core flow predicted by three dimensional model is lower. This is due to the close positioning of pipes and the tendency for the flow from the intact pipes connected to pump 2 to bypass the core through the ruptured path (Fig. 3.8) which is not accounted in the 1D analysis. Pressure drop offered by grid plate under primary pipe ruptured condition predicted by the 1D and 3D models (2.31 m and 2.15 m) are also very close.

A reduction in average core flow under pipe rupture condition by 2.5 % from the one dimensional model estimate causes marginal increase in clad and sodium hotspot temperatures, viz., 20 °C and 15 °C respectively only. These temperature estimates are carried out using plant dynamics code DYANA-P. The increase possible due to one dimensional approximation is negligible compared to the large margins (375 °C and 227 °C) available against the respective design safety limits.

The axial velocity distribution in the core subassembly along the radial direction at various pipe locations and angular locations are shown in Figs. 3.10 and 3.11 respectively. It

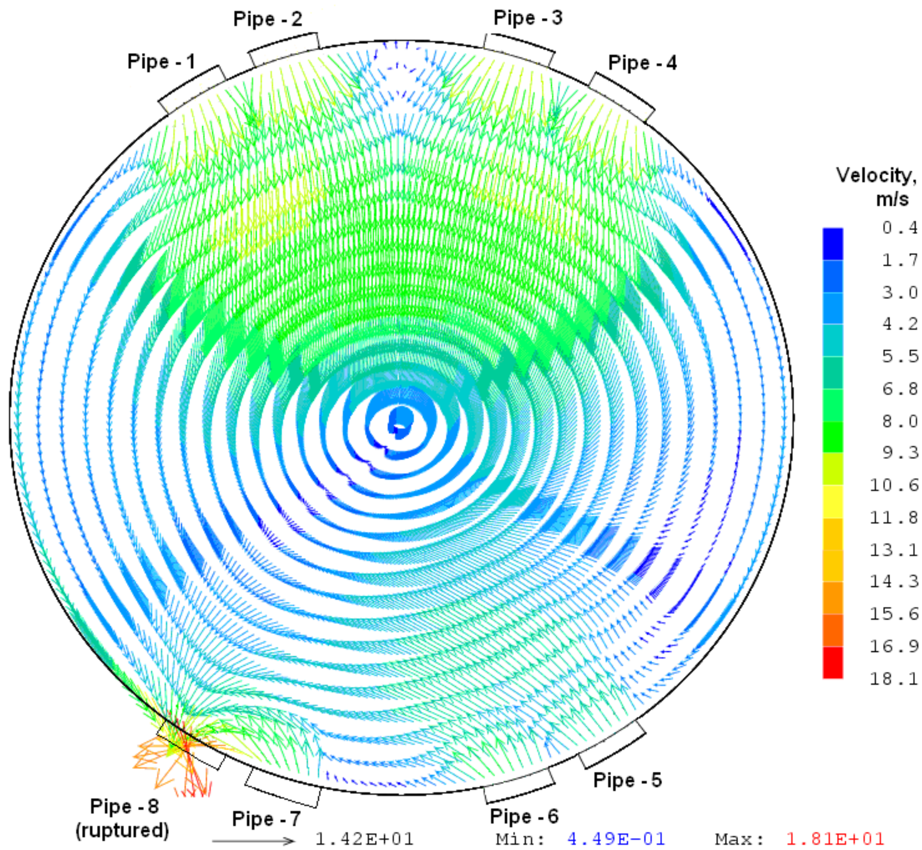

Fig. 3.8: Velocity profile in grid plate during pipe rupture condition

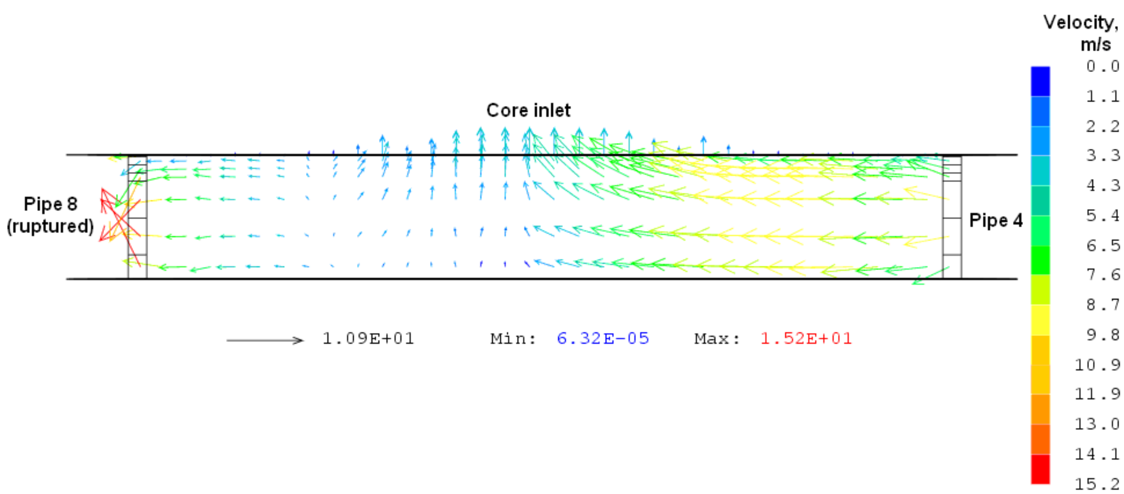

Fig. 3.9: Velocity profile in the vertical plane through discharge pipes during rupture condition

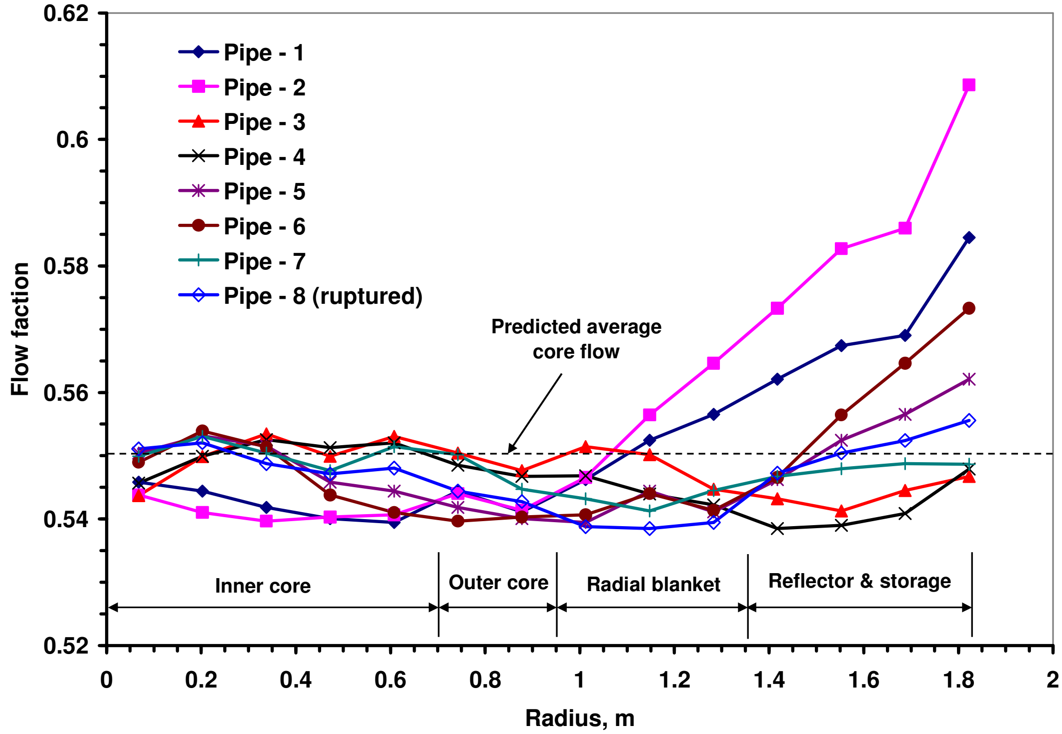

Fig. 3.10: Radial distribution of flow through various subassembly in the core under rupture condition (along various circumferential planes near pipe locations)

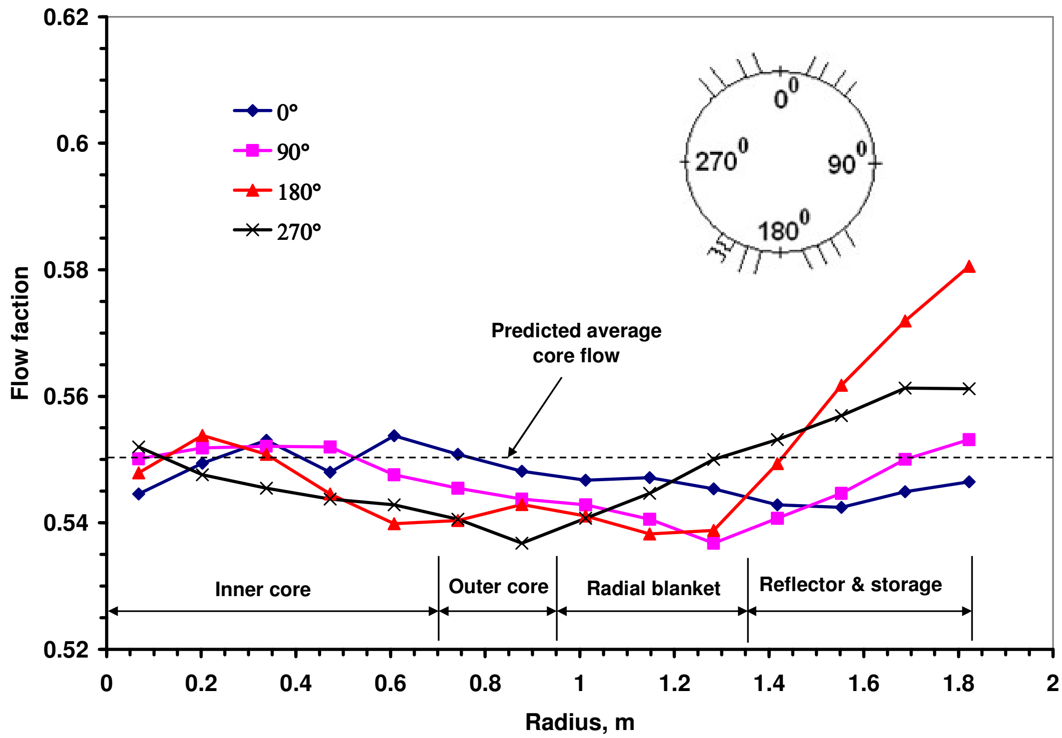

Fig. 3.11: Radial distribution of flow through various subassembly in the core under rupture condition (along various circumferential planes)

can be seen from the figures that the flow velocity through various subassemblies varies over a range of 54 % to 61 % of nominal. The maximum variation in the flow through various subassemblies from the mean core flow value is of the order of +0.5 % to -1 % in the fuel region of core. Deviation in the flow through blanket subassemblies compared to the mean core flow is + 2 % to – 1 %. The deviation is maximum in the peripheral region where the sodium flow itself is very small. The maximum positive deviation of +6 % occurs in the peripheral subassemblies which are very close to the intact pipes. Maximum negative deviation observed is -1 % only. Thus, it can be concluded that there is no significant flow redistribution through the fuel and blanket regions of core under pipe rupture condition. This is in agreement with the conclusion derived for the grid plate with two pipe concept [38]. Therefore, the plant dynamics modeling does not require special consideration for simulation flow re-distribution caused by the grid plate. The point pressure approximation for grid plate is valid for all transients addressed by plant dynamics codes.

3.3 THERMAL HYDRAULICS OF HOT POOL

Significant effects due to thermal stratification in hot pool would be observed after reactor SCRAM due to sudden reduction in heat generation in the reactor core. To understand this, transient multi-dimensional analysis of hot pool is carried out using a detailed three dimensional model as well as using an approximated axi-symmetric two dimensional model. Predictions by these models are compared against one dimensional model predictions of hot pool. In the one dimensional model, the entire hot pool is represented through a single control volume as shown in Fig. 3.12. Sodium flow from various core zones (Q_{Ci}) at different temperatures (T_{Ci}) enters the hot pool and gets perfectly mixed before entering the IHX. The IHX flow is represented as (Q_I) and IHX receives sodium from the hot pool at the mixed mean temperature of hot pool (T_{HP}). In the one dimensional model, the continuity and energy balance equations are represented as Eqn. (3.8) and (3.9) respectively.

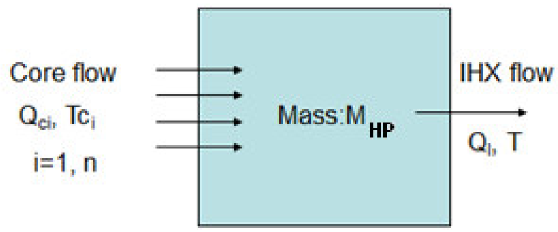

Fig. 3.12: Representation of perfect mixing model

$$\frac{dM_{HP}}{dt} = \sum_{i=1}^{n} Q_{Ci} - Q_I \tag{3.8}$$

$$\frac{d(M_{HP}\ CpT_{HP})}{dt} = \sum_{1}^{n} Q_{Ci}CpT_{Ci} - Q_I CpT_{HP} \tag{3.9}$$

3.3.1 Three Dimensional Modeling of Hot Pool

The geometry of hot pool is symmetric about 90^0cylindrical sector. Hence, a sector model is developed. The computational domain and mesh pattern considered for the analysis are shown in Fig. 3.13. Mesh pattern for the geometry is generated using trimmed cell approach. Total number of computational meshes in the domain is ~ 55000. Subassemblies in the reactor core are arranged in a hexagonal geometry. Each hexagonal ring of the core is represented through an equivalent cylindrical ring in the three dimensional model. Radial width of each cylindrical ring is modelled such that the outlet area of all the subassemblies located in the ring matches with area of the inlet boundary condition. Thus, the core outlet velocity is simulated exactly. Velocity and temperature boundary conditions are specified at the 11 different inlet rings. The one dimensional model represents the core through 10 radial channels. Each channel consists of several subassemblies. Power and flow per subassembly in each radial channel is modelled to be the same based on averaging approach. Each core ring considered in the three dimensional model consists of subassemblies from different one dimensional channels. Number of subassemblies of different core channels present in each core ring is known. Based on this information, flow and temperature of sodium through each core ring essential for the three dimensional model are established based on the one dimensional analysis results.

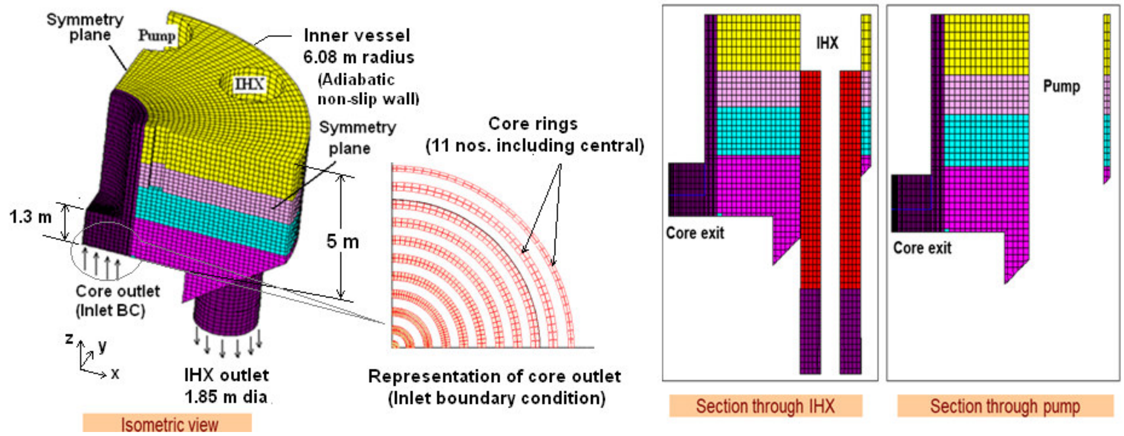

Fig. 3.13: Model and mesh pattern considered for three dimensional modelling of hot pool

Inlet velocity and temperature are specified at these boundaries. There is a porous plate and a shell provided below the control plug in hot pool. The effects of these porous structures are modeled through sinks in the respective momentum balance equations. Pressure loss coefficient of these structures are defined based on the equation (3.10). The pressure loss coefficient, Ω is specified using Ward Smith correlation [39] given in equation (3.11) for porous plates.

$$\Delta P = \Omega\frac{\rho v^2}{2} \tag{3.10}$$

$$\Omega = \left(\frac{1}{0.608\gamma(1-\gamma^{2.6})\left(1+\left(\frac{\delta}{\varphi}\right)^{3.5}\right)+\gamma^{3.6}} - 1\right)^2 \tag{3.11}$$

For, $0 < \delta/\varphi < 0.6$, $0 < \gamma < 0.75$, $0.57 < \Omega < 35000$

Where ΔP is the pressure drop, Ω is the pressure loss coefficient, ρ is density of fluid, v is the superficial velocity of fluid approaching the porous plate, δ is thickness of plate, φ is diameter of circular holes in the plate and γ is the surface porosity of the porous plate. There is additional pressure drop offered tube bundle of IHX. The pressure drop offered by the tube bundle would be anisotropic, in that it would offer different resistances to each component of flow. Individual tubes are not modeled owing to large computational resources required. The tube bundle is modeled as a porous volume with separate pressure drop coefficients defined for axial, radial and circumferential directions. For pressure drop in axial direction, Blasius relation [40] for turbulent flow is used. For radial and circumferential directions, Zukauskas correlation [36] discussed in section 3.2.1 is employed. Outlet from the domain is considered at the bottom of IHX. Apart from this, heat transferred from the primary sodium to the secondary sodium circuit is modelled though uniformly distributed heat sink in the energy balance equation within IHX. Free surface is simulated through frictionless wall and all physical walls in the domain are modeled as non-slip adiabatic walls with smooth wall resistance conditions. Turbulence is treated through standard high Reynolds number k-ε model with first order upwind scheme adopted for convective terms. Higher order scheme is not adopted in the present study as there are no regions where sharp velocity gradient exists in the hot pool. The Reynolds number of flow is also high enough to justify the usage of upwind scheme. Hence, in order to ensure faster convergence, upwind scheme is adopted. Analysis is carried out using finite volume based unstructured mesh CFD code.

3.3.2 Axi-symmetric Two Dimensional Modeling of Hot Pool

Flow entry into the hot pool is through various subassemblies in the core. Core is located centrally in the hot pool. Hence, axi-symmetric approximation is applicable for this boundary. Flow exit from the hot pool is through four IHX located at a pitch circle diameter from the core center. Sodium flow from the hot pool enters the IHX through inlet windows located at 1400 mm from the free surface of hot pool. However, for the sake computational simplicity, the inlet window is considered to be located axi-symmetrically. This approximation is adopted as the purpose of the hot pool model is to predict the temperature evolution of sodium at the inlet of IHX during plant transients in a realistic manner while compared to the simplified one dimensional approach. The axi-symmetric model of hot pool developed along with boundary conditions is shown in Fig. 3.14. The axi-symmetric domain is generated by extracting a two dimensional plane from the three dimensional mesh pattern discussed above. Number of computational cells in the domain is 1510. With the selected mesh pattern, the y+ values for initial steady state condition are below 200. Geometry of core outlet is modelled in a similar manner as discussed in section 3.3.1. Velocity and temperature boundary conditions are specified at the hot pool inlet (core outlet).

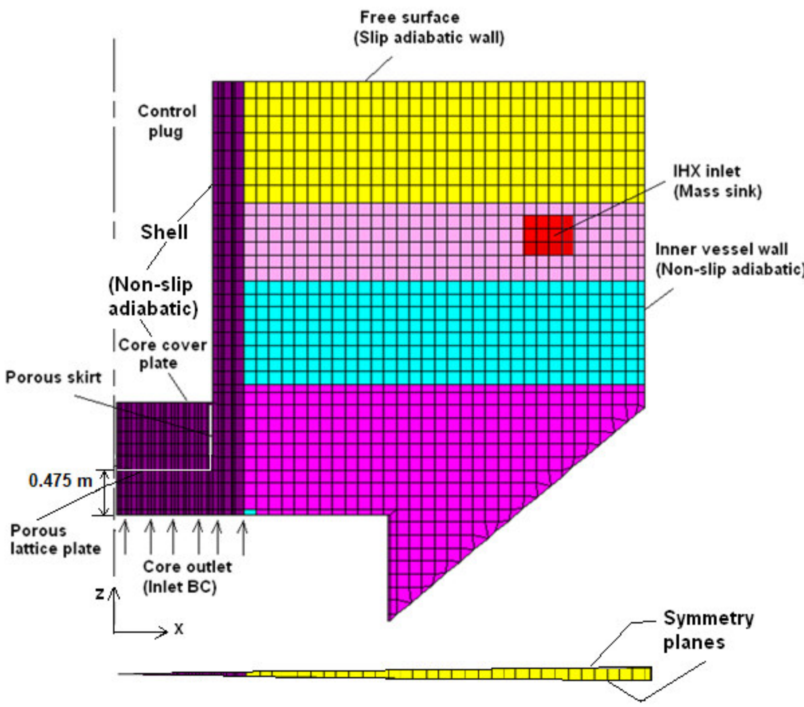

Fig. 3.14: Axi-symmetric model of hot pool with boundary conditions

In this model also, hydraulic resistances offered by the porous lattice plate and the shell (lattice plate and skirt) provided in the hot pool are simulated through sinks in the momentum balance equation. Free surface is simulated through frictionless wall and all the physical walls in the domain are modeled as non-slip adiabatic walls with smooth wall resistance conditions. Outlet from the domain is simulated through mass sink in the continuity equation at a location corresponding to the radial and axial positions of inlet window of IHX. The volume of the mass sink region matches with the volume of all the four

IHX inlet windows in the reactor. Turbulence is treated through standard high Reynolds number k-ε model (details of the choice of the turbulence model are discussed subsequently in section 3.3.6) with first order upwind scheme adopted for convective terms. Pressure velocity coupling is achieved through the SIMPLE algorithm [41].

3.3.3 Boundary Conditions

As already mentioned, the transient scenario following spurious SCRAM event is considered for the analysis. During initial steady state conditions, velocity and temperature distributions at the core outlet correspond to that during full power operating conditions. The transient is simulated by considering that reactor SCRAM happens leading to abrupt (within 1 s) power reduction in the core to decay heat conditions. Along with reactor SCRAM, the speeds of sodium pumps coast down (governed by their flywheel inertia) to 20 % speed. Due to sudden reduction in core power, there will be sharp reduction in temperature of sodium coming out of core subassemblies. Transient evolutions of flow through the reactor core and temperature at the outlet of the core during this event are predicted using the one dimensional whole plant modeling code DYANA-P. The predicted flow and temperature evolutions at the outlet of central subassembly in the core are shown in Fig. 3.15. Velocity and temperature evolutions of sodium at the outlet of various core zones modeled in DYANA-P are specified as transient boundary conditions for the three dimensional and axi-symmetic models of hot pool and thermal hydraulic responses of hot pool during the event are studied.

3.3.4 Steady State Velocity and Temperature Distributions

Velocity distributions predicted by the three dimensional model in the circumferential planes through IHX and the symmetry plane between two IHX are shown in Fig. 3.16. Sodium emanating from the core, flows vertically upwards and gets deflected radially by the control plug. The porous skirt causes the flow to turn downwards before flowing radially towards the inner vessel. Thus, the flow coming out of the core makes a ‘U’ turn in the region

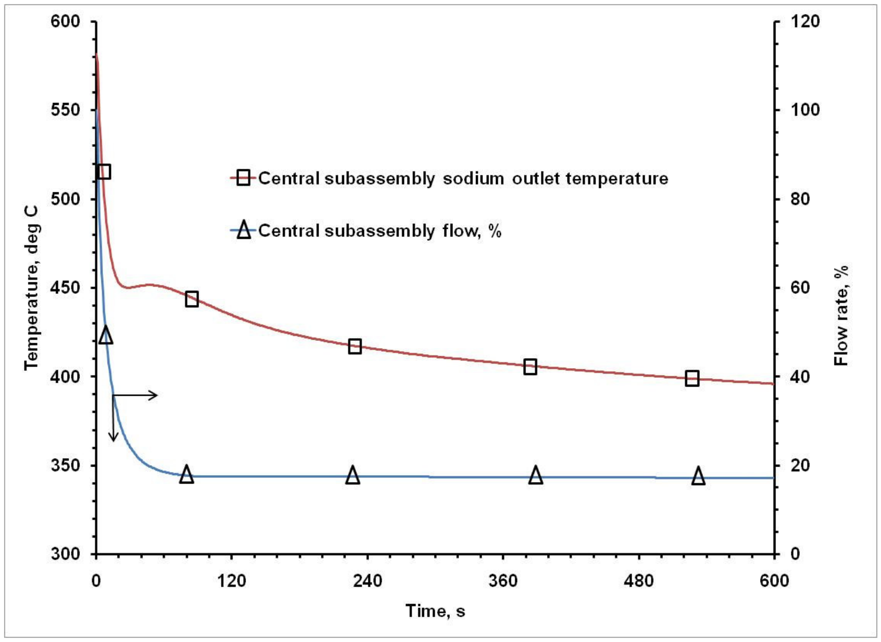

Fig. 3.15: Evolution of flow and temperature at the outlet of central subassembly predicted by DYANA-P

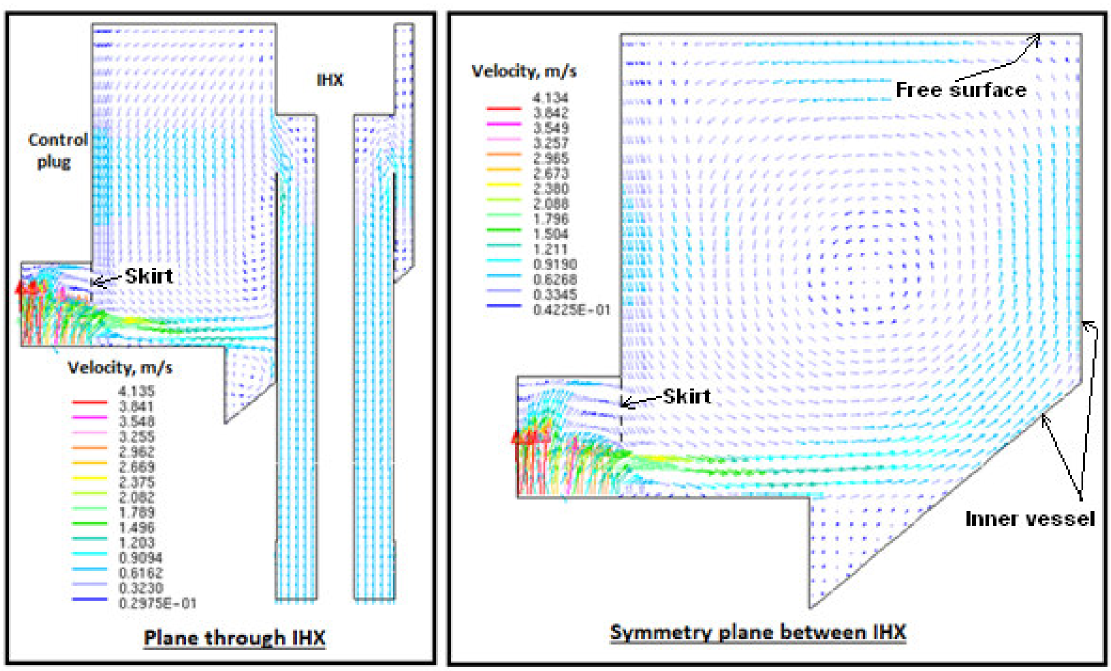

Fig. 3.16: Steady state velocity pattern in the hot pool predicted by 3-D model

between core top and control plug. Near the inner vessel, sodium flows upwards close to the outer shell and reaches free surface. A part of this flow enters IHX inlet window. In the sodium free surface, direction of sodium flow is radially inwards towards the control plug shell. Near the control plug, the flow direction is downwards. Thus, a recirculating pattern is made by sodium in the region of hot pool between two IHX.

Temperature distribution in sodium predicted by the three dimensional model in the circumferential planes through IHX and symmetry plane between two IHX are shown in Fig. 3.17. It can be observed that due to the deflection and mixing effect created by porous skirt, sodium flow reaching the inner vessel from the core is very well mixed. Therefore, stratification layers are not formed in the hot pool. Sodium in the hot pool is well mixed and flow entering the IHX is at the mixed mean temperature of 547 ^{0}C.

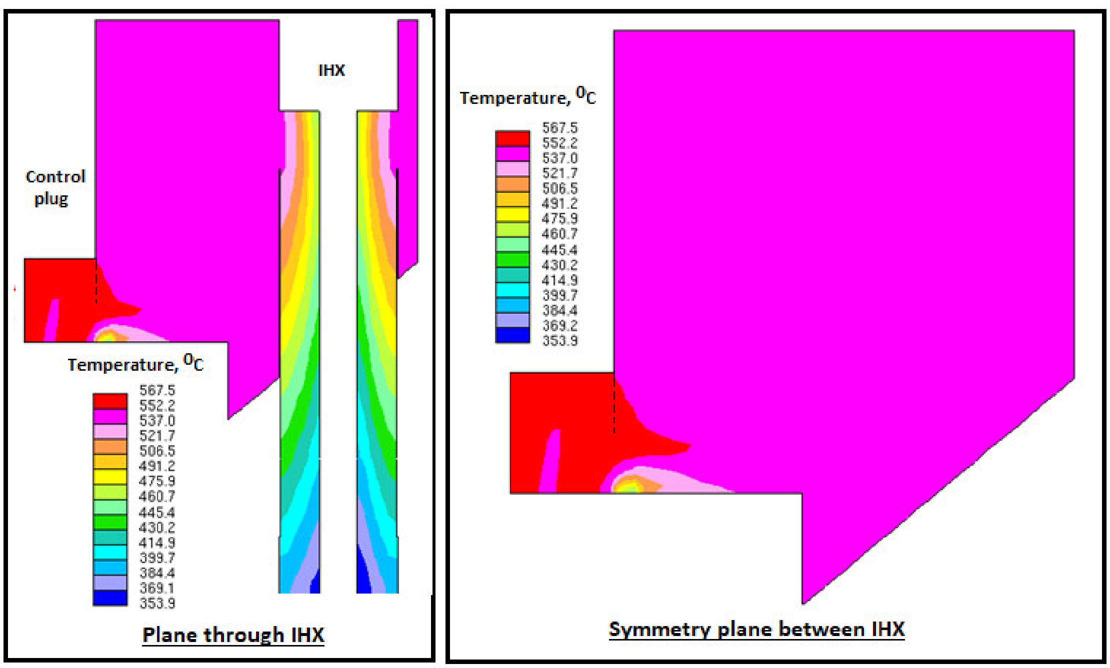

Fig. 3.17: Steady state temperature profile in the hot pool predicted by 3-D model

Velocity and temperature fields of sodium in the hot pool predicted by the two dimensional model are shown in Fig. 3.18. The recirculation flow pattern of sodium in the hot pool is well predicted by the two dimensional model. The U turn of sodium flow emanating from the core in the region between core top and control plug is also well predicted by the two dimensional model. The path followed by sodium from the core is also similar to that observed in the symmetry plane between IHX in the three dimensional model. The perfect mixing nature of sodium flow in the hot pool is also predicted by the two dimensional model. Thus, the overall flow pattern and thermal mixing of coolant in hot pool predicted by the three dimensional and two dimensional models are nearly similar. Therefore, as far as the plant dynamic analysis is concerned, the single control volume based perfect mixing model can accurately represent the coolant temperature entering the IHX inlet window.

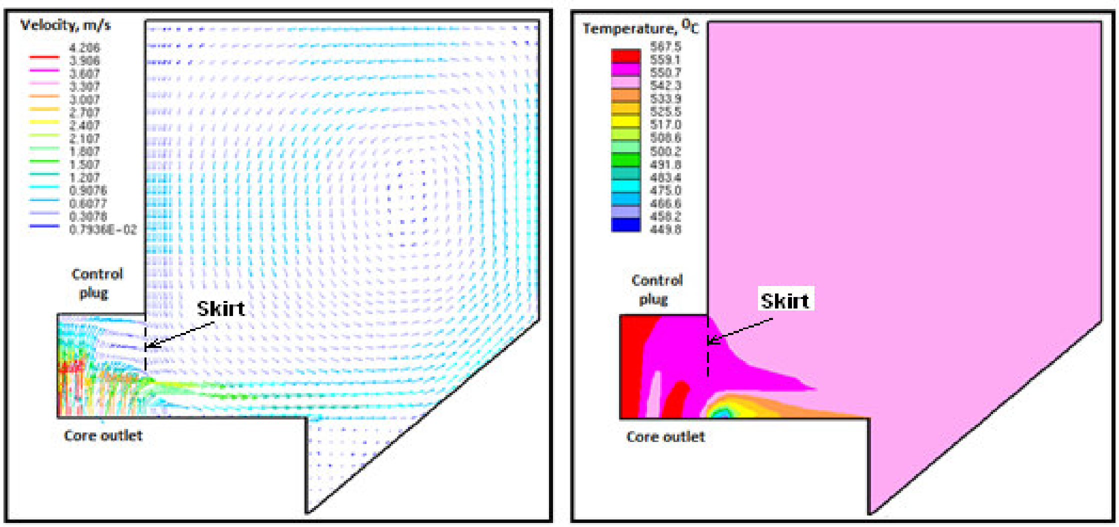

Fig. 3.18: Steady state velocity and temperature pattern in hot pool predicted by 2-D model

3.3.5 Transient Velocity and Temperature Distributions

Temperature distributions of sodium in the hot pool at 300 s after the initiation of reactor SCRAM and primary flow reduction to 20 % as predicted by 3-D and 2-D models are shown in Fig. 3.19. Due to flow reduction to 20 %, the cold sodium streams emanating from reactor core is unable to penetrate up and reach the upper regions of hot pool. Due to the dominance of buoyancy over the fluid inertia, the upper regions of hot pool get stratified. Stratified layers formed near the IHX window can be clearly seen in the figures. It can be noted that the formation of thermally stratified layers is well predicted by both the three dimensional as well as the axi-symmetric models. Temperature distribution of sodium predicted in the axial direction of hot pool is also nearly same. It shows that the axi-symmetric model is capable of representing thermal stratification in the hot pool.

Due to the geometrical nature of control plug and porous skirt, hot pool basically receives sodium through the cylindrical area between core top and bottom of skirt. The height of this cylindrical region (0.475 m) may be considered as the characteristic length to represent Reynolds (Re) and Grashoff (Gr) numbers. Velocity is represented based on the above cylindrical area as the flow area. Since, thermal stratification during plant transients is paid attention, the temperature difference of sodium in the hot pool domain is considered as the ΔT for representation of Grashoff number. Accordingly, Reynolds, Grashoff and Richardson (Ri) numbers at initial steady state conditions and at different times after reactor SCRAM are shown in Table 3.1. It can be observed from the Richardson numbers calculated that sodium flow during initial steady state conditions is dominated by inertia force and as the transient progresses, buoyancy starts dominating over inertia and sodium flow will then be under mixed convection regime.

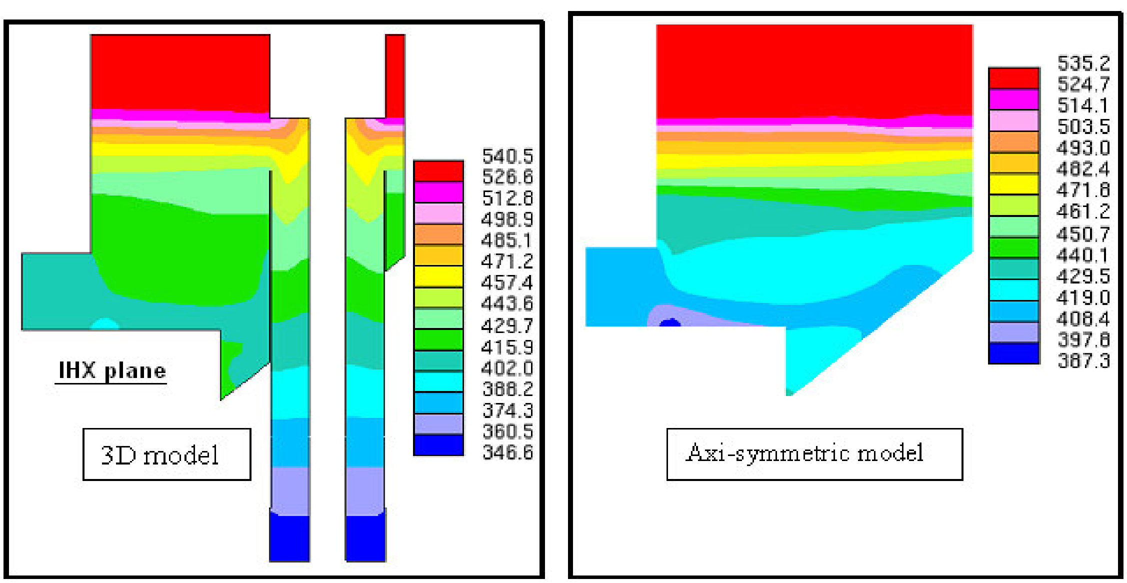

Fig. 3.19: Predicted temperature distribution in hot pool at 300 s during SCRAM event

Table 3.1: Non dimensional number calculated during spurious SCRAM

Time instant	Re	Gr	Ri
Initial	3.6×10^{6}	3.3×10^{11}	0.03
300 s	7.2×10^{5}	5.0×10^{11}	0.98
600 s	7.2×10^{5}	5.2×10^{11}	1.01

As far as system dynamics simulation is concerned, the pool thermal hydraulic parameter important for accurate simulation of whole plant transient is the primary sodium temperature at the IHX inlet. The thermal transient happening in the pool gets communicated to the rest of the plant through this parameter. The average inlet temperature corresponds to flow weighted average at the entry of inlet window in the three dimensional model and in the mass sink region of axi-symmetric model. In the one dimensional model, the mixed mean temperature of hot pool represents the temperature of sodium entering the IHX inlet. Evolutions of average sodium temperature at the IHX inlet predicted by the three dimensional, axi-symmetric and one dimensional models are shown in Fig. 3.20. Three dimensional model represents the thermal stratification in hot pool more accurately compared to other models due to the more realistic representation of the hot pool geometry. But, the computational effort involved for this model is enormously high compared to other models. The one dimensional predictions deviate from the three dimensional model predictions by ~ 17 %. The deviation gets reduced to ~7 % with two dimensional representation of hot pool. For estimating the above deviations, the change in the temperature of sodium predicted at any instant at the inlet of IHX with respect to the initial steady state value is calculated first. These temperature changes predicted by the one dimensional and axi-symmetric models are the compared with respect to the three dimensional model at every instant of time to calculate the instantaneous deviations. This is averaged over a period of 900 s to calculate the above reported deviations. It is worth highlighting here that the CPU time required for three dimensional model is 50 times that required for two dimensional model. Considering the closeness of predictions between the axi-symmetric and three dimensional models, the axi-symmetric modelling can be considered as a good approximation to represent thermal stratification effects in hot pool. Plant dynamics simulations can be carried out with due consideration of thermal stratification effects in hot pool by incorporating a 2-D based mixing model for the hot pool.

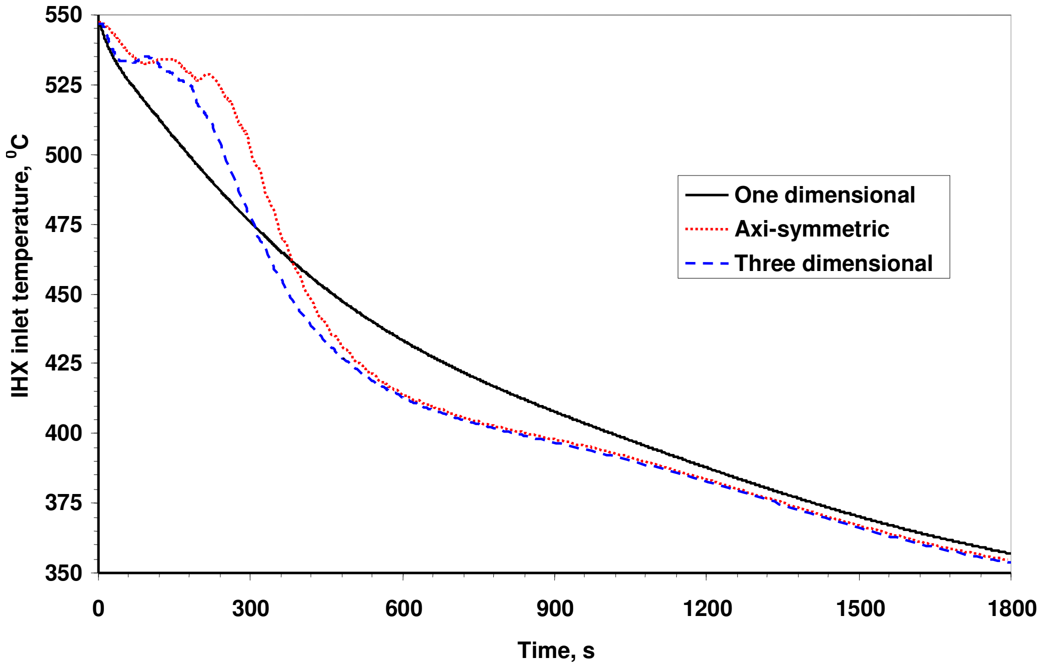

Fig. 3.20: Temperature evolution at IHX inlet predicted by different models during SCRAM

3.3.6 Parametric Studies with various Turbulence Models

The coolant flow encountered in the hot pool is highly turbulent even at low flow conditions as evident from the Reynolds numbers shown in Table 3.1. Turbulence plays a major role in the momentum and energy transport of sodium in the hot pool. An accurate resolution of spatio-temporal details of turbulent flow requires direct numerical simulation using a fine grid model and transient marching with small time steps. This is computationally impossible for the large geometrical size of hot pool. Therefore, a practical approach involves the accounting of thermal hydraulic effects of turbulence on the momentum and heat transport through appropriate models. Commonly adopted approach for turbulence modeling is using the Reynolds-averaged Navier-Stokes (RANS) equations. The Reynolds stresses appearing in these equations can be algebraically evaluated with the help of the turbulent eddy viscosity concept. The eddy viscosity, in turn, can be obtained using approaches of different levels of complexity. The effectiveness of two equation models, viz., k-ε, k-ω in resolving turbulence is well established.

In an improved form for k-ε model, equations for k and ε are derived from the application of a rigorous statistical technique (Renormalization Group Method). These equations include additional term in ε equation to take into account of (i) interaction between turbulence dissipation and mean shear, (ii) the effect of swirl on turbulence, (iii) analytical formula for turbulent Prandtl number and (iv) differential formula for effective viscosity. This model provides improved predictions for high streamline curvature and strain rate, transitional flows and wall heat and mass transfer. It is also possible to solve for the Reynolds stresses using six transport equations, with additional computational effort. Due to the large size of pool, the turbulence behavior in the pool may become anisotropic in nature. The Reynolds stress based model (RSTM) is capable of accounting for the anisotropic nature of turbulence behavior. Transient in the hot pool following reactor SCRAM has been simulated using various turbulence models. The geometrical model considered is axisymmetric model of the hot pool (Fig. 3.14) as explained in the previous section. Time step for the simulation is such that the maximum courant number during the transient varies between 1.1 and 0.2. The corresponding average courant number during the transient varies between from 0.1 and 0.02.

Temperature evolutions predicted at the inlet of IHX by various turbulence models are shown in Fig. 3.21. It is observed that the predictions of transient thermal hydraulic behaviour by various turbulence models are very close. The recirculating nature of flow in the hot pool and the anisotropic turbulence effects do not affect the turbulent mixing nature of sodium flow in the hot pool significantly. Similar conclusion is derived in the numerical study of sodium natural convection in the upper plenum of MONJU reactor vessel which was carried out as part of an IAEA organized coordinated research project [42] (IAEA, 2014). Hence, the popular and generic high Reynolds number k-ε model is concluded to be appropriate for the axi-symmetric modeling of hot pool for the plant dynamic studies.

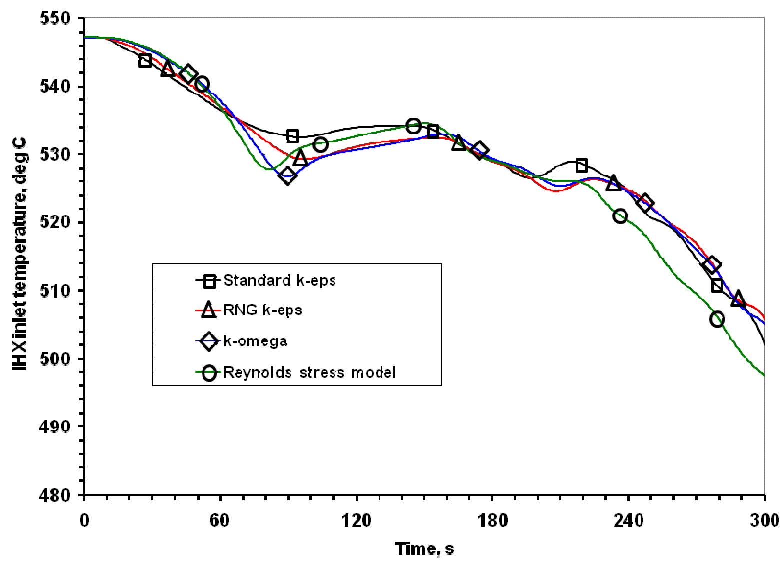

Fig. 3.21: Temperature evolution predicted at the inlet of IHX by various turbulence models

3.4 THERMAL HYDRAULICS OF COLD POOL

Significant multi-dimensional thermal hydraulic features would be developed in cold pool during plant transients, viz., reactor SCRAM and trip of one secondary sodium pump. The boundary of cold pool at the top is occupied by inner vessel above which hot sodium pool is present. Sodium velocity at the outlet of IHX has a significant component in the downward direction. Therefore, sodium flow entering the upper region of cold pool is very small. During transients, when the temperature of sodium at the outlet of IHX changes, it propagates initially to the lower region of cold pool. Temperature of upper region of cold pool changes slowly due to diffusion rather than by convection (due to low velocity of sodium prevailing in this region). Therefore, stratified conditions may be developed in cold pool during transients. Other important transients which can cause imperfect mixing of coolant in the cold pool are trip of one secondary sodium pump or loss of cooling of steam generators connected to one loop. Transient thermal hydraulic analysis of cold pool during reactor SCRAM and one secondary sodium pump trip events have been carried out using three dimensional model of cold pool and the predicted transient behavior are compared against one dimensional as well as multi-zone modeling of cold pool.

3.4.1 Single Zone Model

In the one dimensional model, the entire cold pool is represented through a single control volume as shown in Fig. 3.22. Hence, the sodium flows from various IHX (Q_I) at different temperatures (T_I) enter the cold pool and get perfectly mixed before entering the pump. Pump flow is represented as (Q_{PP}) and pumps receive sodium from the cold pool at the mixed mean temperature of cold pool (T_{CP}). The continuity and energy balance equations are represented as Eqns. (3.12) and (3.13) respectively.

$$\frac{dM_{CP}}{dt} = \sum_{i=1}^{n} Q_{Ii} - \sum_{j=1}^{n} Q_{PPj} \tag{3.12}$$

$$\frac{d(M_{CP}CpT_{CP})}{dt} = \sum_{i=1}^{n} Q_{Ii}CpT_{Ii} - \sum_{j=1}^{n} Q_{PPj}CpT_{CP} \tag{3.13}$$

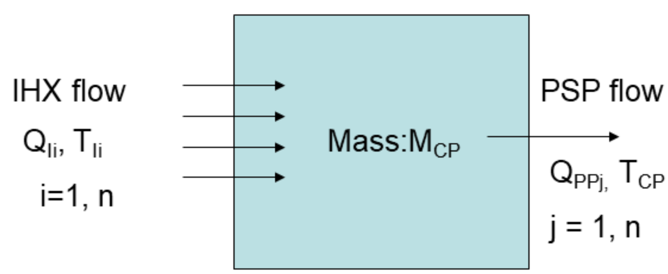

Fig. 3.22: Single control volume representation of cold pool

3.4.2 Multi Zone Model

In the multi zone approach, cold pool volume is divided into 4 sectors in the circumferential direction as shown in Fig. 3.23. Two IHX of a particular secondary loop and one primary sodium pump are located in each of the sectors 1 and 2. Sector 3 and 4 are 60^0 sector volumes between the IHX of two loops. Moreover, each of the cylindrical sectors are divided in the axial direction into two volumes. Volume 2 in Fig. 3.23 represents the region of cold pool falling between the inner vessel redan and main vessel. They are the low velocity zones of cold pool. Thus, the cold pool volume is divided into 8 volumes. Cold pool volumes in sectors 3 and 4 receive sodium from the IHX of both the loops and hence their thermal behaviors are expected to be identical. Hence, these two sectors are combined into a single sector in the multi zone model of cold pool represented as six control volumes as shown in Fig. 3.24.

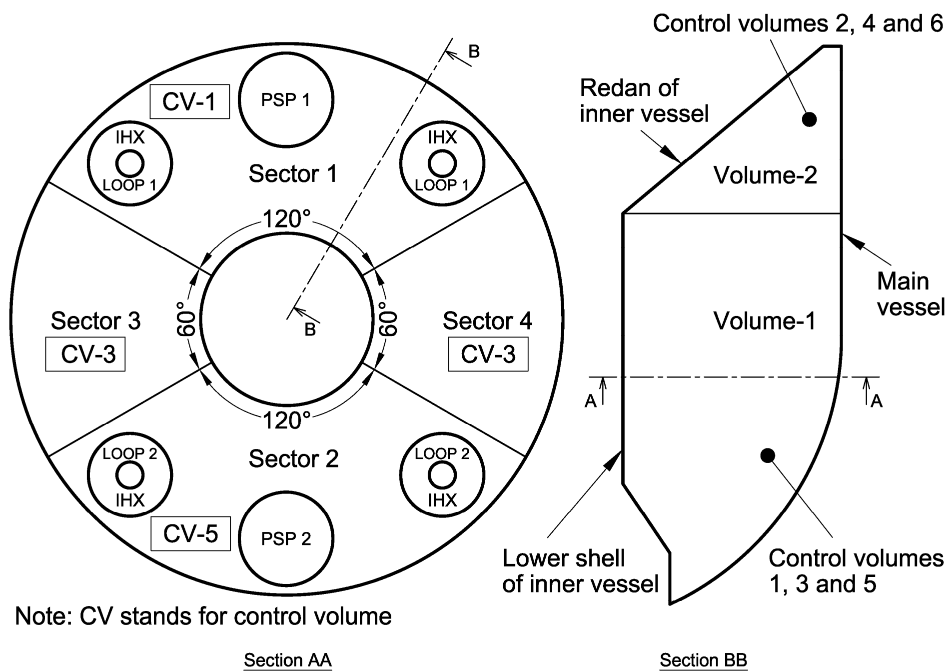

Fig. 3.23: Representation of the division of cold pool into multiple volumes for the multi-zone model

Control volumes 1 & 2 and 5 & 6 represent the cold pool in sectors 1 and 2 respectively. Accordingly, the two pump inlets in the cold pool are located in control volumes 1 and 5 respectively. The control volumes 3 and 4 represent the remaining 120^0 sector of cold pool (i.e., sectors 3 and 4 together). Control volumes 2, 4 and 6 represent the volume of cold pool falling between the inner vessel redan and main vessel. Sodium flow from the IHX connected to secondary sodium loops 1 and 2 enter the control volumes 1 and 5 respectively. A fraction of sodium flow reaching the control volumes 1 and 5 (Q_{f1} and Q_{f2}) enters and mixes with control volumes 2 and 6 respectively. Same amount of flow is assumed to enter the control volumes 1 and 5 from volumes 2 and 6. This fraction is arrived at based on the results of three dimensional simulation. Further, it is assumed that control volumes 1 and 5 interact with control volume 3 through intermixing of 50 % of IHX flow reaching the control volumes 1 and 5. Equations representing energy balance are given in Equations 3.14 to 3.19. Masses of all the control volumes are treated as constant. Temperature of sodium flow received by Pump 1 and 2 are T_1 and T_5 respectively.

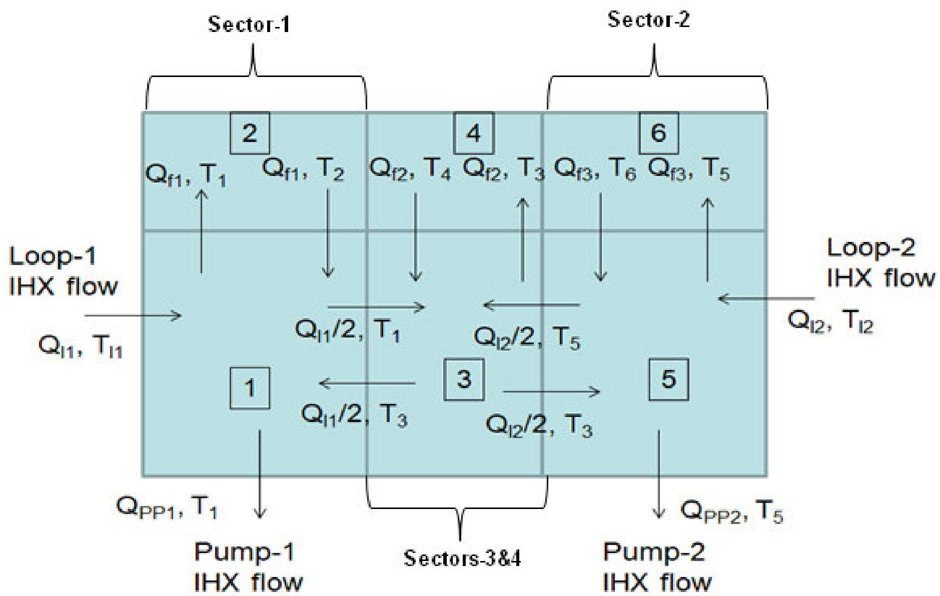

Fig. 3.24 : Representation of four zone model of cold pool

$$\frac{d(M_{CP1}CpT_1)}{dt} = Q_{I1}CpT_{I1} + Q_{F1}CpT_2 + (Q_{I1}/2)CpT_3 - Q_{PP1}CpT_1 - Q_{F1}CpT_1 - (Q_{I1}/2)CpT_1 \qquad (3.14)$$

$$\frac{d(M_{CP2}CpT_2)}{dt} = Q_{F1}CpT_1 - Q_{F1}CpT_2 \qquad (3.15)$$

$$\frac{d(M_{CP3}CpT_3)}{dt} = (Q_{I1}/2)CpT_1 + Q_{F2}CpT_4 + (Q_{I2}/2)CpT_5 - (Q_{I1}/2)CpT_3 - (Q_{I2}/2)CpT_3 - Q_{F2}CpT_3 \qquad (3.16)$$

$$\frac{d(M_{CP4}CpT_4)}{dt} = Q_{F2}CpT_3 - Q_{F2}CpT_4 \qquad (3.17)$$

$$\frac{d(M_{CP5}CpT_5)}{dt} = Q_{I2}CpT_{I2} + Q_{F3}CpT_6 + (Q_{I2}/2)CpT_3 - Q_{PP1}CpT_5 - Q_{F1}CpT_5 - (Q_{I2}/2)CpT_5 \quad (3.18)$$

$$\frac{d(M_{CP6}CpT_6)}{dt} = Q_{F3}CpT_5 - Q_{F3}CpT_6 \quad (3.19)$$

3.4.3 Three Dimensional Model

When the transient thermal hydraulic conditions at the outlet of IHX in both the loops are same (during transients such as reactor SCRAM), then the geometry of cold pool along with boundary conditions are symmetric about 90^0 cylindrical sector. Such scenario can be analysed using 90^0 sector model of cold pool consisting of one IHX and half of a pump included. The main objective of three dimensional model is the representation of direction of flow in the mixing process within the cold pool. The mesh pattern comprising of 50,300 meshes has been selected based on mesh independent analysis carried out between two models, viz., (i) coarse mesh with 50,300 meshes and (ii) fine mesh with 74,800 meshes. Primary sodium flow and temperature conditions predicted by the 1-D code DYANA-P at the IHX outlet are specified as inlet boundary conditions for the 3-D model at an axial location 1 m from the outlet window as shown in Fig. 3.25. Uniform axial velocity is specified at this location. This is to simulate the possible downward axial velocity component of sodium at the exit of the outlet window. Outlet from the 3-D model is specified at the location of pump entry. The volume of stand pipe provided for accommodating the pump and the corresponding sodium volume are not considered in the geometrical model. Similarly, other solid volumes such as spherical header, primary pipes etc. are also not modeled. All the physical walls in the domain are modeled as non-slip adiabatic walls with smooth wall resistance condition. Circumferential end surfaces of the domain are specified as symmetry boundaries. Turbulence is treated through standard high Reynolds number k-ε model with first order upwind scheme adopted for convective terms. Higher order scheme is not adopted in the present study as there are no regions where sharp velocity gradient exists in the cold pool. The Reynolds number of flow is also high enough to justify the usage of upwind scheme. Hence, in order to ensure faster convergence, upwind scheme is adopted. Analysis is carried out using finite volume based unstructured mesh CFD code.

During plant transients which originate from single secondary sodium circuit, the thermal hydraulic conditions at the outlet of IHX connected to the two loops will be different. Analysis of such events requires 180 ^{0} sector model of cold pool consisting of two IHX and two numbers of half pump inlets as shown in Fig. 3.26. Boundary conditions in the domain, viz., inlets, outlets, walls and symmetry boundaries are similar to those described above.

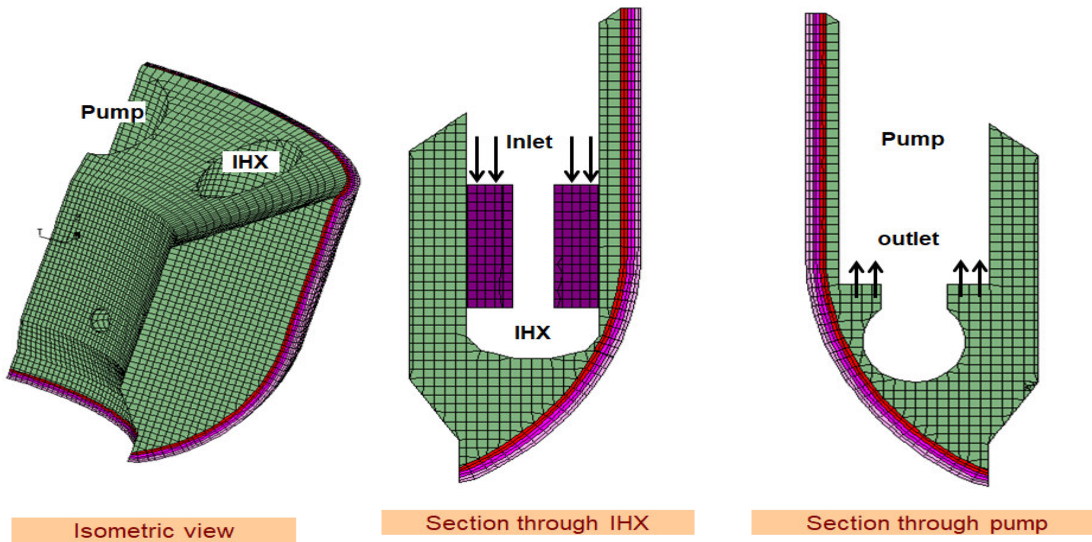

3.25: Model and mesh pattern developed for analysing reactor SCRAM

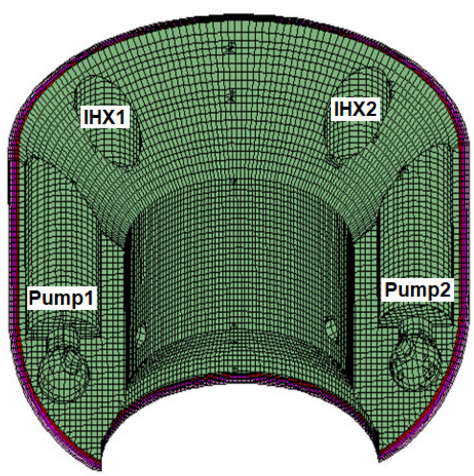

3.26: Model and mesh pattern developed for analysing one secondary sodium pump trip event

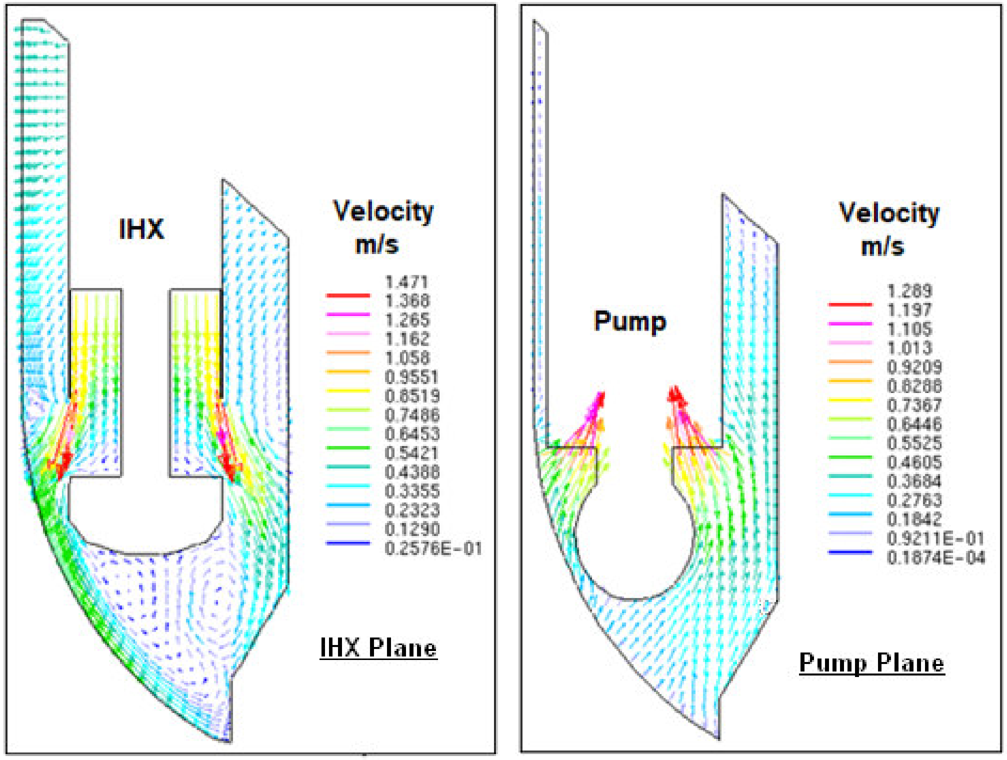

Fig. 3.27: Predicted velocity field in the cold pool along 2 vertical sections during normal operation

3.4.4 Steady State Flow Distribution in Cold pool

Predicted velocity distribution in cold pool during normal operating conditions of reactor in two different circumferential planes passing through IHX and pump are shown in Fig. 3.27. It can be observed that due to the axial downward flow of sodium in the shell side of IHX, the sodium flow entering the cold pool through the outlet window has significant axial component velocity. Outlet window of IHX and pump inlet are located nearly in the same radial as well as axial locations in the cold pool. They are displaced circumferentially by 45 ^{0}. Due to this, the flow exiting from the IHX outlet window has to travel only in the circumferential direction ideally to reach the pump entry. However, due to the significant axial velocity component in the downward direction, the sodium exiting from IHX flows downwards initially and then turns upwards to flow towards pump inlet. Due to this, the region of cold pool above the IHX outlet window does not encounter significant sodium flow velocity. Hence, this region does not participate in the thermal mixing of cold pool in an active manner. This is the motivation behind conceiving a multi zone model for cold pool. It is observed from the analysis of the predicted flow pattern that ~ 10 % of flow emanating from IHX reaches the sodium volume of cold pool between redan portion of inner vessel and main vessel. The value of Q_F in the multi-zone model is selected accordingly.

3.4.4 Transient in Cold Pool during Spurious SCRAM

During this transient, reactor power reduces to decay power conditions within 1 s. Simultaneously, speeds of primary and secondary pumps are reduced to 20 %. Due to sudden reduction in reactor power, temperature of hot pool reduces. As IHX receive sodium from the hot pool, the primary sodium temperature at the outlet of IHX reduces. The flow and temperature evolutions at the outlet of IHX predicted by one dimensional code DYANA-P during this transient is shown in Fig. 3.28. Transient three dimensional analysis of cold pool is carried out by considering the above flow and temperature evolutions at the IHX outlet as boundary conditions.

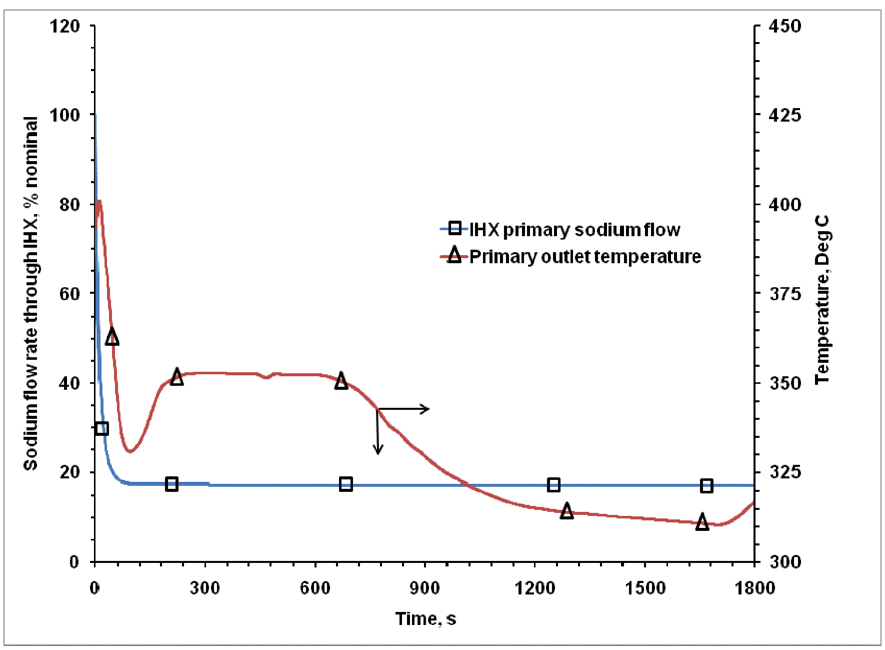

Fig. 3.28: Flow and temperature evolution at the outlet of IHX during spurious SCRAM predicted by DYANA-P

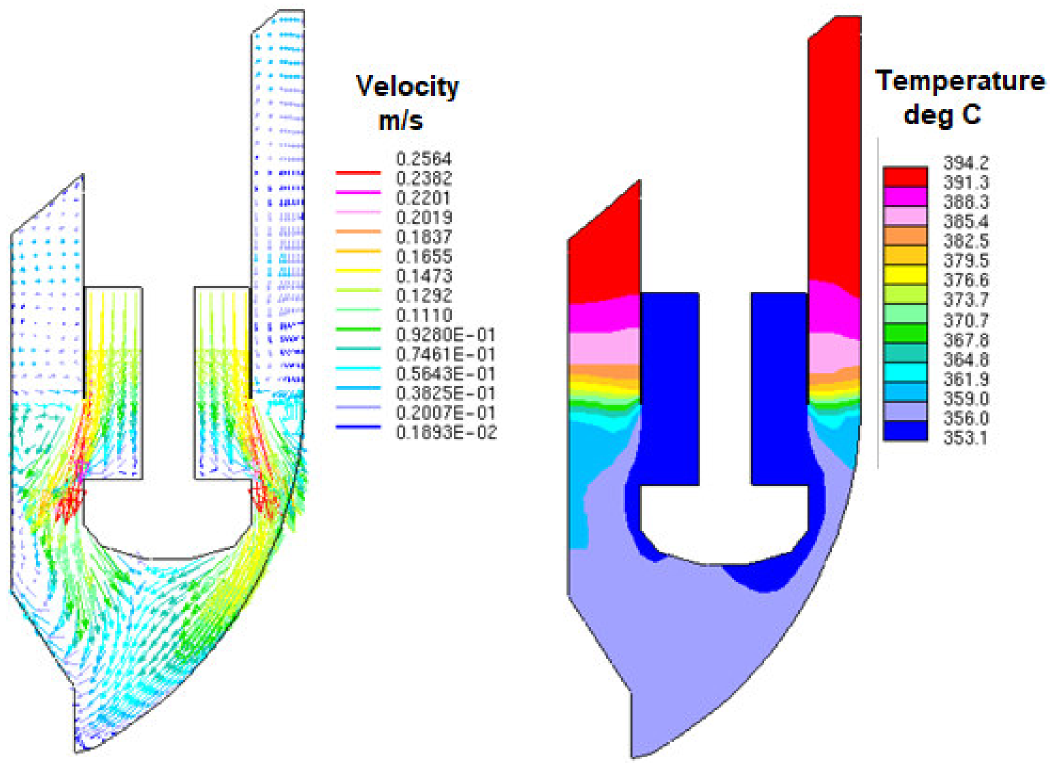

Fig.3.29: Velocity profile and temperature distribution in the plane through IHX at 300 s during spurious SCRAM

From the system dynamics simulation point of view, the parameter of importance is temperature evolution at the suction of primary sodium pump. The predicted velocity and temperature distributions predicted in the plane through IHX at 300 s are shown in Fig. 3.29. It can be observed that the velocity magnitude is reduced compared that during normal operating conditions of the reactor (Fig. 3.27) due to the speed reduction action taken on the pumps. However, there is significant downward (axial) component of velocity at the outlet of IHX which is similar to that during normal operating condition. Therefore, the upper region of cold pool around the redan portion of inner vessel is thermally stratified due to very low amount of flow from IHX reaching this region. Temperature of this region changes relatively slowly compared to the lower region. Temperature of this region reduces only by 3 ^{0}C in

300 s, whereas that of the bottom region reduces by as high as 44 ^{0}C. This justifies the sub-division of cold pool volume into two zones in the axial direction in the multi zone model.

Temperature evolutions at the inlet of pump predicted by the three dimensional, single zone and multi zone models are shown in Fig. 3.30. The average inlet temperature corresponds to flow weighted average at the entry of pump in the three dimensional model. In the single zone model, the mixed mean temperature of cold pool represents the temperature of sodium entering the IHX, whereas in the multi zone model it is temperature of control volumes of 1 or 5. It can be observed that there is large deviation between the temperature evolutions predicted by the three dimensional and single control volume model. The multi zone model predictions are close to that predicted by the three dimensional model. Thus, the six control volume model is able to represent the mixing as well as stratification behavior of cold pool in a more realistic manner compared to the single control volume model. Thus, the multi zone model simulates the thermal hydraulic behavior of cold pool during spurious SCRAM event in a realistic manner compared to single zone model.

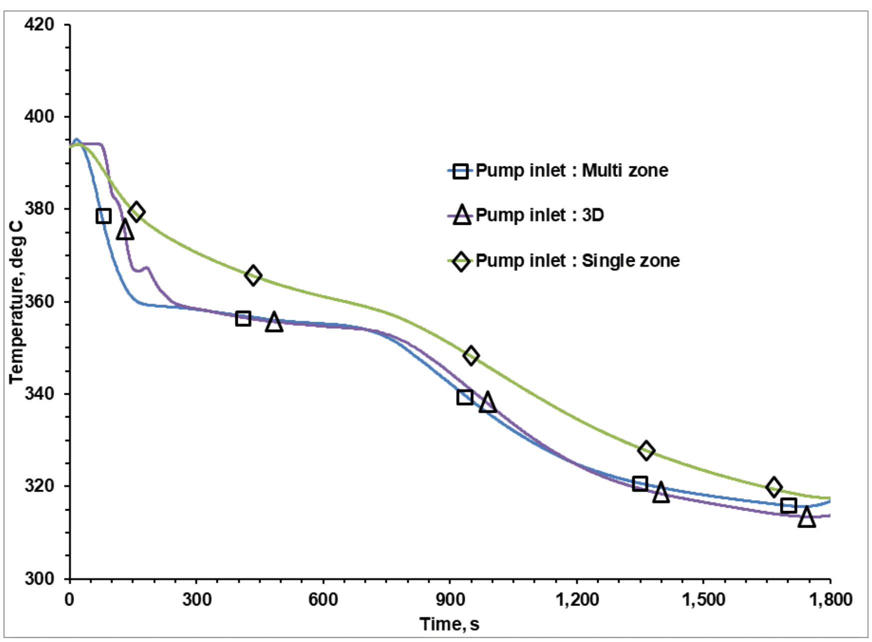

Fig. 3.30: Temperature evolution at the inlet of pump predicted by various models during spurious SCRAM

3.4.5 Transient in Cold Pool during One Secondary Sodium Pump Trip

Trip of secondary sodium pump in one loop causes reduction in cooling of IHX of the affected loop. Due to this, temperature of primary sodium at the outlet of IHX in the affected loop increases and that of the unaffected loop remains nearly unchanged. The increase in temperature of primary sodium reaching the cold pool through two IHX ultimately results in temperature increase of primary sodium entering the pump. Once this temperature increases above the initial steady state value by 10 ^{0}C, reactor SCRAM takes place. Along with reactor SCRAM, coast down of speeds of primary and secondary sodium pumps to 20 % also takes place. Reactor SCRAM is considered to take place at 30 s in the present analysis. DYANA-P predicts the temperature evolution at the inlet of pump through single control volume mixing model for cold pool. The evolution of primary sodium flow and temperature predicted by DYANA-P at the outlet of IHX of the two loops is shown in Figs. 3.31 and 3.32 respectively.

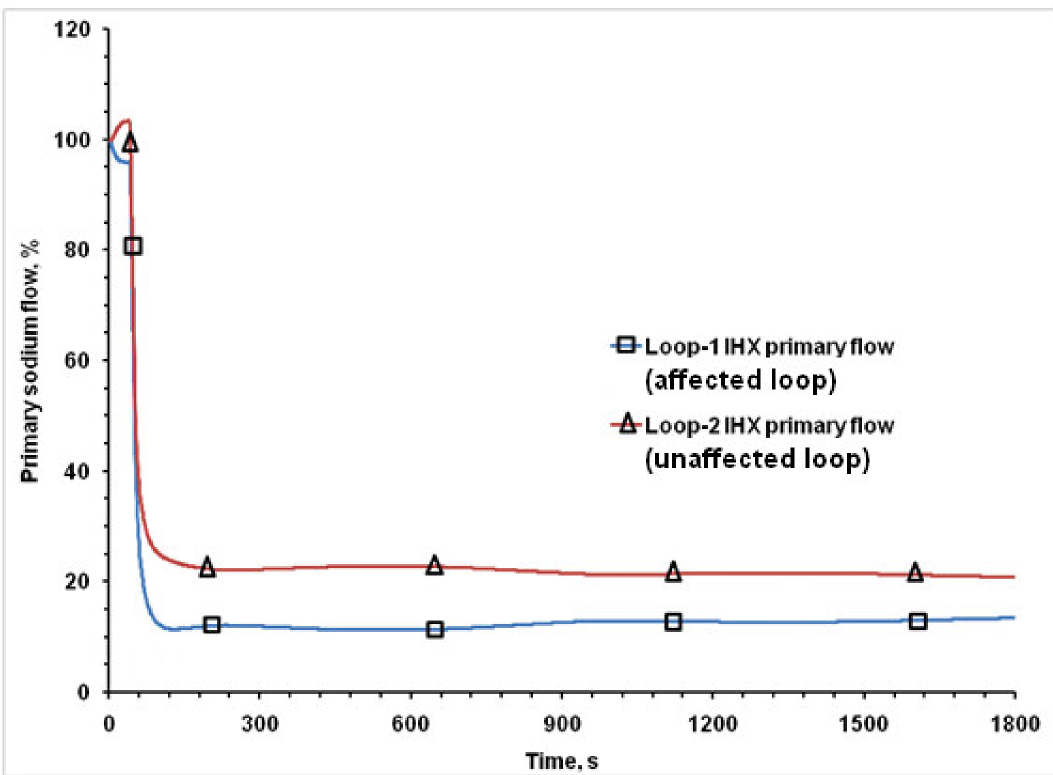

Fig. 3.31: Primary sodium flow evolution through IHX of two loops predicted by DYANA-P during one secondary pump trip

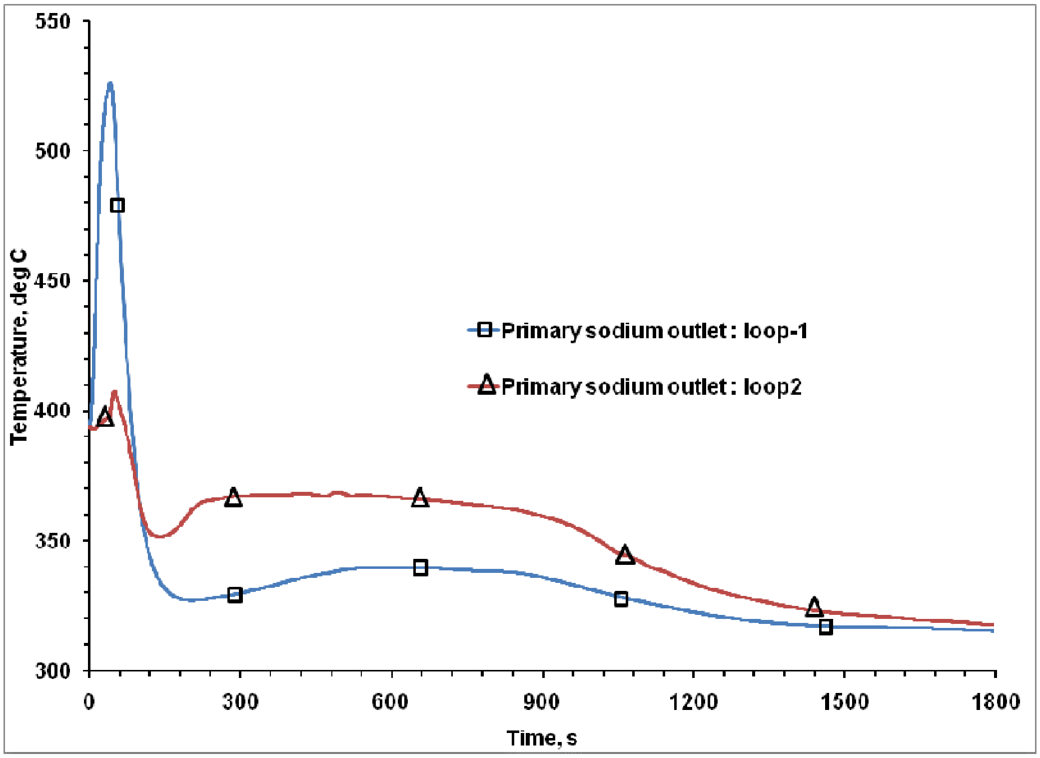

Fig. 3.32 : Temperature evolution at the primary outlet of IHX of the two loop predicted by DYANA-P during one secondary sodium pump trip

It can be observed that due to the difference in the thermal conditions of the primary sides of the IHX of the two loops, the buoyancy conditions prevailing in the primary side of the IHX are also different. Due to this, primary sodium flows through the IHX of two loops are different as evident in Fig. 3.31. The IHX of the unaffected loop-2 receives higher primary sodium flow compared to the loop-1 IHX. Three dimensional simulation of this transient is carried out using the 180^0 sector model of cold pool as discussed in section 3.4.3. Flow and temperature evolutions obtained from DYANA-P code are used as input boundary conditions at the IHX-1 and IHX-2 exit locations in the model.

Temperature distribution predicted in cold pool at 300 s after one secondary sodium pump trip is shown in Figs. 3.33 and 3.34. It can be observed that the sodium exiting through the IHX of the affected loop (IHX-1) is significantly hotter than that exiting through the IHX of the unaffected loop (IHX-2). Pump-1 is located close to the IHX of the affected loop.

Hence, the primary sodium received by Pump-1 is hotter that that received by Pump-2. The predicted evolutions of sodium temperature at the inlets of Pump 1 and Pump 2 in the primary sodium circuit during the transient are shown in Figs. 3.35 and 3.36 respectively.

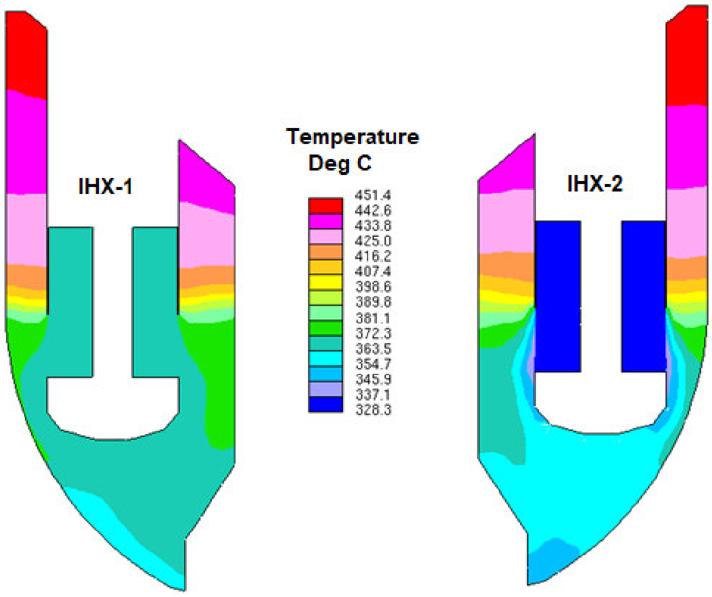

Fig. 3.33: Temperature distribution in cold pool in the planes passing through affected and unaffected Loop IHXs (IHX-1 and IHX-2) at 300 s after one secondary sodium pump trip

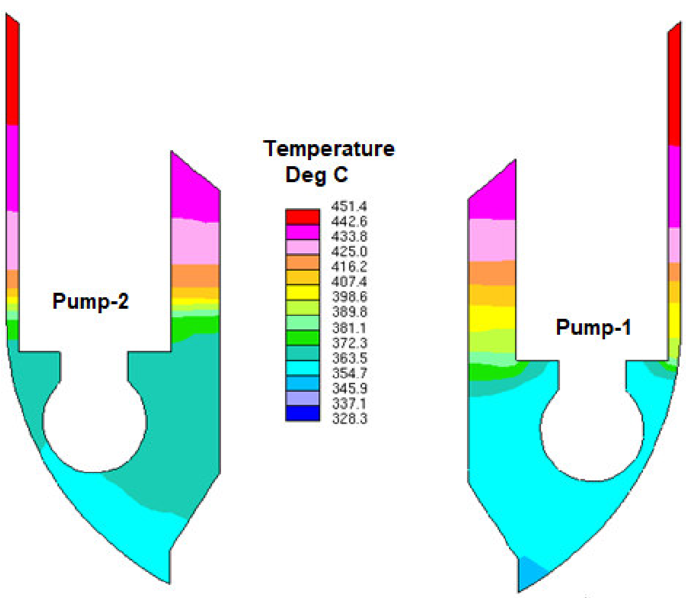

Fig. 3.34: Temperature distribution in cold pool in the planes passing through Pump -1 and Pump-2 at 300 s after one secondary sodium pump trip

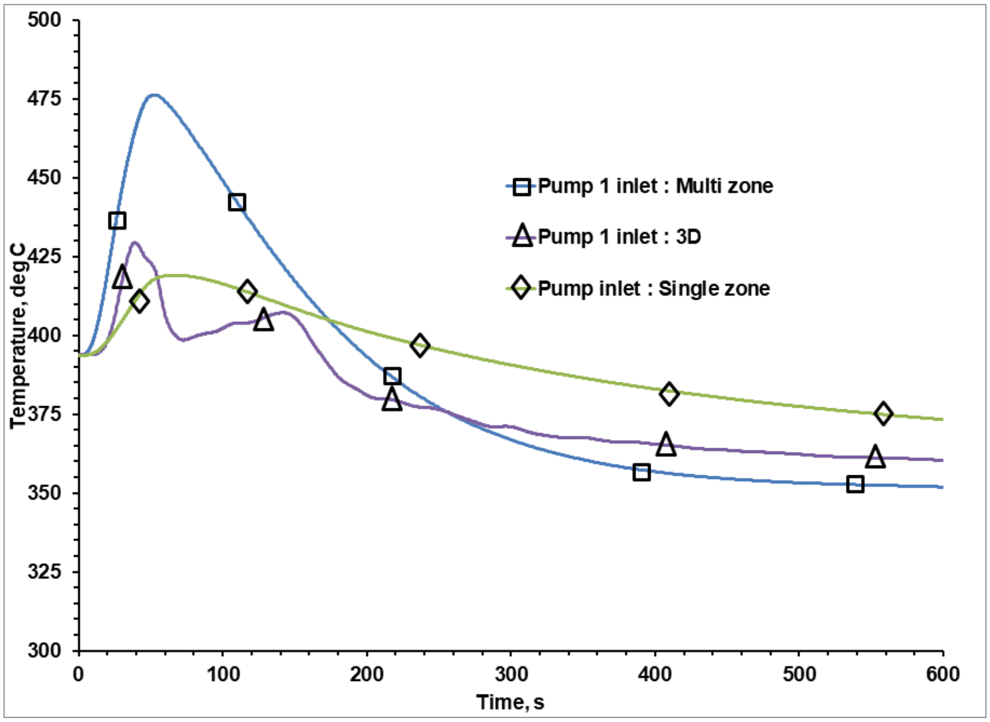

Fig. 3.35: Predicted evolution of sodium temperature at inlet of Pump 1 during one secondary pump trip

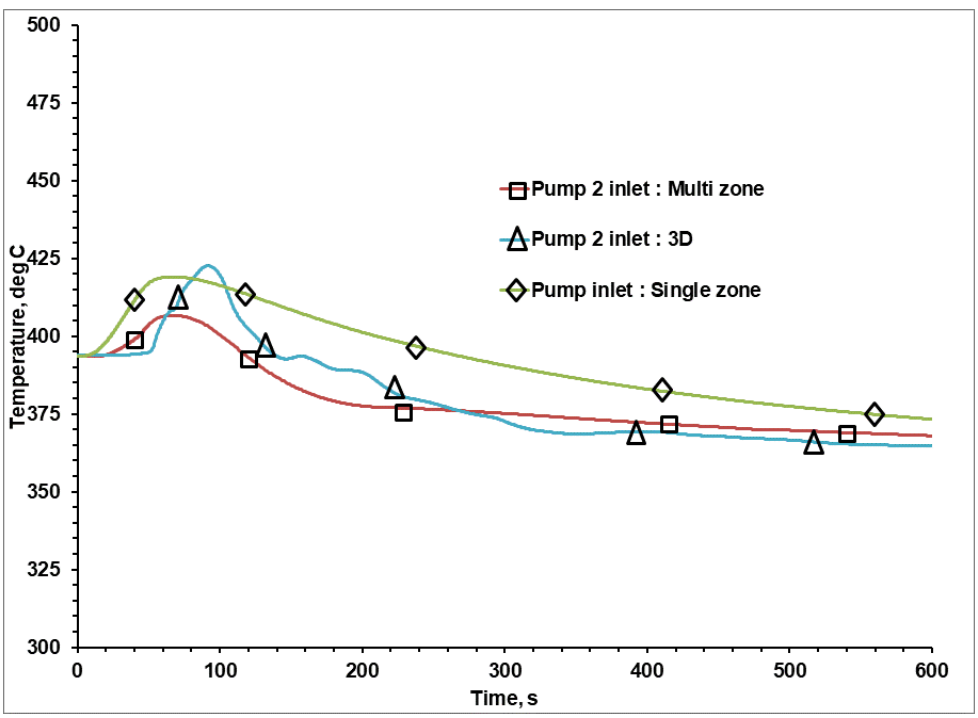

Fig. 3.36: Predicted evolution of sodium temperature at inlet of Pump 2 during one secondary pump trip

The single zone model under predicts the temperature evolution at the inlet of Pump-1 and over predicts the temperature evolution at the inlet of Pump-2 compared to the predictions by the three dimensional model. There is over prediction by the multi-zone model at the Pump-1 location and under prediction at the Pump-2 location. From reactor safety point of view, the important parameter is the time at which the sodium temperature entering the pump increases by 10 ^{0}C above the initial value. Automatic SCRAM of the reactor is based on this signal. Hence, the SCRAM demand time predicted by the three dimensional model is 24.5 s. The same predicted by the multi-zone and single zone models are 14 s and 30 s respectively. Thus, as far as the prediction of SCRAM demand time is concerned, the multi-zone model predictions are not conservative from the point of view of reactor safety. However, the prediction by the single zone model is conservative since it is delayed by 5.5 s compared to the three dimensional model predictions. Thus, it can be concluded that as far as one loop events are concerned, the predictions by the multi-zone model are neither conservative nor realistic. For accurate prediction of thermal transients during events affecting single secondary sodium loop, three dimensional modeling of cold pool is essential. Since, temperature at the inlet of the two pumps are different, grid plate also receives sodium at different thermal conditions from the primary pipes connected to each pump. Thermal mixing of primary sodium flow in the grid plate is another aspect to be addressed in the plant dynamics studies. This is beyond the scope of the present investigations.

3.5 CLOSURE

Thermal hydraulic studies on hot pool during plant transients involving thermal stratification indicate that 2-D axi-symmetric modeling can predict thermal stratification phenomenon very similar to that of three dimensional model predictions. The deviations between axi-symmetric and three dimensional model predictions are acceptable for plant dynamics studies while comparing against the large computational effort associated with three dimensional studies. Hence, axi-symmetric model for hot pool is recommended for plant dynamics studies. Comparison of transient phenomenon predicted in the cold pool with single zone, multi-zone and three dimensional models has brought out the advantages and disadvantages of the multi-zone model. Multi-zone model can realistically predict the thermal hydraulics in cold pool during events in which both the secondary sodium loops participate in a similar manner. However, this model is not conservative for transients originating from one secondary sodium loop. Hence, for accurate representation of transients in the cold pool, three dimensional modeling is essential. Development of axi-symmetric modeling of hot pool for linking with one dimensional modeling of the rest of the plant is taken up as the next activity in the thesis.

CHAPTER – 4

DEVELOPMENT OF HYBRID CODE

4.1 AXI-SYMMETRIC CFD CODESTITH-2D

Detailed knowledge of velocity and temperature distributions in the pool is essential for thermal hydraulic and structural design of SFR. Such information can be derived through the solution of governing equations representing fluid flow and heat transfer in multi-dimensional geometry. A two dimensional computational fluid dynamics (CFD) code named 'STITH-2D' (Structured Turbulent Induced Thermal Hydraulics) has been developed for solving the governing equations in Cylindrical coordinate system using Finite Volume Method (FVM). Details of governing equations, their discretization and method of solutions are presented in this section. Important features of the code are presented in Table 4.1.

Table 4.1: Important features of STITH-2D

Sl. No.	Feature	Details
1	Geometrical modeling	Cartesian and Cylindrical
2	Simulation	Steady state and Transient
3	Buoyancy modeling	Boussinesq assumption
4	Discretization of governing equations	Finite Volume Method (FVM)
5	Schemes for convective terms	Central difference, Upwind, Hybrid and Power law
6	Algorithm for pressure velocity coupling	SIMPLE
7	Turbulence model	Standard k-ε model
8	Solution of discretized equations	Line by line method (TDMA)

4.2 GOVERNING EQUATIONS

Equations governing fluid flow and heat transfer in two dimensional geometry are presented below [43].

4.2.1 Cartesian Coordinate System

Conservation of mass:

$$\frac{\partial \rho}{\partial t}+\frac{\partial}{\partial x}(\rho U)+\frac{\partial}{\partial y}(\rho V)=0 \tag{4.1}$$

Conservation of momentum

$$\rho\left(\frac{\partial U}{\partial t}+U\frac{\partial U}{\partial x}+V\frac{\partial U}{\partial y}\right)=-\frac{\partial P}{\partial x}+\frac{\partial}{\partial x}\left(\mu_{eff}\frac{\partial U}{\partial x}\right)+\frac{\partial}{\partial y}\left(\mu_{eff}\frac{\partial U}{\partial y}\right)+S_U \tag{4.2}$$

$$\rho\left(\frac{\partial V}{\partial t}+U\frac{\partial V}{\partial x}+V\frac{\partial V}{\partial y}\right)=-\frac{\partial P}{\partial y}+\frac{\partial}{\partial x}\left(\mu_{eff}\frac{\partial V}{\partial x}\right)+\frac{\partial}{\partial y}\left(\mu_{eff}\frac{\partial V}{\partial y}\right)+S_V \tag{4.3}$$

Conservation of Energy

$$\rho Cp\left(\frac{\partial T}{\partial t}+U\frac{\partial T}{\partial x}+V\frac{\partial T}{\partial y}\right)=\frac{\partial}{\partial x}\left(K_{eff}\frac{\partial T}{\partial x}\right)+\frac{\partial}{\partial y}\left(K_{eff}\frac{\partial T}{\partial y}\right)+S_T \tag{4.4}$$

Turbulence modeling

$$\frac{\partial}{\partial t}(\rho k)+\frac{\partial}{\partial x}(\rho Uk)+\frac{\partial}{\partial y}(\rho Vk)=\frac{\partial}{\partial x}\left[\left(\mu+\frac{\mu_t}{\sigma_k}\right)\frac{\partial k}{\partial x}\right]+\frac{\partial}{\partial y}\left[\left(\mu+\frac{\mu_t}{\sigma_k}\right)\frac{\partial k}{\partial y}\right]+P_k+G_k-\rho\varepsilon \tag{4.5}$$

$$\frac{\partial}{\partial t}(\rho\varepsilon)+\frac{\partial}{\partial x}(\rho U\varepsilon)+\frac{\partial}{\partial y}(\rho V\varepsilon)=\frac{\partial}{\partial x}\left[\left(\mu+\frac{\mu_t}{\sigma_\varepsilon}\right)\frac{\partial \varepsilon}{\partial x}\right]+\frac{\partial}{\partial y}\left[\left(\mu+\frac{\mu_t}{\sigma_\varepsilon}\right)\frac{\partial \varepsilon}{\partial y}\right]+\left[C_{\varepsilon1}(P_k+C_{\varepsilon3}G_k)-C_{\varepsilon2}\rho\varepsilon\right]\frac{\varepsilon}{k} \tag{4.6}$$

Where

$$P_k=\mu_t\left[2\left(\frac{\partial U}{\partial x}\right)^2+2\left(\frac{\partial V}{\partial y}\right)^2+\left(\frac{\partial U}{\partial y}+\frac{\partial V}{\partial x}\right)^2\right] \qquad G_k=-\frac{\mu_t}{\sigma_t}g\beta\frac{\partial T}{\partial y}$$

$\mu_{eff}=\mu+\mu_t$ $\mu_t=C_\mu\frac{\rho k^2}{\varepsilon}$ and $K_{eff}=K+\frac{\mu_t C_p}{\sigma_t}$

As recommended by Markatos and Pericleous [44], various constants pertaining to the turbulence model have been selected as C_μ = 0.09, $C_{\varepsilon1}$ = 1.44, $C_{\varepsilon2}$ = 1.92, σ_t = 1.0, σ_k = 1.0 and σ_ε = 1.3. $C_{\varepsilon3}$ is taken as tanh(V/U). σ_t, σ_k and $\sigma_\varepsilon$are turbulent Prandtl numbers for energy transfer, k and ε. Above values for the constants and Prandtl numbers are suggested for fluids having Prandtl number in the order of unity. These values need to be improved for accurate simulation of near wall effects in low Prandtl number cases as reported by Jackson et al. [45]. Studies by Kawamura et al. [46] indicate that the turbulent Prandtl number (σ_t) for liquid metal reduces from about 3, close to the wall, to unity far away from the wall. Present study focuses on turbulent mixing phenomenon in bulk of the pool. Hence the use of turbulent Prandtl number as unity is justified.

4.2.2 Cylindrical Coordinate System (r-Z)

Conservation of mass:

$$\frac{\partial \rho}{\partial t}+\frac{1}{r}\frac{\partial}{\partial r}(\rho r U)+\frac{\partial}{\partial z}(\rho V)=0 \tag{4.7}$$

Conservation of momentum

$$\rho\left(\frac{\partial U}{\partial t}+U\frac{\partial U}{\partial r}+V\frac{\partial U}{\partial z}\right)=-\frac{\partial P}{\partial r}+\left[\frac{\partial}{\partial r}\left(\frac{\mu_{eff}}{r}\frac{\partial}{\partial r}(rU)\right)+\frac{\partial}{\partial z}\left(\mu_{eff}\frac{\partial U}{\partial z}\right)\right]+S_U \tag{4.8}$$

$$\rho\left(\frac{\partial V}{\partial t}+U\frac{\partial V}{\partial r}+V\frac{\partial V}{\partial z}\right)=-\frac{\partial P}{\partial z}+\left[\frac{1}{r}\frac{\partial}{\partial r}\left(r\mu_{eff}\frac{\partial V}{\partial r}\right)+\frac{\partial}{\partial z}\left(\mu_{eff}\frac{\partial V}{\partial z}\right)\right]+S_V \tag{4.9}$$

Conservation of Energy

$$\rho Cp\left(\frac{\partial T}{\partial t}+U\frac{\partial T}{\partial r}+V\frac{\partial T}{\partial z}\right)=\left[\frac{1}{r}\frac{\partial}{\partial r}\left(rK_{eff}\frac{\partial T}{\partial r}\right)+\frac{\partial}{\partial z}\left(K_{eff}\frac{\partial T}{\partial z}\right)\right]+S_T \tag{4.10}$$

Turbulence modeling

$$\rho\left(\frac{\partial k}{\partial t}+U\frac{\partial k}{\partial r}+V\frac{\partial k}{\partial z}\right)=\left[\frac{1}{r}\frac{\partial}{\partial r}\left(r\left[\mu+\frac{\mu_t}{\sigma_k}\right]\frac{\partial k}{\partial r}\right)+\frac{\partial}{\partial z}\left(\left[\mu+\frac{\mu_t}{\sigma_k}\right]\frac{\partial T}{\partial z}\right)\right]+P_k+G_k-\rho\varepsilon \tag{4.11}$$

$$\rho\left(\frac{\partial \varepsilon}{\partial t}+U\frac{\partial \varepsilon}{\partial r}+V\frac{\partial \varepsilon}{\partial z}\right)=\left[\frac{1}{r}\frac{\partial}{\partial r}\left(r\left[\mu+\frac{\mu_t}{\sigma_\varepsilon}\right]\frac{\partial \varepsilon}{\partial r}\right)+\frac{\partial}{\partial z}\left(\left[\mu+\frac{\mu_t}{\sigma_\varepsilon}\right]\frac{\partial \varepsilon}{\partial z}\right)\right]+[\mathrm{C}_{\varepsilon 1}(P_k+C_{\varepsilon 3}G_k)-C_{\varepsilon 2}\rho\varepsilon]\frac{\varepsilon}{k} \tag{4.12}$$

Where

$$P_k = \mu_t \left[2\left(\frac{\partial U}{\partial r}\right)^2 + 2\left(\frac{\partial V}{\partial z}\right)^2 + \left(\frac{\partial U}{\partial r} + \frac{\partial V}{\partial z}\right)^2 + \frac{U^2}{r^2} \right] \qquad G_k = -\frac{\mu_t}{\sigma_t} g\beta \frac{\partial T}{\partial z}$$

The source term in the axial momentum equation (S_V) includes buoyancy induced momentum source (S_{VB}), which is calculated based on Boussinesq approximation [47] as,

$$S_{VB} = \rho\beta g_y \left[T - T_{ref}\right] \tag{4.13}$$

Where T_{ref} is the reference temperature for estimation of buoyancy effects in the domain. The temperature difference that sodium in the domain is likely to face during the time period of calculation is ~ 200 ^{0}C. The corresponding value of ($\beta\times\Delta T$) is ~ 0.05. Hence, the Boussinesq approximation is valid. The applicability of Boussinesq approximation for the theoretical simulation of thermally stratified liquid sodium flow in the SUPERCAVNA facility has been demonstrated by Bieder et al. [48].

4.3 DISCRETIZATION OF GOVERNING EQUATIONS

The finite volume method (FVM) is a discretization method which is well suited for the numerical solution of conservation equations governing fluid flow and heat transfer [41]. An important feature of FVM is ensuring of local conservation of fluxes in various discretizations cells considered for solution. Discretization cells considered are called control volumes. That is, the numerical flux is conserved from one control volume to its neighbors. Thus, the FVM always gives physically realistic solution and therefore is very attractive for modeling problems in which conservation of flux is of importance such as in fluid mechanics and heat & mass transfer. In STITH-2D, the governing partial differential equations are discretized based on FVM. Further, mesh staggering approach is adopted between continuity and momentum balance equations to avoid pressure-velocity decoupling in the solution. In this approach, fluid pressure and temperature are stored at one grid point and flow velocities are stored at different grid points. These grid points are staggered by half the width of control volume. The representation of grid points for U-momentum and V-momentum equations are shown in Figs. 4.1 and 4.2 respectively. Properties of fluid are stored at the node where pressure and temperature are represented. Fluid properties are considered to be constant in the formulation corresponding to that at average temperature. The influence of buoyancy force on the fluid flow is modeled through Boussinesq approximation. The discretized form of governing equations in cylindrical coordinate system are discussed below.

U-momentum (Fig. 4.1)

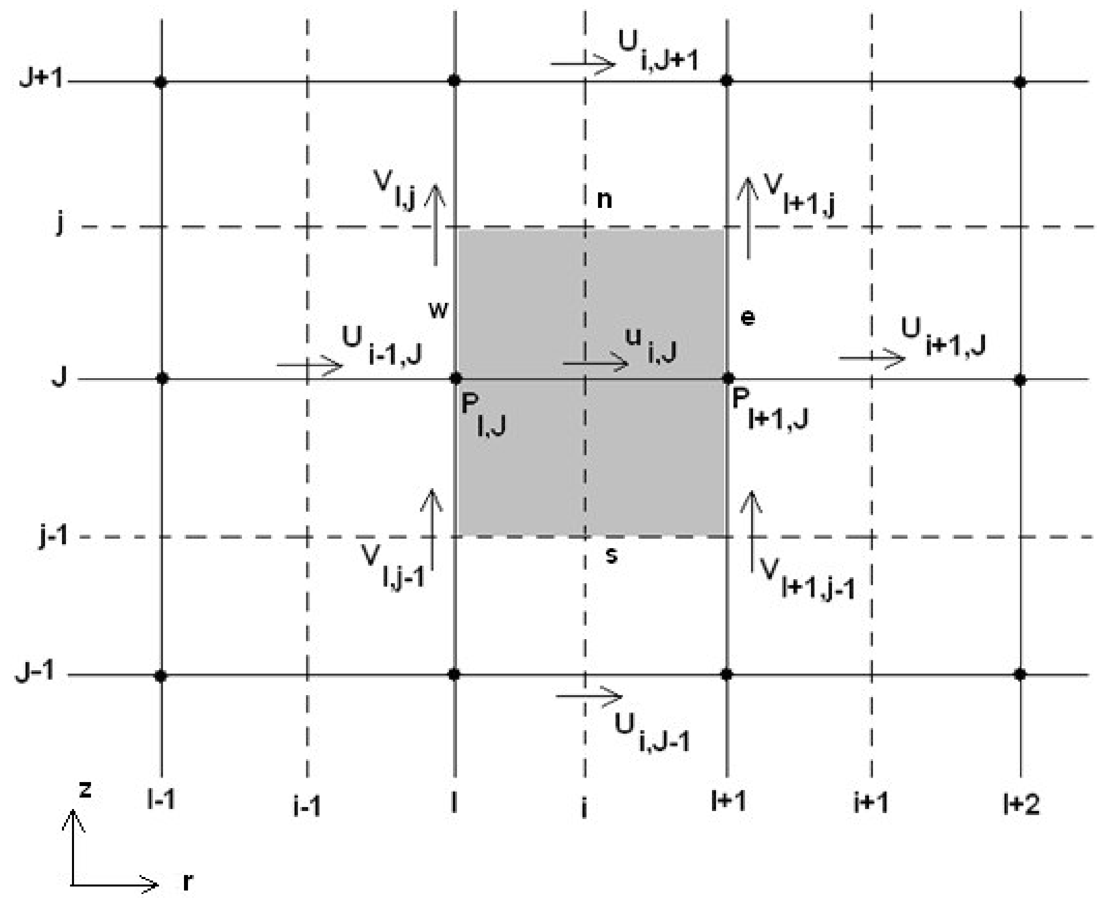

Fig. 4.1: Representation of control volume for U

$$a_P U_{i,J} = a_E U_{i+1,J} + a_W U_{i-1,J} + a_N U_{i,J+1} + a_S U_{i,J-1} + b_{i,J} \tag{4.14}$$

Where the coefficients a_P, a_E, a_W, a_N and a_S are evaluated based on convective and diffusive fluxed at the boundary of control volumes given by,

$$F_e = (\rho AU)_e = \frac{(\rho AU)_{i+1,J} + (\rho AU)_{i,J}}{2}$$
$$= r_J \frac{(r_j - r_{j-1})}{2} \left[\rho U_{i+1,J} + \rho U_{i,J}\right] \tag{4.15}$$

$$F_w = (\rho AU)_w = \frac{(\rho AU)_{i,J} + (\rho AU)_{i-1,J}}{2}$$
$$= r_J \frac{(r_j - r_{j-1})}{2} \left[\rho U_{i,J} + \rho U_{i-1,J}\right] \tag{4.16}$$

$$F_n = (\rho AV)_n = \frac{(\rho AV)_{I,j} + (\rho AV)_{I+1,j}}{2}$$
$$= r_j \frac{(z_{I+1} - z_I)}{2} \left[\rho V_{I,j} + \rho V_{I+1,j}\right] \tag{4.17}$$

$$F_s = (\rho AV)_s = \frac{(\rho AV)_{I,j-1} + (\rho AV)_{I+1,j-1}}{2}$$
$$= r_{j-1} \frac{(z_{I+1} - z_I)}{2} \left[\rho V_{I,j-1} + \rho V_{I+1,j-1}\right] \tag{4.18}$$

$$D_e = r_J \frac{\mu_{I+1,J}(r_j - r_{j-1})}{z_{i+1} - z_i} \tag{4.19}$$

$$D_w = r_J \frac{\mu_{I,J}(r_j - r_{j-1})}{z_i - z_{i-1}} \tag{4.20}$$

$$D_n = r_j \frac{\mu_{I,J} + \mu_{I+1,J} + \mu_{I,J+1} + \mu_{I+1,J+1}}{4} \frac{(z_{I+1} - z_I)}{(r_{J+1} - r_J)} \tag{4.21}$$

$$D_s = r_{j-1} \frac{\mu_{I,J} + \mu_{I+1,J} + \mu_{I,J-1} + \mu_{I+1,J-1}}{4} \frac{(z_{I+1} - z_I)}{(r_J - r_{J-1})} \tag{4.22}$$

Now, the coefficients a_P, a_E, a_W, a_N and a_S are calculated based on equations (4.23) to (4.28) depending on the numerical scheme adopted for representing the profile variation between nodal points.

$$a_E = D_e A(|P_e|) + Max(-F_e, 0) \tag{4.23}$$

$$a_W = D_w A(|P_w|) + Max(F_w, 0) \tag{4.24}$$

$$a_N = D_n A(|P_n|) + Max(-F_n, 0) \tag{4.25}$$

$$a_S = D_s A(|P_s|) + Max(F_s, 0) \quad (4.26)$$

Where P represents the cell Reynolds number given by

$$P_e = \frac{\rho U_e (x_{i+1} - x_i)}{\mu_e} = \frac{\rho (U_{i,J} + U_{i+1,J})}{2} \frac{(x_{i+1} - x_i)}{\mu_{I+1,J}} \quad (4.27)$$

Values of A(|Pe|) for various schemes are given by Table 4.2.

Table 4.2: Function A(|Pe|) for various schemes

Sl. No.	Scheme	Formula for A(|Pe|)
1	Central difference	1-0.5 |Pe|
2	Upwind	1
3	Hybrid	Max (0, 1-0.5 |Pe|)
4	Power law	Max (0, (1-0.1 |Pe|)^5)

$$a_P = a_E + a_W + a_N + a_S + F_e + F_n - F_w - F_s + \rho r_J (z_{I+1} - z_I)(r_j - r_{j-1}) \frac{1}{\Delta t} \quad (4.28)$$

$$b_{i,J} = (P_{I,J} - P_{I+1,J}) r_J (r_j - r_{j-1}) - \Gamma U_{i,J} (r_j - r_{j-1})(z_{I+1} - z_I) \frac{1}{y_J} + S_u r_J (r_j - r_{j-1})(z_{I+1} - z_I)$$
$$+ \rho r_J (r_j - r_{j-1})(z_{I+1} - z_I) U^0{}_{i,J} \frac{1}{\Delta t} \quad (4.29)$$

For steady state solution, last terms in the RHS of eqns. (4.28) and (4.29) are not required to be considered.

<u>V-momentum (Fig. 4.2)</u>

$$a_P V_{I,j} = a_E V_{I+1,j} + a_W V_{I-1,j} + a_N V_{I,j+1} + a_S V_{I,j-1} + b_{I,j} \quad (4.30)$$

Where the coefficients a_P, a_E, a_W, a_N and a_S are evaluated based on convective and diffusive fluxed at the boundary of control volumes given by,

$$F_e = (\rho A U)_e = \frac{(\rho A U)_{i,J} + (\rho A U)_{i,J+1}}{2}$$
$$= r_j \frac{(r_{J+1} - r_J)}{2} \left[\rho U_{i,J} + \rho U_{i,J+1}\right] \quad (4.31)$$

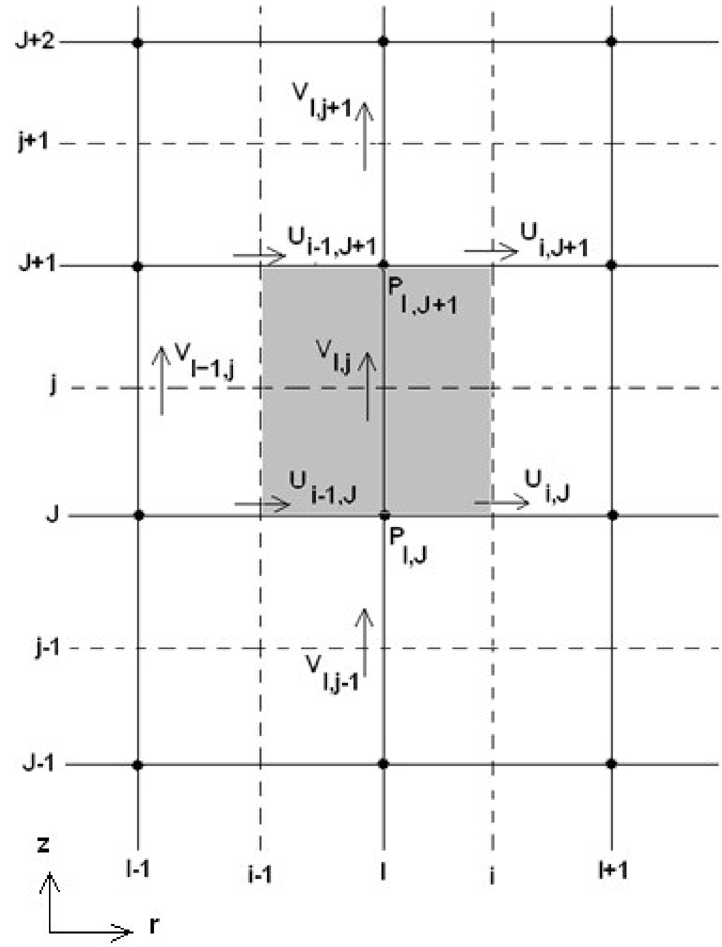

Fig. 4.2: Representation of control volume for V

$$F_w = (\rho AU)_w = \frac{(\rho AU)_{i-1,J} + (\rho AU)_{i-1,J+1}}{2} \tag{4.32}$$
$$= r_j \frac{(r_{J+1} - r_J)}{2}\left[\rho U_{i-1,J} + \rho U_{i-1,J+1}\right]$$

$$F_n = (\rho AV)_n = \frac{(\rho AV)_{I,j} + (\rho AV)_{I,j+1}}{2} \tag{4.33}$$
$$= r_{J+1} \frac{(z_i - z_{i-1})}{2}\left[\rho V_{I,j} + \rho V_{I,j+1}\right]$$

$$F_s = (\rho AV)_s = \frac{(\rho AV)_{I,j-1} + (\rho AV)_{I,j}}{2} \tag{4.34}$$
$$= r_J \frac{(z_i - z_{i-1})}{2}\left[\rho V_{I,j-1} + \rho V_{I,j}\right]$$

$$D_e = \frac{\mu_{I,J+1} + \mu_{I,J} + \mu_{I+1,J+1} + \mu_{I+1,J}}{4} r_j \frac{(r_{J+1} - r_J)}{z_{I+1} - z_I} \tag{4.35}$$

$$D_w = \frac{\mu_{I-1,J+1} + \mu_{I-1,J} + \mu_{I,J+1} + \mu_{I,J}}{4} r_j \frac{(r_{J+1} - r_J)}{z_I - z_{I-1}} \tag{4.36}$$

$$D_n = \frac{\mu_{I,J+1} r_{J+1} (z_i - z_{i-1})}{r_{j+1} - r_j} \tag{4.37}$$

$$D_s = \frac{\mu_{I,J} y_J (x_i - x_{i-1})}{y_j - y_{j-1}} \tag{4.38}$$

Now, the coefficients a_P, a_E, a_W, a_N and a_S are calculated based on eqns. (4.23) – (4.28) and Table 4.2 depending on the numerical scheme adopted for representing the profile variation between nodal points.

$$a_P = a_E + a_W + a_N + a_S + F_e + F_n - F_w - F_s + \rho r_j (z_i - z_{i-1})(r_{J+1} - r_J) \frac{1}{\Delta t} \tag{4.39}$$

$$b_{I,j} = (P_{I,J} - P_{I,J+1}) r_j (z_i - z_{i-1}) + S_V y_j (z_i - z_{i-1})(r_{J+1} - r_J) + \rho r_j (z_i - z_{i-1})(r_{J+1} - r_J) V^0{}_{I,j} \frac{1}{\Delta t} \tag{4.40}$$

For steady state solution, the last term of equations (4.39) and (4.40) are not required to be considered.

<u>Continuity (Fig. 4.3)</u>

By using a guessed pressure field, P^*, momentum balance equations can be solved for an approximate velocity field. The approximate solution of velocity field does not necessarily satisfy the continuity equation. In order to impose the restriction from the continuity equation the following pressure correction equation (Poisson equation) can be formulated.

$$\nabla^2 P' = \frac{1}{\Delta t} \nabla . \mathrm{U} \tag{4.41}$$

Where p' is the correction for P* to obtain the true pressure field

$$a_P P'_{I,J} = a_E P'_{I+1,J} + a_W P'_{I-1,J} + a_N P'_{I,J+1} + a_S P'_{I,J-1} + b'_{I,J} \tag{4.42}$$

$$a_E = (\rho dA)_{i,J} = \rho \frac{r_J (r_j - r_{j-1})}{a_{P(i,J)}} r_J (r_j - r_{j-1}) \tag{4.43}$$

$$a_W = (\rho dA)_{i-1,J} = \rho \frac{r_J (r_j - r_{j-1})}{a_{P(i-1,J)}} r_J (r_j - r_{j-1}) \tag{4.44}$$

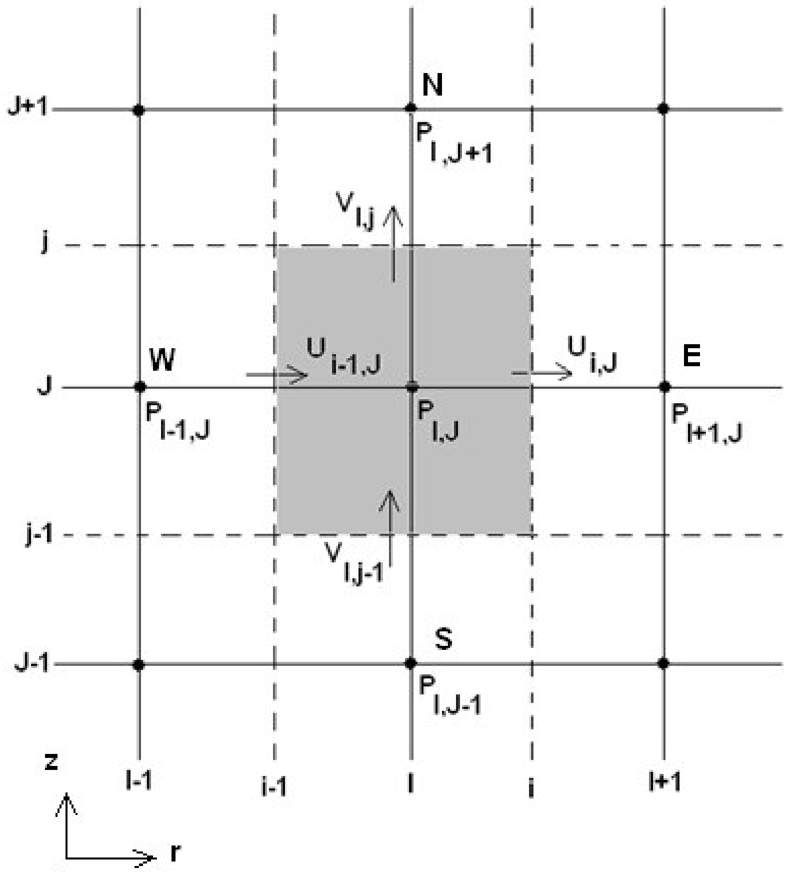

Fig. 4.3: Representation of control volume for P and T

Where $a_{P(i,J)}$ and $a_{P(i-1,J)}$ are the a_P coefficients of x momentum equations for the control volumes (i, J) and (i-1,J) respectively.

$$a_N = (\rho dA)_{I,j} = \rho \frac{r_j(z_i - z_{i-1})}{a_{P(I,j)}} r_j(z_i - z_{i-1}) \tag{4.45}$$

$$a_S = (\rho dA)_{I,j-1} = \rho \frac{r_{j-1}(z_i - z_{i-1})}{a_{P(I,j-1)}} r_{j-1}(z_i - z_{i-1}) \tag{4.46}$$

Where $a_{P(I,j)}$ and $a_{P(I,j-1)}$ are the a_P coefficients of y momentum equations for the control volumes (I, j) and (I, j-1) respectively.

$$a_P = a_E + a_W + a_N + a_S \tag{4.47}$$

$$b'_{I,J} = \rho U_{i-1,J} r_J (r_j - r_{j-1}) - \rho U_{i,J} r_J (r_j - r_{j-1}) + \rho V_{I,j-1} r_{j-1}(z_i - z_{i-1}) - \rho V_{I,j} r_j (z_i - z_{i-1}) \tag{4.48}$$

Conservation of Energy

The discretized form of energy balance equation is obtained with respect to the nodal representation shown in Fig. 4.6. Temperature is stored at the same nodal location where pressure is stored.

$$a_P T_{I,J} = a_E T_{I+1,J} + a_W T_{I-1,J} + a_N T_{I,J+1} + a_S T_{I,J-1} + b_{I,J} \tag{4.49}$$

$$F_e = (\rho CpAU)_e = \rho Cpr_J (r_j - r_{j-1}) U_{i,J} \tag{4.50}$$

$$F_w = (\rho CpAU)_w = \rho Cpr_J (r_j - r_{j-1}) U_{i-1,J} \tag{4.51}$$

$$F_n = (\rho CpAV)_n = \rho Cpr_j (z_i - z_{i-1}) V_{I,j} \tag{4.52}$$

$$F_s = (\rho CpAV)_s = \rho Cpr_{j-1} (z_i - z_{i-1}) V_{I,j-1} \tag{4.53}$$

$$D_e = \frac{2K_{I,J} K_{I+1,J}}{K_{I,J} + K_{I+1,J}} \frac{r_J (r_j - r_{j-1})}{(z_{I+1-} z_I)} \tag{4.54}$$

$$D_w = \frac{2K_{I-1,J} K_{I,J}}{K_{I-1,J} + K_{I,J}} \frac{r_J (r_j - r_{j-1})}{(z_{I-} z_{I-1})} \tag{4.55}$$

$$D_n = \frac{2K_{I,J} K_{I,J+1}}{K_{I,J} + K_{I,J+1}} \frac{r_j (z_i - z_{i-1})}{(r_{J+1-} r_J)} \tag{4.56}$$

$$D_s = \frac{2K_{I,J} K_{I,J-1}}{K_{I,J} + K_{I,J-1}} \frac{r_{j-1} (z_i - z_{i-1})}{(r_{J-} r_{J-1})} \tag{4.57}$$

Now, the coefficients a_P, a_E, a_W, a_N and a_S are calculated based on eqns. (4.23) – (4.28) and Table 4.2 depending on the numerical scheme adopted for representing the profile variation between nodal points.

$$a_P = a_E + a_W + a_N + a_S + F_e + F_n - F_w - F_s + \rho Cpr_J (z_i - z_{i-1})(r_j - r_{j-1}) \frac{1}{\Delta t} \tag{4.58}$$

$$b_{I,J} = S_T r_J (z_i - z_{i-1})(r_j - r_{j-1}) + \rho Cpr_J (z_i - z_{i-1})(r_j - r_{j-1}) T^0{}_{I,J} \frac{1}{\Delta t} \tag{4.59}$$

For steady state solution, the last term of equations (4.58) and (4.59) are not required to be considered. Discretized equations for k and ε are obtained in the same manner as that obtained for the energy balance equation.

Discretized equations for the Cartesian coordinate system are formulated in a similar manner as discussed above and are given in Annexure.

4.4 ALGORITHM FOR SOLUTION

The system of PDEs are solved by SIMPLE algorithm [41]. SIMPLE stands for Semi-Implicit Method for Pressure Linked Equations. This is a method based on guess-and-correct procedure for the calculation of pressure on a staggered grid. The flow chart of the SIMPLE Algorithm is shown in Fig. 4.4. Under relaxation of the solution is found essential for obtaining converged solution over iterations. The under relaxation is implemented in the solutions by modifying the coefficients [41] as follows.

$$b_{I,J} = b_{I,J} + \frac{1 - F_{relax}}{F_{relax}} a_{I,J} U_{I,J} \quad and$$

$$a_{I,J} = \frac{a_{i,J}}{F_{relax}}$$

Similar relaxation is applied for other variables, viz., V and P.

4.5 SOLUTION OF DISCRETIZATION EQUATIONS

The algebraic equations obtained by discretizing the governing equation over a control volume will have five terms involving nodal variables. These system of equations are solved by Line by Line method. In this method, each discretized equation is rewritten, to have only three nodal variable terms. The other two nodal variable terms are combined along with the source term. With this assumption, the system of equations are represented through a tri-diagonal matrix and solution for this system is obtained by forward elimination and backward substitution as follows.

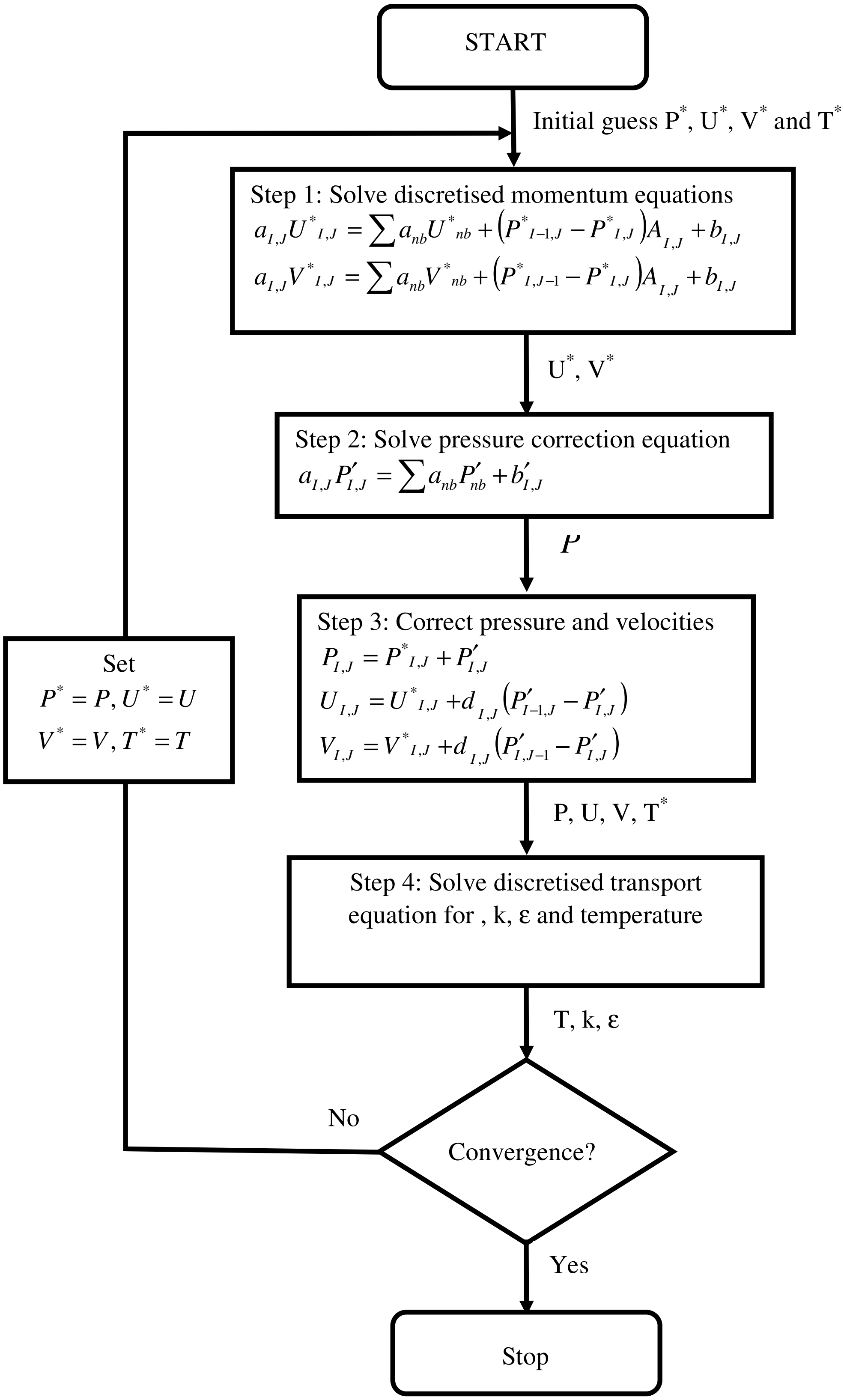

Fig. 4.4: Flow chart of SIMPLE algorithm for any time step

Let the system of N algebraic equations be represented as follows.

$$a_i\phi_i = b_i\phi_{i+1} + c_i\phi_{i-1} + d_i$$

In the backward substitution process from N, the equation can be represented as

$$\phi_i = P_i\phi_{i+1} + Q_i$$

Where $P_i = \dfrac{b_i}{a_i - c_iP_{i-1}}$ *and* $Q_i = \dfrac{d_i + c_iQ_{i-1}}{a_i - c_iP_{i-1}}$

Now for the last node N,

$$P_N = 0 \textit{ and } Q_N = \phi_N$$

which is known from the boundary condition. Parameter at all other nodes can now be evaluated by backward substitution. In order to achieve convergence, several internal iterations are carried out for the Line-by-Line method to avoid divergence.

4.6 VALIDATION

Validation of the STITH computer code has been carried out by comparing its predictions against results published in literature. Four different problems have been considered for the validation.

(1) Lid driven square cavity under laminar flow

(2) Laminar flow between two parallel plates maintained at constant wall temperature

(3) Laminar flow through a pipe at constant wall temperature

(4) Turbulent flow through a backward facing step

The above class of problems selected for validation confirm the applicability of code for solving fluid flow and heat transfer problems involving various aspects, viz., (i) laminar flow, (ii) turbulent flow, (iii) Cartesian geometry, (iv) cylindrical geometry and (iv) fluid flow with wall heat transfer.

4.6.1 Lid Driven Square Cavity

A square cavity has been modeled in Cartesian coordinate system and the top wall is considered to move at constant velocity. Schematic of the model with boundary conditions is shown in Fig. 4.5. The grid pattern considered for the analysis 120 X 120. The study has been carried out for two different Reynolds numbers, viz., 400 and 1000. The predicted vertical velocity distributions at the horizontal mid plane are shown in Figs. 4.6 and 4.7 respectively. Published results by Ghia et al. [49] are also shown in these plots. Good comparison can be observed between the two solutions.

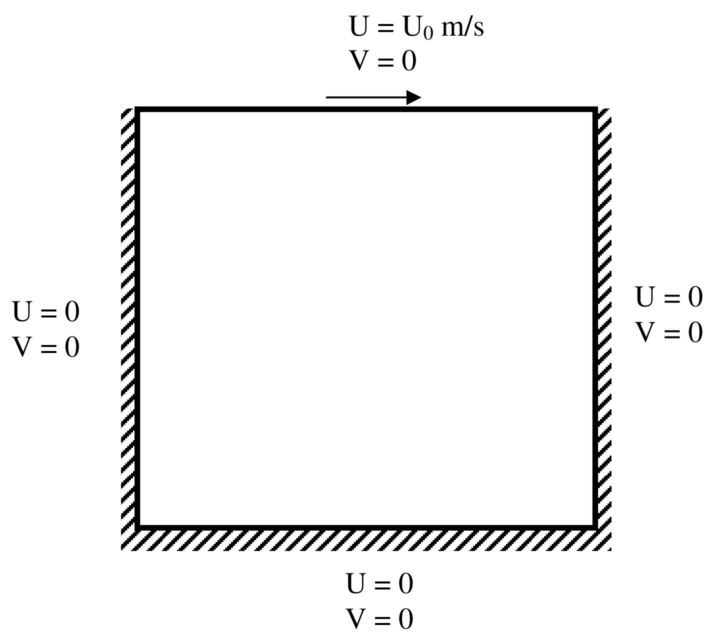

Fig. 4.5: Schematic and boundary conditions of cavity

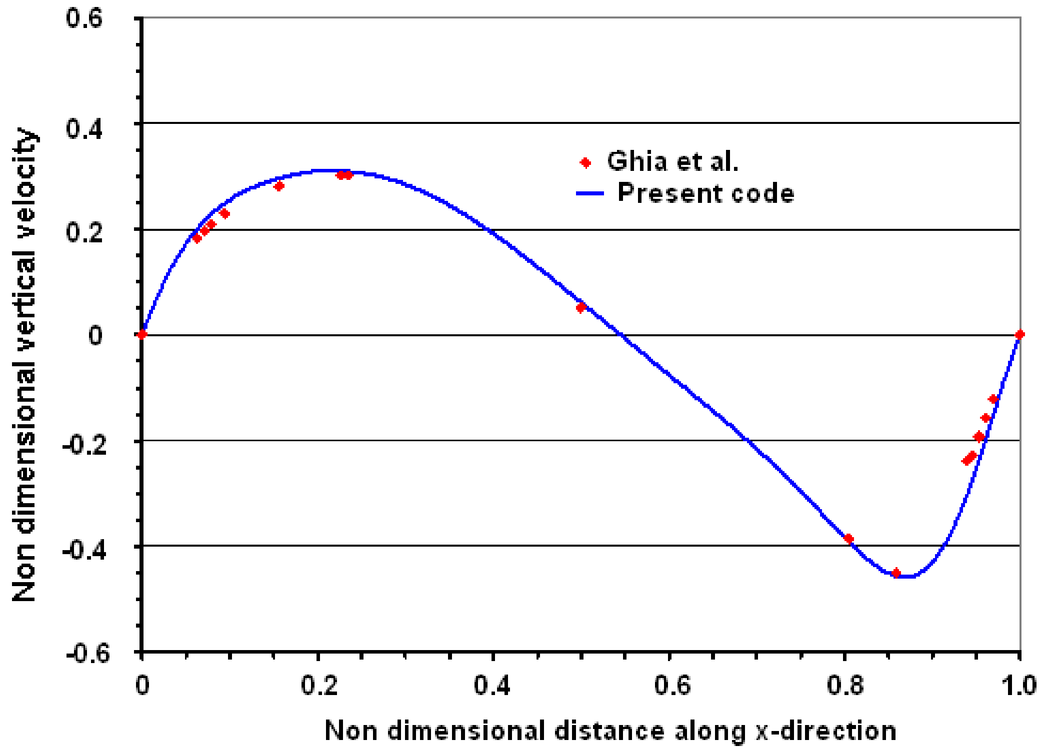

Fig. 4.6: Predicted y-velocity distribution at mid plane for Re=400

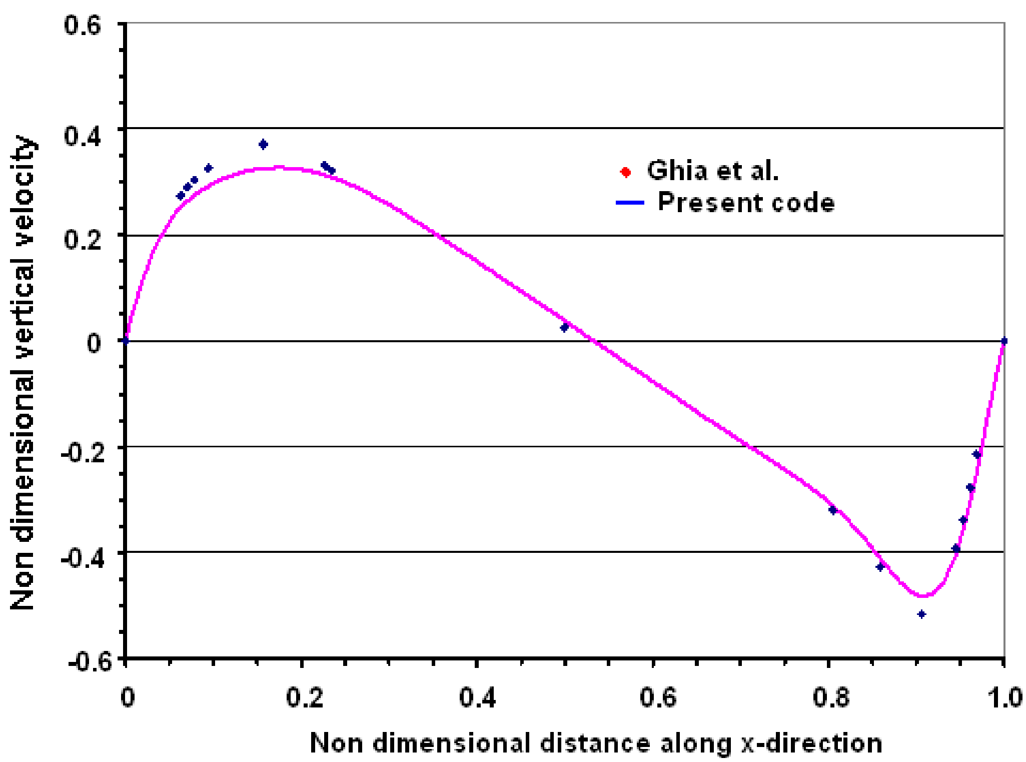

Fig. 4.7: Predicted y-velocity distribution at mid plane for Re=1000

4.6.2 Flow between Two Parallel Plates

Laminar flow between two parallel plates has been modeled using Cartesian coordinate system. The geometry and boundary conditions considered are shown in Fig. 4.8. Both plates are at isothermal temperature conditions. Flow is considered to enter the duct at uniform velocity and development of flow and temperature are estimated using STITH-2D. Predicted velocity distribution after full development is shown in Fig. 4.9. Also shown in this figure is the analytical solution of velocity. Predicted evolutions of velocity at the mid plane of duct and Nusselt numbers are shown in Figs. 4.10 and 4.11 respectively. Published results for this case by Shah and London [50] are plotted in these figures. Good comparison can be observed on the predictions of velocity and Nusselt number developments. The fully developed Nussult number predicted is 7.5 (Fig. 11). As far as development of friction factor is concerned, the friction factor predicted after full development (24 / Re) matches with the published data. Thus, the prediction of thermal hydraulic behavior by the Cartesian geometry system of the code can be considered to be validated.

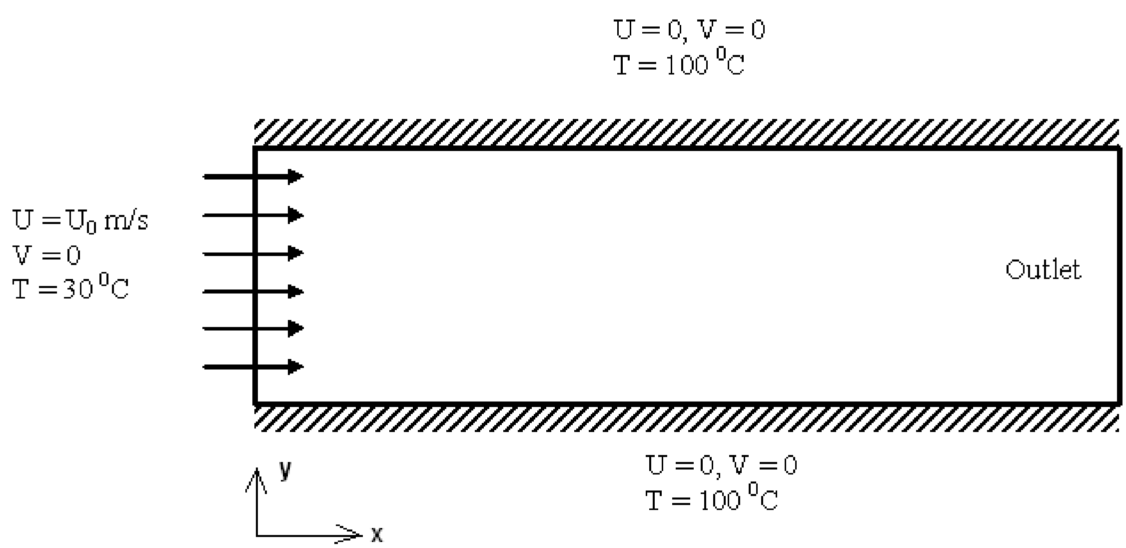

Fig. 4.8: Schematic of flow between two parallel plates with boundary conditions

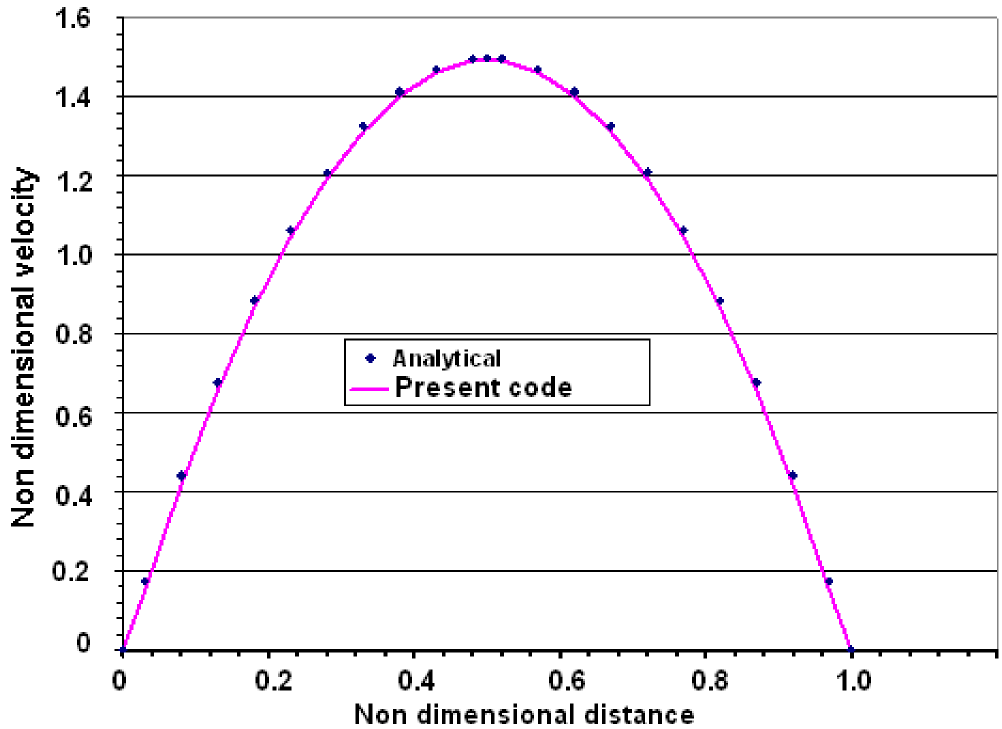

Fig. 4.9: Predicted velocity profile along the width of duct

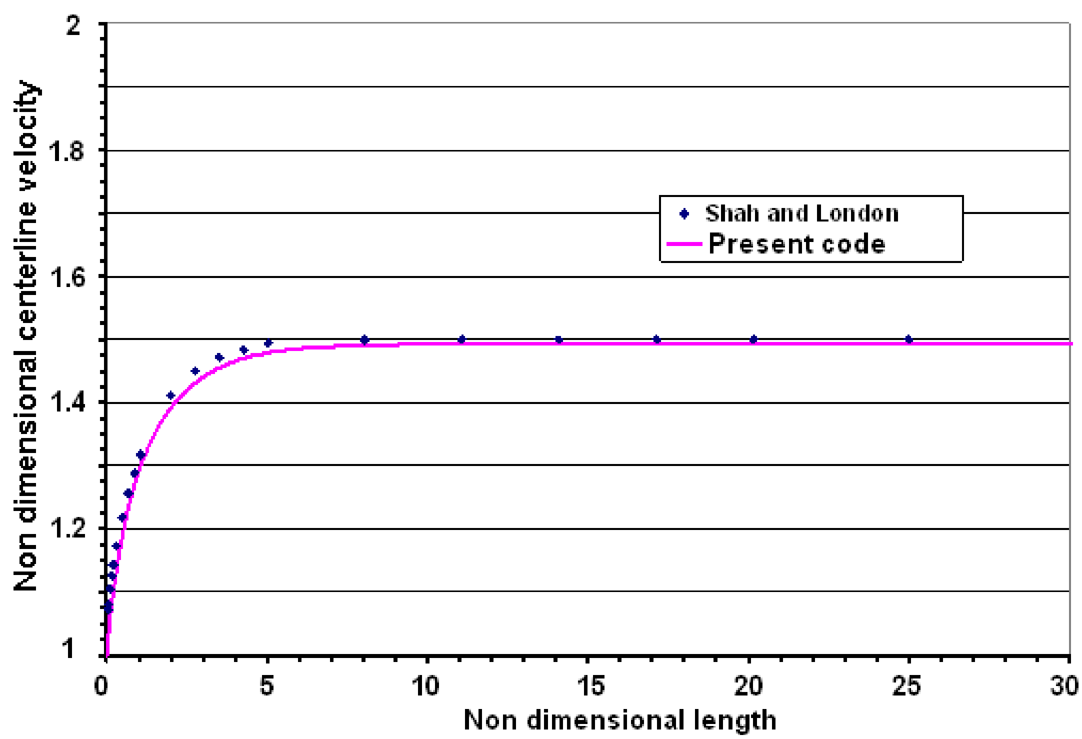

Fig. 4.10: Predicted development of velocity a the central plane of duct

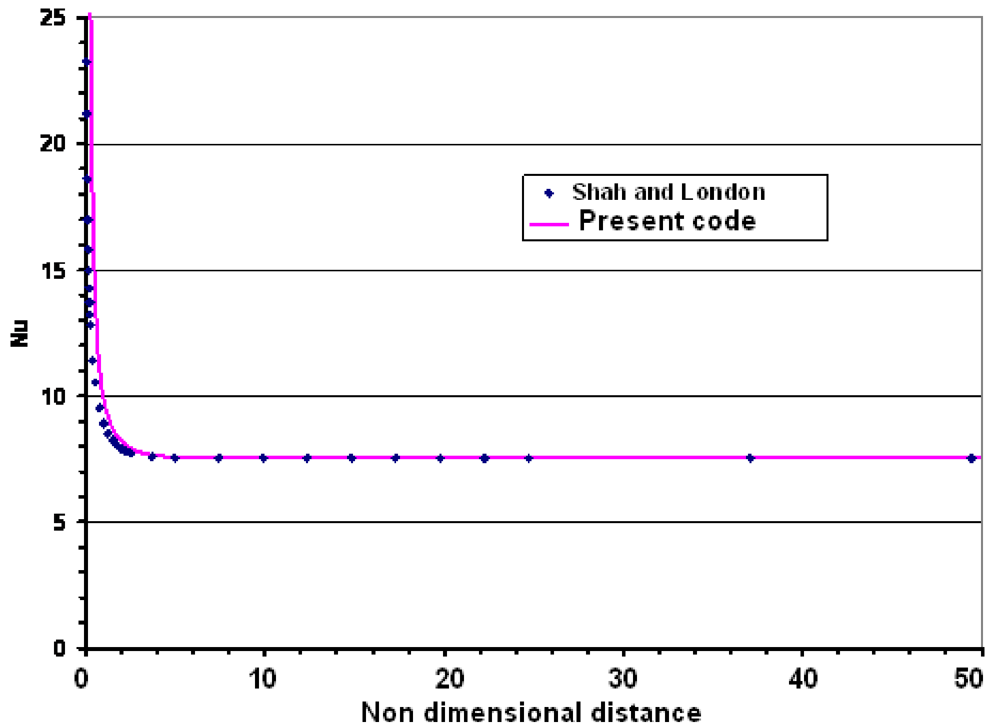

Fig. 4.11: Predicted development of Nusselt number along the length of duct

4.6.3 Flow development in a circular Pipe

Flow development in a circular pipe has been modeled using Cylindrical coordinate system. The geometry and boundary conditions considered are shown in Fig. 4.12. Pipe wall is considered to be at isothermal temperature condition. Flow is considered to enter the pipe at uniform velocity and development of flow and temperature are estimated using STITH-2D. Predicted velocity distribution after full development is shown in Fig. 4.13. Also shown in this figure is the analytically predicted distribution of velocity. Predicted evolutions of velocity at the centre of the pipe and Nusselt numbers are shown in Figs. 4.14 and4.15 respectively. In these figures the length is non dimensionalized with respect to radius of pipe. Published results for this case by Shah and London [50] are also plotted in these figures. Good comparison can be observed on the predictions of velocity and Nusselt number developments. The fully developed Nussult number predicted is 3.66. The friction factor predicted after full development (16 / Re) matches with the analytical data. Thus, the prediction of thermal hydraulic behavior by the Cylindrical geometry system can be considered to be validated.

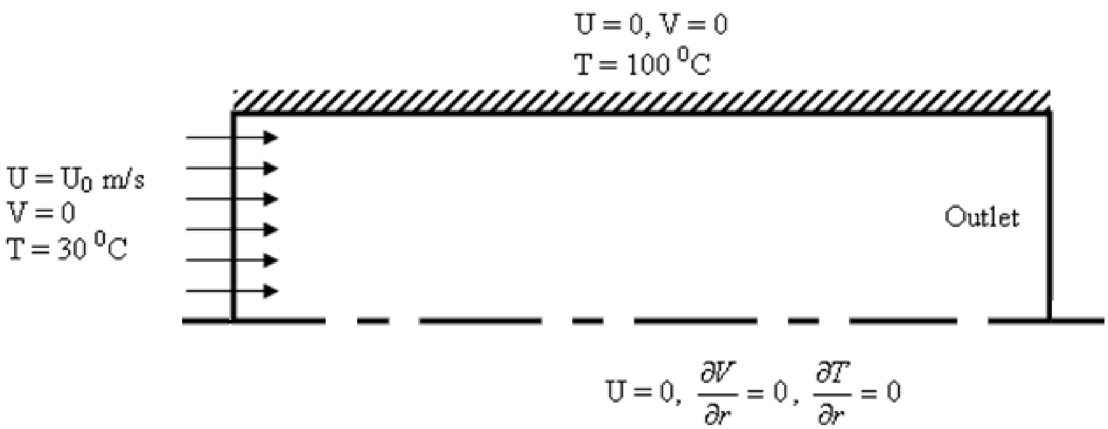

Fig. 4.12: Schematic of flow through pipe with boundary conditions

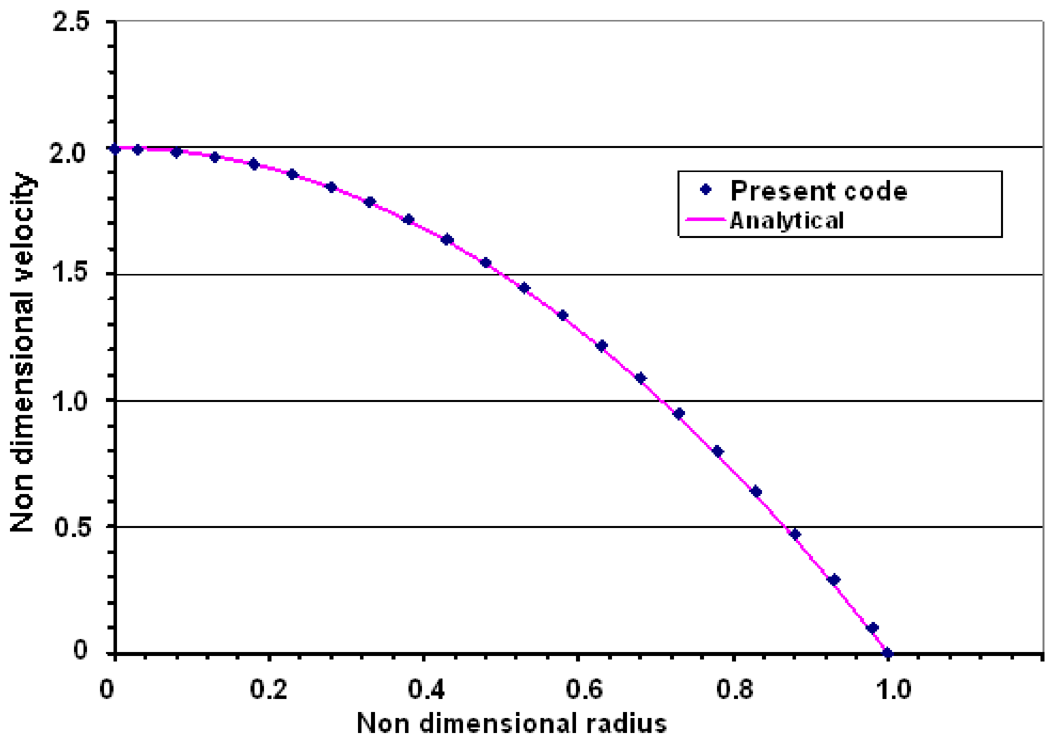

Fig. 4.13: Predicted radial distribution of velocity after development

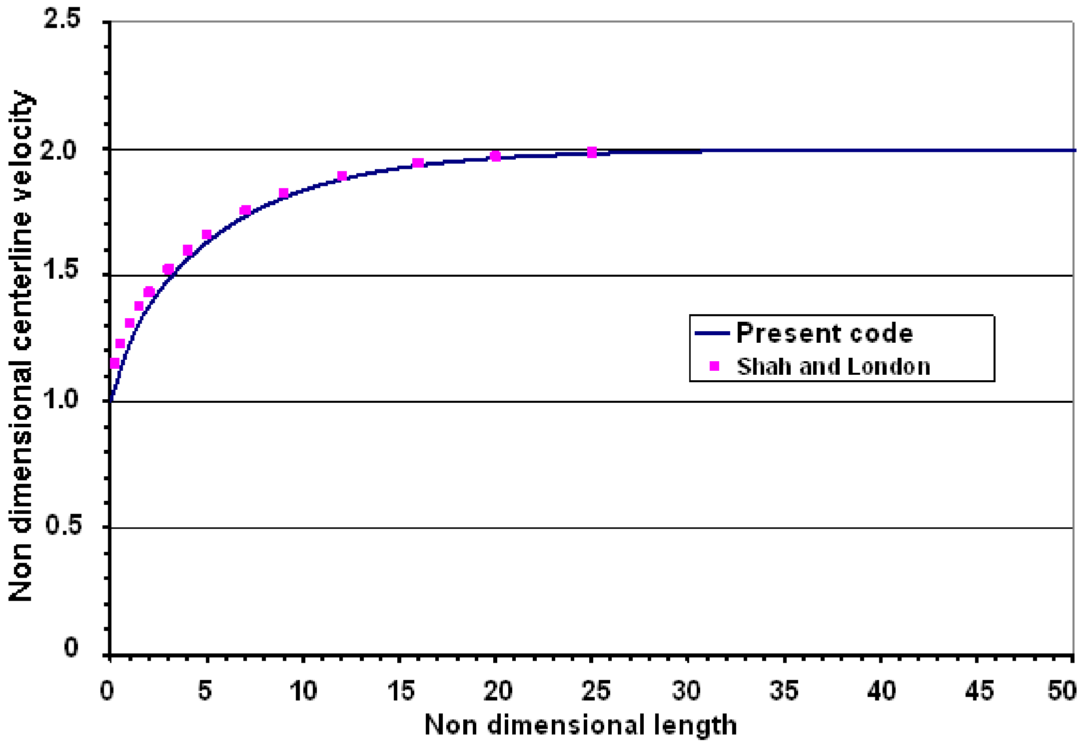

Fig. 4.14: Predicted development of velocity at the centre of the pipe

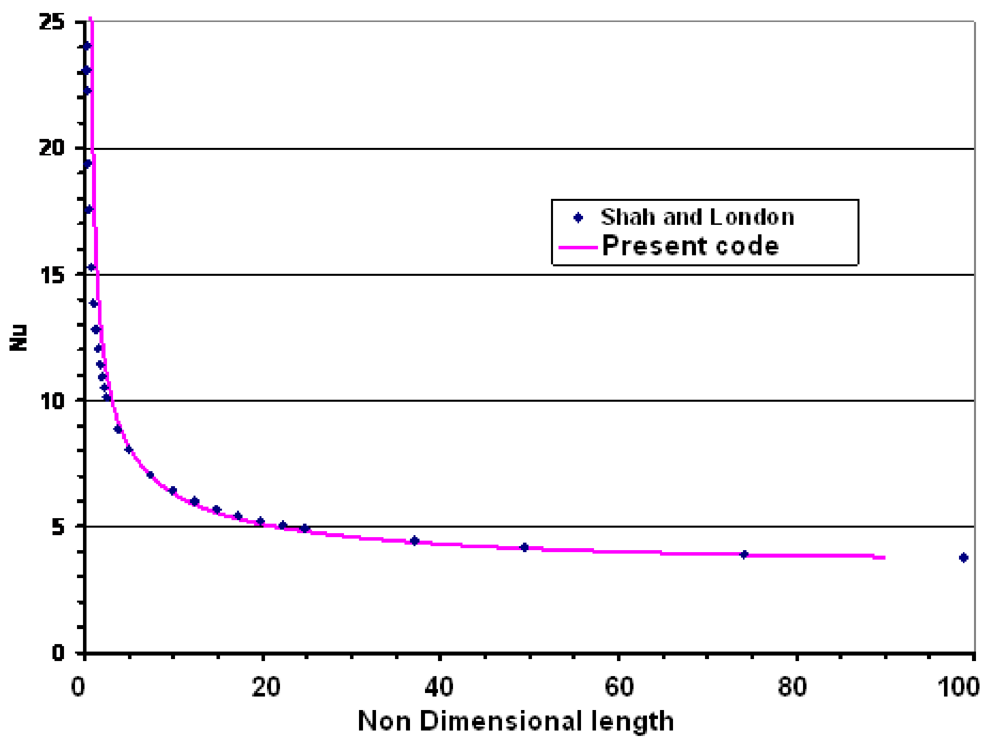

Fig. 4.15: Predicted evolution of Nusselt number development along the length of pipe

4.6.4 Turbulent Flow through a Backward Facing Step

For the computation of turbulent behavior, the flow configuration of backward facing step [51] has been selected. In this case, the ratio of step height to outlet channel height is 1:3 and the Reynolds number based on the step height and entry velocity is 44,580. The geometrical details are shown in Fig. 4.16. Comparison of the predicted velocity distribution against the experimental data at x/H = 13.33 is shown in Fig. 4.17. It can be observed that the predictions are close to the experimental data.

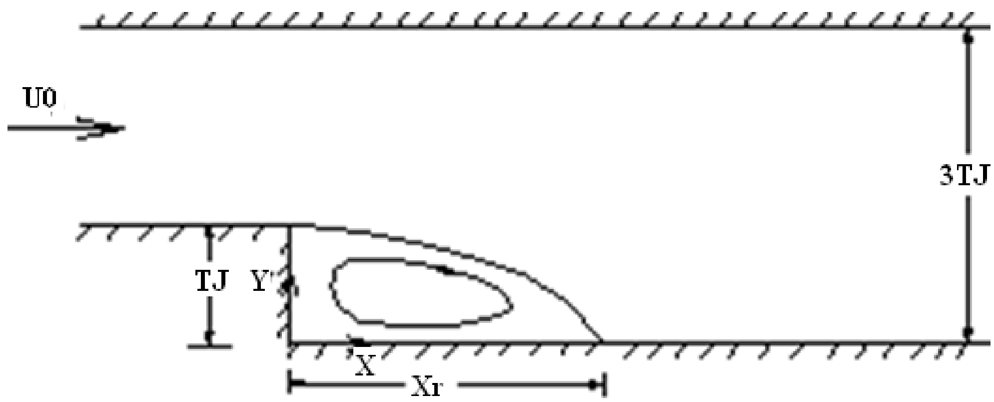

Fig. 4.16: Geometry of the backward facing step flow

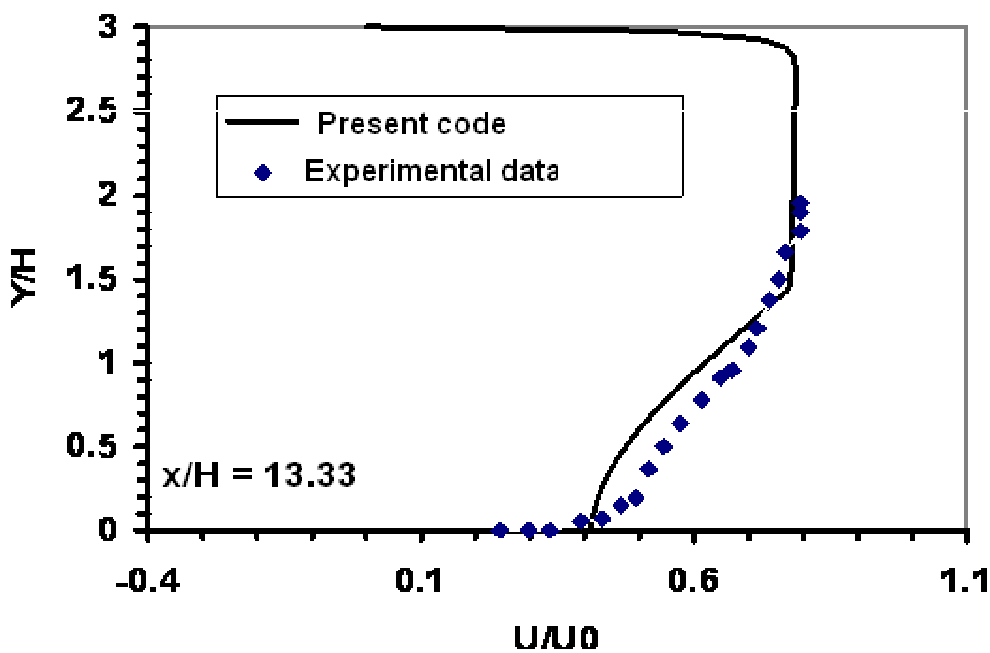

Fig. 4.17 : Comparison of the turbulent model predictions against experimental data

4.6.5 Inter-Code Comparison

In order to demonstrate the applicability of the code in the prediction of transient thermal hydraulic behavior of large sodium pools of reactor size, axisymmetric analysis of hot pool of the reactor during steady state operating conditions of the reactor has been carried out. This approach has been adopted due to the non-availability of experimental data for benchmarking. The geometrical modeling and boundary conditions adopted for this calculation are same as to those discussed in section 3.3.2 of Chapter 3 for the axisymmetric model of hot pool. The predicted velocity pattern in the hot pool by STITH-2D is shown in Fig. 4.18 along with the velocity pattern predicted by Star CD 3.26 code. It can be observed that the both the predictions are very close. The particular nature of flow in the region above the core as well as near the inner vessel are predicted similarly by both the codes. Moreover, the predictions of recirculating flow pattern in the hot pool are also similar.

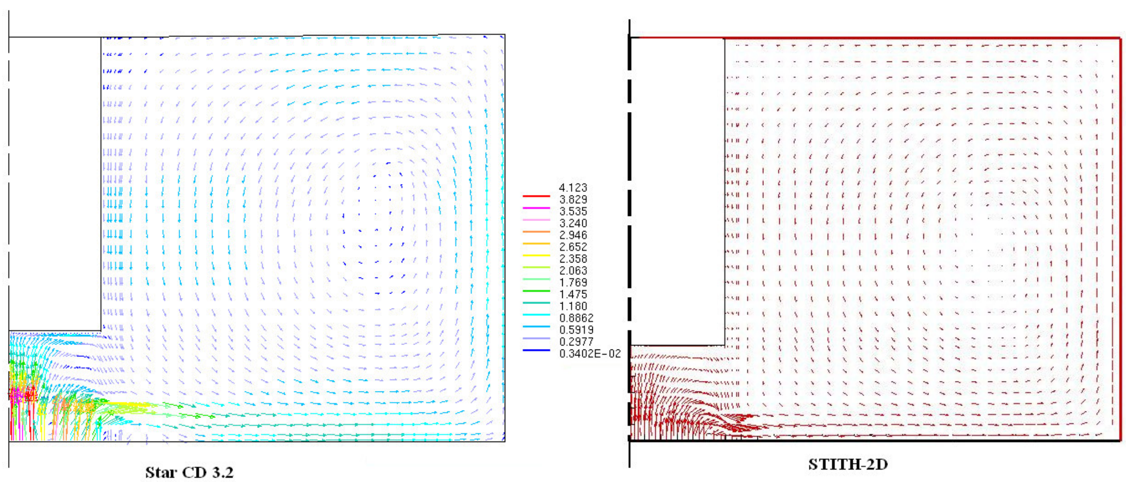

Fig. 4.18: Comparison of predicted velocity pattern in hot pool by the 2D models of Star-CD with STITH-2D

4.7 DEVELOPMENT OF ONE DIMENSIONAL - CFD COUPLED SYSTEM DYNAMICS TOOL (HYBRID MODEL)

Two dimensional axi-symmetric model of SFR hot pool of fast reactor has been formulated using the using the STITH-2D code and the rest of the plant, viz. reactor core, cold pool, intermediate heat exchangers, secondary sodium circuit and steam generators are modeled using the one dimensional formulations available in the plant dynamics code DYANA-P. The coupled code system is named as DYANA-HM. Modeling of hot pool in STITH-2D code is similar to that shown in Fig. 3.14. The only difference is that the conical redan of inner vessel is modeled as flat, as shown in Fig. 4.19 from the point of view of simplifying the computational model. However, the total volume of hot pool is conserved. In this model, hydraulic resistances offered by porous plates and shells provided in the hot pool are simulated through sinks in the momentum balance equations. Free surface is simulated through frictionless wall and all the physical walls in the domain are modeled as non-slip walls. The main focus of the CFD model for hot pool is the simulation of coolant mixing phenomenon within the pool. This does not require accurate simulation of wall shear effects. Hence, wall function is not included in the model. Outlet from the domain is simulated using

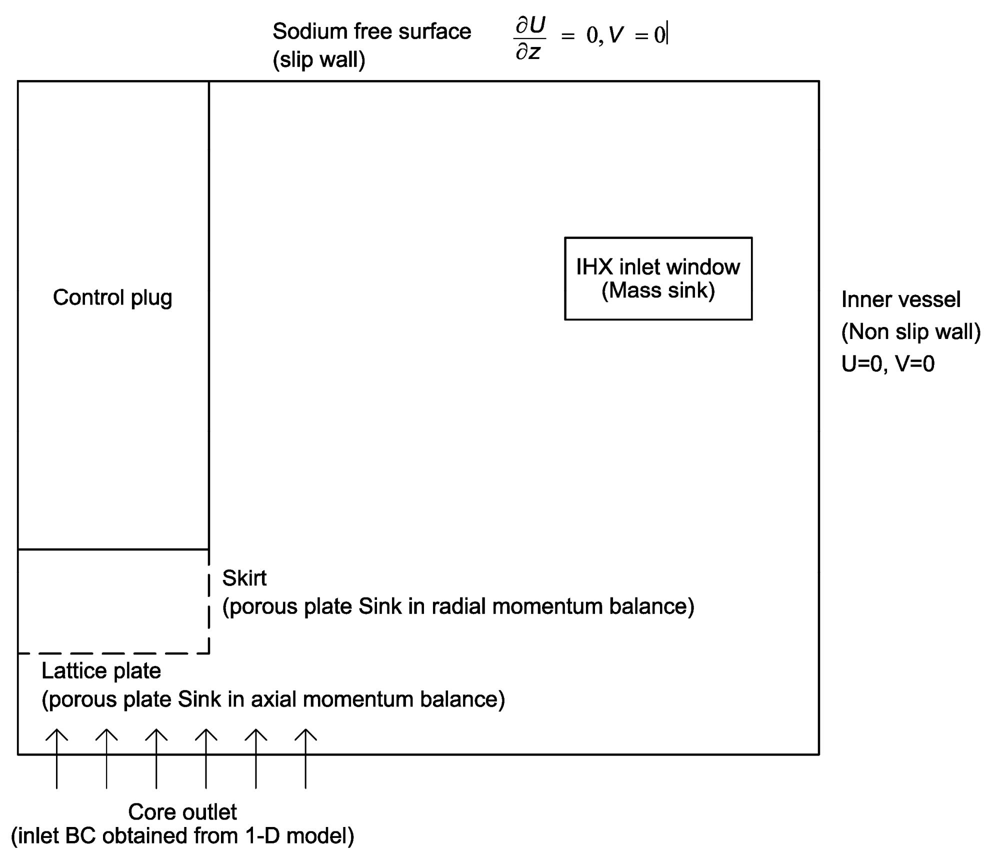

Fig. 4.19: Axi-symmetric model of hot pool with boundary conditions

mass sink in the continuity equation at a location corresponding to the radial and axial position of inlet windows of IHX. Turbulence is treated through standard high Reynolds number k-ε model.

Flow and outlet temperature distributions in various radial zones on reactor core obtained from the one dimensional multi-region modeling of core (from DYANA-P) is specified as inlet boundary condition in the axi-symmetric model of hot pool. Schematic representation of primary and secondary sodium circuits modeled in DYANA-P code are shown in Figs. 4.20 and 4.21 respectively. The nodalization scheme followed in DYANA-P for SFR modeling is shown in Fig. 4.22. Regarding spatial nodalisation, the reactor core is divided in the 10 radial zones and19 axial zones. In each core zone, a SA pin has been modeled with two radial zones for the fuel, one for cladding and one for the coolant.

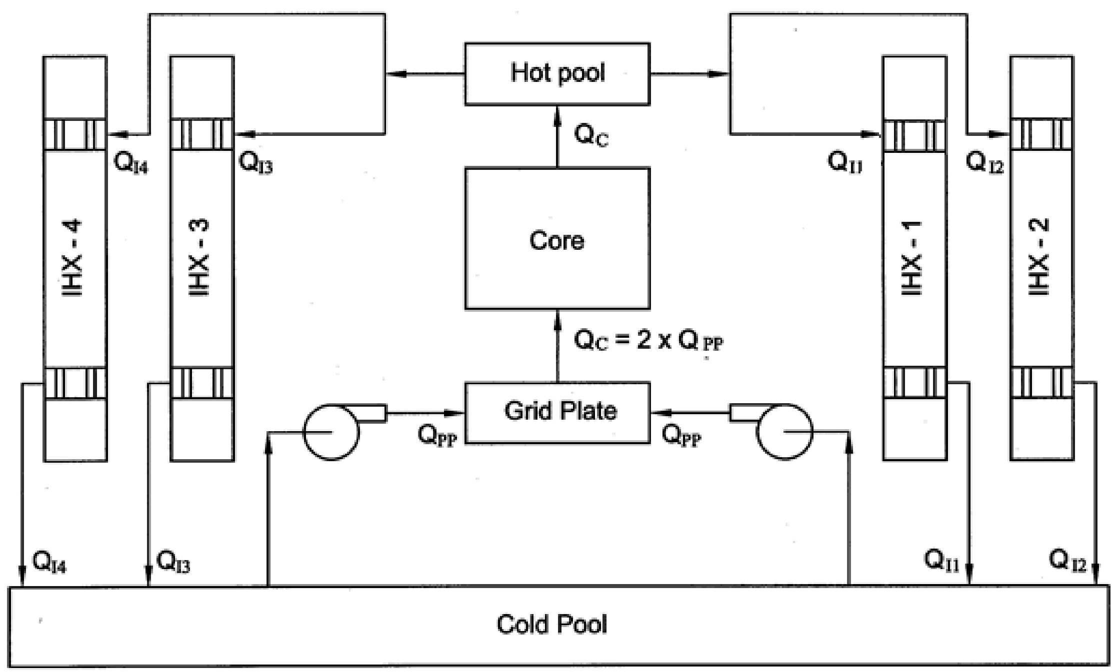

Fig. 4.20: Schematic model of primary sodium circuit

In a similar manner, multiple zones are considered along the length of IHX and SG. For each axial volume of heat exchanger, four nodes, viz., one each for primary and secondary coolant, one node for tube wall and another node for shell wall are modeled. In the volumes representing the coolant piping, three radial nodes are considered. These represent coolant, pipe wall and insulation regions respectively. As already mentioned, primary and secondary sodium pumps are modeled based on homologous characteristics for the applicable range of specific speed. Flow rate and inlet temperature of feed water flow are specified as boundary condition and steam conditions at the exit of the SG is calculated based on the two phase heat exchange model included in the code. Cold pool is represented through six zones, with three volumes considered in the circumferential and two volumes in the axial direction. Other modeling aspects of the code are presented in details in section 2.2.10.

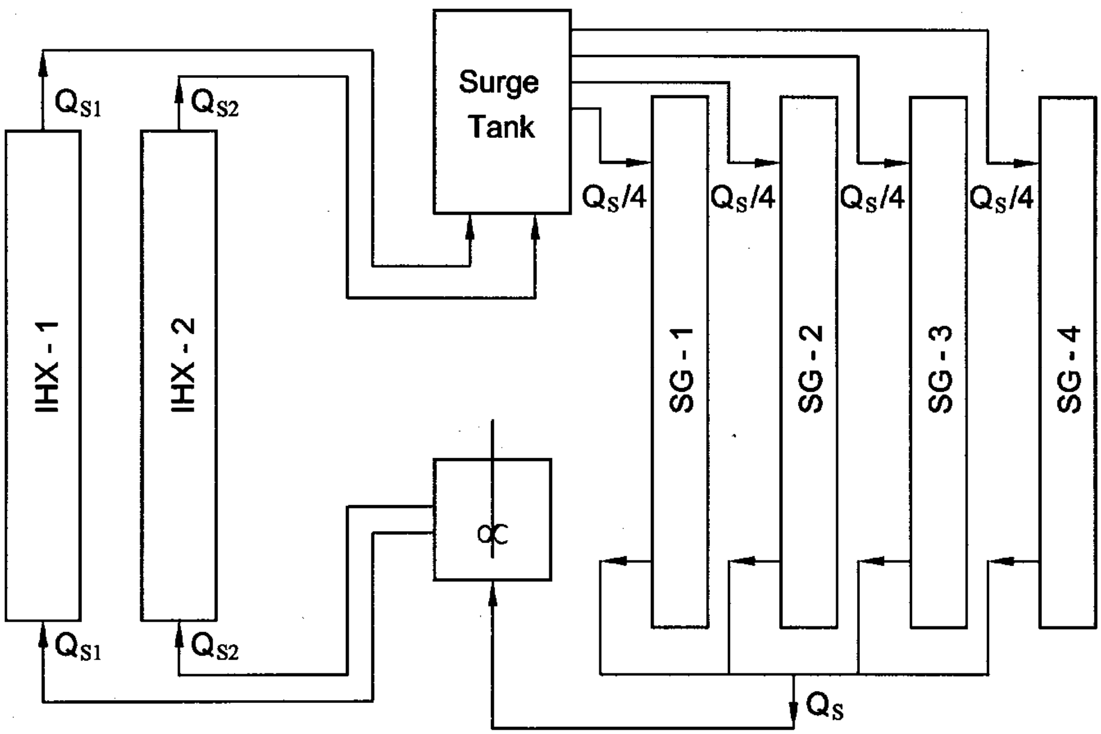

Fig. 4.21: Schematic model of a secondary sodium circuit

The calculation sequence followed in DYANA-HM is shown in Fig. 4.23. At first, steady state calculations are performed for the entire plant along with two dimensional steady state calculations for hot pool. IHX inlet temperature required for the system model is evaluated as the average temperature of fluid entering the IHX inlet window in the axi-symmetric model of hot pool. Similar approach is adopted in the transient calculation also.

For each time step, numerical integration of governing equations representing fluid flow and heat transfer in the hot pool is performed through an iterative approach till the specified convergence levels are achieved. Based on the inlet temperature of primary sodium predicted through the axi-symmetric model, the system dynamics calculations for the rest of the plant is carried out to obtain the flow and temperature distribution in various parts of the plant. The nodalization scheme of DYANA-HM is shown in Fig. 4.27.

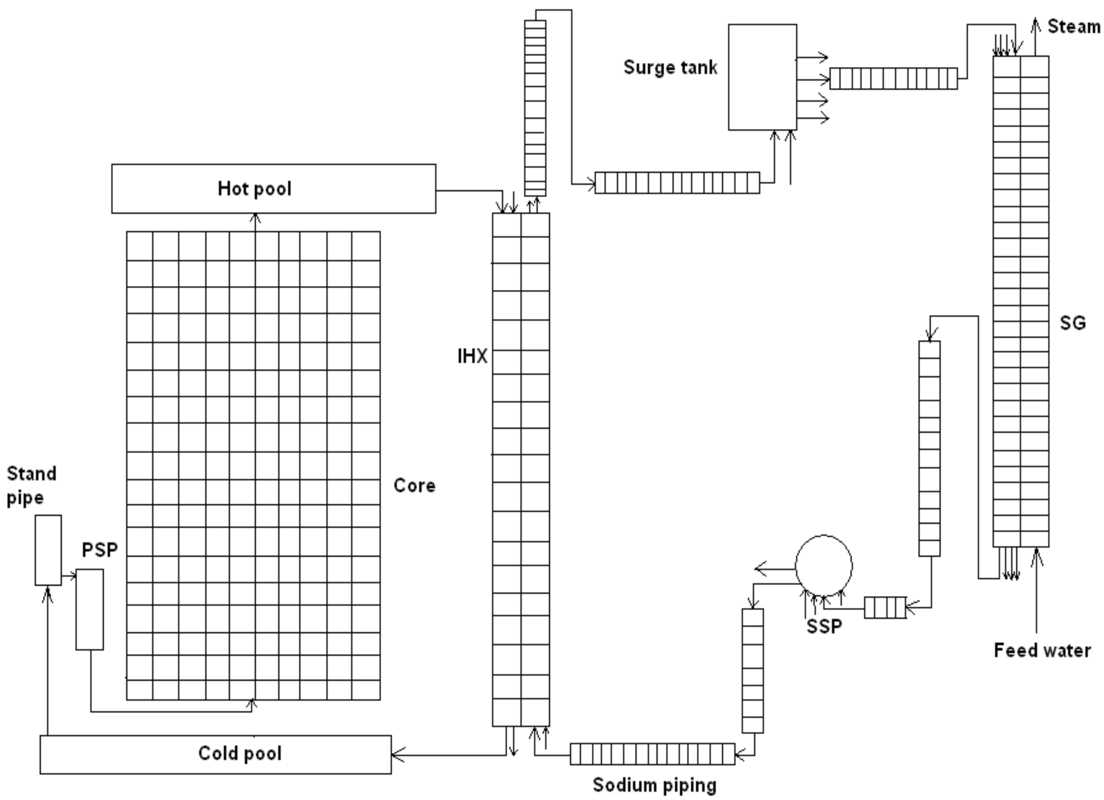

Fig. 4.22: Nodalisation scheme in DYANA-P to model FBR plant (single primary and secondary sodium circuits alone are shown)

4.8 CLOSURE

An axi-symmetic model for transient simulation of thermal hydraulics of hot pool of fast reactor based on CFD approach has been developed. The CFD code developed for turbulent flow simulations has been validated by comparison of code predictions against benchmark solutions reported in literature. Subsequently, an axi-symmetric modeling of hot pool developed using the CFD code which is coupled with system dynamics code (DYANA-P) for the rest of the plant. The coupled hybrid code system is named as DYANA-HM.

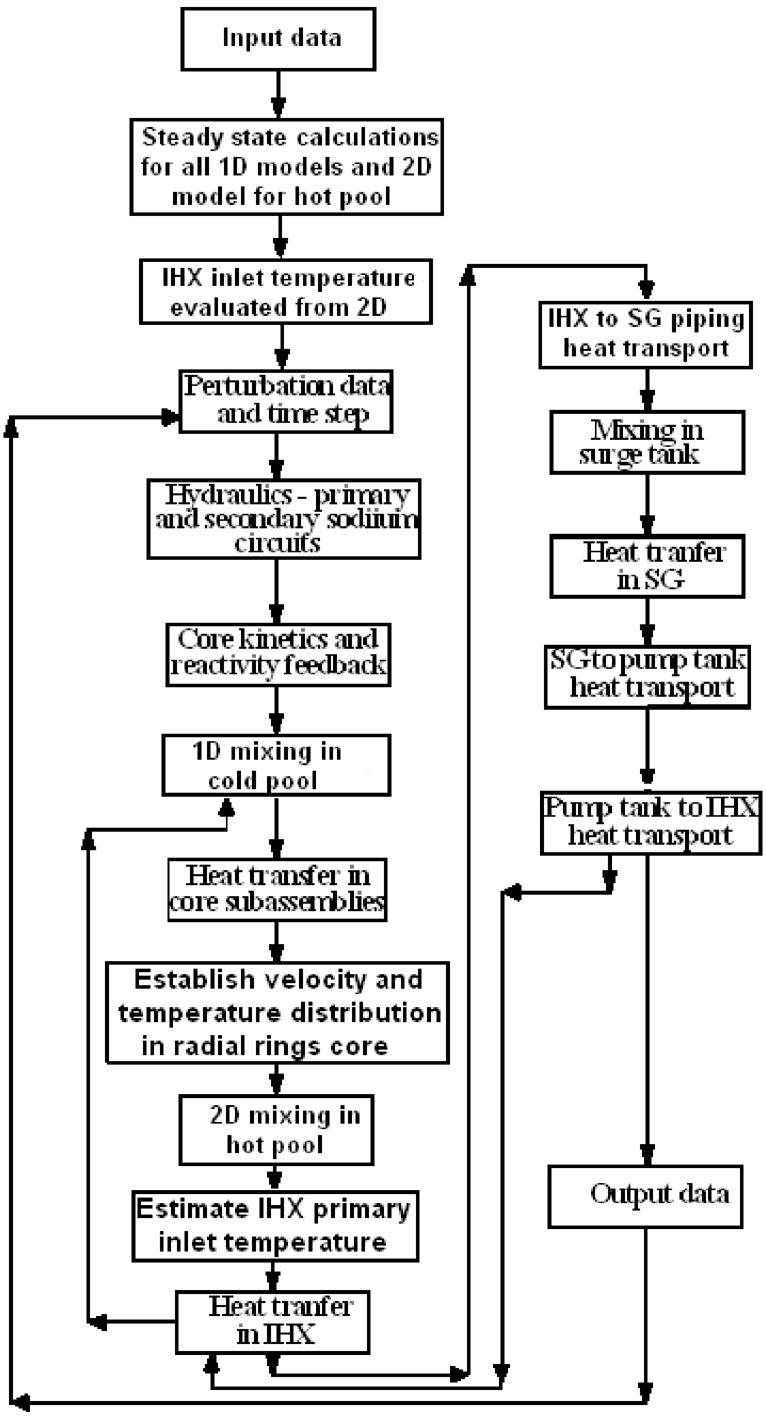

Fig. 4.23: Calculation sequence followed in DYANA-HM

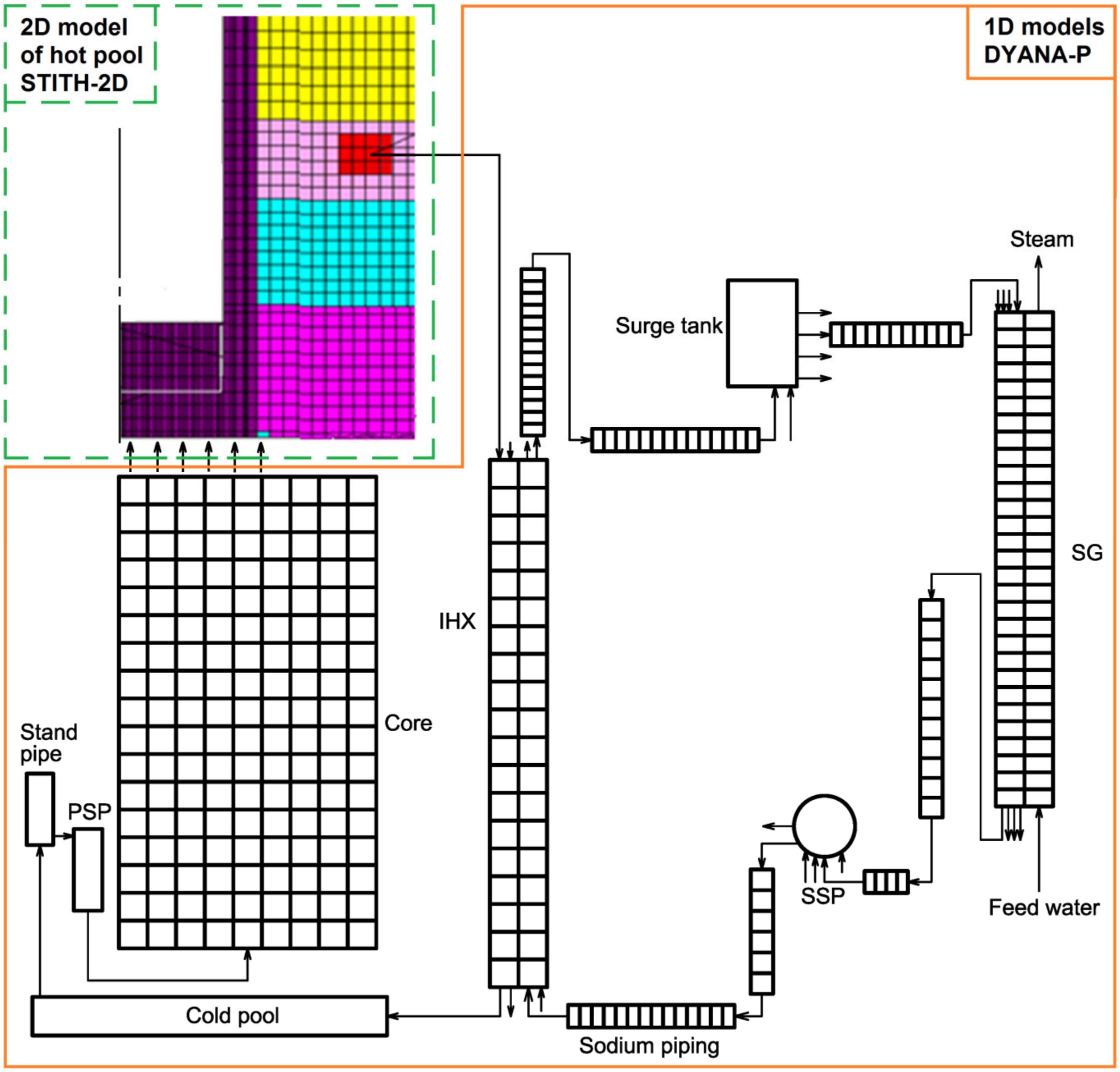

Fig. 4.24: Nodalization scheme of DYANA-HM

CHAPTER – 5

ANALYSIS OF PLANT TRANSIENTS USING DYANA-HM

5.1 DESCRIPTION OF TRANSIENTS

Four different typical plant transients, viz., (i) spurious SCRAM, (ii) loss of steam water system, (iii) class IV power failure and (v) station blackout events have been considered for the analysis. These transients are selected with the consideration that the transient behavior in the plant especially in the hot pool during various design basis events is enveloped by these four events. Further, these transients lead to symmetric evolution of parameters in the cold pool in both the loops. A brief scenario and description of these events is given in Table 5.1. During spurious SCRAM and loss of steam water system events, the primary and secondary sodium circuits will be under forced flow conditions with flow rates reduced to 20 %. During spurious SCRAM, the heat removal from the sodium systems takes place through the normal heat removal path (steam generators) whereas under loss of steam water system, heat removal takes place through a dedicated decay heat removal system. However, during the time period of analysis reported in this section (about ½ h), it is considered that the dedicated decay heat removal system is not deployed and the decay heat generated in the core is considered to be absorbed by the sodium systems itself. Heat removal and primary sodium flow conditions during class IV power failure event are similar to that during loss of steam water system event. Secondary sodium circuit will be under natural convection conditions in this case as emergency diesel power supply is provided only for the operation of primary sodium pumps at a reduced speed. Both primary as well as secondary sodium circuits will enter into natural convection conditions during a station blackout event. Heat removal condition during station blackout event is similar to that during loss of steam water system or class IV power failure events. Analyses of these events have been carried out using DYANA-P (fully one dimensional model) and DYANA-HM (coupled one dimensional and CFD model for hot pool) and results are discussed in the following sections.

Table 5.1: Scenario of events considered for analysis

Sl. No.	Event title	Scenario
1	Spurious SCRAM	• Reactor SCRAM at t= 0s • Coast down of primary sodium pumps to 20 % speed during t = 0 to 80 s • Coast down of secondary sodium pumps to 20 % speed during t = 0 to 40 s • Feed water flow to SG reduced to 15 % (during t= 0 to 30 s) gradually by the SG sodium outlet temperature controller
2	Loss of steam water system	• Total loss of feed water flow to steam generator (SG) at t= 0 s • Reactor SCRAM at t = 30 s • Coast down of primary sodium pumps to 20 % speed during t = 30 to 110 s • Coast down of secondary sodium pumps to 20 % speed during t = 30 to 70 s • Decay heat removal system deployed after ½ h
3	Class IV power failure	• Coast down of primary sodium pumps to 18 % • Trip of secondary sodium pumps (speed reducing to zero in 55 s) and total loss of feed water flow to SG at t = 0 s • Reactor SCRAM at t = 0.5 s • Primary pumps speed reach 18 % at 90 s • Decay heat removal system deployed after ½ h
4	Station blackout	• Trip of primary sodium pumps. Speed reducing to zero in 100 s • Trip of secondary sodium pumps. Speed reducing to zero in 55 s • Total loss of feed water flow to SG at t = 0 s • Reactor SCRAM at t = 0.5 s • Decay heat removal system deployed after ½ h

5.2 SPURIOUS SCRAM

As explained earlier, the transient simulated is reactor trip followed by reduction in primary and secondary flows to 20 %. Due to the action of feed water flow controller, which manipulates the feed water flow through steam generator to control the sodium temperature at the outlet of steam generators, the feed water flow reduces gradually to 15 % in line with the reduction in sodium temperature. Predicted velocity and temperature distributions in the hot pool at the beginning of the transient (initial steady state condition) and 600 s after reactor SCRAM are shown in Fig. 5.1. It is observed that during initial steady state conditions, the sodium flow emanating from the core is deflected by the bottom plate and the porous shell of control plug. Due to the high kinetic energy of sodium flow after being deflected by the control plug compared to the buoyancy force, it flows radially towards the periphery of the hot pool. It then rises up to the free surface making a counter clockwise recirculation pattern in the hot pool before entering the inlet window of IHX. Temperature condition in the hot pool appears to be well mixed except in the region close to core exit. The average temperature of sodium entering the IHX inlet is 547 ^{0}C.

Predicted flow field in hot pool at 600 s after reactor SCRAM is much different from that during initial steady state condition. Reduced core flow rate at 600s (20 %) and the influence of buoyancy, cause the sodium from core to flow radially outwards initially and then to flow inwards towards the control plug. It then rises up close to the control plug shell and makes a clockwise recirculation pattern below IHX window before entering the IHX. Due to the low velocity and low temperature, core exit sodium is unable to penetrate the hot stratified layers formed in the upper region of hot pool. This is evident from the velocity and temperature distribution of sodium in hot pool predicted at 600 s.

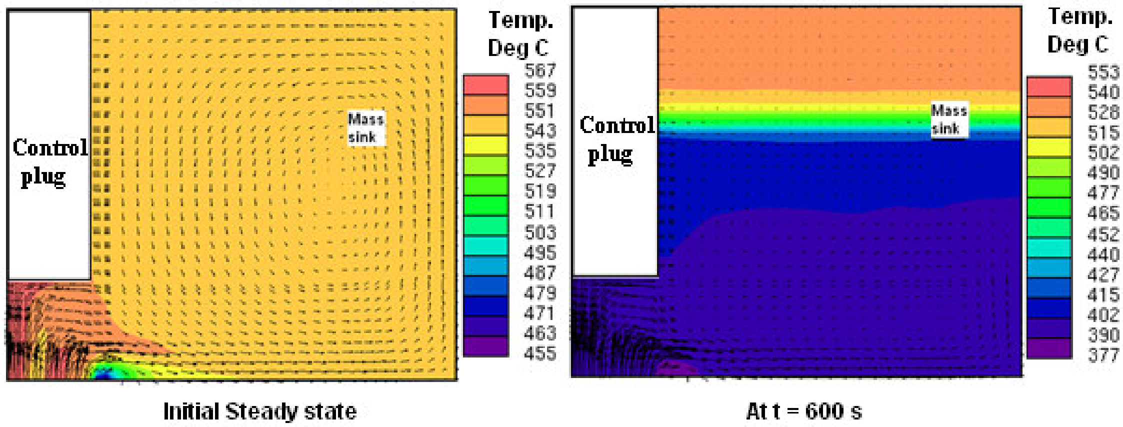

Fig. 5.1: Velocity and temperature distributions in hot pool predicted by DYANA-HM during spurious SCRAM

Comparison of temperature evolutions in the primary and secondary sides of IHX predicted respectively by DYANA-HM and DYANA-P are shown in Figs. 5.2 and 5.3. It can be observed that due to the modeling of thermal stratification in DYANA-HM, the IHX primary inlet temperature reduction is gradual during the initial period compared to that predicted by DYANA-P. Significant difference between the predictions exists up to 400 s. However, predictions of primary sodium temperature at the outlet of IHX by both the codes are nearly the same. This is due to the fact that the secondary inlet temperature to IHX predicted by both the codes are nearly the same, as a consequence of feed water flow controller action trying to control the sodium temperature at the outlet of SG. Moreover, after reactor SCRAM, primary and secondary sodium flow rates are reduced to 20 % and the power transferred across the IHX also reduces. As a result, the temperature differences between primary and secondary sodium at the cold end as well as hot end of IHX reduce significantly. Thus, secondary sodium outlet temperature starts following primary sodium inlet temperature and primary sodium outlet temperature starts following secondary sodium inlet temperature closely. Effectively, the prediction of secondary hot leg temperature in the IHX alone is affected due to the consideration of thermal stratification in hot pool. Prediction of reactor inlet temperature is also not affected by the consideration of thermal stratification in hot pool during this transient as the primary sodium temperature at the outlet of IHX is negligibly affected.

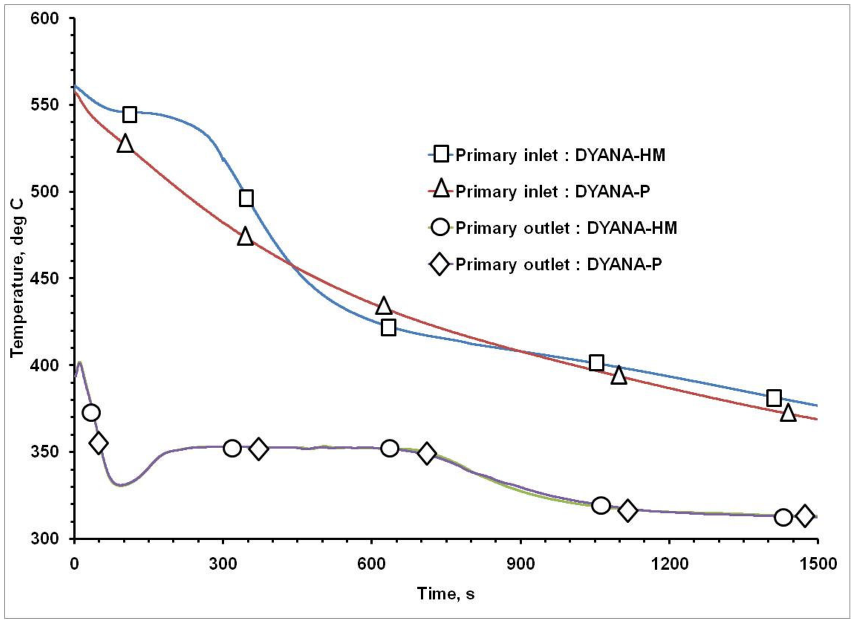

Fig. 5.2: Evolutions of IHX primary temperature during spurious SCRAM

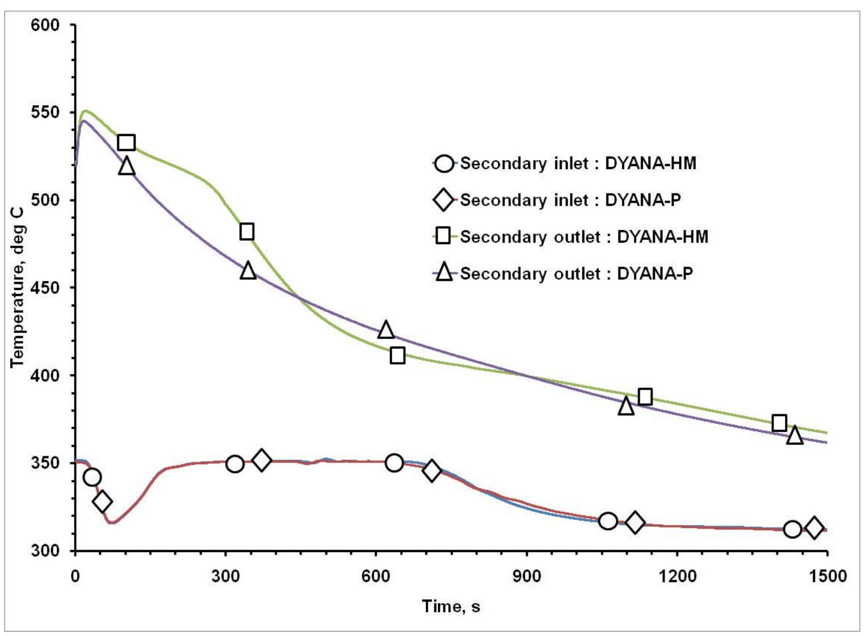

Fig. 5.3: Evolutions of IHX secondary temperature during spurious SCRAM

Predicted temperature evolutions in the sodium and steam sides of steam generators respectively by DYANA-HM and DYANA-P are compared in Figs. 5.4 and 5.5. Here also, it is evident that predictions of hot leg temperature alone are different. Moreover, significant difference is observed only during the initial ~ 500 s of the transient. Cold leg temperature is nearly unaffected mainly due to the action of feed water flow controller and the feed water inlet temperature is considered to be the same in both the cases. It can be summarized from these studies that during transients in which heat removal is continued to be available through the steam generators and when the primary sodium circuit is under forced convection conditions, the cold leg temperatures of heat exchangers are not affected due to the thermal stratification phenomenon in the hot pool. Hence, the prediction of core temperature is also not affected under these transients. Thus, the analysis of core safety during this class of transients does not require detailed modeling of thermal stratification phenomenon in hot pool.

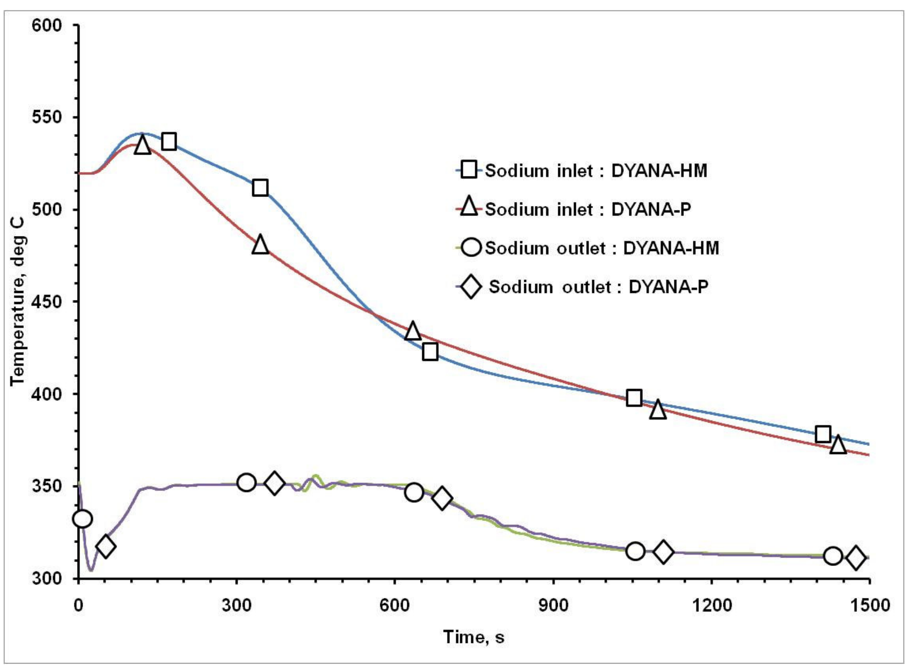

Fig. 5.4: Evolutions of SG sodium temperature during spurious SCRAM

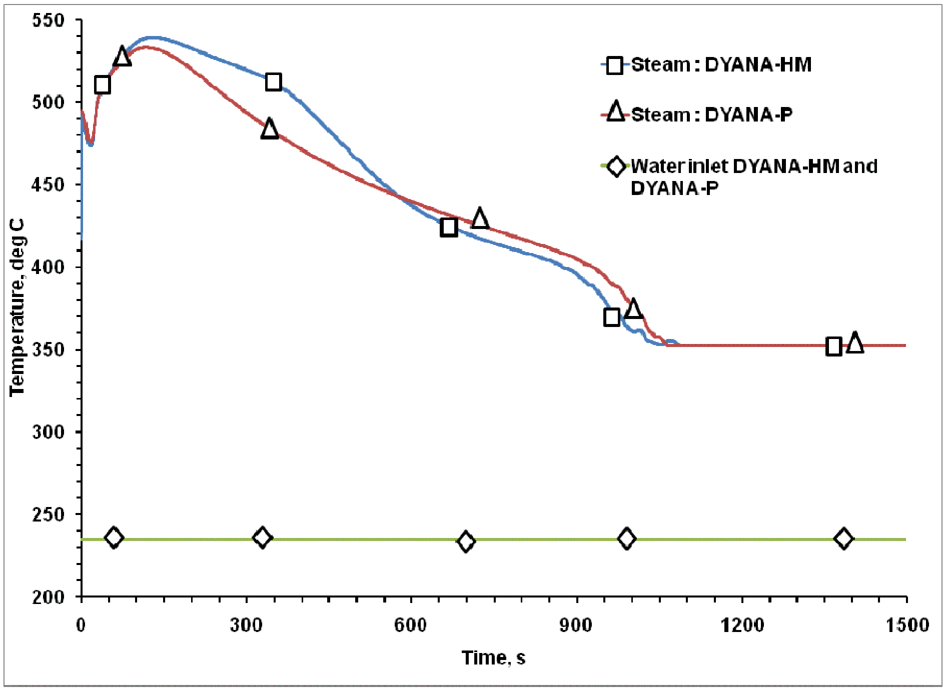

Fig. 5.5: Evolutions of steam temperature during spurious SCRAM

5.3 LOSS OF STEAM WATER SYSTEM

This event is simulated by considering that the heat sink to all the SG is lost instantaneously. Due to the loss of cooling caused by the event, sodium temperatures start increasing. As the reactor inlet temperature increases by 10 ^{0}C above its initial level, reactor trips automatically due to the action of plant protection system. Accordingly, reactor SCRAM is considered to take place at 30 s in this analysis. Predicted velocity and temperature distributions in the hot pool at 180 s and 360 s during the transient are shown in Fig. 5.6. It can be observed that when the sodium coming out of the core is colder than that in the pool, due to thermal stratification, the cold front is not able to penetrate freely into the sodium pool. Hence, the flow pattern in the hot pool is similar to that observed in the case of spurious SCRAM at 600 s (Fig. 5.1). The thermal stratification interface is formed near the bottom of control plug. Two major recirculation paths between inner vessel and control plug shell are observed. At 360 s, the sodium coming out of core is hotter than that present in the lower region of hot pool. Hence, due to the influence of buoyancy, the flow coming out of core splits up into two parts. One part, which crosses the lattice plate, flows upwards close to the control plug shell. Another part flowing below the lattice plate travels radially towards inner vessel and makes a recirculation path before entering IHX. Stratification layer is found to be shifted upwards towards IHX inlet.

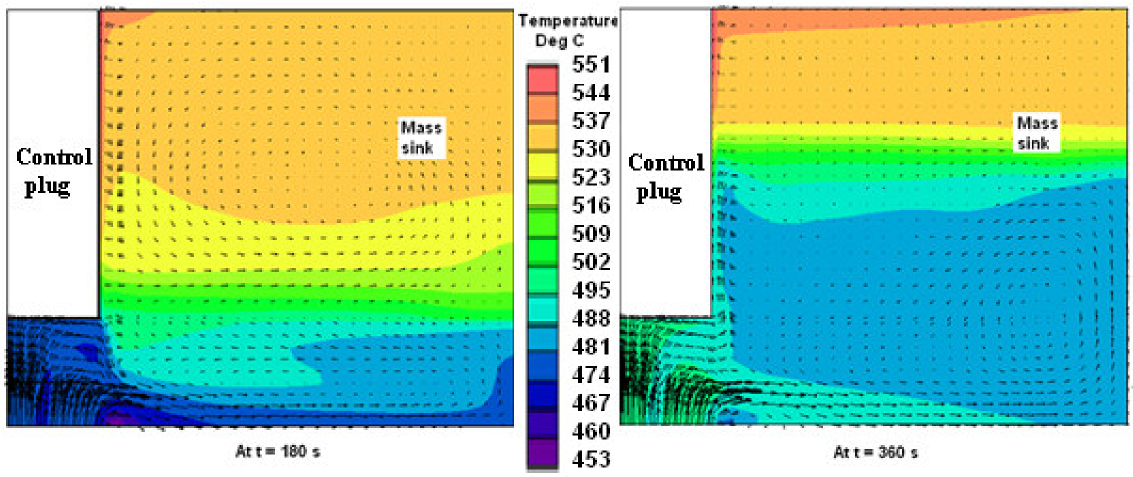

Fig. 5.6: Velocity and temperature distribution in hot pool predicted by DYANA-HM during loss of steam water system

Predicted temperature evolutions in the primary and secondary sides of IHX respectively by DYANA-HM and DYANA-P codes are compared in Figs. 5.7 and 5.8. It can be observed that significant difference between the predictions exists both in the hot leg as well as in cold leg of IHX. The differences between the predictions continue to be present throughout the transient. Predicted temperature evolutions at the IHX outlet by both the codes are close during the first 200 s of the transient. Subsequently, the effect of thermal stratification in the hot pool gets propagated to the outlet of IHX after some time delay. This delay is due to the fact that initial evolution of primary outlet temperature is mainly governed by the large increase in secondary sodium inlet temperature which happens immediately following the initiating event (as evident in Fig. 5.8). With respect to the evolution of secondary sodium temperature, secondary sodium outlet of IHX is the one which gets affected initially due to the thermal stratification effects in hot pool. This effect gets

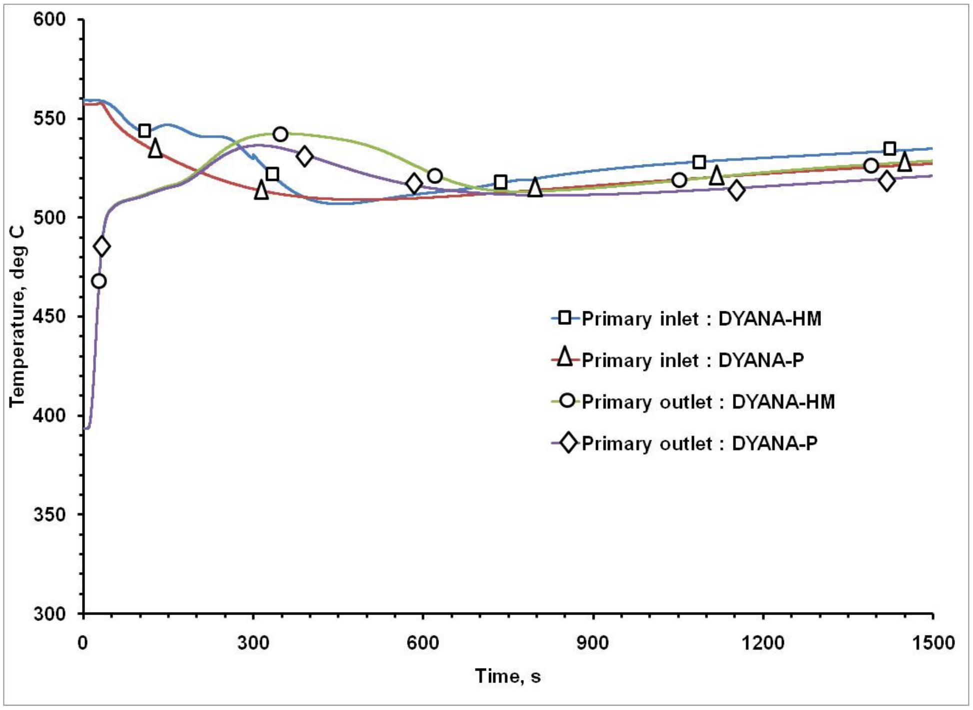

Fig. 5.7: Evolutions of IHX primary temperature during loss of steam water system

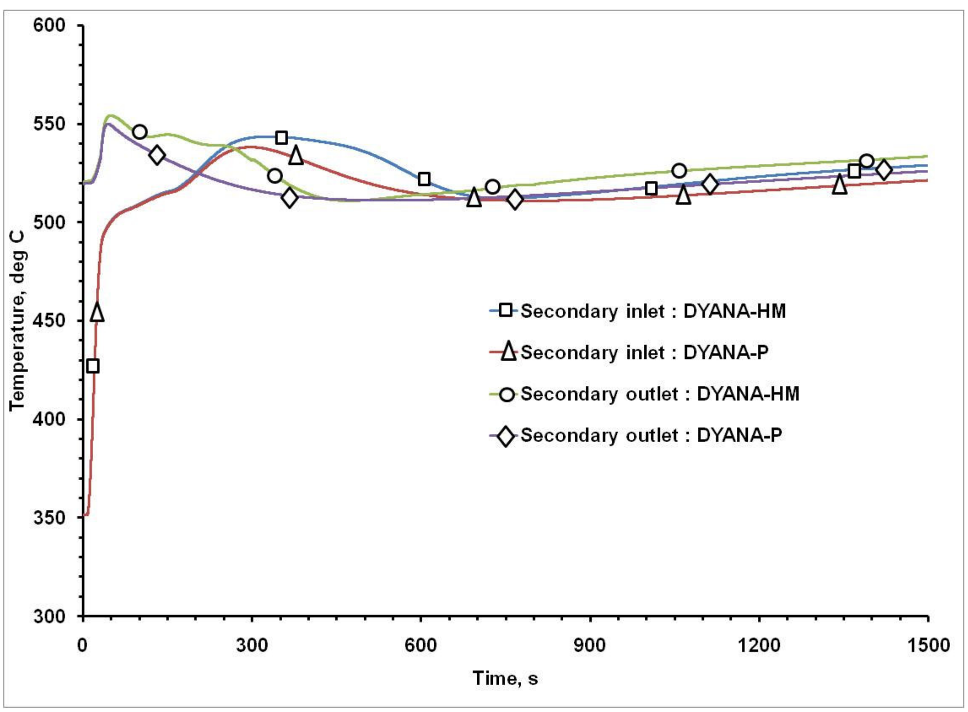

Fig. 5.8: Evolutions of IHX secondary temperature during loss of steam water system

propagated to the inlet of SG after some time delay (at about 100 s) in the surge tank and hot leg piping (as evident in Fig. 5.9). Subsequently, the effect gets communicated to the outlet of SG after a further delay in the SG (at about 150 s). Secondary inlet of IHX faces this effect after a further delay in the pump tank and cold leg piping (at about 200 s). Thus, it can be concluded that thermal stratification in hot pool affects the temperature evolution of entire plant during this event. In spite of secondary sodium circuit under forced flow mode, the effect of thermal stratification in the hot pool on the secondary sodium temperature remains unabated under the conditions when SG cooling is not available.

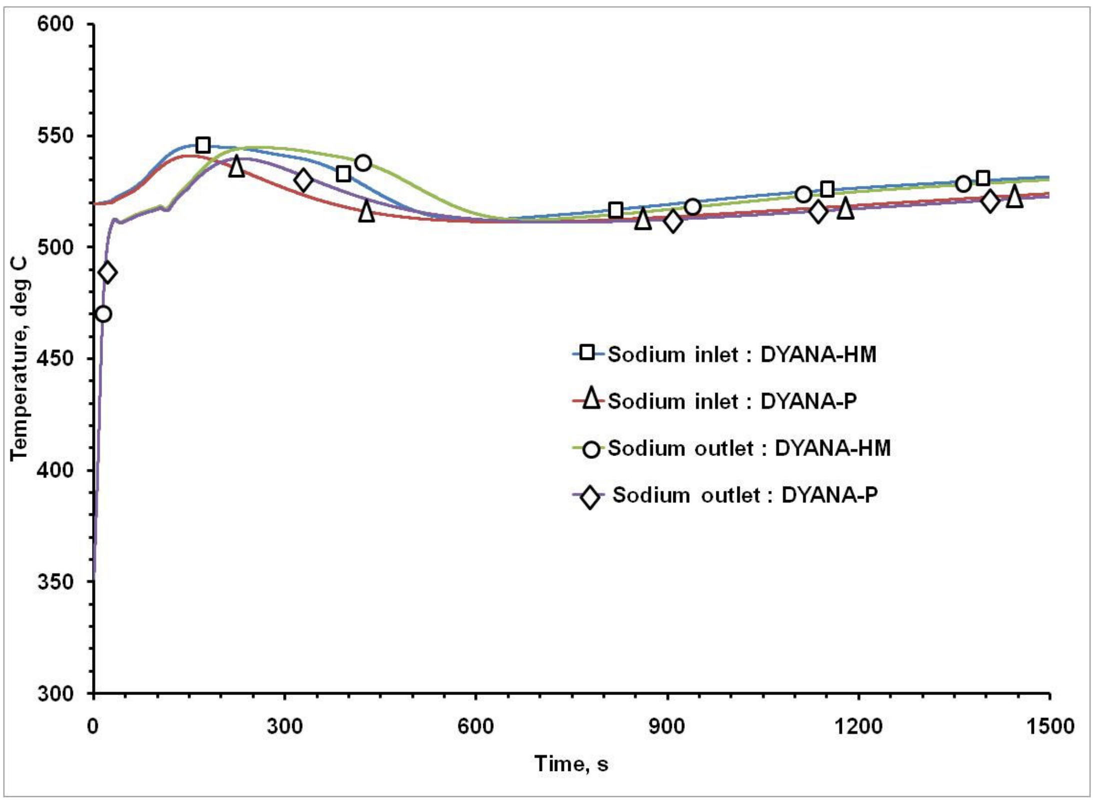

Fig. 5.9: Evolutions of SG sodium temperature during loss of steam water system

5.4 CLASS IV POWER FAILURE

This event is simulated by considering the primary sodium pumps coast down to 18 % speed (taking over by emergency power), secondary sodium pumps coast down to zero speed and heat sink to all the SG is lost instantaneously. Due to the speed reduction of primary sodium pumps, reactor trips automatically due to the action of the plant protection system. Accordingly, reactor SCRAM is considered to take place at 0.5 s in this analysis. Predicted velocity and temperature distributions in the hot pool at 180 s and 360 s during the transient are shown in Fig. 5.10. It can be observed that when the sodium coming out of the core is colder than that in the pool, due to thermal stratification, the cold front is not able to penetrate freely into the sodium pool. The thermal stratification interface is formed near the bottom of control plug. Two major recirculation paths between inner vessel and control plug shell are observed. At 360 s, the sodium coming out of core is hotter than that present in the lower region of hot pool. Hence, due to the influence of buoyancy, the flow coming out of core splits up into two parts. One part, which crosses the lattice plate, flows upwards close to the control plug shell. Another part flowing below the lattice plate travels radially towards inner vessel and makes a recirculation path before entering IHX. Stratification layer is found to be moving upwards towards IHX inlet. The flow and temperature profile in this case are similar to that observed in the case of loss of steam water system event.

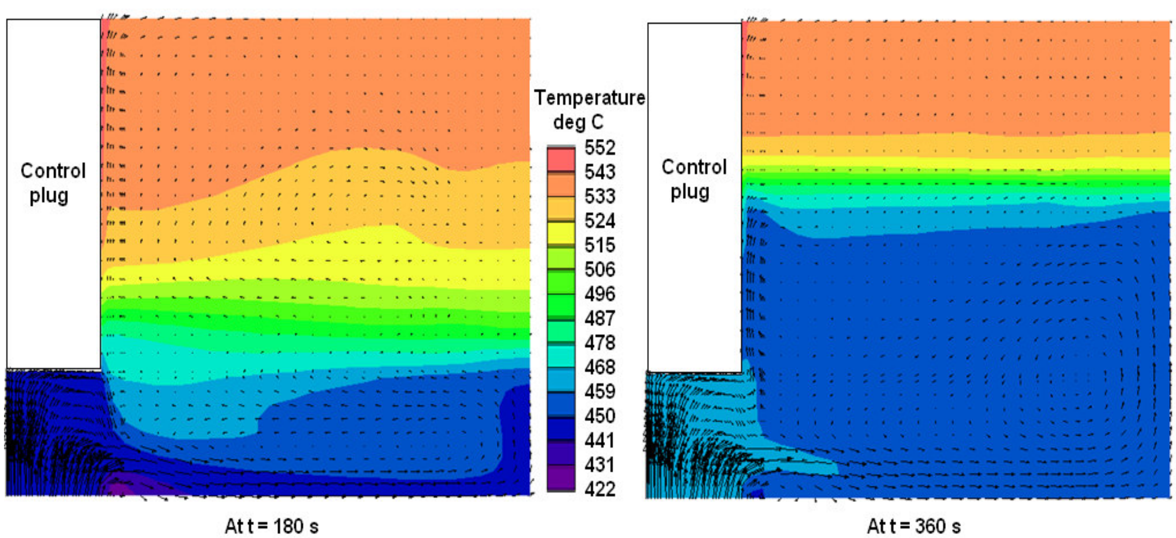

Fig. 5.10: Velocity and temperature distribution in hot pool predicted by DYANA-HM during power failure

Comparison of predicted temperature evolutions in the primary and secondary sides of IHX respectively by DYANA-HM and DYANA-P codes is shown in Figs. 5.11 and 5.12. It can be observed that significant differences between the predictions exist both in the hot leg as well as in the cold leg temperature of IHX. The differences continue to be present throughout the transient. Reduction in hot pool temperature following reactor trip causes secondary sodium temperature at the outlet of IHX to reduce. After about 300 s, the outlet temperature decreases below the inlet temperature indicating heat transfer from secondary sodium circuit to primary circuit. This causes adverse buoyancy head to be developed in the secondary sodium circuit resulting in flow reversal and flow oscillations.

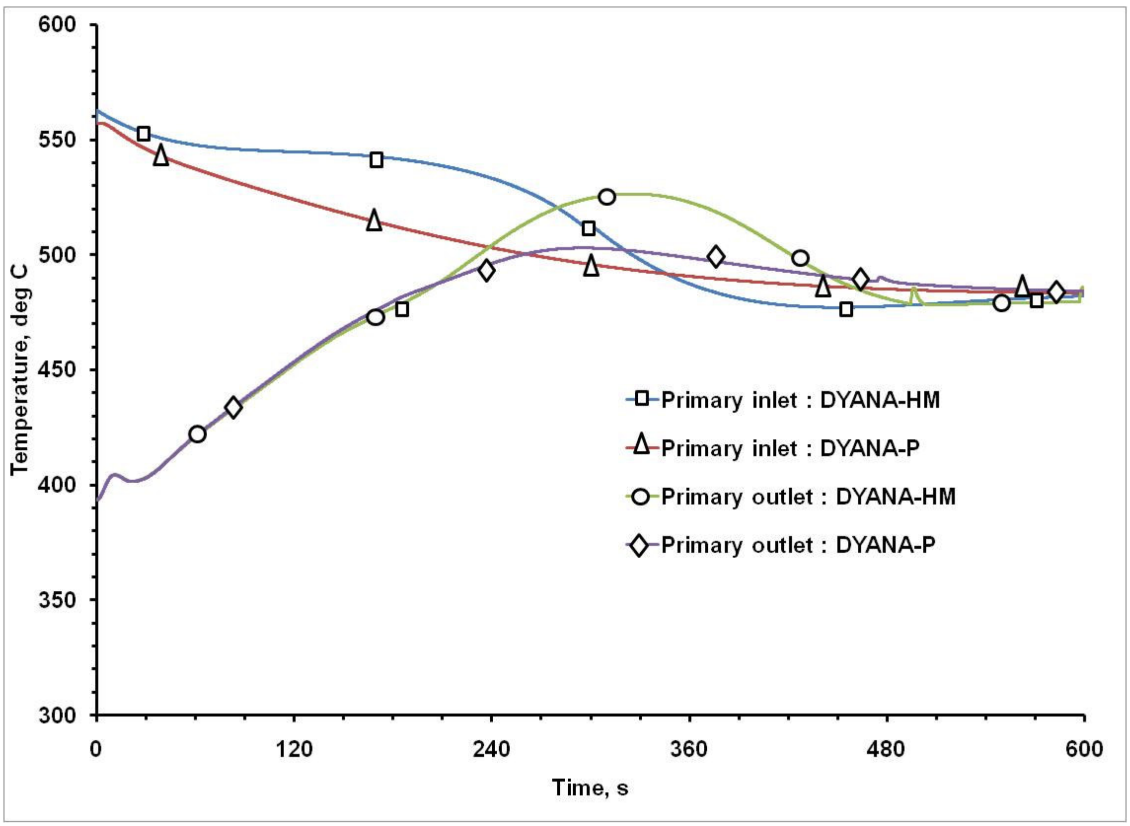

Fig. 5.11: Evolutions of IHX primary temperature during class IV power failure

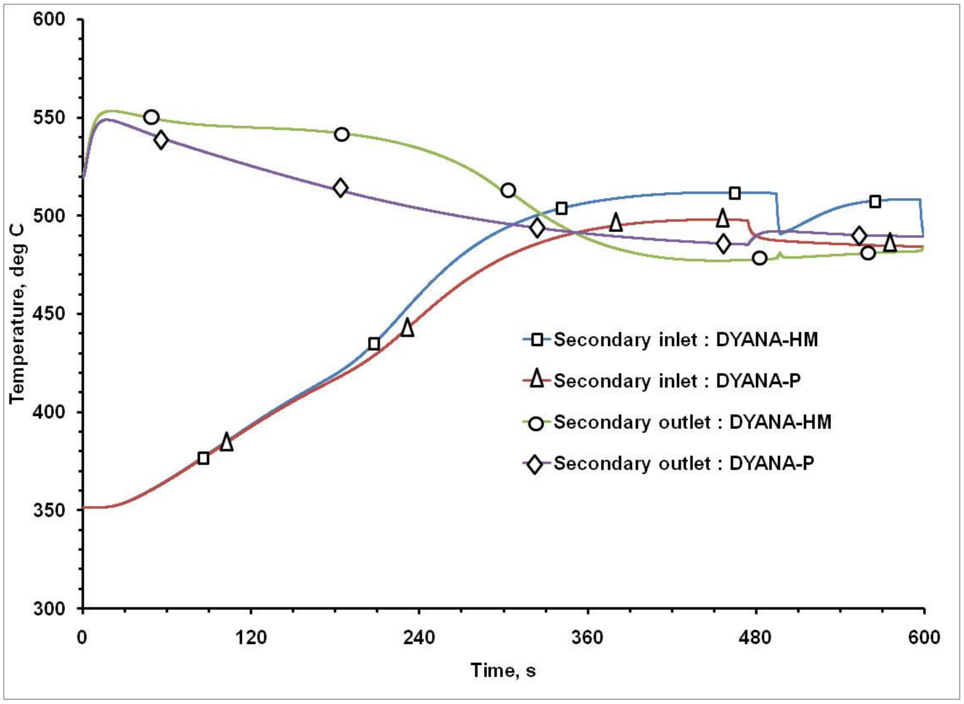

Fig. 5.12: Evolutions of IHX secondary temperature during class IV power failure

The first appearance of flow reversal in the secondary sodium circuit is predicted by DYANA-P code at 470 s and the same predicted by DYANA-HM is at 490 s. This difference is due to the relatively slower reduction in the primary sodium temperature at the inlet of IHX due to thermal stratification in hot pool. Flow oscillations continue in the secondary sodium circuit after this time. For the clarity of presentation, temperature evolutions are plotted for a time duration of 600 s only. The reversal of secondary sodium flow predicted by DYANA-P is sustained for the longer duration, whereas that predicted by DYANA-HM is in the form for short time pulses. This is the reason for the typical difference in the behavior of secondary sodium inlet and outlet temperature evolutions of IHX predicted by DYANA-P and DYANA-HM at the instant of flow reversal.

Temperature evolutions at the outlet of IHX predicted by both the codes are similar during the first 200 s of the transient. Subsequently, the effect of thermal stratification in the hot pool gets propagated to the outlet of IHX also. The propagation of thermal stratification effects into the secondary sodium circuit is slightly delayed in this case compared to that in the case of loss of steam water system event. This is due to the absence of forced flow in the secondary sodium system. Thus, thermal stratification in hot pool affects the temperature evolution of entire plant (Figs. 5.11 to 5.14) during this event. Sudden reductions in sodium temperature at the outlet of SG observed after 470 s in Fig. 5.13 are due to the reversal of secondary sodium flow in the circuit as shown in Fig. 5.14. It is evident from Fig. 5.14 that the evolution of natural convection predicted in the secondary sodium circuit is also influenced by thermal stratification in hot pool. At the first instant of flow reversal in the secondary sodium circuit, the temperature change predicted in the secondary sodium across IHX by DYANA-HM code is higher than that predicted by DYANA-P. Therefore, the moment flow reversal happens, the temperature reduction caused at the secondary sodium inlet of IHX is higher in the case of DYANA-HM and hence the adverse buoyancy head in the circuit gets nullified immediately. The flow again sets up in the forward direction in the circuit. This does not happen in the case of prediction by DYANA-P and hence the reverse flow sustains for a longer duration.

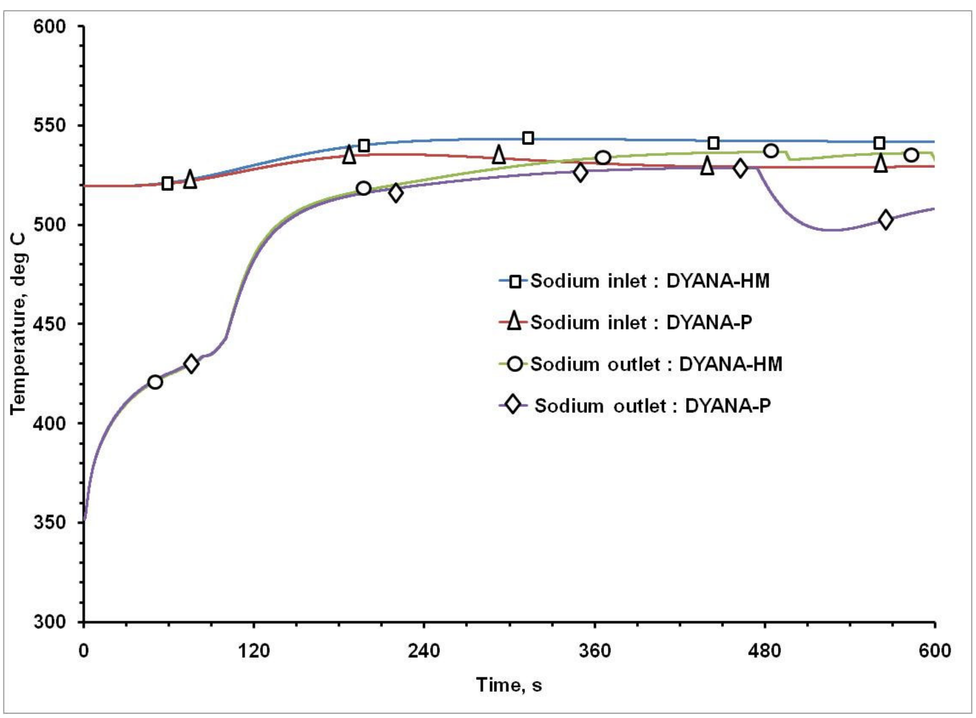

Fig. 5.13: Evolutions of SG sodium temperature during class IV power failure

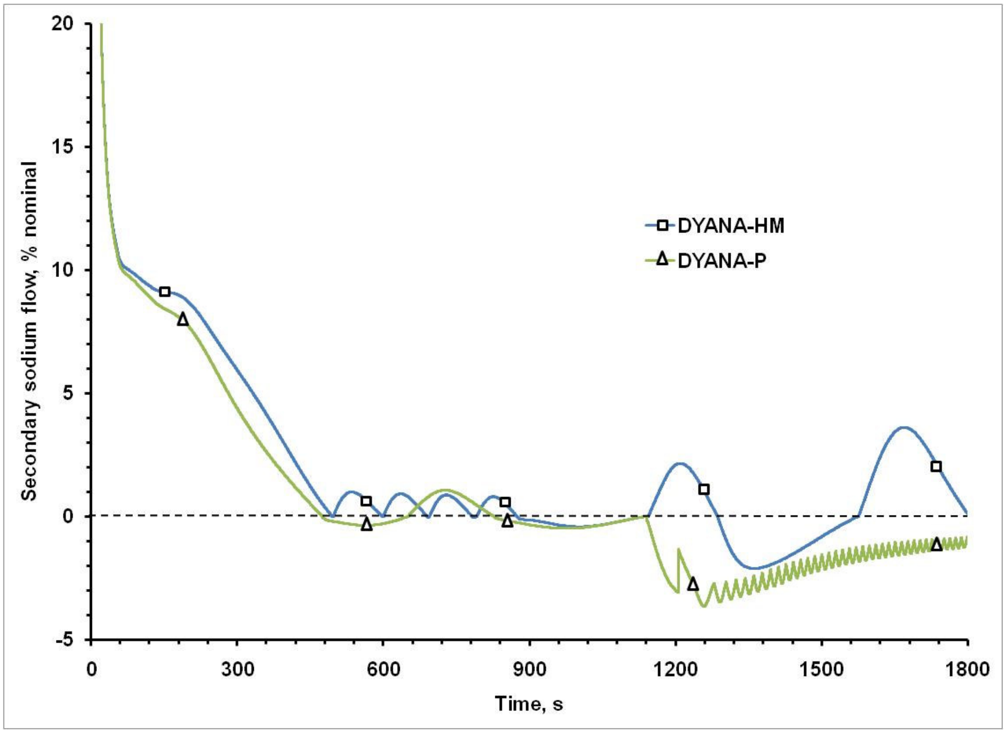

Fig. 5.14: Evolutions of natural convection flow in secondary sodium circuit during class IV power failure

5.5 STATION BLACKOUT

This event is simulated by considering that primary and secondary sodium pumps get tripped simultaneously and coast down to zero speed. Heat sink to all the SG is also lost instantaneously. Due to the speed reduction of primary sodium pumps, reactor trips automatically by the action of the plant protection system. Accordingly, reactor SCRAM is considered to take place at 0.5 s in this analysis. Sodium flows in both primary and secondary sodium circuits enter into natural convection conditions during this event. Predicted velocity and temperature distributions in the hot pool at 180 s and 360 s during the transient are shown in Fig. 5.15. It can be observed that most of the hot pool is in stagnant condition due to low natural convection induced flow rate through the core. The temperature evolution in the pool is governed by diffusion rather than convection. Sodium flow coming out of the core is hotter than that present in the pool. Due to this favorable buoyancy, the sodium from the core rise to the free surface by flowing along the control plug shell. The core flow being only 3 % of nominal flow (natural convection flow), the convective mixing region in the hot pool by the sodium emanating from the core is confined to a small volume close to the control plug shell. In the rest of the region the thermal mixing is mainly by conduction.

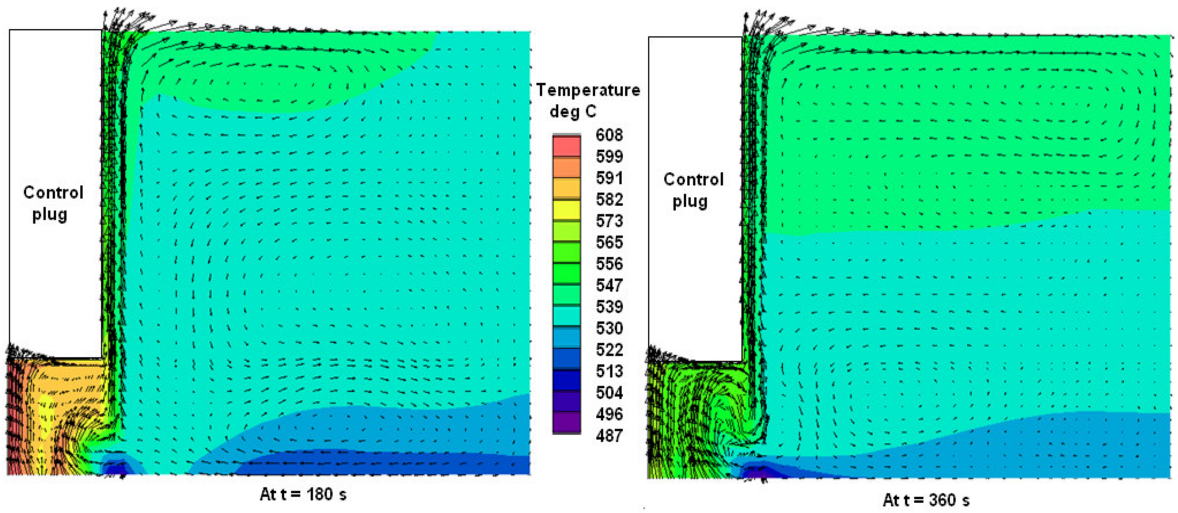

Fig. 5.15: Velocity and temperature distribution in hot pool predicted by DYANA-HM during station blackout

Evolution of sodium flows through the core predicted by DYANA-P and DYANA-HM are shown in Fig. 5.16. It can be observed that both the predictions are similar. Evolution of primary sodium temperature at the inlet and outlet of IHX is shown in Fig. 5.17. It can be observed that the evolutions of IHX primary sodium inlet temperature predicted by both the models are similar. Thus, the consideration of thermal stratification effect does not influence the temperature evolution of various parts of the plant during this event.

Temperature evolution of sodium in the hot pool is governed by diffusion due to low flow rate of sodium through the core. The buoyancy force developed in the primary sodium circuit results in a core flow rate of only ~ 3% as evident in Fig. 5.16. In the case of power failure event, the core flow (forced flow) maintained after reactor SCRAM is ~ 18 % due to the running of primary sodium pumps by the emergency power supply. When the core flow is in the order of 3 %, the decay power produced in the core is significant enough to heat up the

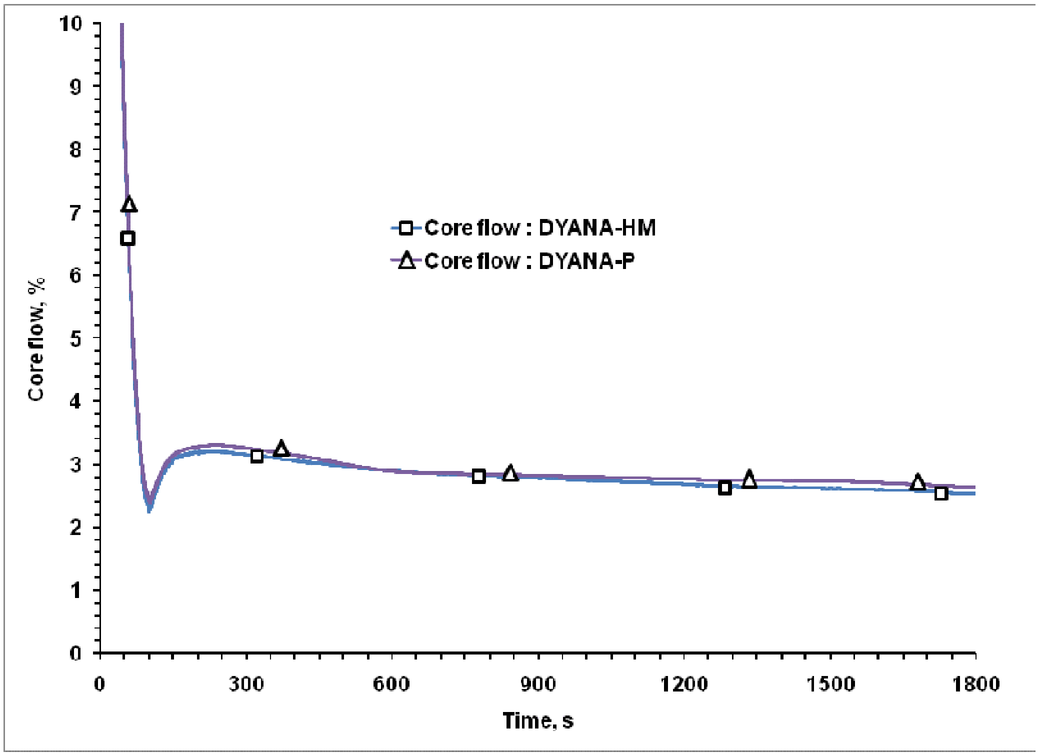

Fig. 5.16: Evolution of core flow during station blackout

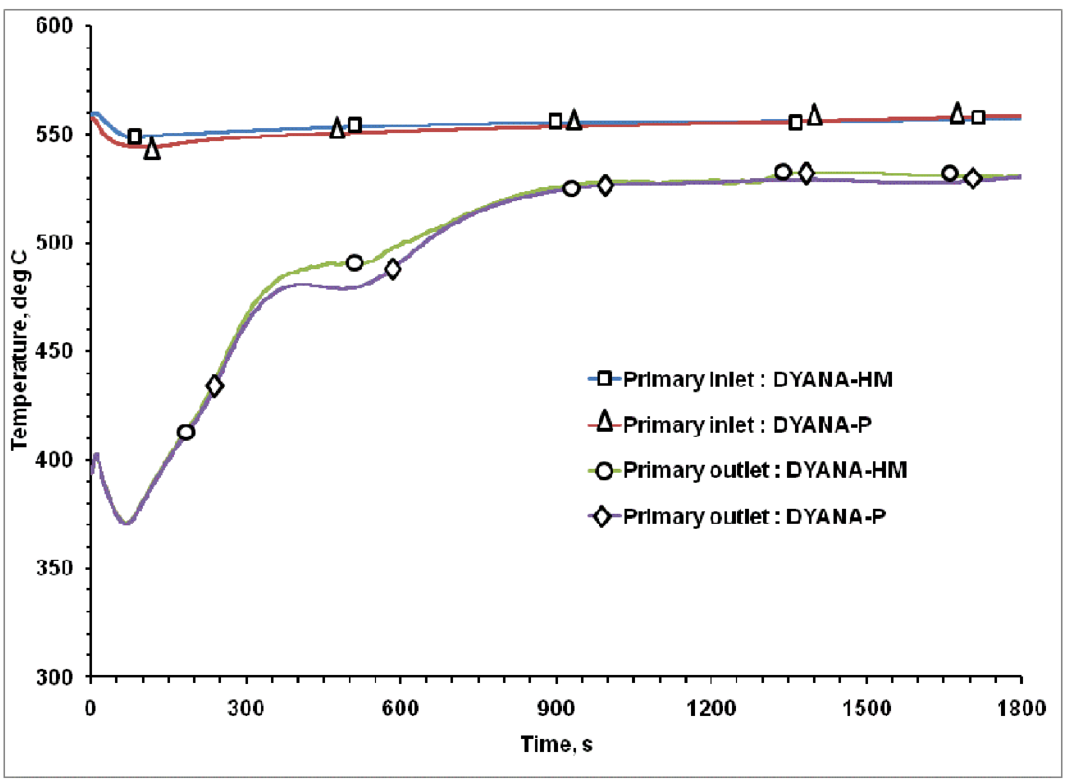

Fig. 5.17: Evolution of primary sodium temperature at the inlet of IHX during station blackout

sodium passing through the core significantly above the mean temperature hot pool sodium. The primary sodium flow rate in the hot pool being very low, thermal mixing of hot pool would be governed by diffusion rather than convection. Because of the good conductivity of sodium, temperature hot pool sodium evolve in a well mixed manner. Therefore, stratification effects are absent in this case. In the case of power failure, core flow is in the order of 18 % after reactor SCRAM. This results in sodium to exit from the core at a temperature much lower than that of hot pool sodium resulting in significant thermal stratification effects in the hot pool. During station blackout event, the temperature of hot pool changes gradually and nearly in a well mixed manner due to very weak natural convection flow developed in the primary sodium circuit.

5.6 CLOSURE

Investigation of typical transients suggest that when heat removal is continued in steam generator units, then the prediction of hot leg temperatures of heat exchangers alone are affected due to hot pool thermal stratification. Prediction of cold leg temperatures and hence the core temperatures under these class of transients are not affected. However, when no heat removal takes place through SG, hot pool thermal stratification significantly influences temperature evolution in various parts of the plant. This occurs even when the secondary sodium circuit is under forced flow conditions. During transients in which secondary sodium circuit is under natural convection and primary circuit is under forced flow, the evolution of natural convection flow behavior in the secondary sodium circuit is influenced by the thermal stratification.

Hot pool is in well mixed condition during normal operating conditions and thermal stratification effects develop only after reactor SCRAM. Therefore, the actuation time of plant protection system during various design basis events do not get affected due stratification effects. Moreover, plant protection system gets triggered within a few seconds after the occurrence of initiating events having serious implications on core safety. Therefore, multi-dimensional model based studies are not essential for the design of plant protection system and demonstration of core safety. However, multi-dimensional model based studies provide accurate information with respect to transient thermal loading on various structures and components which form an essential part of the thermo-mechanical design and life prediction of systems and components. Moreover, realistic prediction of transient scenario in the plant under post shutdown cooling conditions can be obtained only with the inclusion of multi-dimensional based thermal stratification models. Thus, development of capability to address above two scenario is the main benefit of DYANA-HM over DYANA-P.

CHAPTER – 6

PRIMARY FLOW HALVING TIME AND SYMPATHETIC SAFETY ACTION

6.1 INTRODUCTION

It is known that the heat removal capacity of coolant system is strongly linked to flow rate of coolant. During transients resulting from loss of pumping power, coolant flow through reactor core reduces with time. Thermal consequences in the core under such conditions depend on the rate of reduction of coolant flow and the time of initiation of safety actions. Flow coast down characteristics of circuit depends on hydraulic inertia of the system. The inherent hydraulic inertia derived from the piping and pumping systems is low in the primary system with pool type concept. Considerable inertial effects can be derived by mounting a flywheel on pump shaft. This retards the speed reduction of pump following trip and thereby ensures the pumping of coolant in the circuit for a significant duration even after the trip of pump motor. Coast down duration of the pump is very important from safety considerations of the plant as it (i) slows down the rate of rise of temperatures in the core, (ii) provides comfortable time for initiating safety actions, (iii) reduces the peak temperature of reactor core components reached during transients and (iv) provides time for smooth take over from main heat transport system to decay heat removal system.

Larger coast down time for pumps is desirable from the above considerations. However, since the coast down time is directly linked to size of flywheel mounted on pump shaft, large coast down time leads to an expensive design. Formation of cold stagnation layer above the core top can cause momentary flow reversal in the core. Flow reversal in core will have serious thermal consequences on clad and coolant temperatures inside the subassembly. Moreover, the flow reversal phase would be associated with momentary flow stagnation resulting in very poor heat transfer from cladding to coolant. Thus, flow reversal in core should be prevented from safety considerations. During transients resulting in natural convection flow evolution in core, high primary flow halving time (FHT) results in formation of stratification layers in the hot pool above the core. FHT is the time in which the flow in the circuit reduces to 50 % of the initial value. It was observed from earlier studies [52] that for any selected value of primary system inertia, higher value of secondary system inertia is beneficial for better core flow and heat removal in a loop type SFR. For a given secondary system inertia, increasing of primary system inertia beyond a value causes reduction in minimum core flow. The core flow even reverses for very high values of primary system inertia. The flow reversal can lead to coolant boiling if the flow does not recover immediately. Thus, a loop type SFR requires large inertia for the secondary pump to avoid flow reversal effects. It may be highlighted that this is not applicable for a pipe rupture event.

Similar studies for pool type SFR [53] indicate the requirement of higher flow halving time for secondary sodium system compared to that for primary sodium system to avoid flow reversal in core. Thermal stratification in the pool plays an important role in the thermal hydraulics linked to coast down time of pumps [54, 55, 56]. A medium range coast down time for the primary sodium system induces development of a high density layer near the core exit. This layer contributes to an adverse buoyancy effect in the core coolant flow, and finally results in increasing the peak coolant temperature in the core. Hence, there is a need for optimization of coast down time of primary to ensure establishment of a smooth natural convection flow through the core.

6.2 CONSIDERATION FOR DECIDING FLOW HALVING TIME

There are several considerations for deciding coast down of coolant in heat transport systems. Important factors are listed below:

(i) To ensure plant safety under loss of flow events

(ii) Avoid reactor trip during short term power fluctuations

(iii) Smooth take over of decay heat removal system from normal heat transport system under loss of heat sink events

(iv) Avoid stratification effects in the pool

Careful investigation of these factors is carried out for selecting the coast down time. The first two considerations listed above impose conflicting requirements on fixing threshold values on reactor SCRAM parameters. To ensure plant safety, it is desirable to have the threshold values on SCRAM parameter as close as possible to the values of parameters during normal operating conditions. Normal fluctuations in the parameters, uncertainties in measurement and drift in setting of threshold values are considered in fixing the threshold values from the point of view of operator comfort. Under short term power fluctuations, the electrical systems undergo short term perturbations. As a result the pumping systems in the reactor would go through a transient phase leading to short term flow reduction and pick up. During this phase, if the SCRAM parameters are challenged, then reactor would get tripped automatically irrespective of the normal electrical power being restored. Reactor trip under short term power fluctuations can be avoided through (a) suitably fixing threshold for SCRAM parameters without compromising safety (such that SCRAM parameters do not cross the threshold value), (b) selecting longer flow coast down time for pumping systems (flow reduction caused is benign) and (c) combination of (a) and (b).

The consideration (iii) plays a key role in reactor system which adopt decay heat removal systems connected to secondary sodium circuit. Under loss of pumping conditions, the decay heat is removed through natural convection flow established in the primary and secondary sodium systems. The driving force for natural convection developed due to buoyancy depends on the thermal centre difference between the heat source and heat sink. In the primary sodium circuit, the thermal centre difference between reactor core and IHX is responsible for the buoyancy induced driving force, whereas in the secondary sodium system the same is between IHX and decay heat exchanger. During the coast down phase of pumps, when the sodium flows in the primary and secondary sides are of comparable magnitude, then the thermal centre of IHX coincides with the geometrical centre. Hence, it is desirable to have higher flow coast down time for secondary compared to primary. In the primary side, the effect of thermal centre difference between core and IHX gets masked to a great extent by the thermal capacities of sodium pools which delay the temperature evolution of inlet and outlet plenums allowing for smooth establishment of stable natural convection flow in both primary as well as secondary.

Following reactor SCRAM, reactor power reduces in the core and cold sodium starts coming out of fuel subassemblies. This causes cold shock on above core structures. In order to reduce the cold shock, one of the important automatic procedure adopted in the plant is to reduce speeds of sodium pumps to a lower value after the reactor power reduces to decay power level. Lower coast down time is beneficial to produce desirable results from this consideration. Nevertheless, under pump trip conditions, the hot shock on various components can be reduced by selecting a longer coast down time. A case study presented to elaborates this aspect.

6.3 FLOW HALVING TIME Vs SAFETY

A case study has been carried out towards bringing out the strong link between the SCRAM threshold and coast down time. Objectives of the case study are to ensure core safety and at the same to avoid reactor trip due to short term power perturbations.

6.3.1 SCRAM Parameters for Power Failure Event

Thermal hydraulic analysis of off-site power failure event has been carried out using the DYANA-P code. This event is simulated by assuming instantaneous dryout all SG and setting the drive torques of primary and secondary sodium pumps to zero. Thus, the primary and secondary pumps coast down are governed by their inertia. SCRAM parameters protecting the plant through reactor trip during a power failure event are low primary pump speed (N_P), high power to flow ratio (P/Q), high central SA sodium outlet temperature (θ_{CSAM}) and high coolant temperature rise across central SA ($\Delta\theta_{CSAM}$). θ_{CSAM} and $\Delta\theta_{CSAM}$ evolve at the same time for events occurring at full power conditions. Therefore, for practical purpose of analysis, these two parameters can be treated as a single one.

6.3.2 Flow Halving Time to Ensure Safety

Primary coast down time helps in reducing the rate of rise of core temperatures during loss of flow events and thereby allows more time for safety action, before the core temperatures exceed the respective design safety limits. The design safety limits for this category of events [57] are (i) maximum clad hotspot temperature is less than 800 ^{0}C, (ii) there is no coolant boiling inside the core and (iii) there is no melting of the fuel. The SCRAM parameters N_P and P/Q are the first two parameters appearing and are connected to the first shutdown system. The third parameter, θ_{CSAM} is connected to the second shutdown system. A parametric study has been carried out by varying the primary coast down time, which is represented in terms of flow halving time (FHT). Secondary FHT is considered constant at 4 s in this study. Summary of results of the study are given in Table 6.1. Threshold for triggering SCRAM by θ_{CSAM} parameter in this case is considered as 10 K rise in this parameter above the initial steady state value.

It can be observed from Table 6.1 that when the FHT of primary sodium system is less than 3 s, the maximum value of clad hotspot temperature exceeds 800 ^{0}C. Table 6.1 discusses only about the peak temperatures reached in the core at the time of initiating reactor SCRAM. Subsequently, the core temperatures may again rise due to the continued reduction in core flow before stable natural convection flow is established in the core. This can lead to the formation of a second peak during the transient. Evolution of normalized 'core flow to core power' during the transient for various values of primary FHT is shown in Fig. 6.1. It can be observed from the figure that the core flow reduces to a minimum before a stable natural convection flow is established.

Table 6.1: Off-site power failure event :Minimum FHT for ensuring safety

Sl. No.	Primary FHT, s	Time at which process parameter (θ_{CSAM}) reaches SCRAM threshold, s	Time of initiation of reactor SCRAM, s	Maximum clad hotspot temperature, ^{0}C	Maximum average sodium hotspot temperature, ^{0}C
1	8.0	1.22	1.51	731	640
2	6.0	1.1	1.39	743	650
3	4.0	0.96	1.25	766	670
4	3.0	0.89	1.18	792	692
5	2.0	0.82	1.11	855	748

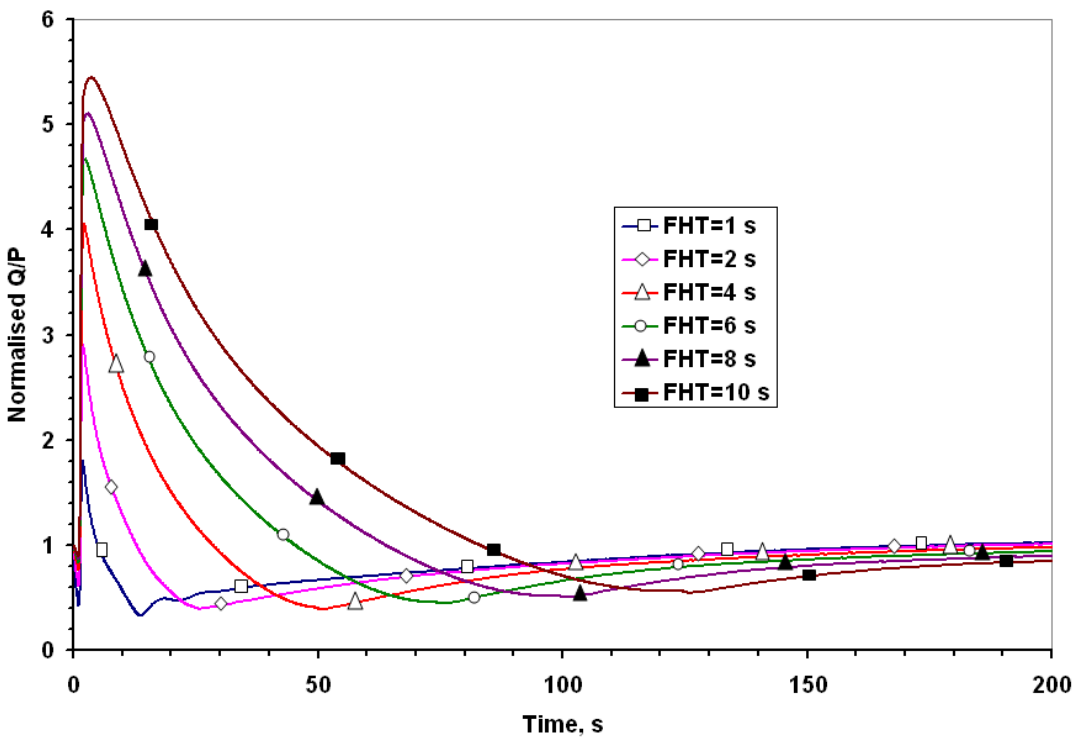

Fig. 6.1: Evolution of normalized core flow to power ratio during power failure

Variation of minimum core flow against primary FHT is shown in Fig. 6.2. It can be observed that initially up to a FHT of 5 s, an increase in FHT causes reduction in minimum core flow reached during the transient. This is due to the interaction of buoyancy developed in the primary sodium circuit during the transient. However, this reduction does not affect the Q/P ratio significantly. This is due to the fact that the time at which minimum core flow is reached in the core gets extended with increase in FHT. Therefore, power produced in the core at the instant of minimum core flow reduces with increase in FHT. However, from the point of view of having increased core flow during the transient with increase in FHT, it is desirable to have it more than 5 s.

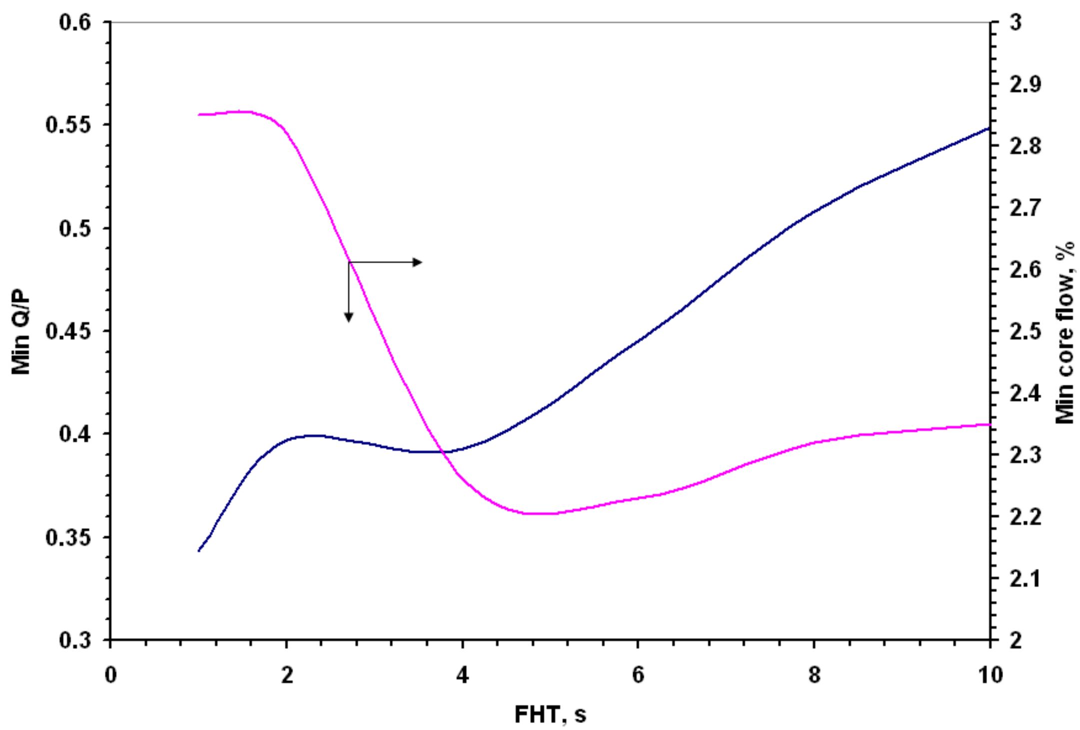

Fig. 6.2: Minimum core flow reached during power failure event

Due to the reduction of Q/P ratio below 1 during the transient, a second peak in clad hotspot temperature occurs as shown in Fig. 6.3. It can be seen that the second peaks are higher than the first peak. In order to limit the clad hotspot temperature below category 2 limit of 800 ^{0}C, the FHT required in the primary sodium circuit is 8 s. Thus, from the point of view of core safety primary FHT of 8 s is essential.

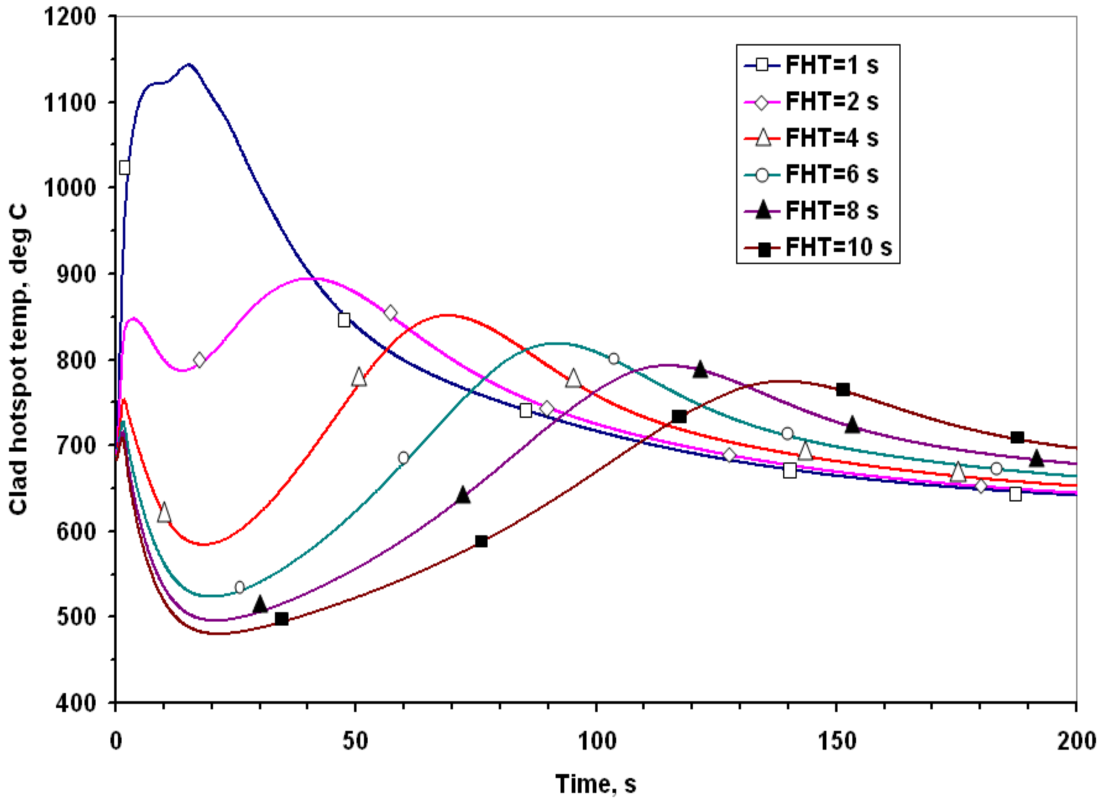

Fig. 6.3: Evolution of clad hotspot temperature during power failure

Apart from the above aspects, an examination of the dynamics of SFR [58-63] suggests that reactors with larger primary sodium FHT are beneficial from the point of view of having a benign response to an Unprotected Loss of Flow (ULOF) event. Unprotected transients are important in the design of fast reactor systems as they are the initiators for energetic power excursion in the core. The coasting down time of the pump has been found to play an important role in reactivity dynamics, by bringing in sufficient negative feedback reactivity due to structural expansions in reactor assembly in case of ULOF. Thus, apart from analysis of protected transients, unprotected transients are also required to be considered in proper selection of FHT from the point of view of safety.

6.4 FLOW HALVING TIME TO AVOID SCRAM DURING SHORT TERM POWER FAILURE

When off-site power failure occurs in the plant, all the pump motors get tripped and flows in the respective circuits start reducing. This in turn causes rise in coolant temperature. In case power comes back within short time, then the coolant flows and hence the coolant temperatures will be restored back. If any of the SCRAM parameters crosses its trip threshold during this transient, then reactor SCRAM happens and restoration of power cannot ensure continued plant operation. Reactor will have to be taken to cold shutdown state and plant startup will have to be initiated for bringing the reactor back to operation. This affects the plant availability seriously. Therefore, it is desirable to avoid reactor SCRAM during short term power disturbances lasting for a few seconds. This can be achieved if the reactor SCRAM parameters do not increase to their respective SCRAM threshold values during the short term power failure conditions. In order to accomplish this, coast down times of coolant circuits have to be chosen accordingly. Minimum value of SCRAM parameter N_P and maximum values of parameters P/Q and θ_{CSAM} reached against primary FHT are shown in Figs. 6.4-6.6 respectively. The analysis has been carried out for various values of power failure duration. It may be noted that the threshold values of SCRAM parameters N_P, P/Q and θ_{CSAM} are 95 % nominal, 110 % and 10 K above nominal respectively.

It can be observed from these figures that when power failure extending beyond 0.5 s happens, in order to limit the SCRAM parameters below their respective trip threshold values, the FHT required for the primary system is 10 s. It can also be observed that approaching of the threshold of SCRAM parameters in various durations of power failure can be prevented by increase in the FHT. FHT requirement for various cases of power failure to avoid reactor SCRAM has been determined and is shown in Fig. 6.7. In order to prevent reactor SCRAM when power failure extend for 2 s duration, the requirement of FHT is 38 s.

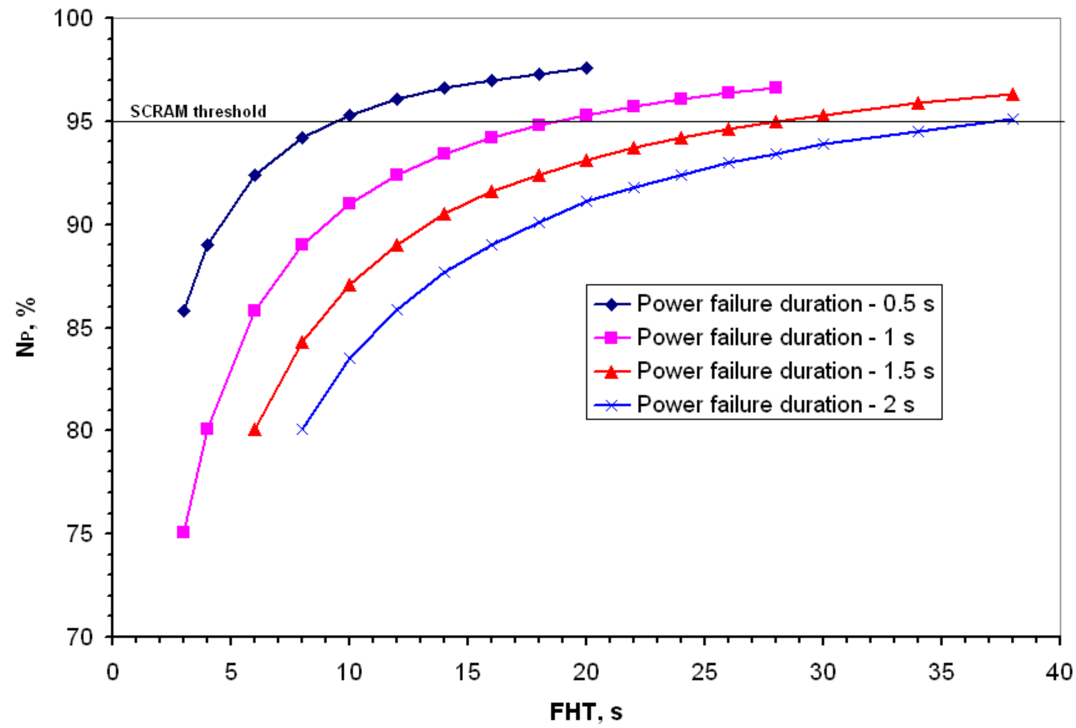

Fig. 6.4: Minimum value of speed parameter reached during power failure event

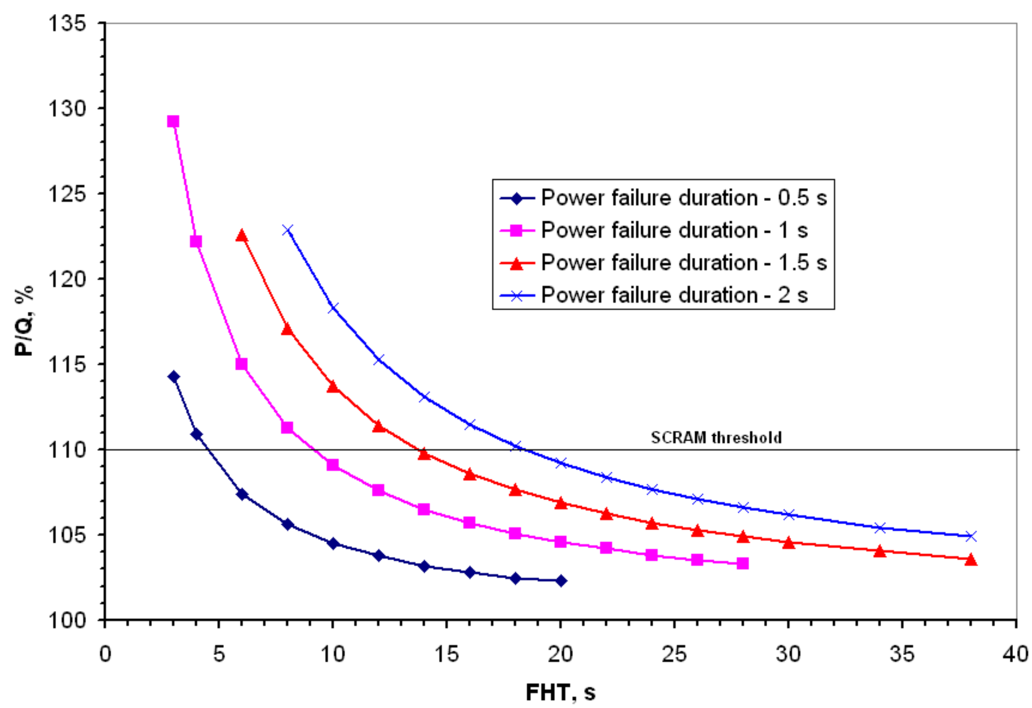

Fig. 6.5: Maximum value of P/Q parameter reached during power failure

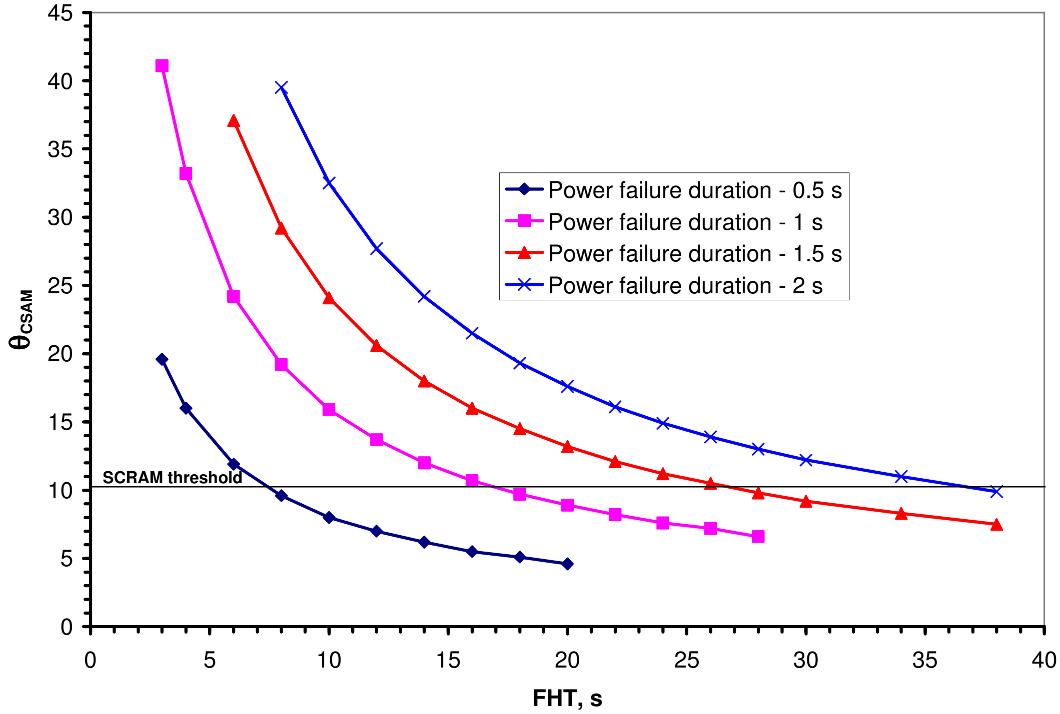

Fig. 6.6: Maximum value of θ_{CSAM} reached during power failure

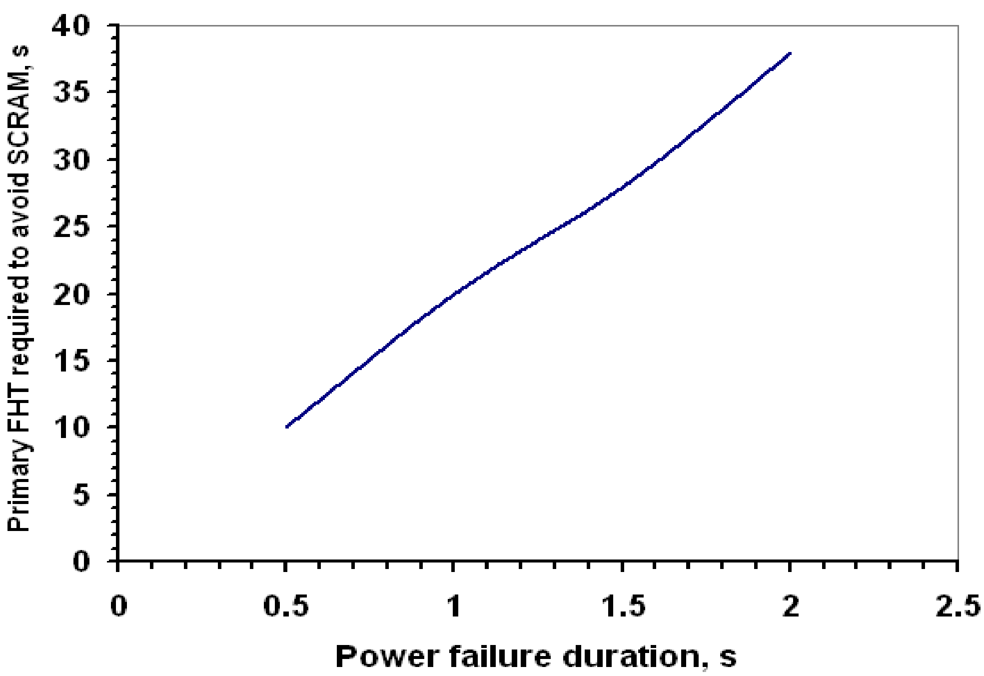

Fig. 6.7: Requirement of FHT to avoid SCRAM during short term power failure

This value can be brought down if the threshold values of SCRAM parameters are revisited. With the threshold values of SCRAM parameters revised to meet the safety requirements, a FHT of 8 s can eliminate reactor SCRAM during short term power failure for a duration extending up to 0.75 s.

6.5 SYMPATHETIC SAFETEY ACTION AND THERMAL STRATIFICATION

Reactor SCRAM suddenly reduces the power produced in the core to decay power levels. This results in sharp reduction in sodium temperature at the outlet of core subjecting the upper core structures to cold shock. To weaken the effect of cold shock, speeds of sodium pumps are reduced to a lower value (20 %) after SCRAM. This action known as sympathetic safety action delays the reduction of hot pool temperature following SCRAM and thereby reduces the rate of temperature reduction faced by the hot pool components. However, the primary sodium flow entering hot pool can lead to thermal stratification effects in the hot pool due to reduction in inertial force with respect to buoyancy force. The scenario being a cool down transient, adverse buoyancy effect is only developed in the hot pool causing the upper layers of hot pool subjected to significant thermal stratification as discussed in Section 5.2. Flow reduction action aids in the development of stratification layer and delays the breaking of the same. In order to ascertain the effect of sympathetic safety action on the thermal stratification phenomenon in hot pool, transient thermal hydraulic analysis of spurious SCRAM event has been carried out using DYANA-HM without considering sympathetic safety action. The predicted temperature evolution in hot pool is compared against those obtained in the case with sympathetic safety action (discussed in Section 5.2).

Predicted temperature distributions in hot pool at 300 s and 600 s after the initiation of spurious SCRAM are shown in Figs. 6.8 and 6.9 respectively. Also shown in these figures are the temperature distributions in the case with sympathetic action considered. It can be observed that when sympathetic safety action is not adopted the formation of stratification layers is prevented due to the good mixing offered by the full sodium flow emanating from the core. However, the hot pool gets cooled down faster when the sympathetic safety action is not considered. The flow pattern of primary sodium in the hot pool during the entire duration of the transient without sympathetic safety action also continues to be same as that during initial steady state conditions. When sympathetic safety action is adopted, the adverse buoyancy effects significantly influence the development of flow pattern in hot pool.

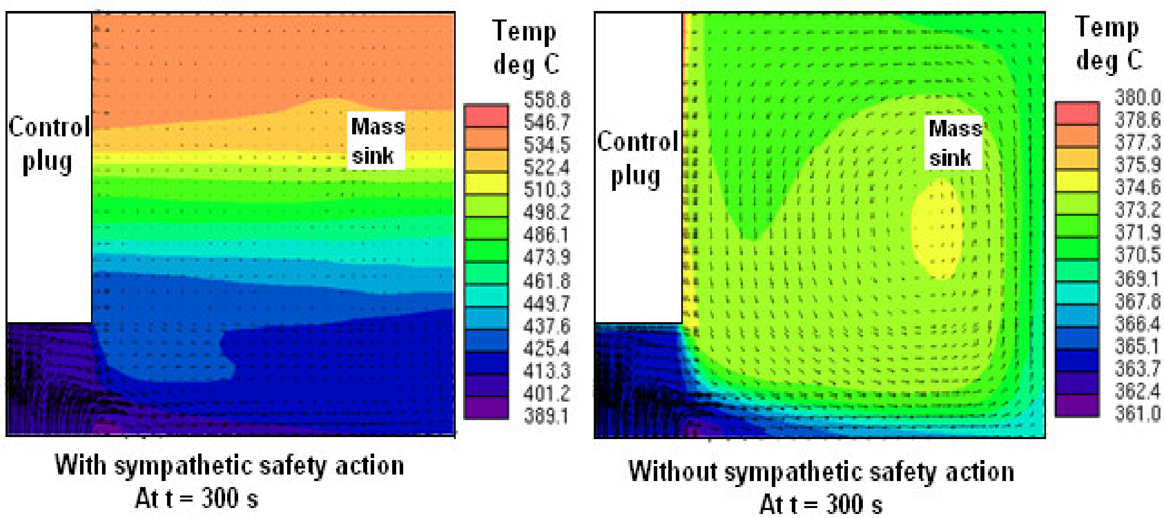

Fig. 6.8: Velocity and temperature distributions in hot pool at 300 s after SCRAM with and without sympathetic safety action adopted

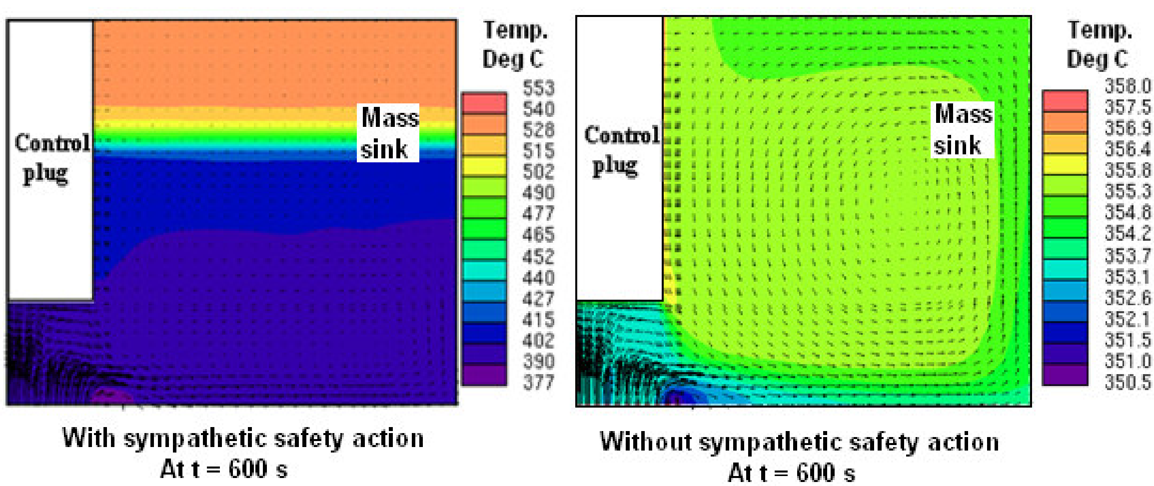

Fig. 6.9: Velocity and temperature distributions in hot pool at 600 s after SCRAM with and without sympathetic safety action adopted

Comparison of temperature evolutions at the inlet of IHX during the transient with and without sympathetic safety action is shown in Fig. 6.10. It can be observed from the figure that the sympathetic safety action helps retarding the rate of reduction of sodium temperature in the hot pool. The predicted rate of reduction sodium temperature at the inlet of IHX in the cases with and without sympathetic safety action, which is a representative of the cold shock seen by the components in hot pool, is shown in Fig. 6.11. It can be observed that sympathetic safety action helps in reducing the thermal shock from ~ 110 ^{0}C/min to 30 ^{0}C/min. The duration for which the rate of temperature reduction remains more than 10 ^{0}C/min is the same in both the cases. Thus, though the sympathetic safety action results in development of thermal stratification in hot pool for about 15 minutes after reactor SCRAM, a significant reduction in thermal shock faced by components is the benefit of this procedure.

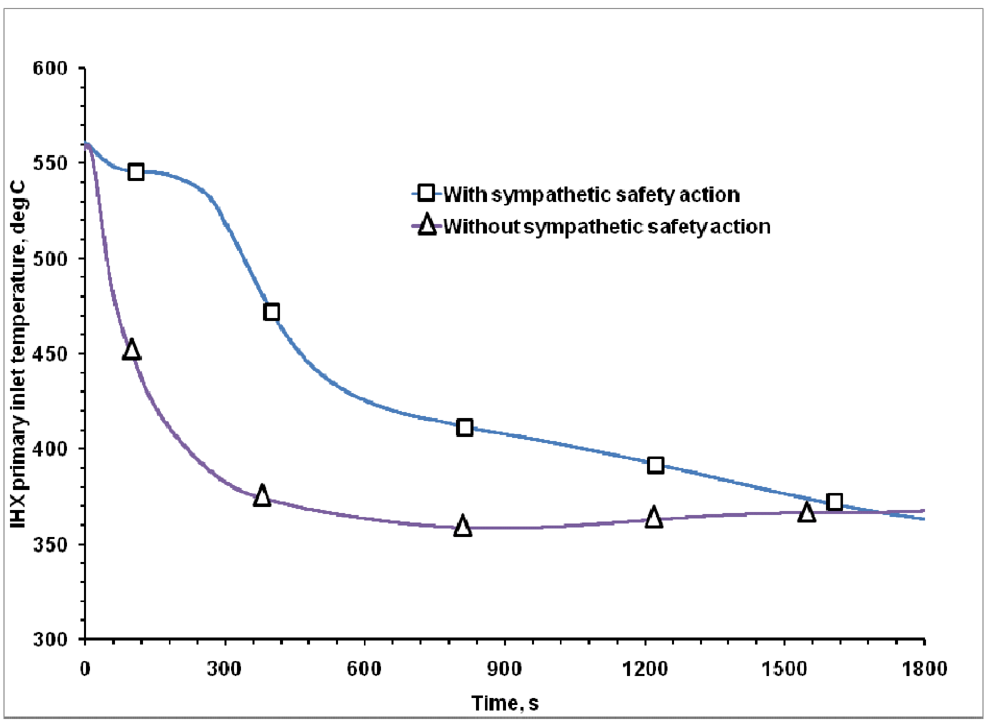

Fig. 6.10: Primary sodium temperature evolution at IHX inlet after SCRAM with and without sympathetic safety action adopted

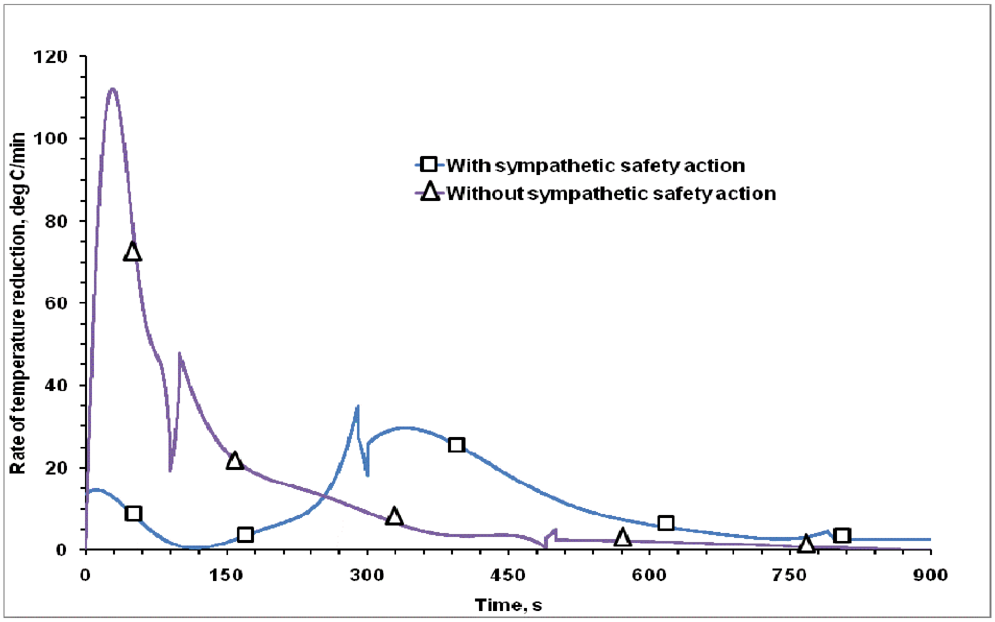

Fig. 6.11: Rate of reduction sodium temperature at the inlet of IHX after SCRAM with and without sympathetic safety action

6.6 CLOSURE

Large value of primary coast down time is an important safety feature from the point of view of thermal consequences in the reactor core during loss of flow events. Consequences of unprotected loss of flow events have been made benign by the choice of large primary coast down times. In order to limit the consequences of power failure event within design safety limits for a 500 MWe pool type reactor, a primary flow halving time of 8 s has been found to be essential. Apart from safety benefits, the large coast down time has also an operational benefit by way of improving plant availability through the elimination of reactor SCRAM during short term power failure events. It is seen that a primary flow halving time of 8 s can eliminate reactor SCRAM during short term power failure for a duration extending up to 0.75 s. Analysis of hot pool with and without the consideration of sympathetic safety action shows that though the sympathetic safety action results in development of thermal stratification in hot pool for about 15 minutes after reactor SCRAM, significant reduction in thermal shock faced by components is the main benefit of this procedure.

Sympathetic safety action following reactor trip weakens the inertial force of coolant flow significantly with respect to buoyancy force resulting is adverse buoyancy effects (thermal stratification) to be developed in hot pool. However, this action is established to be essential for improving the fatigue life of components. In this context, in order to have accurate prediction of thermal hydraulic scenario during reactor transients, models incorporating multi-dimensional analysis capability for sodium pools becomes essential.

REFERENCES

[1] Chetal, S. C., et al., 2006. Design of the prototype fast breeder reactor, Nuclear Engineering and Design, 236, 852-860.

[2] Albright, D.C., Bari, R.A., 1978. ‘Primary pipe rupture accident analysis for Clinch River Breeder Reactor’, Nuclear Technology, vol. 39, pp. 225–257.

[3] Gregory J. Van Tuyle, 1982. ‘Analysis of CRBRP station blackout using SSC/MINET’, BNL-NUREG-31110.

[4] Perkins, K. A, Bari, R. A, and Pratt, W. T., 1979. ‘In-vessel natural convection during a hypothetical loss of heat sink accident in the Fast Flux Test Facility’, BNL-NUREG-26131.

[5] Agrawal, A.K., et al., 1978. ‘An advanced thermo hydraulic simulation code for transients in LMFBRs (SSC-L Code)’, BNL-NUREG-50773.

[6] Guppy, J. G., 1978. ‘Application of multi time step integration method in SSC’, BNL-NUREG-25519.

[7] Horak, W. C., Guppy, J. G. and Kennett, R. J. ‘Validation of SSC using the FFTF natural circulation tests’, BNL-NUREG-31437.

[8] Yong-Bum Lee et al., 2002. ‘Development of a two-dimensional model for the thermohydraulic analysis of the hot pool in liquid metal reactors’, Annals of Nuclear Energy, vol. 29, pp. 21-40.

[9] Zhu, J., 1991. A low-diffusive and oscillation free convection schemes. Communications in Applied Numerical Methods, vol. 7, pp. 225.

[10] Van Doormal, J.P., Raithby, G.D., 1984. Enhancements of the SIMPLE method for predicting incompressible fluid flows. Numerical Heat Transfer, vol. 7, pp. 147–163.

[11] Gregory J., 1986. ‘A momentum integral network method for thermal hydraulic system analysis’, Nuclear Engineering and design, vol. 91, pp.17-28.

[12] Geffraye et al., 2009. ‘CATHARE 2 V2.5_2 : a Single Version for Various Applications’, The 13th International Topical Meeting on Nuclear Reactor Thermal hydraulics (NURETH-13), Japan.

[13] Tenchine, D., et al., 2012. ‘Status of CATHARE code for sodium cooled fast reactors’, Nuclear Engineering and Design, vol. 245, 140-152.

[14] Dufour Ph., 1995. ‘OASIS : an Interactive Simulation Case’, Simulation Multi-conference, Phenix, Arizona, USA.

[15] Mochizuki, H., 2010. ‘Development of plant dynamics analysis code NETFLOW++’, Nuclear engineering and Design, vol. 240, pp. 577-587.

[16] CHVETSOV. A. VOLKOV, 1998. ‘3-D Thermal Hydraulic Analysis of Transient Heat Removal from Fast Reactor Core Using Immersion Coolers’, IAEA Technical Committee meeting on: Methods and Codes for Calculations of Thermal hydraulic Parameters for Fuel, Absorber Pins and Assemblies of LMBFR with Traditional and Burner Cores, Obninsk, Russia.

[17] Hu, B. X., et al., 2013. ‘Development of a transient thermal-hydraulic code for analysis of China Demonstration Fast Reactor’, Annals of Nuclear Energy 55, 302–311

[18] IAEA, 2000. Transient and accident analysis of a BN-800 type LMFR with near zerovoid effect. IAEA, -TECDOC-1139.

[19] Zaiyong Ma, et al., 2015, Basic verification of THACS for sodium-cooled fast reactor system Analysis, Annals of Nuclear Energy 76, 1–11.

[20] Natesan, K. et al., 2011. ‘Dynamic Simulation of Accidental Closure of Intermediate Heat Exchanger Isolation Valve in a Pool Type LMFBR’, Annals of Nuclear Energy, Vol. 38, pp. 748–756.

[21] Vaidyanathan, G., et al., 2010. Dynamic model of Fast Breeder Test Reactor, Annals of Nuclear Energy, Vol. 37 (4), pp. 450–462.

[22] Dunn, F.E., et al., 1985. 'The SASSYS-1 LMFBR systems analysis code', Int. Topical Meeting on Fast Reactor Safety, Knoxville, Tennessee, USA, April 21-25.

[23] Cahalan, O. E. and Wei, T. Y. C., 1990. 'Modeling developments for the SAS4A and SASSYS computer codes', International Conference on Fast Reactor Safety, American Nuclear Society, Snowbird, Utah.

[24] Aurelia Chenu, et al., 2009.One- and Two-dimensional Simulations of Sodium Boiling under Loss-of flow Conditions in a Pin Bundle with the TRACE Code, 13th International Topical Meeting on Nuclear Reactor Thermal Hydraulics (NURETH-13) Kanazawa City, Ishikawa Prefecture, Japan.

[25] Wadim Jaeger and Victor Sánchez, 2013. Validation of the heat transfer enhancement models for spacer gridsin the system code TRACE, Nuclear Engineering and Design 265, 272– 287.

[26] Bottoni, M., et al., 1990. 'Experimental and Numerical Investigations of Sodium Boiling Experiments in Pin Bundle Geometry', Nuclear Technology, 89, 56-82.

[27] Tobita, Y., et al., 2002. 'The development of SIMMER-III, an advanced computer program for LMFR safety analysis', Proceedings of the IAEA/NEA Technical Meeting on Use of Computational Fluid Dynamics (CFD) Codes for Safety Analysis of Reactor Systems Including Containment, Pisa, Italy.

[28] Yamano, H., et al., 2003. SIMMER-III: A Computer Program for LMFR core Disruptive Accident Analysis, Version 3. A Model Summary and Program Description, JNC Report. Japan Atomic Energy Agency, JNC TN9400 2003-071.

[29] Martin, L., et al., 2009. 'The Phenix reactor: assessment of 35 years operation', Revue Générale du Nucléaire 1.

[30] IAEA, 2013. ‘Benchmark analyses on the natural convection test performed during the PHENIX End-of-Life experiments’, Final report of a coordinated research project 2008-2011, IAEA-TECDOC No. 1703.

[31] Tenchine, D., 2010. ‘Some thermal hydraulic challenges in sodium cooled fast reactors’, Nuclear Engineering and Design, 240, 1195-1217.

[32] Ieda, Y., et al., 1990. ‘Experimental and analytical studies of the thermal stratification phenomenon in the outlet plenum of fast breeder reactors’. Nuclear Engineering and Design, 120, 403–414.

[33] Chellapandi, P., and Velusamy, K., 2015. Thermal hydraulic issues and challenges for current and new generation FBRs, Nuclear Engineering and Design, 294, 202-225.

[34] Mohamad, A. A., and Viskanta, R., 1991. Transient low Prandtl number fluid convection in a lid-driven cavity. Numerical Heat Transfer, Part A, Vol. 19, pp. 187-205.

[35] Gresho, P. M., and Upson, C. D., 1983. Application of a modified finite element method to the time-dependent thermal convection of a liquid metal. In Proceedings of 3rd International Conference on Numerical Methods in Laminar and Turbulent Flow (Edited by C. Taylor, C. Johnson, J. A. Smith and W. Ramsey), pp. 750-762, Pineridge Press.

[36] Zukauskas. A, and Ulinskas. R, 1983. ‘Heat Exchanger Design Handbook’, Vol.2, Hemisphere Publishing Corporation.

[37] CHAM, PHOENICS code version 3.5.1, 2010.

[38] Natesan, K., Velusamy, K., Selvaraj, P. and Chellapandi, P, 2000. ‘3D hydraulic analysis of grid plate under pipe ruptured condition in PFBR’, Proc. 27 th National Conference of FMFP, FCRI, Palghat, India, pp. 191-198.

[39] Ward Smith, A. W., 1971. Pressure Losses in Ducted Flows, Butterworths, London, pp. 188.

[40] BLASIUS, P. R. H. 1913. Das AehnlichkeitsgesetzbeiReibungsvorgangen in Flüssigkeiten. Forschungsheft 131,1- 41.

[41] S. V. Patankar, ‘Numerical Heat Transfer and Fluid Flow’, Hemisphere Publishing Corporation, New York, 1980.

[42] IAEA, 2014. ‘Benchmark analyses of sodium natural convection in the upper plenum of the MONJU reactor vessel’, Final report of the coordinated research project 2008-2012, IAEA-TECDOC No. 1754.

[43] Byron Bird, R., Warren E. Stewart and Edvin N. Lightfoot, 1994. ‘Transport Phenomena’, John Wiley & Sons, Singapore.

[44] Markatos, N. C., and Pericleous, K. A., 1984. Laminar and turbulent natural convection in an enclosed cavity, Int. J. Heat Mass Transf., 27, pp. 755-772.

[45] Versteeg, H. and Malalasekra, W., 2007. ‘An Introduction to Computational Fluid Dynamics’, Pearson Education Limited.

[46] Jackson, J. D., Axcell, B. P., and Walton, A., 1994. ‘Mixed-convection heat transfer to sodium in a vertical pipe’, Experimental Heat Transfer, Vol. 7, pp. 71-90.

[47] Kawamura et al., 1998. ‘DNS of turbulent heat transfer in channel flow with low to medium-high Prandtl number fluid’, Int. J. Heat Fluid Flow, 19, pp. 482-491.

[48] Bieder. U., et al., 2018. ‘CFD analysis and experimental validation of steady state mixed convection sodium flow’, Nuclear Engineering and Design, Volume 326, pp. 333-343.

[49] Ghia, U., Ghia, K. N., and Shin, C, T, 1982. High-Re Solutions for Incompressible Flow Using the Navier-Stokes Equations and a Multigrid Method, Journal of Computational Physics, 48, 387-411.

[50] Shah, R. K. and London, A. L., 1978. Laminar Flow Forced Convection in Ducts, Advances in Heat Transfer, Supplement 1, 1978.

[51] Kim, J., Kline, S. J. and Johnston, J. P., 1980. Investigation of a reattaching turbulent shear layer: Flow over a backward facing step, J. Fluids Eng., ASME Trans., Vol. 102, pp. 302-308.

[52] Madni, I. K. and Agrawal, A. K., 1980. LMFBR system analysis: impact of heat transport system on core thermal-hydraulics, Nuclear Engineering and Design, Vol. 62, pp. 199-218.

[53] Durham, M. E., 1970. Journal of British Nuclear Energy Society, Vol. 15 (4), pp. 305-310.

[54] Han, J. W., et al. 2009. Investigation into the effects of a coastdown flow on the characteristics of early stage cooling of the reactor pool in KALIMER-600, Annals of Nuclear Energy, Vol. 36, pp. 1325–1332.

[55] Garner, P. L., Blomquist, R. N., Gelbard, E. M., 1992. COMMIX-1AR/P: a three dimensional transient single-phase computer program for thermal hydraulic analysis of single and multi-component systems, Vol. 2, User's Guide, ANL-92/33.

[56] Han, J. W., et al., 2012. Comparison of various design parameters' effects on the early-stage cooling performance in a sodium-cooled fast reactor, Annals of Nuclear Energy, Vol. 40, pp. 65–71.

[57] Puthiyavinayagam et al., 2002. Design safety limits in Prototype Fast Breeder Reactor, 1st National Conference on Nuclear Reactor Safety, Mumbai, INDIA.

[58] Essig, C., 1985. Dynamic behaviour of RAPSODIE in exceptional transient experiments. In: Proceedings ANS International Topical Meeting on Reactor Safety, Knoxville, USA.

[59] Planchon, H.P., Golden, G.H., Sackett J.I., 1987. Demonstration of Passive Safety Features in EBR-II, CONF-870415-3.

[60] Gregory, C.V., et al., 1979. Natural convection tests in support of dounreay PFR. Proceedings ANS/ENS Int. Conf. on Fast Reactor Safety Technology, Seattle.

[61] Valentin, B., et al., 1990. Natural convection tests in PHENIX coltemp experiments, Proceedings Int. Fast Reactor Meeting, Snowbird, vol. 4, pp. 269–277.

[62] Gouriou, A. et al., 1982. Dynamic behavior of super PHENIX reactor under unprotected transient. In: Proceedings LMFBR Safety Topical Meeting, Lyon.

[63] Jensen, S. E. and Olgaard, P. L., 1995. Description of prototype fast reactor at Dounreay, NKS/RAK-2(95)TR-C1, Rio National Laboratory.

Annexure

Discretization of Governing Equations in Cartesian Coordinate System

U-momentum (Fig. A.1)

$$a_P U_{i,J} = a_E U_{i+1,J} + a_W U_{i-1,J} + a_N U_{i,J+1} + a_S U_{i,J-1} + b_{i,J} \tag{A.1}$$

Where the coefficients a_P, a_E, a_W, a_N and a_S are evaluated based on convective and diffusive fluxes at the boundary of control volumes given by,

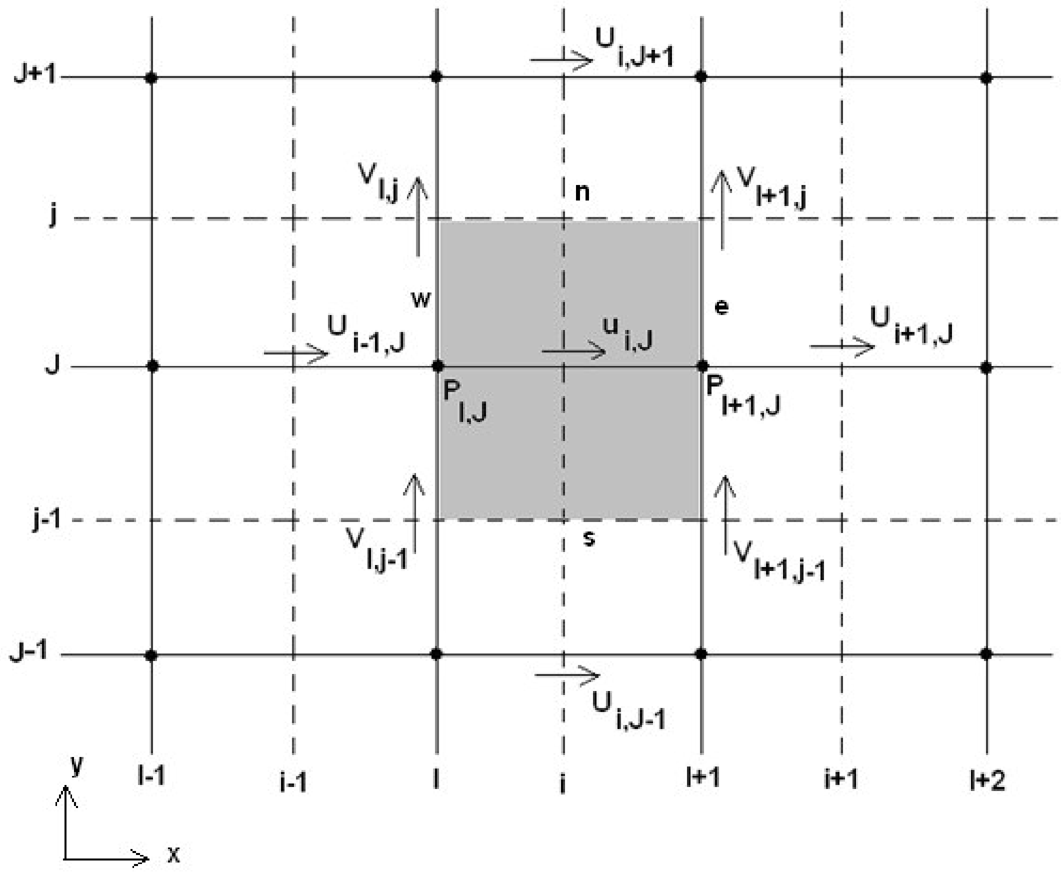

Fig. A.1: Representation of control volume for U (Cartesian)

$$\begin{aligned} F_e = (\rho AU)_e &= \frac{(\rho AU)_{i+1,J} + (\rho AU)_{i,J}}{2} \\ &= \frac{(y_j - y_{j-1})}{2}\left[\rho U_{i+1,J} + \rho U_{i,J}\right] \end{aligned} \tag{A.2}$$

$$F_w = (\rho AU)_w = \frac{(\rho AU)_{i,J} + (\rho AU)_{i-1,J}}{2}$$
$$= \frac{(y_j - y_{j-1})}{2}\left[\rho U_{i,J} + \rho U_{i-1,J}\right] \tag{A.3}$$

$$F_n = (\rho AV)_n = \frac{(\rho AV)_{I,j} + (\rho AV)_{I+1,j}}{2}$$
$$= \frac{(x_{I+1} - x_I)}{2}\left[\rho V_{I,j} + \rho V_{I+1,j}\right] \tag{A.4}$$

$$F_s = (\rho AV)_s = \frac{(\rho AV)_{I,j-1} + (\rho AV)_{I+1,j-1}}{2}$$
$$= \frac{(x_{I+1} - x_I)}{2}\left[\rho V_{I,j-1} + \rho V_{I+1,j-1}\right] \tag{A.5}$$

$$D_e = \frac{\mu_{I+1,J}\left(y_j - y_{j-1}\right)}{x_{i+1} - x_i} \tag{A.6}$$

$$D_w = \frac{\mu_{I,J}\left(y_j - y_{j-1}\right)}{x_i - x_{i-1}} \tag{A.7}$$

$$D_n = \frac{\mu_{I,J} + \mu_{I+1,J} + \mu_{I,J+1} + \mu_{I+1,J+1}}{4}\frac{(x_{I+1} - x_I)}{(y_{J+1} - y_J)} \tag{A.8}$$

$$D_s = \frac{\mu_{I,J} + \mu_{I+1,J} + \mu_{I,J-1} + \mu_{I+1,J-1}}{4}\frac{(x_{I+1} - x_I)}{(y_J - y_{J-1})} \tag{A.9}$$

Now, the coefficients a_P, a_E, a_W, a_N and a_S are calculated based on the numerical scheme adopted for representing the profile variation between nodal points.

$$a_E = D_e A(|P_e|) + Max(-F_e, 0) \tag{A.10}$$

$$a_W = D_w A(|P_w|) + Max(F_w, 0) \tag{A.11}$$

$$a_N = D_n A(|P_n|) + Max(-F_n, 0) \tag{A.12}$$

$$a_S = D_s A(|P_s|) + Max(F_s, 0) \tag{A.13}$$

Where P represents the cell Reynolds number given by

$$P_e = \frac{\rho U_e (x_{i+1} - x_i)}{\mu_e} = \frac{\rho(U_{i,J} + U_{i+1,J})}{2}\frac{(x_{i+1} - x_i)}{\mu_{I+1,J}} \tag{A.14}$$

Values of A(|Pe|) for various schemes are given by Table 4.2.

$$a_P = a_E + a_W + a_N + a_S + F_e + F_n - F_w - F_s + \rho(x_{I+1} - x_I)(y_j - y_{j-1})\frac{1}{\Delta t} \quad \text{(A.15)}$$

$$\begin{aligned} b_{i,J} = &(P_{I,J} - P_{I+1,J})(y_j - y_{j-1}) + S_u(x_{I+1} - x_I)(y_j - y_{j-1}) + \\ &\rho(x_{I+1} - x_I)(y_j - y_{j-1})U^0{}_{i,J}\frac{1}{\Delta t} \end{aligned} \quad \text{(A.16)}$$

For steady state solution, last terms in the RHS of eqns. (A.15) and (A.16) are not required to be considered.

S_u includes buoyancy induced momentum source calculated based on Boussinesq approximation [47] as

$$S_{uB} = \rho\beta g_x\left[\frac{(T_{I,J} + T_{I+1,J})}{2} - T_{ref}\right] \quad \text{(A.17)}$$

<u>V-momentum (Fig. A2)</u>

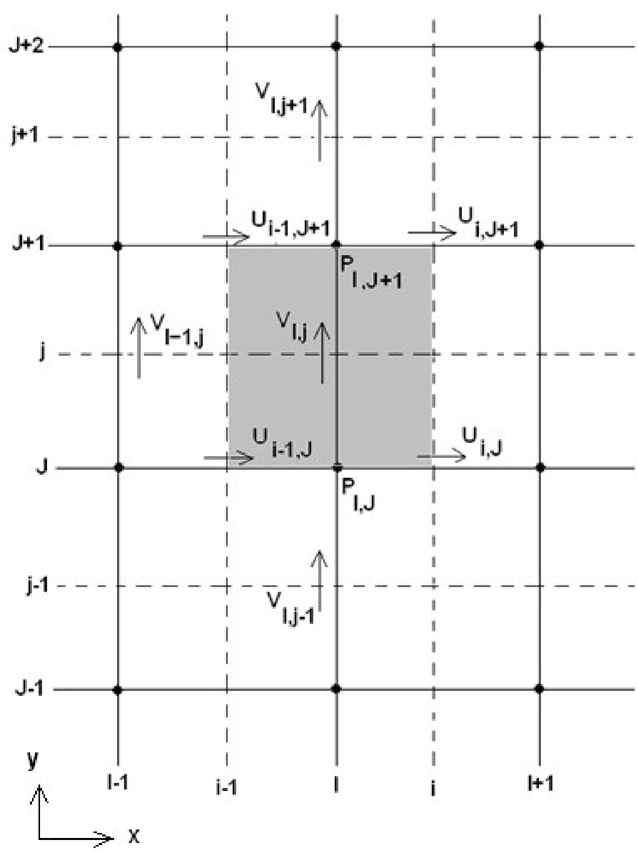

Fig. A.2: Representation of control volume for V (Cartesian)

$$a_P V_{I,j} = a_E V_{I+1,j} + a_W V_{I-1,j} + a_N V_{I,j+1} + a_S V_{I,j-1} + b_{I,j} \tag{A.18}$$

Where the coefficients a_P, a_E, a_W, a_N and a_S are evaluated based on convective and diffusive fluxed at the boundary of control volumes given by,

$$\begin{aligned} F_e = (\rho AU)_e &= \frac{(\rho AU)_{i,J} + (\rho AU)_{i,J+1}}{2} \\ &= \frac{(y_{J+1} - y_J)}{2}\left[\rho U_{i,J} + \rho U_{i,J+1}\right] \end{aligned} \tag{A.19}$$

$$\begin{aligned} F_w = (\rho AU)_w &= \frac{(\rho AU)_{i-1,J} + (\rho AU)_{i-1,J+1}}{2} \\ &= \frac{(y_{J+1} - y_J)}{2}\left[\rho U_{i-1,J} + \rho U_{i-1,J+1}\right] \end{aligned} \tag{A.20}$$

$$\begin{aligned} F_n = (\rho AV)_n &= \frac{(\rho AV)_{I,j} + (\rho AV)_{I,j+1}}{2} \\ &= \frac{(x_i - x_{i-1})}{2}\left[\rho V_{I,j} + \rho V_{I,j+1}\right] \end{aligned} \tag{A.21}$$

$$\begin{aligned} F_s = (\rho AV)_s &= \frac{(\rho AV)_{I,j-1} + (\rho AV)_{I,j}}{2} \\ &= \frac{(x_i - x_{i-1})}{2}\left[\rho V_{I,j-1} + \rho V_{I,j}\right] \end{aligned} \tag{A.22}$$

$$D_e = \frac{\mu_{I,J+1} + \mu_{I,J} + \mu_{I+1,J+1} + \mu_{I+1,J}}{4} \frac{(y_{J+1} - y_J)}{(x_{I+1} - x_I)} \tag{A.23}$$

$$D_w = \frac{\mu_{I-1,J+1} + \mu_{I-1,J} + \mu_{I,J+1} + \mu_{I,J}}{4} \frac{(y_{J+1} - y_J)}{(x_I - x_{I-1})} \tag{A.24}$$

$$D_n = \frac{\mu_{I,J+1}(x_i - x_{i-1})}{y_{j+1} - y_j} \tag{A.25}$$

$$D_s = \frac{\mu_{I,J}(x_i - x_{i-1})}{y_j - y_{j-1}} \tag{A.26}$$

Now, the coefficients a_P, a_E, a_W, a_N and a_S are calculated based on eqns. (A.10) – (A4.15) and Table A.1 depending on the numerical scheme adopted for representing the profile variation between nodal points.

$$a_P = a_E + a_W + a_N + a_S + F_e + F_n - F_w - F_s + \rho(x_i - x_{i-1})(y_{J+1} - y_J)\frac{1}{\Delta t} \quad (A.27)$$

$$\begin{aligned} b_{I,j} &= (P_{I,J} - P_{I,J+1})(x_i - x_{i-1}) + S_V(x_i - x_{i-1})(y_{J+1} - y_J) \\ &\quad + \rho(x_i - x_{i-1})(y_{J+1} - y_J)V^0{}_{I,j}\frac{1}{\Delta t} \end{aligned} \quad (A.28)$$

S_V includes buoyancy induced momentum source calculated based on Boussinesq assumption as

$$S_{VB} = \rho\beta g_y\left[\frac{(T_{I,J} + T_{I,J+1})}{2} - T_{ref}\right] \quad (A.29)$$

For steady state solution, the last term of equations (A.27) and (A.28) are not required to be considered.

<u>Continuity</u>

The pressure velocity coupling is achieved by deriving transport equation for pressure correction from the continuity equation. The discretized form of pressure correction equation with respect to the nodal representation shown in Fig. A.3 is given below.

$$a_P P'_{I,J} = a_E P'_{I+1,J} + a_W P'_{I-1,J} + a_N P'_{I,J+1} + a_S P'_{I,J-1} + b'_{I,J} \quad (A.30)$$

$$a_P P'_{I,J} = a_E P'_{I+1,J} + a_W P'_{I-1,J} + a_N P'_{I,J+1} + a_S P'_{I,J-1} + b'_{I,J} \quad (A.31)$$

$$a_P P'_{I,J} = a_E P'_{I+1,J} + a_W P'_{I-1,J} + a_N P'_{I,J+1} + a_S P'_{I,J-1} + b'_{I,J} \quad (A.32)$$

$$a_P P'_{I,J} = a_E P'_{I+1,J} + a_W P'_{I-1,J} + a_N P'_{I,J+1} + a_S P'_{I,J-1} + b'_{I,J} \quad (A.33)$$

$$a_E = (\rho dA)_{i,J} = \rho\frac{(y_j - y_{j-1})}{a_{P(i,J)}}(y_j - y_{j-1}) \quad (A.34)$$

$$a_W = (\rho dA)_{i-1,J} = \rho\frac{(y_j - y_{j-1})}{a_{P(i-1,J)}}(y_j - y_{j-1}) \quad (A.35)$$

Where $a_{P(i,J)}$ and $a_{P(i-1,J)}$ are the a_P coefficients of x momentum equations for the control volumes (i, J) and (i-1,J) respectively.

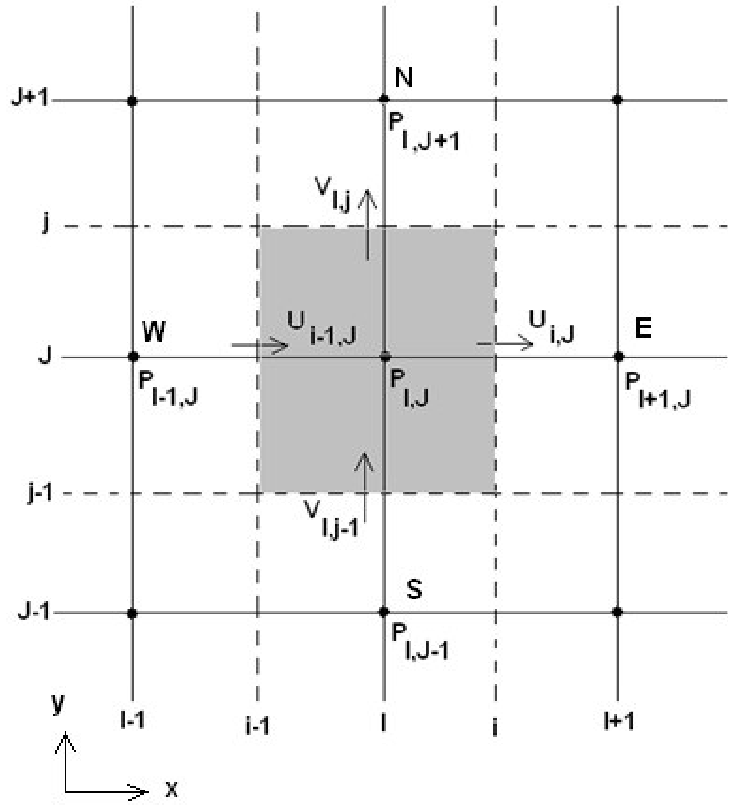

Fig. A.3: Representation of control volume for P and T (Cartesian)

$$a_N = (\rho dA)_{I,j} = \rho \frac{(x_i - x_{i-1})}{a_{P(I,j)}}(x_i - x_{i-1}) \tag{A.36}$$

$$a_S = (\rho dA)_{I,j-1} = \rho \frac{(x_i - x_{i-1})}{a_{P(I,j-1)}}(x_i - x_{i-1}) \tag{A.37}$$

Where $a_{P(I,j)}$ and $a_{P(I,j-1)}$ are the a_P coefficients of y momentum equations for the control volumes (I, j) and (I, j-1) respectively.

$$a_P = a_E + a_W + a_N + a_S \tag{A.38}$$

$$b'_{I,J} = \rho U_{i-1,J}(y_j - y_{j-1}) - \rho U_{i,J}(y_j - y_{j-1}) + \rho V_{I,j-1}(x_i - x_{i-1}) - \rho V_{I,j}(x_i - x_{i-1}) \tag{A.39}$$

Conservation of Energy

The discretized form of energy balance equation is also obtained with respect to the nodal representation shown in Fig. 4.3. Temperature is stored at the same nodal location of storage of pressure.

$$a_P T_{I,J} = a_E T_{I+1,J} + a_W T_{I-1,J} + a_N T_{I,J+1} + a_S T_{I,J-1} + b_{I,J} \tag{A.40}$$

$$F_e = (\rho CpAU)_e = \rho Cp(y_j - y_{j-1})U_{i,J} \tag{A.41}$$

$$F_w = (\rho CpAU)_w = \rho Cp(y_j - y_{j-1})U_{i-1,J} \tag{A.42}$$

$$F_n = (\rho CpAV)_n = \rho Cp(x_i - x_{i-1})V_{I,j} \tag{A.43}$$

$$F_s = (\rho CpAV)_s = \rho Cp(x_i - x_{i-1})V_{I,j-1} \tag{A.44}$$

$$D_e = \frac{2K_{I,J}K_{I+1,J}}{K_{I,J} + K_{I+1,J}} \frac{(y_j - y_{j-1})}{(x_{I+1-}x_I)} \tag{A.45}$$

$$D_w = \frac{2K_{I-1,J}K_{I,J}}{K_{I-1,J} + K_{I,J}} \frac{(y_j - y_{j-1})}{(x_{I-}x_{I-1})} \tag{A.46}$$

$$D_n = \frac{2K_{I,J}K_{I,J+1}}{K_{I,J} + K_{I,J+1}} \frac{(x_i - x_{i-1})}{(y_{J+1-}y_J)} \tag{A.47}$$

$$D_s = \frac{2K_{I,J}K_{I,J-1}}{K_{I,J} + K_{I,J-1}} \frac{(x_i - x_{i-1})}{(y_{J-}y_{J-1})} \tag{A.48}$$

Now, the coefficients a_P, a_E, a_W, a_N and a_S are calculated based on eqns. (4.10) – (4.15) and Table 4.2 depending on the numerical scheme adopted for representing the profile variation between nodal points.

$$a_P = a_E + a_W + a_N + a_S + F_e + F_n - F_w - F_s + \rho Cp(x_i - x_{i-1})(y_j - y_{j-1})\frac{1}{\Delta t} \tag{A.49}$$

$$b_{I,J} = S_T(x_i - x_{i-1})(y_j - y_{j-1}) + \rho Cp(x_i - x_{i-1})(y_j - y_{j-1})T^0{}_{I,J}\frac{1}{\Delta t} \tag{A.50}$$

For steady state solution, the last term of equations (A.49) and (A.50) are not required to be considered. Discretized equations for k and ε are obtained in the same manner as that obtained for the energy balance equation.